THE STUDY OF LIGHT INDUCED STRUCTURES IN LIQUIDS AND SOLIDS

MICHAEL ANTHONY CUTTER

Department of Physics

Royal Holloway College

This thesis is submitted in fulfilment for the degree of Doctor of Philosophy in the University of London

1976

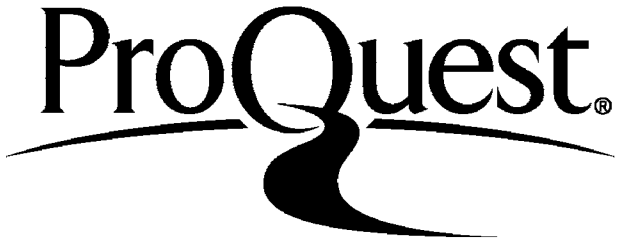

ABSTRACT

A number of interaction mechanisms of laser light with matter are reviewed; these include laser induced damage, nonlinear optics and various types of scattering.

A comprehensive experimental study of laser induced damage is described. This damage is caused to a glass surface bearing a thin gold film while being illuminated by an argon ion laser beam.

Small diffraction gratings can be produced by placing thin metallic films inside a ruby laser cavity. In such an arrangement the intense light of the laser is obliquely incident on the thin partially absorbing film simultaneously from two opposite directions, heating occurs, therefore, much more rapidly at the antinodes than at the nodes of the resulting standing wave. This heating can cause evaporation and ionization of the film. Since the film intersects the antinodes of the standing wave in a series of lines, this removal of the film material results in the creation of a diffraction grating. A time resolved investigation has been made of the development of such gratings in a number of metallic films, and the effect of film thickness, incident laser intensity, and angular orientation of the film has been studied.

A solution of the time dependent stimulated scattering equations is obtained. Using a new approach it is shown that by suitable convolutions, the time dependent stimulated scattering gain profile for absorbing and non-absorbing liquids can be directly obtained from the steady state scattering results.

Laser mode locking techniques are detailed and a description is given of a ruby ring laser system. This system was able to deliver pulses as short as 25 picoseconds in duration and with peak intensities of 100 MW/cm^2.

CONTENTS

CONTENTS
(continued)

C O N T E N T S

(continued)

CHAPTER I

INTERACTION MECHANISMS OF LASER LIGHT WITH MATTER

1.1 DEVELOPMENT OF THE LASER

The underlying principles of the laser and even the relevant technology for the construction of a simple laser, have been known since 1917 when Einstein[1] postulated the existence of the stimulated emission of radiation from an atomic system. This stimulated radiation is proportional to the radiation density at the emission frequency, and is emitted in phase with the external stimulating radiation. Up until then only the spontaneous emission process had been accounted for, and as the name implies, this process of radiation emission requires no external influence.

During the early 1920's Fuchauer and Landenburg produced a relationship linking the integral of the absorption coefficient of an atomic line with Einstein's stimulated emission process and with the distribution of the atomic populations among the different energy levels. The great importance of this formula lies in the possibility of gaining information about the population distribution among the energy states of a given material by simply measuring the fractional power absorbed over the entire absorption line.

During the late 1920's and the 1930's much work was performed by spectroscopists on the change in the absorption of atomic lines by changing the population of the atomic state from that experienced when the atoms are in thermal equilibrium, but no negative absorption was obtained.

It wasn't until after the Second World War, which had fostered a considerable effort in the microwave region, that the production of stimulated emission of microwaves became a reality, with Purcell and Pound[2] in 1951, inverting the population of a nuclear spin system by the sudden reversal of an external magnetic field and hence detecting a

stimulated emission signal at 50 kHz. This then led to the search in the early 1950's for suitable materials and processes in order to obtain stimulated emission, culminating in 1954 with Townes' [3] successful microwave amplifier.

With the advent of the MASER (Microwave Amplification of Stimulated Emission of Radiation), many people speculated on the possibility of extending the principle of the maser operation to the optical region. This led Schawlow and Townes[4] in 1958, to present a paper proposing the construction of an optical maser, outlining the minimum inversion necessary to achieve oscillation within an active medium which was undergoing absorption of radiation for an energy pump, such as a flash lamp, and incorporating regenerative feedback in the system, as would be achieved if the system was bounded by two colinear mirrors. By 1960 Maiman[5] had successfully constructed an optical maser using a 0.05% chromium-ion concentration ruby crystal of 1 cm dimensions, with two parallel faces coated with evaporated silver, forming a parallel plate resonator; this produced a train of 3kW, 2 μs pulses, lasting approximately 1 ms.

Within a year, Hellwarth[6] had extended the output power level to the megawatt region, by a process known as 'Q' switching, in which a lossy component is inserted into the laser cavity to build up a large inversion population which is suddenly released in a few tens of nanoseconds, by the removal of this lossy component. The switching of the lossy component can be achieved by a variety of methods, although originally Hellworth obtained 'Q' switching by use of an optical Kerr cell in conjunction with crossed polarisers. Pulsing the Kerr cell at its $\lambda/4$ voltage, increases the transmission of the system for the duration of the electrical pulse.

A much more convenient method of 'Q' switching was later developed by Sorokin[7,8] in 1964, by the use of an absorbing dye cell in the laser

cavity. This technique worked on the principle that above a certain laser radiation intensity, the dye's absorption level would become saturated and therefore incapable of acting as a lossy component. This bleaching process performed the same function as the switched Kerr cell.

In addition to the above two mentioned methods of 'Q' switching is the use of a Pockel cell[9,10] and Glan-Thompson prism as an electro-optic shutter.

While research work was continuing on the ruby lasers, a parallel set of work was being undertaken on trying to obtain lasing action in other materials not necessarily solid state. By 1961 Javan[11] had developed the C W helium-neon laser, which had a power of only a few milliwatts, but exhibited a much better spectral and spatial purity than that of the ruby.

Since 1960 the laser field has seen a rapid increase in the literature published and experiments performed on the subject, with lasing having being accomplished in many varieties of materials and in the solid, liquid, gaseous and semiconductor phase. Power levels for the pulsed lasers are now in excess of terawatts/cm^2, with pulse durations of less than 5ps while the C W CO_2 lasers have been reported with tens of kilowatts output and efficiencies of up to 30%.

1.2 LASER INDUCED DAMAGE

The types of interaction mechanisms which may play a role in the initiation and development of laser induced damage, can basically be divided into five main headings, i.e.

(i) thermal
(ii) stimulated Brillouin
(iii) avalanche breakdown
(iv) self focusing
(v) impurity inclusions.

Although there exists a limited number of damage mechanisms, the ways in which they lead to damage are numerous and if a particular experiment is

to be duplicated, then a detailed description of the variables involved are needed, such as pulse duration, beam diameter, laser frequency and details of material growth and preparation.

1.2.1 Thermal

In general, thermal damage occurs in those materials which have a reasonably high absorption either at the surface or in the bulk of the material. In principle the determination of the surface temperature is achieved by solving the differential equation for the flow of heat:

$$\nabla^2 T(x,y,z,t) - \frac{1}{K} \frac{\partial T}{\partial t}(x,y,z,t) = - A(x,y,z,t)/K ,$$

where T is the temperature as a function of position (x,y,z) and time t, K is the thermal diffusivity, K the thermal conductivity, and A the heat produced per unit volume per unit time, as a function of position and time.

In 1964 Ready[12] discovered the validity of using an ordinary thermodynamic approach for calculating the effects produced by high-power laser beams absorbed at opaque surfaces, and found that his calculations were in reasonable agreement with the observed effects.

In actual experiments where the absorbed flux densities are high, such things as melting, vapourization and ionization may play a significant role in governing the extent of the damage, and hence severely confuse the analysis. In these studies the use of a phenomenological model to describe the process involved is of tremendous value. One such model was described by Ready[13] in order to explain the observed minute explosions which took place at the surface of a metal irradiated by a 'Q' switched laser. In this model he describes how the surface rises to the vapourization temperature and begins to vapourize. Then this material recoils against the surface producing a high pressure. This becomes superheated as more heat is conducted into the interior. Eventually at a

critical point the temperature has risen high enough so that the heat of vapourization falls to zero at which point there is no distinction between the super heated solid and a highly condensed gas. The emission of vapourised material then proceeds like a thermal explosion.

A similar approach has been undertaken by other research workers[14] with a reasonable amount of success. On a very similar tack to that discussed above, some work[15,16] has been undertaken on calculating the impulse shock waves that are generated on the removal by vapourization of the target material. In this instance a measure of the material resistance to the generation of shock waves can be calculated, and a deduction can therefore be made as to which materials would be most useful in the fabrication of pulsed laser mirrors.

In addition to the formation of plumes of vapourised materials, it has also been reported[17-21] that when the target material has reached a high enough temperature, ionization can occur. This ionized material has been detected by observing ionized emission lines in the spectra of the laser generated microplasmas[22,23], and also by directly collecting the ions emitted from the surface[24-26]. By observing the current produced from a plasma on an oscilloscope, a direct measure of the plasma formation in time is thus obtained and by noting which ionized lines are present in the spectra, an estimate of the electron temperature can be made.

Although most of the discussion so far has been on the removal of material from the irradiated surface where the temperature has exceeded the vapourization temperature, thermal damage may also occur from the stresses developed during thermal expansion of the material, and where the surface temperature has reached the melting point. One might expect such a phase change to be reversible, with the melted region cooling down after the removal of the incident light, leaving the surface in much the same

condition as before it was irradiated. Work has been reported[27] which suggests that this is not always the case, and a comprehensive discussion on this effect can be found in Chapter II.

1.2.2 Stimulated Brillouin Scattering

In 1922, Brillouin[28] analysed the random fluctuations of a medium into its acoustic modes, and showed that the light scattered from such a medium will be shifted in frequency by a Doppler shift due to the velocity of the acoustic waves. This frequency shifted light was subsequently detected[29] and is now known as spontaneous Brillouin scattering. It was later found[30,31] that if laser light of sufficient intensity was passed through such a medium, then the weak spontaneous scattering would beat with the main laser light, and a hypersonic wave would build up at the difference frequency due to electrostrictive coupling. A very strong interaction can therefore occur, with the Brillouin scattered light and the hypersonic wave being amplified at the expense of the laser light. It was subsequently reported[32] in 1964, that when powerful laser light was focused into a transparent solid, damage occurred from the mechanical stresses associated with the generation of these acoustic waves.

It has been shown by Bliss[33] that when the incident laser pulse is short compared to the relaxation time of the acoustic phonons, then the damage threshold for a particular medium occurs at a constant energy density. For longer pulses, however, where a steady state approximation can be made, the damage threshold occurs at a constant power density. In the latter instance it was calculated that intensity levels of the order of 10^4 MW/cm^2 were needed in order to establish damage in quartz.

1.2.3 Avalanche Breakdown

It has been suggested by a number of research workers[33-38] that in some instances laser induced damage in transparent solids could be attributed to electron avalanche breakdown.

If an intense laser beam is focused into a transparent dielectric which has an electron in the conduction band, then it is possible that the electron will derive sufficient energy from the laser field to be accelerated to an energy greater than the band gap[35]. Each such electron would then be capable of exciting another electron into the conduction band by impact ionization, leading to an exponential increase in the number of conduction electrons. If the rate of increase of the electron's energy exceeds the losses, by diffusion, trapping, recombination or impurity and phonon scattering, then the avalanche ensues, leading to a strongly absorbing region. The energy absorbed by the electrons is eventually lost to the lattice of the material by electron-phonon scattering. The release of a large amount of energy in a small volume, leads to the destruction of the material at that point. Intensities of the order of 10^{10} W/cm^2 are needed to produce avalanche breakdown in ruby[35]. The initial production of electrons could be caused by easily ionized impurities, metallic inclusions or multiphoton absorption.

To cause damage in a material by the electron avalanche mechanism, two conditions must be fulfilled. First, the laser intensity must be high enough so that the rate of gain of energy by the electrons exceeds their losses. Secondly, the laser energy density must be sufficient to create a critical number of conduction electrons within the duration of the pulse. Therefore if the laser pulse is long compared with the time required for the avalanche to occur, one would expect the damage threshold to be dependent on the power density of the laser. For shorter pulses, however, where the laser intensities are high enough to deposit the energy

faster than the rate at which losses occur, the damage thresholds are expected to be dependent on the energy density of the laser pulse.

An interesting consequence of the fact that energy is imparted to the material lattice by phonon-electron interaction, is that the threshold level at which damage occurs increases with an increase in the material's temperature[35], since the phonon-electron collision frequency increases with higher temperatures.

Lastly, it can be shown[35] that the theoretical threshold intensity for laser damage, increases with increasing laser frequency, since more energy can be obtained by an electron during a longer optical period and the probability that a collision will occur before the electric field amplitude changes in direction, is higher for lower frequencies.

1.2.4 Self-focusing

The refractive index of any transparent dielectric will exhibit a weak dependence on the intensity of the light passing through the material. This dependence can be written in the form[39]:

$$n = n_0 + n_2 E^2$$

where E is the amplitude of the local electric field and n_2 is a constant dependent on the material. If a laser pulse, with a beam intensity profile which decreases smoothly from the centre, passes through such a material, then the refractive index of the medium will increase towards the centre of the beam due to the higher light intensities. This results in a refractive index gradient across the beam profile which acts as a convex lens on the light. If the light beam intensity is high enough, complete self-focusing of the beam will occur[40-42].

It has been calculated by Akhmonov[43] that the power level required to compensate for the diffraction spreading in a collimated Gaussian

beam is given by:

$$P_c = \frac{\lambda^2 c}{32\pi^2 n_2}$$

where λ is the wavelength of the light in the medium in absence of the nonlinearity, and c is the velocity of light in vacuum.

The approximate focusing length, which represents the distance in which an initially collimated beam will be brought to a self-focus within the nonlinear medium for power levels in excess of the critical power P_c, is given by the following expression, derived from detailed numerical studies undertaken by Marburger[44]:

$$Z_f = kr^2 \left\{ \frac{0.136}{[(P/P_2)^{\frac{1}{2}} - 0.858]^2 - 0.0202} \right\}^{\frac{1}{2}}$$

where r is the $1/e$ radius of the Gaussian intensity profile of the beam, k is the wave vector and P_2 is given by

$$P_2 = 0.0116 \lambda^2 c/n_2$$

It can be seen from this equation that for $P \gg P_2$, Z_f is inversely proportional to the square root of the total laser power. With a pulse, therefore, the effective focusing length will decrease on the rise of the pulse, and then increase to infinity as the pulse decays. This therefore leads to a moving focus, which has been observed[42,45].

The values calculated for the critical power P_c and the self-focusing length Z_f are based on the assumption that the refractive index change takes place in a time short compared with the duration of the pulse. Under the converse condition the critical power P_c required so that self-focusing just compensates for the diffraction spreading is given by:

$$P_c \propto \frac{\lambda^2 c}{n_2 \Delta t}$$

and the self-focusing distance is given by:

$$Z_f \propto \frac{1}{P^{\frac{1}{2}} \Delta t}$$

where Δt is the duration of the laser pulse.

Four mechanisms have been identified that contribute to the non-linear refractive index in solids:

(i) electrostriction[39];
(ii) electronic distortion[46,47];
(iii) molecular librations[48];
(iv) absorptive heating[49-51].

The approximate time required for electrostrictive effects to occur in a beam of radius r, is given by $\tau = r/v_s$ where v_s is the velocity of sound in the medium. This puts a value of 10^{-6} sec on τ for a 4 mm radius beam passing through glass, which is long compared to 'Q' switched laser pulses. Therefore it is expected that I_c, the critical intensity corresponding to P_c, will be large for both 'Q' switched and mode locked pulses. An estimate[33] of the value of I_c, for 10 ns and 30 ps laser pulses travelling through glass gives 5×10^8 W/cm^2 and 3×10^{15} W/cm^2 respectively, where the variation in refractive index has been caused solely be electrostriction.

We would therefore expect that for picosecond pulses any self-focusing present should be attributed to either electronic distortion or molecular libration since these processes have much shorter relaxation times, although the nonlinear refractive index n_2 for these processes is smaller ($\tau \simeq 10^{-13}$ s for molecular libration and 10^{-16} s for electronic distortion). A qualitative analysis of the electrostriction mechanism has shown[52], however, that self-focusing can occur even in the transient case, provided the pulse power is large enough.

The process of self-focusing is itself not a destructive process, but could easily initiate an avalanche electron breakdown due to the high electric fields present in the focal region.

1.2.5 Particle Inclusions

Small inclusions in laser materials and optical components can lead to localised heating which may result in damage[53,54], caused by thermal expansion or by melting of the surrounding region. These inclusions may come from the impurities in the raw materials or the crucible material (i.e. platinum, iridium, SiO_2 or refractory materials) used to fabricate the optical components.

If we consider these inclusions to be spherical and of radius r then the energy absorbed by the particles, if the incident light intensity is given by I is

$$\Delta E = 2\pi r^2 I \Delta t \int_0^{\pi/2} \left[1 - \exp(-2\alpha r \cos\theta)\right] \sin\theta \cos\theta \, d\theta$$

or

$$\Delta E = \pi r^2 I \Delta t \left\{1 + \frac{1}{2r^2\alpha^2}\left[-1 + \exp(-2r\alpha) + 2r\alpha \exp(-2r\alpha)\right]\right\}$$

where Δt is the pulse duration and α the material absorption coefficient.

The temperature rise experienced by such a particle will be given by:

$$T = \frac{3 \Delta E}{4 c_i \rho_o \pi r^3}$$

where c_i is the specific heat at constant volume and ρ_o the density of the inclusion material.

Thus for thick particles ($\alpha r \gg 1$) the temperature is proportional to $1/r$, while for thin particles ($\alpha r \ll 1$) the temperature is dependent on $1/r^2$. If the particle is much smaller than the wavelength of the incident light a partial wave analysis is needed to determine the absorption cross-section.

Therefore if a platinum inclusion is irradiated by a 30 ns laser beam of 20 J/cm^2 the temperature T attained is

$$T \simeq 1.6 \times 10^4/R \ ^\circ K ,$$

where R is the radius of the particles in microns. This figure is very

large but not necessarily correct since we have neglected conduction of heat into the host material. If we therefore consider the conduction of heat from the inclusions to the host material, we find that for large particles no change is found for T, but for small particles the temperature T attained is given by[55];

$$T \simeq \frac{Ir}{4K_h}\left[1 - \frac{r}{(\pi D_h \Delta t)^{\frac{1}{2}}} - \frac{r^3(2-q)}{2q\,\pi^{\frac{1}{2}}(D_h \Delta t)^{\frac{3}{2}}} \cdots\right]^{\circ}K \qquad \ldots (1.1)$$

where $q = 3C_h/c_i$, C_h and D_h are the specific heat and diffusivity of the host material respectively.

Now since the fractional change in the volume of the inclusion is directly proportional to the energy deposited in the inclusion, an estimate of the tensile stress developed can be easily made[56], that is

$$\sigma \simeq 6B_i G_h \alpha_i T/(4G_h + 3B_i)$$

where σ is the tensile stress at the periphery of the inclusion, directed tangential to the inclusion. B_i is the bulk modulus of the inclusion and G_h the shear modulus of the host material. For the particular case of platinum inclusions in a typical glass, this is equal to

$$\sigma \simeq 60\,T \text{ psi} .$$

The value of σ drops off as $1/r^3$ where r is the distance from the centre of the inclusion.

Most glasses have a strength of approximately 6×10^5 psi, therefore if failure is to occur, temperatures of the order of $10{,}000\,^{\circ}K$ are required. Equation (1.1) predicts that for a 30 ns laser pulse of 700 MW/cm^2 incident on platinum particles in glass, particles with radii between about 300 Å and 2 μ result in failure, while smaller and larger particles should be safe.

The above calculation is based on the assumption that no phase change occurs, but this is unlikely to be the case and the effect of a molten glass layer between the glass and platinum will be to lower

significantly the tensile stress and decrease the chances of failure for the smaller particles. If the molten layer is therefore considered[55], the size of particles which will result in failure, lie between 1000 Å and 2 μ.

Because of the rapid decrease in stress with increasing distance from the particle, a 1 μ particle or smaller, will produce cracks less than 10 μ in size for stresses between the liquid-solid boundary of five times the material strength (which is not unreasonable). Such cracks are appreciably smaller than those regularly observed, and may in many cases be undetected. These minor cracks could eventually develop over a number of laser shots, and might explain the fatigue phenomenon observed[54] in several studies of laser damage.

1.3 NONLINEAR OPTICS

The discovery of a number of new nonlinear optical processes, resulting from the interaction of laser light with matter, can be attributed to the high electric fields associated with laser light. From a macroscopic point of view, some of these processes can be considered to have arisen from the polarization of the medium by the electric field.

If we consider a weak electric field E applied to a medium, then the polarization P is simply given by:

$$P = \chi_1 E$$

where χ_1 is the ordinary linear susceptibility. This term is responsible for the familiar linear phenomena of refraction and attenuation[57].

Quite often in physics linear laws turn out to be only an approximation of a much more general formulation, and often these linear laws only hold true where the extent of perturbation of the system is small. Therefore at high field strengths we would expect the polarization to be given by[58-60]

$$P = \chi_1 E + \chi_2 E^2 + \chi_3 E^3 + \ldots \qquad \ldots (1.2)$$

where $\chi_2, \chi_3 \ldots$ are the nonlinear susceptibilities.

1.3.1 Quadratic Polarization

Let us just consider the second term in equation (1.2), and suppose that we want to examine the interaction in a crystal of two travelling waves:

$$E_1(z,t) = A_1 \cos(\omega_1 t + k_1 z)$$

and

$$E_2(z,t) = A_2 \cos(\omega_2 t + k_2 z) \ .$$

Substituting the superposition of these two waves into the second term, we have

$$P_2 = \frac{\chi_2}{2}\left(A_1^2 + A_2^2\right) + \frac{\chi_2}{2} A_1^2 \cos(2\omega_1 t + 2k_1 z) + \frac{\chi_2}{2} A_2^2 \cos(2\omega_2 t + 2k_2 z)$$
$$+ \chi_1 A_1 A_2 \cos\left\{(\omega_1 + \omega_2)t + (k_1 + k_2)z\right\}$$
$$+ \chi_1 A_1 A_2 \cos\left\{(\omega_1 - \omega_2)t + (k_1 - k_2)z\right\} .$$

We find therefore, that the polarization consists of a number of components with different frequencies. Each component of the polarization will emit an electric field at its own frequency.

If the incident applied field only contained one frequency, then the resulting polarization contains a d.c. term and a component oscillating at twice the applied frequency. The d.c. term produces a d.c. applied field proportional to the intensity of the oscillating field. This rectification phenomenon has been observed[61] both in potassium dihydrogen phosphate and potassium dideuterium phosphate, when the light from a ruby laser passed through the crystal. The term oscillating with a frequency of twice that of the applied electric field, results in the generation of second harmonic light, which has been extensively investigated[62-66].

If the applied optical field contains two frequencies, then a number of other interesting effects arise. For instance, if one of the frequencies is zero, that is we apply a d.c. electric field to a medium

through which monochromatic light is passing, then there exists a term in the quadratic polarization which is linear in the optical field, but whose magnitude is proportional to the product of the optical and d.c. fields. This modification of the polarization amplitude results in a change in the refractive index of the medium which is proportional to the d.c. field. This is known as the linear electro-optic or Pockel's effect[57,67].

There also exists the possibility of producing sum $(\omega_1 + \omega_2)$[63,68,69] and difference $(\omega_1 - \omega_2)$[70-72] frequencies of the two travelling waves. These will only be efficiently produced if phase matching conditions exist, i.e.[58,64,65]

$$\omega_3 = \omega_1 \pm \omega_2$$

$$k_3 = k_1 \pm k_2$$

where ω_3 and k_3 are the frequency and wavevector of the new wave.

When a photon at the difference frequency $(\omega_1 - \omega_2)$ is generated the laws governing the conservation of energy indicates that the photon of higher frequency ω_1 will be destroyed to produce not only a photon at the 'idler' frequency $(\omega_1 - \omega_2)$ but also an additional photon at a frequency ω_2. This process is known as parametric amplification and has been known for many years in the microwave region, it was first observed[73] in the optical region in 1964 by Peterson and Yariv.

In media with inversion symmetry, the quadratic polarization vanishes[67] and the first nonlinear term in the total polarization is then the cubic polarization $\chi_3 E^3$. Liquids are a particular case where the quadratic polarization vanishes, and thus do not exhibit the Pockel effect.

1.3.2 Cubic Polarization

If we consider the combination of three independent travelling waves in a medium exhibiting a cubic polarization, then the polarization will have components oscillating with frequencies at all possible sum and difference permutations of ω_1, ω_2, ω_3.

One very obvious possibility is that of producing third harmonic generation, which was first observed by Terhune et al[74].

One of the first nonlinear optical effects to be discovered was the quadratic electro-optic or Kerr effect[57], which arises from terms in the polarization similar to

$$\chi_3 A_1 A_2^2 \cos\left[(2\omega_2 + \omega_1)t + (2k_2 + k_1)z\right]$$

where $\omega_2 = k_2 = 0$. If we propagate a monochromatic wave through the medium in the presence of a d.c. field (A_2), then the cubic polarization will lead to a change in the refractive index proportional to the square of the d.c. field.

The Kerr effect is employed in making electronically controllable optical switches[75]. The nonlinear medium is usually an organic liquid, e.g. nitrobenzene. In the absence of a d.c. field the liquid is optically isotropic in the linear regime. When a d.c. field is applied, a preferred direction is introduced and the medium becomes optically uniaxial. The phase difference which occurs between the ordinary and extraordinary waves as they propagate through the medium, may be adjusted by varying the d.c. field so as to rotate the plane of polarization of an incident beam. By employing a polarization analyser such as a sheet of polaroid or a Glan-Thompson prism, an optical shutter can thus be made. The Pockel effect is also often employed in the same manner as the Kerr effect to produce optical switches.

1.3.3 Nonlinear Transitions

In addition to the effects described, there also exists two other very important nonlinear phenomena which arise from nonlinear transitions induced by the high light fluxes created by lasers. The first of these is known as two photon absorption[76], and occurs in materials where there exists no absorption transition for either of two photons with frequencies

ω_1 and ω_2, but where a transition exists at the frequency $\omega_3 = \omega_1 + \omega_2$. Under the influence of sufficiently high light fluxes, the simultaneous absorption of one photon of each frequency has been observed, both in the cases where $\omega_1 = \omega_2$ [76] and where $\omega_1 \neq \omega_2$ [77].

From a quantum mechanical point of view the absorption of the two photons takes place via a virtual stage of the atom. Excitation to this level occurs through the absorption of a photon of frequency ω_1. If a photon of frequency ω_2 then arrives within a sufficiently short time, the absorption of the two photons will result. Three photon absorption has also been reported[78]. From the excited state established by multiphoton absorption, the atomic system decays to an intermediate level, generally by non-radiative processes, and finally radiates a broad fluorescence line.

The phenomenon of two photon absorption has been used successfully in establishing the duration of picosecond pulses from mode-locked lasers[79]. If a high intensity laser pulse is incident on a 50% beam splitter and the resulting two beams travel in opposite directions along the same path in a cell containing a two photon absorption liquid, then enhanced fluorescence will result at the point where the two beams overlap. By photographing the fluorescence track, a record of the pulse shape is obtained. The photograph can be analysed by a microdensitometer to give an indication of the pulse duration. This technique, although extensively used by research workers, has many shortcomings, e.g. the fluorescence trace gives no indication of the pulse shape and the contrast ratio of the peak fluorescence intensity to the background is low (3:1 maximum). A modification of this technique has been employed[80], where three photons are simultaneously absorbed to give information on both the pulse shape and width, also a higher contrast ratio of up to 10:1 is obtained.

The second nonlinear phenomenon arising from the high light fluxes produced by lasers is that of saturated absorbers. It has been shown[7]

that a number of highly absorbant organic dyes can reach a stage during the absorption of laser radiation in which the population of the excited state is equal to that of the ground state, thus effectively making the dyes transparent to laser radiation since no further absorption transitions can take place. Such dyes have been used[7] to switch the 'Q' of laser cavities and thus produce 'giant' laser pulses. A dye which is highly absorbant at the laser frequency is inserted into the laser cavity so limiting the feedback of light into the active medium. If the concentration of the dye is correctly chosen, there will come a point in the evolution of the laser pulse when the dye becomes saturated, and thus appears transparent to the laser light. This saturated state then allows the build up of the pulse to rapidly ensue.

1.4 SPONTANEOUS SCATTERING

In general if a transparent medium has a uniform density, then no light is scattered from it. Where inhomogeneities exist in the density, or more generally the dielectric constant, scattering will occur. One such medium which is inhomogeneous is the atmosphere which appears to have a uniform density, but only when a large volume element is considered. In reality it consists of a vacuum containing a dilute concentration of small particles, i.e. molecules, and thus capable to some extent of scattering any incident light. In 1881, Lord Rayleigh[81] showed that the intensity of light scattered from small particles is inversely proportional to the fourth power of the wavelength λ of the incident light. In this instance small particles are defined as those particles which are small compared to λ. When the particles are larger than λ then no particular wavelength is preferentially scattered. If each particle has a polarizability, α, Rayleigh showed that the scattered intensity I_s varied as:

$$I_s \propto \frac{\rho \alpha^2}{\lambda^4 r^2} (1 + \cos^2\theta)$$

where ρ is the density of particles, r the distance of the observer, and θ the angle through which the light has been scattered.

Rayleigh's analysis was based on a dilute gas of non-interacting particles, and thus clearly invalid in describing scattering from liquids or solids, where molecular interaction takes place.

The scattering from dense media was later developed by Einstein[82] in 1910. In his theory he divided the sample into small volume elements large enough to contain many molecules, but small compared to the wavelength of light. The incident light induces a dipole moment in each volume element which oscillates in sympathy with the electric field of the incident light and becomes the source of scattered radiation. If the induced polarization is constant throughout the medium, the net scattered radiation in all directions but the forward will be zero due to the destructive interference. This will be the case in a homogeneous medium. In real media, however, there will be small random fluctuations in the local dielectric constant and the induced polarization will not be constant throughout the medium. If the fluctuations in a volume element do not influence the fluctuations in a neighbouring volume, then the total scattering intensity is just the sum of the intensities of the dipole radiation from the fluctuating components of the polarization in each volume element. Einstein was able to show that the scattered intensity followed Rayleigh's equation quite closely except that the square of the particle polarizability α^2 must be replaced by $\langle(\Delta\epsilon)^2\rangle$, which is the square of the fluctuation in dielectric constant averaged over the volume elements v.

$$\therefore \frac{I_s}{I_o} = \frac{\pi^2}{r^2\lambda^4} v^2 \langle(\Delta\epsilon)^2\rangle$$

where I_s and I_o are the scattered and incident intensities respectively.

The total spontaneous scattering spectrum is therefore the result of combining a number of different types of fluctuations. The total

fluctuation can be described in terms of statistically independent variables. There are basically four main processes contributing to the spontaneous spectrum; they are the Brillouin doublet, Rayleigh line, Rayleigh wing, and the Raman lines. These arise from the variation in the dielectric constant of a medium caused by fluctuations in the pressure, entropy, anisotropy and molecular polarizability respectively. It can be shown that each of these components has, in general, a scattered intensity profile given by

$$I(\Delta\omega) \propto \frac{1}{\left(1-\frac{\Delta\omega^2}{\Omega^2}\right)^2 + \left(\frac{2\Gamma\Delta\omega}{\Omega^2}\right)^2}$$

where $\Delta\omega$ is the difference in frequency between the incident and scattered light, and Ω and Γ are the frequency shift and width associated with a particular spontaneous scattering process and scattering medium. The inverse of the frequency width Γ is the relaxation time characteristic of each spontaneous scattering process and scattering medium.

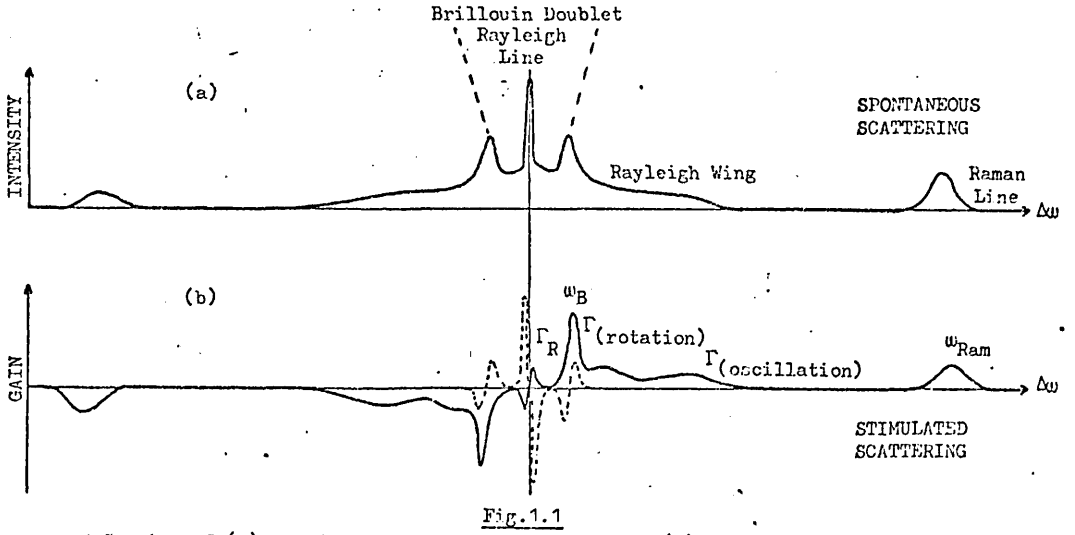

Fig.1.1

Spectra of (a) spontaneous scattering intensity; (b) stimulated scattering gain, as a function of radial frequency shift $\Delta\omega$. The continuous line shows the spectrum of a transparent medium and the dotted line the additional contribution in the presence of absorption. (These spectra must be convolved with that of the laser line to give the experimentally observed spectra.)

The total spontaneous scattering spectrum is displayed in Fig.1.1; the central peaks occur for processes where $\Omega/\Gamma < \sqrt{2}$ and double peaks occur where $\Omega/\Gamma > \sqrt{2}$.

In 1922 Brillouin[28] predicted the existence of a doublet in the spontaneous spectrum by using Debye's[83] method of analysing the fluctuations of a medium into its acoustic modes. He showed that although there exists sound waves of all frequencies propagating in every direction in a medium, scattering of the incident light by the medium in a particular direction will only be significant where the light reflected from consecutive wavefronts is in phase. This is similar to that of the Bragg condition in the diffraction of electrons by crystals.

If we denote the wave-vector of the incident light, scattered light, and acoustic wave by k_L, k_S and k_A respectively, then phase matching is achieved when

$$k_L = k_S + k_A ,$$

which leads to the conclusion that

$$\omega_B = \pm 2n \omega_L \left(\frac{v}{c}\right) \sin\tfrac{1}{2}\theta$$

where ω_L is the frequency of the incident light, v is the velocity of an acoustic wave at the frequency ω_B in a medium of refractive index n, and c is the free space velocity of light.

It can be seen, therefore, that the light scattered from such a medium will be shifted up or down in frequency by a Doppler shift due to the velocity of the acoustic wave. The acoustic wave relaxation time, and hence the frequency width Γ of the Brillouin component are determined by the shear and bulk viscosities of the medium, and is typically of the order of 10^8 Hz.

Experimental confirmation of the existence of the doublet was made by Gross[29] in 1930, and subsequently by many others.

Brillouin's theory predicting the doublet was developed in more detail by Mandelshtam[84] and Landau and Placzek[85], who showed that there also existed a central line in the spontaneous spectrum due to

scattering from non-propagating entropy fluctuations. This central line has come to be known as the Rayleigh line.

The fluctuations in entropy will decay by a thermal process towards an equilibrium state and we therefore expect the Rayleigh line width to be determined by thermal diffusion. In fact the line width Γ_R is:

$$\Gamma_R = D \left[\frac{4\pi n}{\lambda_o} \sin\left(\frac{\theta}{2}\right) \right]^2$$

where D is the thermal diffusivity, n the refractive index of the sample, λ_o the free space wavelength of the incident light and θ the angle through which the light is scattered. For liquids Γ_R is typically 10^7 Hz and thus difficult to measure spectroscopically. Homodyne and heterodyne light beating techniques, which are capable of resolving a few Hz have been developed[86-89] to overcome the problems involved in analysing the fine line widths associated with the Rayleigh line.

In 1928, Raman and Krishnan[90] considered the problem of scattering from anisotropic molecules and showed that there exists a depolarised component of the scattered light. This depolarised light contributes a broad wing to the scattered spectrum, and has a frequency spread which is the inverse of the molecular reorientation time. This phenomena which is now known as the Rayleigh Wing, is caused by a number of different processes all of which produce fluctuations in the anisotropy of the medium.

At present three processes are known to contribute to the total Rayleigh Wing, these are: rotational Brownian motion, angular oscillation of molecules in the local fields of their neighbours, and the change in polarizability of anisotropic media as a result of transverse shear waves. Out of these three processes only the contribution due to the transverse shear waves will propagate in the medium, and thus produce a Doppler shifted doublet. This doublet is diffuse and has a smaller frequency shift than that of the Brillouin peaks, since the velocity of

propagation of transverse waves is less than that of longitudinal waves. The oscillational and rotational processes give rise to the very broad wing centred on the incident frequency, with the high frequency contribution coming mainly from the faster molecular oscillations.

The intensity profiles of the depolarized scattered light due to the three types of fluctuations in the anisotropy are given by [212,216]

$$I_s \propto \frac{1}{\left(1-\frac{I}{4K}\Delta\omega^2\right)^2 + \Delta\omega^2\left(\frac{\varepsilon}{6KT}\right)^2} \qquad \text{Brownian motion}$$

$$I_s \propto \frac{1}{\left(1-\frac{I}{\mu}\Delta\omega^2\right)^2 + \Delta\omega^2\left(\frac{\varepsilon}{\mu}\right)^2} \qquad \text{Oscillations}$$

$$I_s \propto \frac{\rho^2\Delta\omega^2}{\left(1-\frac{\rho\Delta\omega^2}{gk^2}\right)^2 + \Delta\omega^2\left(\frac{\rho}{\varepsilon k^2}\right)^2} + \frac{k^4\varepsilon^2}{1+\Delta\omega^2\frac{\varepsilon^2}{g^2}} \qquad \text{Shear waves}$$

where I_s is the scattered intensity, I the molecular moment of inertia, K is Boltzmann's constant, T the temperature of the medium, ε the viscosity of the medium, $\Delta\omega$ the frequency shift of the scattered light, μ the elastic constant for the oscillations, ρ the density, g the shear modulus of the medium, and k the wavevector of the shear waves.

The three processes described above are interdependent since they all involve a variation in the orientation of anisotropic molecules. Therefore the total Rayleigh wing cannot be calculated by simply adding the three contributions, but the three intensity profiles do give an indication as to the frequency dependence of the separate processes involved. For instance the Brownian motion produces the broad central peak of the Rayleigh Wing, while the molecular oscillations contribute to the extreme wings of the Rayleigh line, and the shear waves produce the diffuse doublet.

The last effect contributing to the spontaneous scattering spectrum was that of the Raman effect[91] which was discovered in 1928. The spectrum of the light scattered by this effect consists of sharp doublets which

are frequency shifted by integral multiples of certain fixed frequencies, characteristic of the medium. The intensity of the up-shifted components is much less than that of the down shifted components.

From a classical physics point of view the Raman effect is described in terms of a change in the polarizability of molecules. Both rotatational and vibrational motion of the molecules will contribute to a change in the molecular polarizability. In the case of rotation, the polarizability may be dependent on the orientation of the molecules with respect to the incident wave, and in the case of vibration, the polarizability may be a function of the intermolecular distance. Therefore from the classical picture the modulation of the polarization $\underline{P}$ of a medium by the rotation and vibration of its molecules will result in scattered light.

Unfortunately the classical view predicts that the up-shifted (anti-Stokes) line and down-shifted (Stokes) line will be of equal intensity, whereas experimental evidence shows that the Stokes lines are far more intense. This discrepancy can be explained satisfactorily by the quantum mechanical theory.

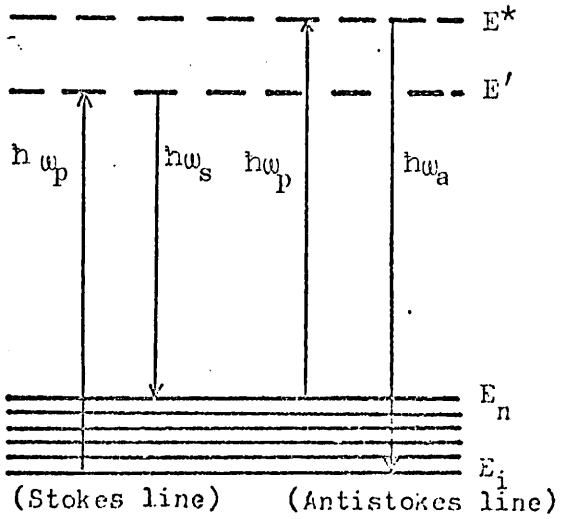

Fig.1.2
Energy level diagram of Raman scattering

The energy levels, Fig.1.2, of a Raman active medium will consist of both discrete rotational and discrete vibrational energy levels. Absorption of a photon by the molecule, will raise the energy of the molecules to $E' = E_i + \hbar\,\omega_p$, where E_i is the initial energy of the molecules, ω_p the radial frequency of the incident photon, and E' the total energy of the molecules. In general this energy E' will not correspond to a stationary state of the system. The molecules will therefore make a virtual transition

to an energy level with energy E', from which it will rapidly decay to a rotational or vibrational level E_n emitting a photon of energy $\hbar\omega_s = \hbar\omega_p - E_n$ (Stokes line). Similarly, if the incoming photon interacted with a molecule in the excited state of energy E_n, then the molecule may return to the ground state with the emission of a photon of higher energy $\hbar\omega_a = \hbar\omega_p + E_n$ (anti-Stokes).

According to the Boltzmann's distribution law, where a medium is in thermal equilibrium, the number of molecules in the ground state will exceed those in an excited state. Therefore the majority of molecules will gain energy from the incident photons, so producing a much more intense Stokes line.

1.5 STIMULATED SCATTERING

When low light levels are used the intensity in the spontaneous Raman line is small, typically of the order of 10^{-6} of the incident intensity. It was accidentally discovered by Woodbury and Ng[92] in 1962, that when the incident light pulse was of very high intensity, a stimulated emission at the frequency of the Raman line existed, having an energy of approximately 20% of that of the incident light and a beam divergence and pulse duration similar to that of the ruby laser pulse used in the experiment.

The process of stimulated Raman scattering can be explained in terms similar to those describing the parametric amplifier[73]. The very weak wave produced by spontaneous Raman scattering beats with the main laser wave at the difference frequency, thus modulating the dielectric constant of the medium.

The coupling between the electromagnetic waves of the incident and scattered light, is achieved via the variation of the nonlinear molecular polarizability. This modulated medium driven at the difference frequency,

which is also the characteristic frequency of the atoms, will interact strongly with the incident light in such a way that the scattered light and atomic excitation is amplified at the expense of the laser beam. During the interaction of the incident light with the Raman active medium, the total energy must be preserved (i.e. conservation of energy), and so a photon at the higher frequency ω_p of the incident light is annihilated to create a photon at the difference frequency of the scattered radiation ω_s and an optical phonon at the difference frequency ω_R,

$$\therefore \qquad \omega_p = \omega_s + \omega_R \quad .$$

It should be noted that stimulated scattering will only exist when a coupling mechanism oscillating at the difference frequency $(\omega_p - \omega_s)$ is established between the two electromagnetic waves and the medium. This scattering will only be of any significance when the difference frequency $(\omega_p - \omega_s)$ approaches a resonance frequency of the medium.

If the above coupling condition is established for each type of spontaneous scattering, then in principal there should exist a corresponding stimulated scattering process, although this may be obscured by competition between different processes. In the steady state regime where the duration of the light pulses are long compared with the characteristic life time $\tau = 2/\Gamma_R$ of the different spontaneous processes, the gain contributed by each process as a function of frequency is of the form:

$$G \propto \frac{2\Gamma \Delta\omega / \Omega^2}{\left(1 - \frac{\Delta\omega^2}{\Omega^2}\right)^2 + \Delta\omega^2 \left(\frac{2\Gamma}{\Omega}\right)^2}$$

where the constants are the same as in the spontaneous scattering equation. The overall gain curve (Denariez and Bret, 1968)[93], shown in Fig.1.1(b), is a sum of such terms.

In 1964, Chiao et al[32] observed stimulated Brillouin scattering. This process can be considered as the simultaneous generation of an

acoustic phonon and a scattered wave from a high intensity incident light pulse, due to nonlinear electrostrictive coupling. Electrostriction is the phenomenon which describes the tendency of a dielectric medium to move into the regions of high electric field.

The year after Chiao's discovery, Mash et al[94] detected stimulated Rayleigh wing scattering in which coupling exists between the electric fields and the medium via molecular orientations.

The last stimulated process to be discovered was that associated with the Rayleigh central line in which coupling between the light wave and the entropy wave of a transparent medium is normally achieved by the very weak electrocaloric effect. Stimulated Rayleigh scattering due to the electrocaloric coupling[57] was first observed by Zailsev[95], although stimulated Rayleigh scattering had previously been detected by Bespalov and Kubarov[96] from concentration fluctuations in a mixture of liquids. In the same year, Herman and Grey[97] suggested using absorbing liquids to enhance the coupling of the light wave to the medium. Under these conditions the stimulated Rayleigh scattering shows a gain for the anti-Stokes line, and also modifies the stimulated Brillouin spectrum. Rank et al[98] observed the stimulated Rayleigh scattering due to absorption in both liquids and gases, and the modification of the stimulated Brillouin scattering spectrum was observed by Pohl[99].

CHAPTER II

DAMAGE PRODUCED IN GLASS BY A C W LASER

2.1 INTRODUCTION

Often the laser has been acclaimed as the answer to many unsolved problems, but one area where it created numerous difficulties was where the power levels used resulted in laser damage either to the optical component or in the active medium. As the development and application of high power lasers progressed, so an inevitable interest was generated in the behaviour of optical materials and coatings under intense illumination.

Up until recently the mass of information published on laser damage and laser damage mechanisms, has never been systematically correlated or usefully directed, and much too much work has been duplicated by different research groups, often with quite different results. To be able to fully analyse, understand and duplicate laser damage, a considerable amount of work needs to be done on quantitatively characterizing the material properties and regulating the laser beam profile.

By the late sixties, it was clear that the advance of high power laser system performance was being impeded by the limitations imposed by material failure. Quite often manufacturers of laser components would have no adequate information on the standard of their optical materials, by which users could specify the power levels at which they expected components to perform without damage. Even to this present day in the U.K. only a handful of optical components have a specification assay.

In response to this situation the American Society for Testing and Materials established a committee in 1969 on lasers and laser materials, who were responsible for formulating standards for laser materials, components and devices. In that same year they held a one-day symposium on damage in laser glass, and every year since 1969 the National Bureau of Standards has held a conference on laser induced damage.

This conference, headed by A.J. Glass and A.H. Guenther, has shown remarkable leadership in being able to affect considerably the direction in which current laser damage work in optical materials has progressed.

Now it appears that a much more coherent and useful effort is being made, not only in the understanding of damage mechanisms, but also in surface preparation and material characterization. In the design of large laser fusion programmes, financial considerations impose severe restrictions on system design. The improvement in the understanding of damage mechanisms and surface preparations has made it possible to design systems with an optimised damage threshold. Correspondingly in CW systems, the understanding of thermally induced distortions, and the availability of reliable material parameters, makes it possible to design such systems to operate safely within the limits imposed by thermal distortions.

Laser instrumentation very often incorporates components that involve transparent substrates, coated with thin metallic or dielectric films. Damage to such films is itself a serious problem which has been the subject of considerable investigation. Even more serious, however, is damage to the substrate material, which in the presence of an absorbing film, may occur at intensities very much less than those required to damage the uncoated material. In the following sections of this chapter, a series of experiments is reported on the comprehensive investigation of the damage caused to a glass surface bearing a gold film which was illuminated by a continuous argon ion laser. Damage to the substrate surface has been observed for power levels as low as 0.1 W and for intensities of less than 5 KW cm^{-2}.

2.2 EXPERIMENTAL DETAILS OF LASER DAMAGE STUDY

In the study of laser damage produced to transparent substrates coated with thin films, a Coherent Radiation 52B continuous argon ion laser was used. A power meter incorporated in the design of the laser ensured a system noise of less than 0.1% (1 sec to 10 hours). During the entire experiment the laser was operated at 5145 Å since this line exhibited the strongest output.

The output from the laser occurred in a single TEM_{oo} transverse mode, and had a divergence of 1 mrad measured at the $1/e^2$ points, and a maximum power output of 3 W. The initial beam diameter at the $1/e^2$ point was 1.4 mm.

The majority of the substrates used in the experiment were microscope slides, which are commercially produced by the tin floatation method and therefore had an optical flatness of better than $\lambda/40$. These substrates were coated with gold films evaporated from an electrically heated molybdenum dish in a vacuum chamber at approximately 10^{-6} torr. Film thicknesses were measured interferometrically.

The light output from the laser was focused in air onto the surface of the glass microscope slides bearing a thin film of gold. The duration of the illumination was determined by a conventional mechanical shutter, while the use of lenses of 5, 10, 25 cm focal length gave focal spots of 0.05, 0.1 and 0.25 mm respectively. (Throughout this chapter the diameter of an illuminated area will refer to the diameter of that region within which the light intensity was greater than $1/e^2$ times the intensity at the centre of the area.)

To test whether the presence of air had any effect on the results, the films were grown and left in vacuum until after they had been illuminated by the argon ion laser. In addition the laser beam was focused on

to the glass substrate during the actual deposition of the gold film, to see whether inhibition of condensation occurs under these conditions. A diagram of this arrangement is shown in Fig.2.1. It was necessary for this part of the experiment to have the glass microscope slide inclined at an angle in order that it could simultaneously be illuminated by the laser and coated with gold.

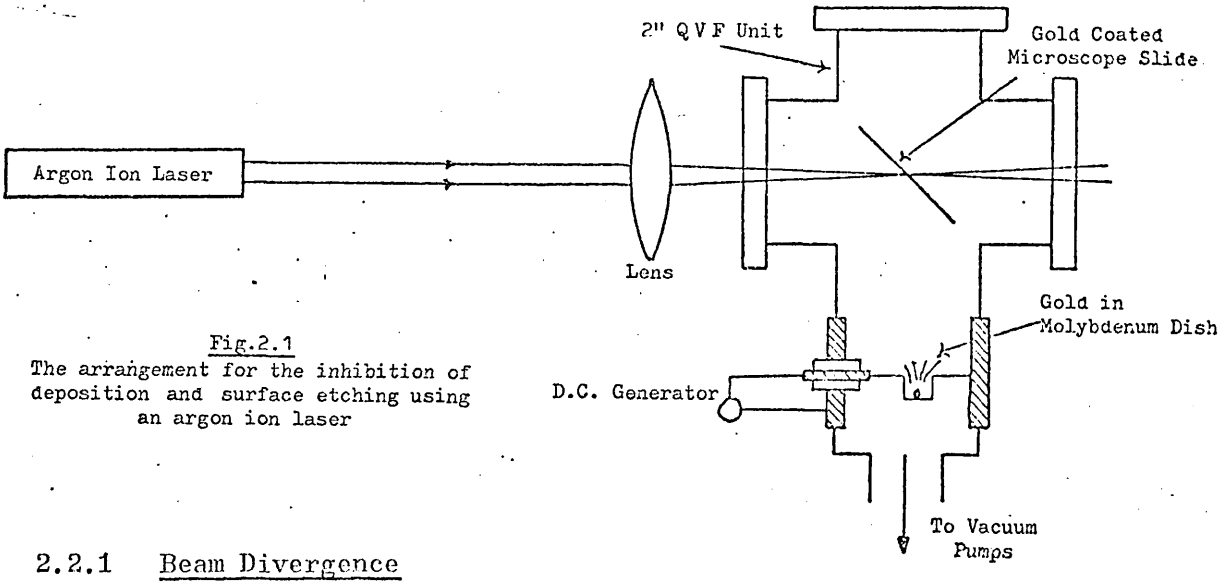

Fig.2.1
The arrangement for the inhibition of deposition and surface etching using an argon ion laser

2.2.1 Beam Divergence

To determine the diameter d of the spot at the focus of a lens with a focal length f, an estimate of the beam divergence θ is required since d is approximately given by the relationship:

$$d = f\theta .$$

The beam width a of the laser at the $1/e^2$ points, was determined by scanning a razor blade edge through the beam and thereby progressively blocking the beam and reducing the power incident on a power meter behind the scanning edge. The position along the scan direction x and power P transmitted past the edge was recorded. The total incident power P_0 was also recorded.

Now, for a Gaussian beam

$$I = I_0 \, e^{-2r^2/a^2} ,$$

and the ratio P/P_0 is given by:

$$\frac{P}{P_o} = \frac{1}{\sqrt{2\pi}} \int_{-\infty}^{\gamma} e^{-z^2/2}\, dz \qquad \ldots (2.1)$$

where $\gamma = \dfrac{2(x - x_o)}{a}$ and x_o is the position of the intensity maximum. P/P_o is determined at each value of x and consequently the left-hand side of the equation is known. The tables of the normal distribution function provides values for the integral on the right-hand side of equation (2.1), and thus the values of γ are determined. Since

$$x = \frac{a}{2}\gamma + x_o ,$$

a plot of x versus γ will yield a straight line whose slope is $a/2$.

Using this procedure a beam divergence of 1.00 ± 0.07 mrads was measured.

2.3 DAMAGE ANALYSIS TECHNIQUES

The damage produced to the substrate surfaces was analysed using two interferometric techniques and from direct observations through an optical microscope.

2.3.1 Two Beam Interferometric Analysis

This technique employs an adapted Michelson interferometer for the study of the microtopography of the substrate surfaces.

The substrate surface is placed so that it forms the mirror of one arm of a Michelson interferometer and lies in the focal plane of a microscope receiving the light from the interferometer. The instrument was illuminated by a sodium lamp, so adjacent fringes indicate a difference in surface height of 2945 Å.

The apparatus used, as shown in Fig.2.2, was a Watson interference objective which has a magnification of 100 and fits onto almost any microscope having a standard thread. The objective has a focal length of 16 mm

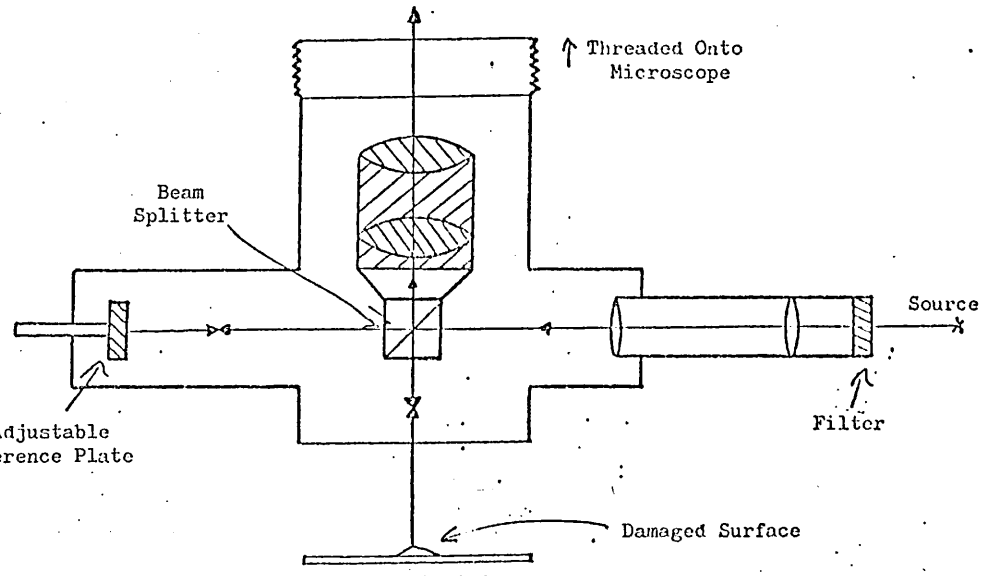

Fig.2.2
The arrangement of the Michelson type interference objective

and a numerical aperture equal to 0.2, giving a lateral resolution of about 1.5 μ, the overall field of view was 1.3 mm diameter.

In obtaining the interferograms of Figs.2.6-2.8, the undisturbed surface bearing the gold film was set perpendicular to the interferometer axis, so that the fringes in these pictures indicate the contours of the surface deformation. The interferograms of Figs.2.9,2.10, however, were obtained by setting the glass slide in such a position that the normal to the undisturbed surface made a small angle to the axis of the instrument. This technique, which shows up the relief rather than the contours of the damaged area, was necessary to illustrate unambiguously the complex structure of the surface deformations shown in Figs.2.9 and 2.10.

Where the surface discontinuities were several wavelengths high the monochromatic light source produced adjacent fringes which were several orders apart, with no way of identifying which fringe was zeroth order, i.e. which corresponds to no path difference. Therefore a white light fringe system was used in which the sodium lamp had been replaced by a white light source. With white light fringes the central fringe can be easily distinguished from all others and a graticule eye piece can be used to note the displacement of the central white fringe.

To obtain maximum fringe visibility from the arrangement, the specimen reflectivity needs to be equal to the reflectivity of the reference mirror, which was approximately 50%. To obtain a reasonable visibility the gold films were left on the substrates, but in the case where only the substrate surface was of interest then the gold film was removed by aqua regia, and the substrates subsequently coated in vacuum with a 50% reflecting film of silver (100 Å) .

2.3.2 Multiple Beam Interferometric Analysis

This interferometric technique used for the study of surface microtopography, employs more than the conventional two beams, and so heightens the sensitivity and accuracy of the resulting interferogram by reducing the fringe width in much the same way as fringe widths are reduced from diffraction gratings by employing more slits.

The surface to be studied is cleaned by the normal techniques and coated with a silver film of approximately 500 Å at which the reflectivity has nearly reached its maximum value, and beyond which there is a rapid increase in absorption with reduced transmission and very little gain in reflectivity. Similarly a reference plate is coated with silver and the two silvered surfaces are mounted close together. The surfaces are then illuminated at normal incidence with a parallel beam using monochromatic light and a set of interference fringes form from the interference of reflected beams between the two silvered surfaces. Each neighbouring fringe corresponds to a change in separation between the two silvered plates of $\lambda/2$. If, therefore, one of the plates is flat and the other has some surface structure, the resulting fringes produce a contour map of the surface. During the experiment the surfaces were illuminated with a mercury lamp and a Kodak Wratten 77A filter was used to select the mercury green line at 5460 Å. This resulted in adjacent fringes representing a change in height of 2730 Å.

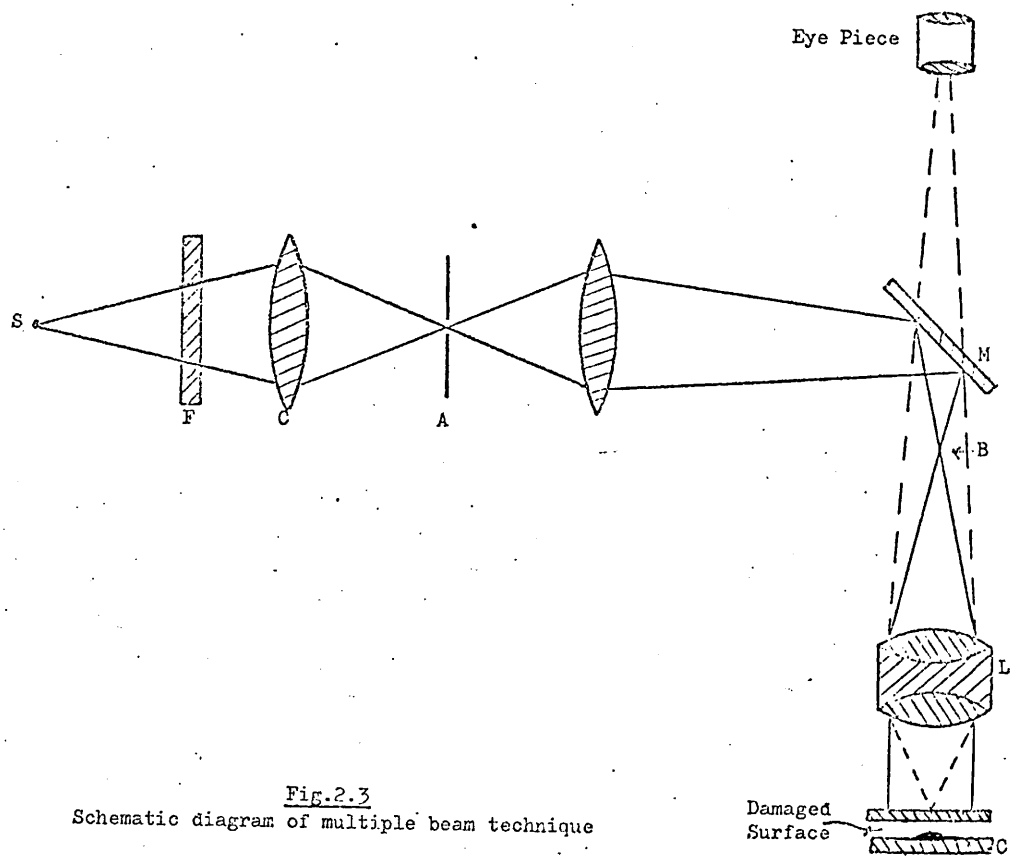

Fig.2.3
Schematic diagram of multiple beam technique

A schematic diagram of the apparatus is shown in Fig.2.3. A source S is used from which a single line is selected by a filter F. The source is imaged by a condenser C onto a slit at A. A glass reflector M then throws an image of A at B and an objective lens L is used to produce a parallel beam incident on to the two silvered surfaces at C, between which the multiple reflections take place. The distance L C is adjusted to give the correct microscope setting to produce an image of C in the eyepiece. The damaged surface under study is represented by the lower of the two plates at C, with its damaged surface facing upwards.

2.4 THEORETICAL CONSIDERATIONS

The model which will be adopted to predict the extent of the damage to the glass substrate, is one of a semi-infinite transparant solid with a thin absorbing layer on the surface.

The temperature of the solid due to a laser beam having a Gaussian spatial profile impinging at normal incidence on the absorbing layer, will

be calculated by solving the equation for the conduction of heat:

$$\nabla^2 T(r,\theta,z,t) - \frac{1}{K} \frac{\partial T}{\partial t}(r,\theta,z,t) = - A(r,\theta,z,t)/K \; . \quad \ldots \; (2.2)$$

The results for the case of a semi-infinite solid are applicable to solids of finite thickness L if $L^2/4Kt \gg 1$, where t is the time of interest. In addition we need to assume that the thermal properties of the absorbing material are independent of temperature, and that the energy lost through the process of re-radiation or convection is negligible.

The solution of equation (2.2) in its present form is rather cumbersome. The same problem can be solved more easily from an indirect approach if we take the solution of equation (2.2) for an instantaneous point source and integrate it with respect to space and time.

If we consider an instantaneous point source of strength Q incident at the point (r',θ') at time $t=0$ and on the plane defined by $z=0$, then equation (2.2) is satisfied by

$$T_1 = \frac{Q}{4(\pi K t)^{\frac{3}{2}}} e^{-(r^2 + r'^2 - 2rr'\cos(\theta - \theta') + z^2)/4Kt} .$$

As $t \to 0$ this expression tends to zero at all points except $(r',\theta',z=0)$ where T_1 becomes infinite. Also the total quantity of heat in the infinite region can be shown to be $Q \rho_o c_p$ where ρ_o is the density and c_p the specific heat at constant pressure.

Let us consider that the incident energy has a spatial extent which has a Gaussian form, i.e.

$$E = E_o \, e^{-(2r^2/a^2)}$$

where E_o is the energy liberated per unit area at the origin, and a is the radius of the area within which the energy is greater than $1/e^2$ times the energy at the centre of the area.

Therefore the temperature $T_2(r,z,t)$ due to an instantaneous Gaussian distribution of heat is:

$$T_2(r,z,t) = \int_0^{\infty} \int_0^{2\pi} e^{-2r'^2/a^2}\, T_1 r'\, d\theta'\, dr'$$

Substituting for T_1 we get

$$T_2(r,z,t) = \frac{E_o}{4\rho_o c_p (\pi K t)^{\frac{3}{2}}} \int_0^{\infty} \int_0^{2\pi} r'\, e^{-2r'^2/a^2} \exp\left[-\frac{(r^2+r'^2+z^2)}{4Kt}\right] e^{rr'\frac{\cos\theta'}{2Kt}}\, dr'd\theta'$$

By expanding the term $e^{rr'\cos\theta'/2Kt}$ and integrating with the help of the reduction formula

$$n\int \cos^n\theta' d\theta' = \cos^{n-1}\theta' \sin\theta' + (n-1)\int \cos^{n-2}\theta' d\theta'$$

we get

$$\frac{1}{2\pi}\int_0^{2\pi} e^{rr'\cos\theta'/2Kt}\, d\theta' = \sum_{n=o}^{\infty} \frac{\alpha^{2n}}{2^{2n}(n!)^2}$$

where $\alpha = \frac{rr'}{2Kt}$. This series is the modified Bessel function of the zeroth order, and shall be denoted by $I_o\left(\frac{rr'}{2Kt}\right)$

$$\therefore \quad T_2 = \frac{E_o}{2\rho_o c_p (\pi K^3 t^3)^{\frac{1}{2}}} \int_0^{\infty} r' e^{-2r'^2/a^2} \exp\left[-\frac{(r^2+r'^2+z^2)}{4Kt}\right] I_o\left(\frac{rr'}{2Kt}\right) dr' \qquad \ldots (2.3)$$

This integral may be evaluated by using the result of a special Laplace transform, i.e.

$$\frac{1}{p} e^{\alpha/p} = \int_0^{\infty} e^{-pt} I_o(2\sqrt{t\alpha})\, dt .$$

If we let $t = u^2$, then $dt = 2u\, du$. Hence

$$\frac{1}{2p} e^{\alpha/p} = \int_0^{\infty} u\, e^{-pu^2} I_o(2u\sqrt{\alpha})\, du \qquad \ldots (2.4)$$

From equations (2.3) and (2.4) it follows that

$$T_2(r,z,t) = \frac{E_o a^2}{\rho_o c_p (\pi K t)^{\frac{1}{2}}(8Kt + a^2)} \exp\left[-\frac{z^2}{4Kt} - \frac{2r^2}{8Kt + a^2}\right]$$

For a laser source that has a duration in time, the temperature at time t and position (r,z) is obtained by convolving T_2 with $\alpha F(t)$, where $F(t)$ describes the intensity of the light at time t incident on the surface and α is the fraction of light absorbed:

$$\therefore T(r,z,t) = \frac{a^2\alpha}{\rho_o c_p (\pi K)^{\frac{1}{2}}} \int_o^t \frac{F(t-t')}{t'^{\frac{1}{2}}[8Kt'+a^2]} \exp\left[-\frac{z^2}{4Kt'} - \frac{2r^2}{8Kt+a^2}\right] dt' \quad \ldots (2.5)$$

Thus equation (2.5) describes the temperature at a position (r,z) and time t due to a laser pulse defined by

$$F_1(r,t) = F(t)\ e^{-2r^2/a^2}$$

impinging at normal incidence on a semi-infinite solid which has an absorbant layer at $z = 0$.

2.4.1 Surface Temperature due to Heating by a Continuous Laser

Let us consider the case of a continuous laser with a Gaussian spatial profile incident on the surface of a semi-infinite solid with an infinitesimally thin absorbing layer on the surface. Then the temperature on the surface can be determined from equation (2.5) by putting $z = 0$ and integrating from $0 \rightarrow \infty$

$$\therefore \quad T(r) = \frac{a^2\alpha F_o}{\rho_o c_p (\pi K)^{\frac{1}{2}}} \int_o^\infty \frac{\exp[-2r^2/(8Kt+a^2)]}{t^{\frac{1}{2}}[8Kt+a^2]} dt \quad \ldots (2.6)$$

where F_o is the constant flux density at the centre of the Gaussian laser profile.

Equation (2.6) can be solved in the following manner. Let

$$\frac{1}{x^2} = (8Kt+a^2)$$

$$\therefore \quad -\frac{2}{x^3} dx = 8K\,dt\ .$$

Substituting into (2.6) we get

$$T(r) = \frac{2a^2\alpha F_o}{\rho_o c_p (8\pi)^{\frac{1}{2}} K} \int_o^{1/a} \frac{e^{-2r^2x^2}}{(1-x^2a^2)} dx$$

Now let $ax = \cos\theta$

$$a\,dx = -\sin\theta\, d\theta$$

$$\therefore \quad T(r) = \frac{2a\alpha F_o}{\rho_o c_p (8\pi)^{\frac{1}{2}} K} \int_o^{\pi/2} e^{-2r^2/a^2 . \cos^2\theta}\, d\theta$$

Put $2\theta = \varphi$ to give

$$T(r) = \frac{a\alpha F_o}{\rho_o c_p (8\pi)^{\frac{1}{2}} k} \cdot e^{-r^2/a^2} \int_o^{\pi} e^{-r^2/a^2 . \cos\varphi} \, d\varphi$$

or

$$T(r) = \frac{a\alpha F_o \sqrt{\pi}}{2\sqrt{2}\,k} \cdot e^{-r^2/a^2} \, I_o\left(\frac{r^2}{a^2}\right) \qquad \ldots (2.7)$$

where

$$I_o(x) = \frac{1}{\pi} \int_o^{\pi} e^{-x\cos\varphi} \, d\varphi$$

is the modified Bessel function of order zero.

The total power incident on the focal spot is given by

$$P = \int_o^{\infty} 2\pi r F \, dr$$

where

$$F = F_o \, e^{-2r^2/a^2}$$

$$\therefore \quad F_o = 2P/\pi a^2 \, .$$

Substituting this into equation (2.7) we finally get

$$T(r) = \frac{\alpha P}{a\sqrt{2\pi}k} \cdot e^{-r^2/a^2} \, I_o\left(\frac{r^2}{a^2}\right) . \qquad \ldots (2.8)$$

The temperature indicated by equation (2.8) is not achieved instantaneously but is approached asymptotically over a period comparable to τ, where

$$\tau = \frac{a^2 \rho_o c_p}{8k} \qquad \ldots (2.9)$$

Equation (2.8) is displayed in a graphical form in Fig. 2.4, in which the normalised temperature is depicted versus the distance from the centre of the incident Gaussian profile in dimensionless units of r/a.

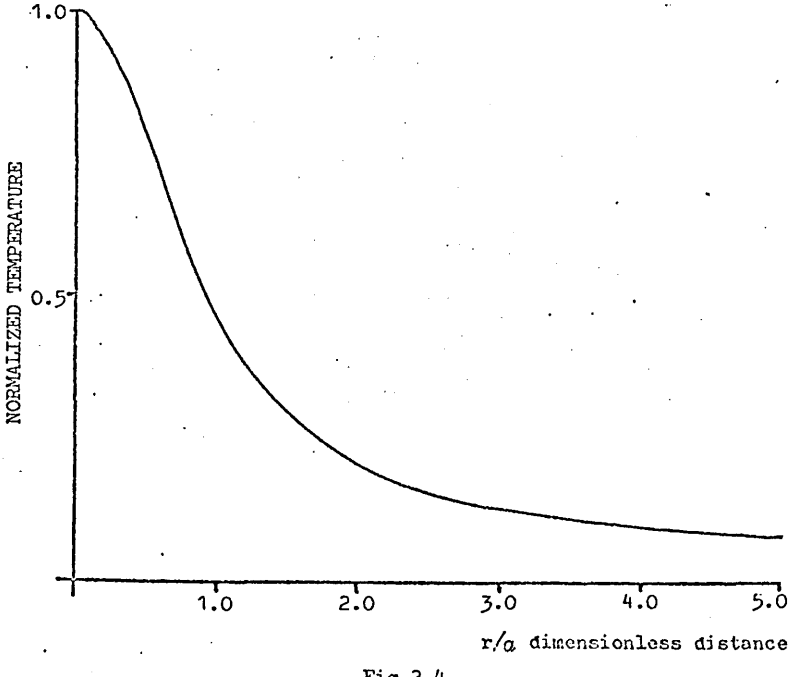

Fig.2.4
The radial temperature on the surface of a semi-infinite slab which is irradiated by a continuous laser beam

2.4.2 Re-radiation from the Surface

In the analysis presented the assumption has been made that the energy lost from the surface through radiation is negligible. However, if the pulse is on for a long time, heat can be conducted over a large area. Thus a large area contributes to re-radiation and, even though the power per unit area may be small, the total power radiated may approach the power absorbed. An approximate estimate of the percentage of power re-radiated can be made by calculating the temperature profile on the surface as a function of position, and then numerically integrating the thermal re-radiation from the surface using the calculated temperature profile and Stefan's law.

The surface temperature due to heating by a continuous laser with a Gaussian profile is given by equation (2.8). Therefore applying Stefan's law to this result we obtain:

$$P_R = \sigma\left[\frac{\alpha P}{a\sqrt{2\pi k}}\right]^4 2\pi \int_0^\infty r\, e^{-4r^2/a^2}\, I_0^4\left(\frac{r^2}{a^2}\right) dr \qquad \ldots (2.10)$$

where σ is Stefan's constant and P_R is the power radiated from the surface.

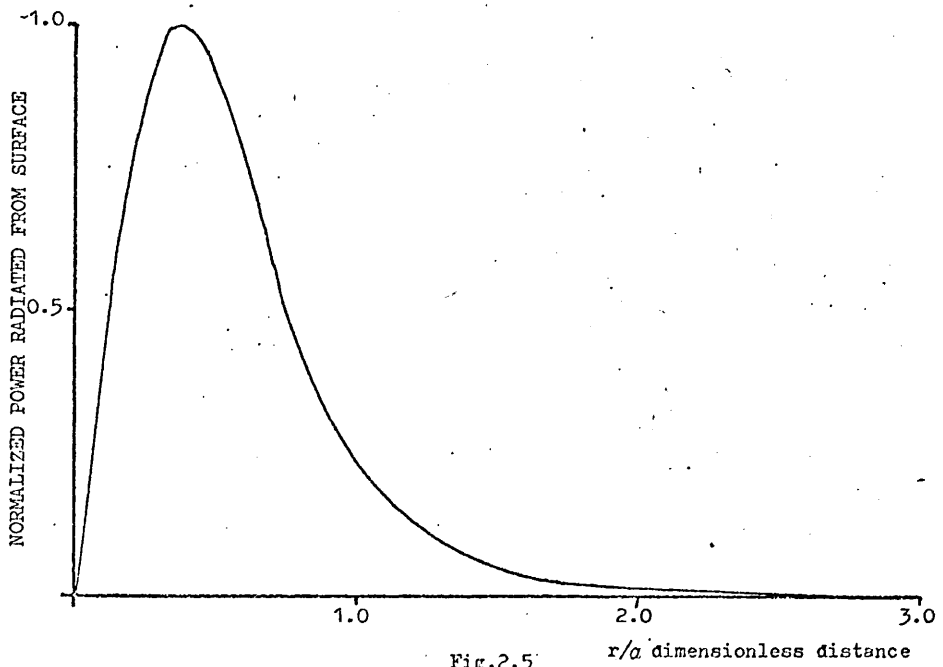

Fig.2.5
Normalized power radiated from an annular surface $2\pi r\, dr/a^2$

The function

$$f(r/a) = \frac{r}{a}\, e^{-4r^2/a^2}\, I_0^4\left(\frac{r^2}{a^2}\right)$$

is displayed in Fig.2.5. By estimating the area under this curve an approximate value for P_R can be obtained.

2.5 DAMAGE CAUSED UNDER VARIOUS CONDITIONS OF LASER ILLUMINATION

Figures 2.6-2.8 show two-beam interferograms of the damage caused to the surface of a glass microscope slide bearing a 200 Å gold film, by focusing laser beams of the indicated powers and durations to spots with diameters of 0.05, 0.1 and 0.25 mm respectively. Further interferometric tests showed that, in every case, the illuminated region had been raised above the level of the undisturbed surface. The surface distortion caused is clearly very large, rising to a height of 2 μm above the surrounding region in the case of the 3 W, 100 s, 0.25 mm focal spot. The minimum power indicated in each figure is the threshold power below which no surface damage could be readily detected.

From the dimensions of the damaged areas in Figs.2.6-2.8, and equation (2.8) a temperature T_T of 1160°C is indicated for the occurrence of laser damage with a r m s error of 60°C. (Here the occurrence of laser damage was defined by the surface being raised by $\lambda/2$, i.e. 2945 Å. This is indicated by the outer dark rings on the interferograms of Figs.2.6-2.8.)

The value of T_T was calculated for each beam diameter from the dimensions of the damaged areas where the lowest power levels had been used. If the other interferograms were used, Figs.2.9, 2.10, then the calculated value of T_T showed a dramatic increase from 2000°C → 5400°C as the incident power level was increased. This indicated that possibly one of two things or both were happening. Either the surface was re-radiating a significant percentage of the absorbed power due to the high

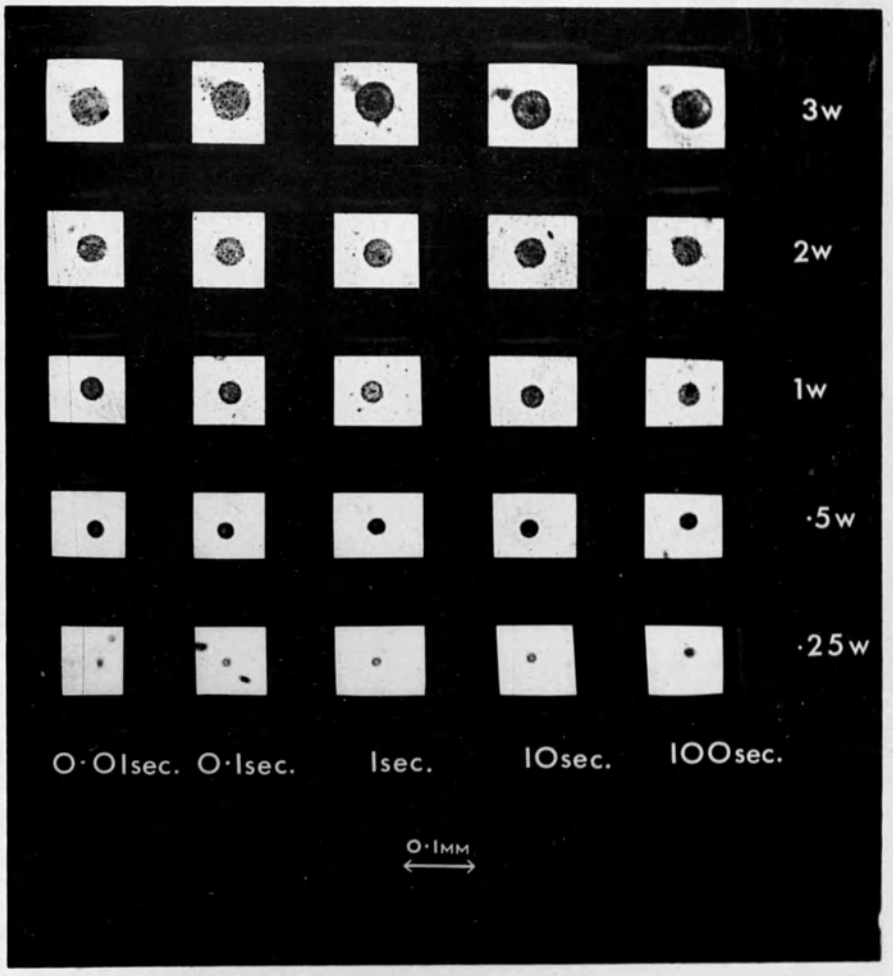

Fig.2.6

Interferograms of the deformation caused to a glass surface bearing a 200 Å gold film by laser illumination of the indicated power and duration. The laser beam of 1 mrad divergence was focused on to the surface by a lens of focal length 5 cm

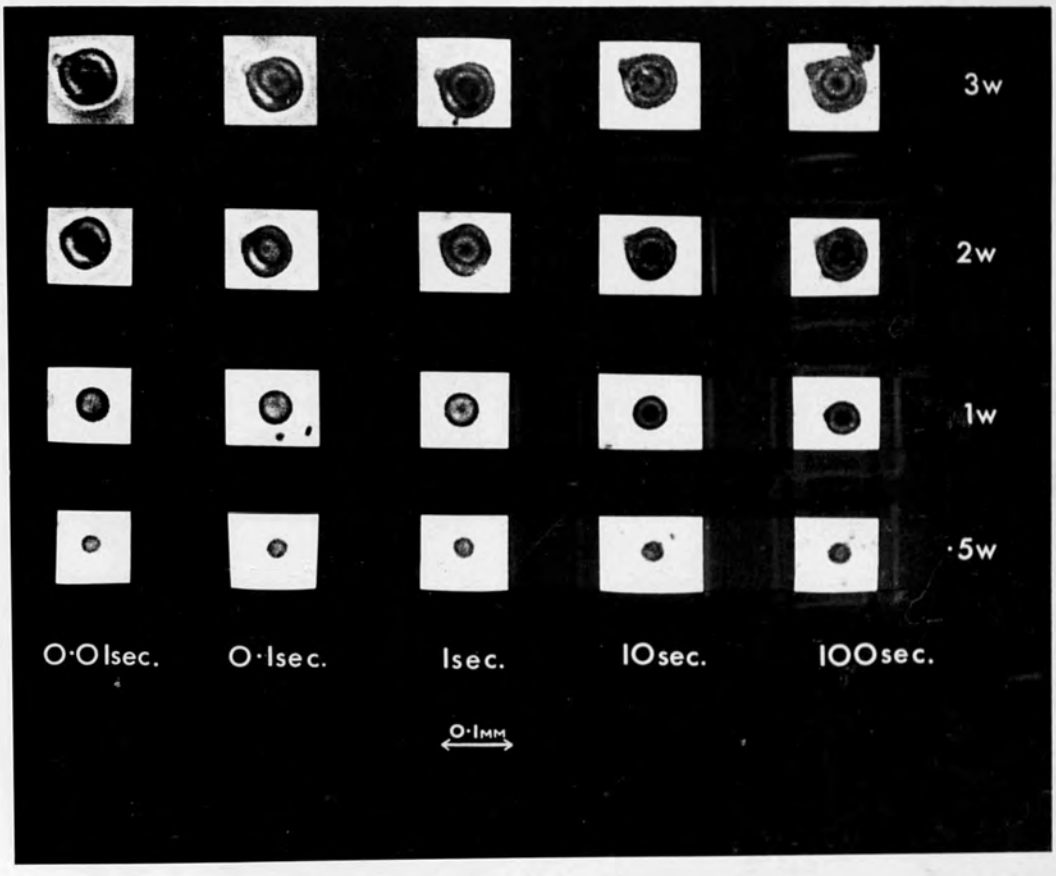

Fig.2.7

Interferograms of the deformation caused to a glass surface bearing a 200 Å gold film by laser illumination of the indicated power and duration. The laser beam of 1 mrad divergence was focused on to the surface by a lens of focal length 10 cm

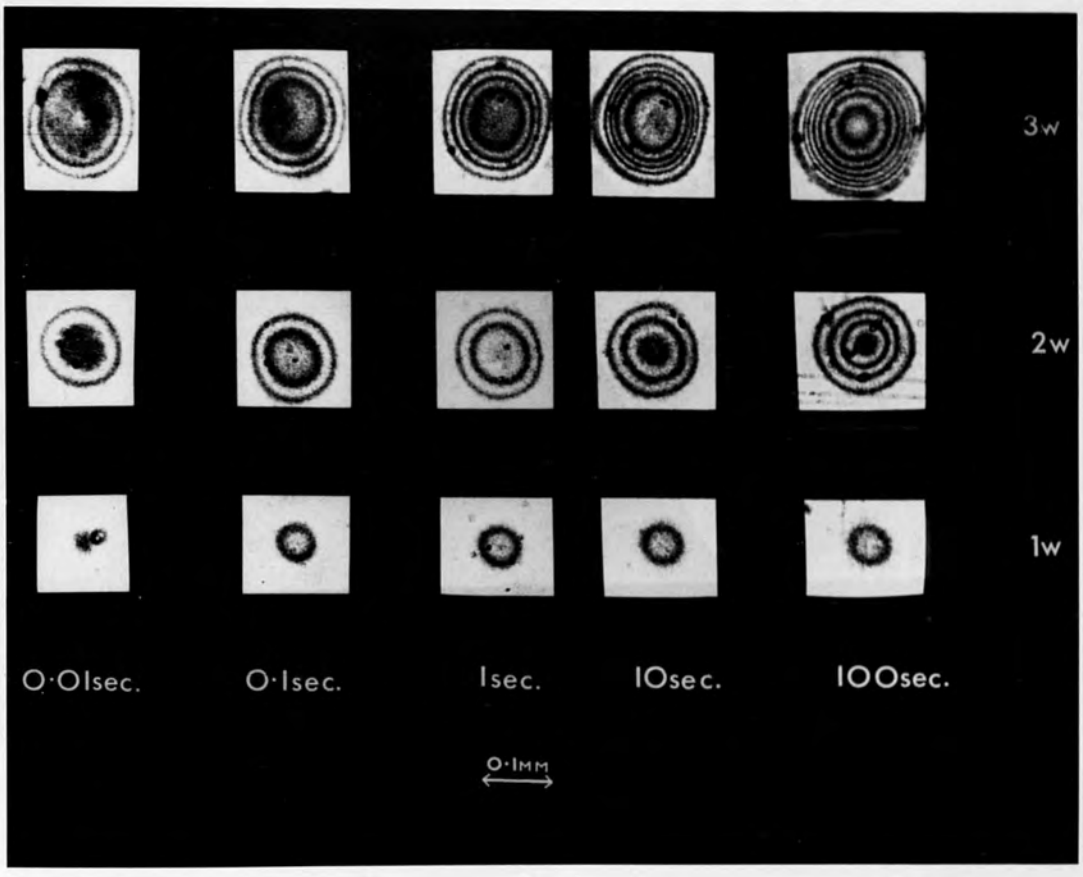

Fig.2.8

Interferograms of the deformation caused to a glass surface bearing a 200 Å gold film by laser illumination of the indicated power and duration. The laser beam of 1 mrad divergence was focused on to the surface by a lens of focal length 25 cm

surface temperatures, or removal of the metallic film was occurring, either by vapourization or flow of liquid gold under gravity, thus reducing the absorption of the laser beam by the surface and therefore limiting the final temperature attained by the surface.

Equation (2.10) and Fig.2.5 indicate that the total power radiated from the surface of the heated slab can vary from 5% of the total absorbed power for the 1W beam focused to a diameter of 0.125mm, to 100% for the 3W beam focused to the same diameter. Although these figures are large they are unlikely to be the only effect contributing to the large variation of T_T.

From observations of the damaged areas it is seen that removal of the gold film occurred for regions where the temperature exceeded approximately 1200°C and in every case a reddish deposit was left. Due to the extensive damage on the surface, and thus the resultant scattering, no value could be placed on the absorption coefficient of the reddish deposit. Since the temperature on the surface is proportional to the absorption coefficient of the surface, the removal of the gold film must therefore modify significantly the resulting temperatures indicated by equation (2.8) for all cases where the temperature has exceeded 1200°C. In establishing the threshold temperature for the occurrence of laser damage, only the results for the focused beams of the lower powers can therefore have any validity.

One very noticeable fact emerging from this damage study is that for the same power level the area damaged by the laser beam increased markedly with an increase in spot diameter.

Equation (2.9) indicates that the time τ during which thermal equilibrium was achieved is comparable to 0.04s, 0.01s and 0.002s, respectively for the cases where the beam was 0.25, 0.1 and 0.05mm diameter. The interferograms show, however, that while all the damaged

regions appeared within 0.01 s , none had reached complete equilibrium within this time. The damage produced by the 5 and 10 cm lenses had, however, reached the maximum width within 0.01 s . Deformation caused by the 0.25 mm spots, continued to grow for more than 10 s , starting as tabular regions with flat tops and steeper sides, but becoming much higher and more rounded with increasing illumination time.

2.6 LASER DAMAGE CAUSED TO GLASS SURFACES BEARING GOLD FILM OF VARIOUS THICKNESSES

The nature of the damage to the glass surface was found to be strongly dependent on the thickness of the gold film. Interferograms showing the distortion caused to surfaces bearing films of (a) 200 Å and (b) 1000 Å are shown in Figs.2.9 and 2.10.

The damage caused to the surface bearing the 200 Å film consisted of a raised region. This region was somewhat depressed in the centre when illuminated for a short period, but became distinctly domed when the illumination was of longer duration. When the damaged area was examined with a transmission microscope, it could be seen that the gold film had been removed from the raised region, leaving a layer of reddish material. This layer, which was of about the same thickness as the original film, was very soft and could easily be scratched off or dissolved in aqua regia. This reddish material was formed even when the surface was illuminated in vacuo.

The surface bearing the 1000 Å film was hardly affected by the focal spots of 0.05 mm diameter, whatever the intensity or duration of the illumination. The gold film was entirely removed from the illuminated region, leaving no red deposit, but the only disturbance caused to the surface of the glass was a slight ridge at the boundary of that region. A much higher ridge was generated at the edge of those regions from which the gold had been removed by light focused to a spot of 0.25 mm diameter.

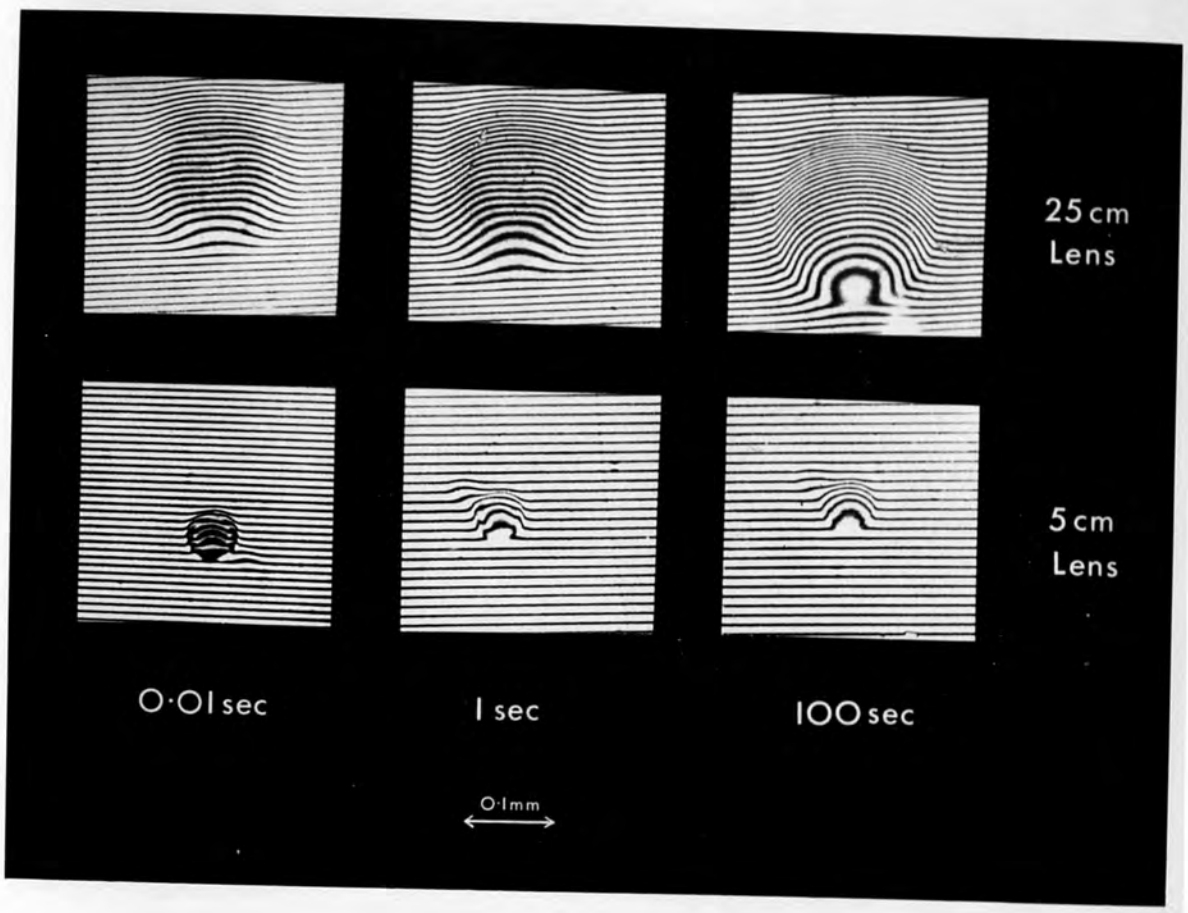

Fig.2.9
Interferograms of the deformation caused by using lenses of the indicated focal length to focus a 3W laser beam on to a glass surface bearing a 200Å gold film for periods of the indicated duration

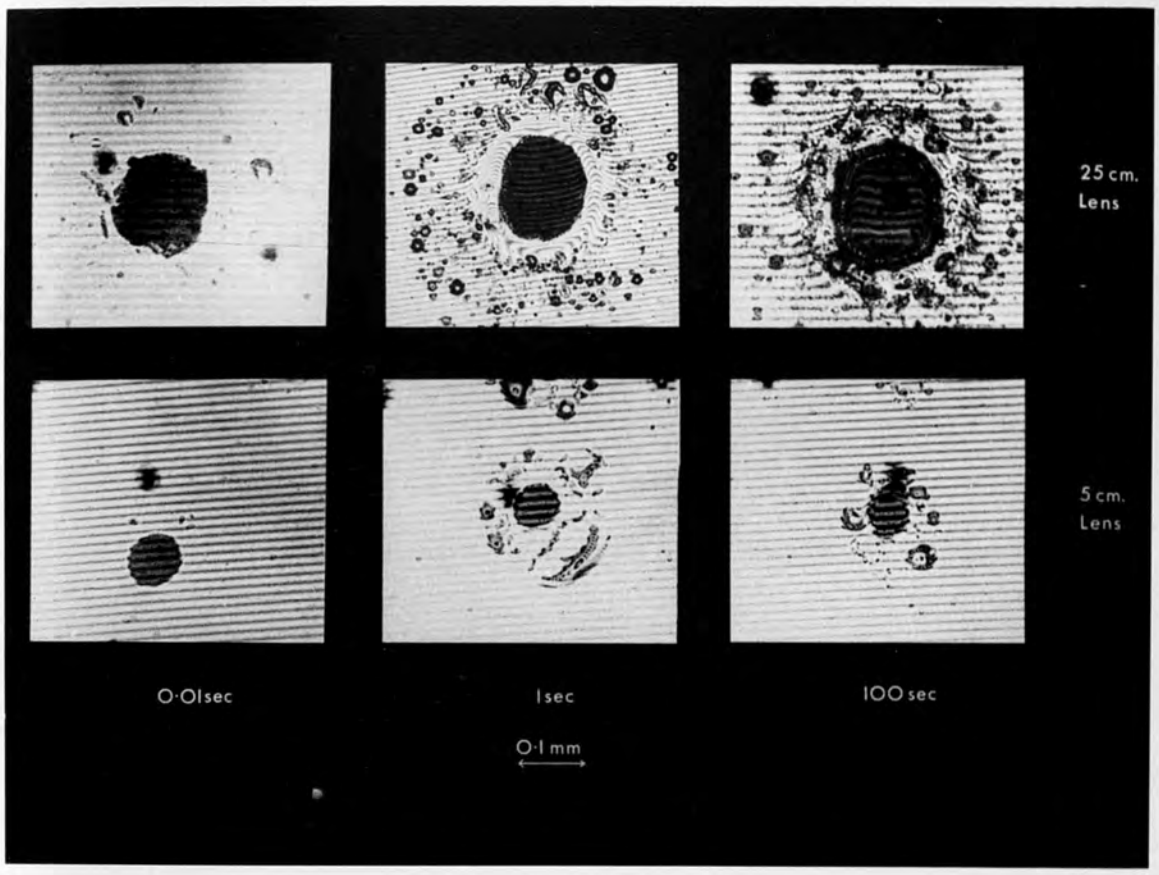

Fig.2.10

Interferograms of the deformation caused by using lenses of the indicated focal length to focus a 2 W laser beam on to a glass surface bearing a 1000 Å gold film, for periods of the indicated duration

In this case the boundary was raised to a height of up to 2 μm ; though the surface in the central region was again left undisturbed (except for a 'moat' developed just inside the boundary ridge). This type of damage took from 10 to 100 s to develop fully, and was so severe it could be examined not only interferometrically but also by direct photography, (Fig.2.11).

It is possible that the reason why little damage occurred to the 1000 Å film was that the thicker film conducted heat away faster from the illuminated region. (Gold has a thermal conductivity 350 times that of glass, while the absorption of the gold film has only increased by 30% in going from the 200 Å to the 1000 Å gold film).

The diameters of the damaged regions again suggest a threshold temperature for surface damage of about 1160°C, while total removal of the gold without surface damage appears to have occurred for regions where the temperature exceeded about 1200°C. This process, however, only occurred in the case of the thicker film, although equation (2.8) indicates that the temperature of the 200 Å film at the centre of the 3 W spot of 0.25 mm diameter would have approached 4 000°C had the film not been destroyed.

2.7 SURFACE DAMAGE DURING INHIBITION OF DEPOSITION

When the laser was focused onto the glass surface during the actual deposition of the gold film[107], very extensive damage could be caused. Fig.2.12 shows a reflection multiple beam interferogram of the damage caused to the glass surface by a 2 W laser beam focused to a spot of 0.1 mm diameter for a period of 1 min, during which time a gold film 500 Å thick was deposited on the surface. Each fringe represents a change in height of 2730 Å.

The interferogram shows that the damaged region has a domed surface, the centre of which has risen about 6 μm above the surrounding area. When

Fig.2.11
Direct photograph of the damage caused to a glass surface bearing a gold film, by using a lens of 25 cm focal length to focus a 2 W laser beam on to the surface for a period of 1 sec

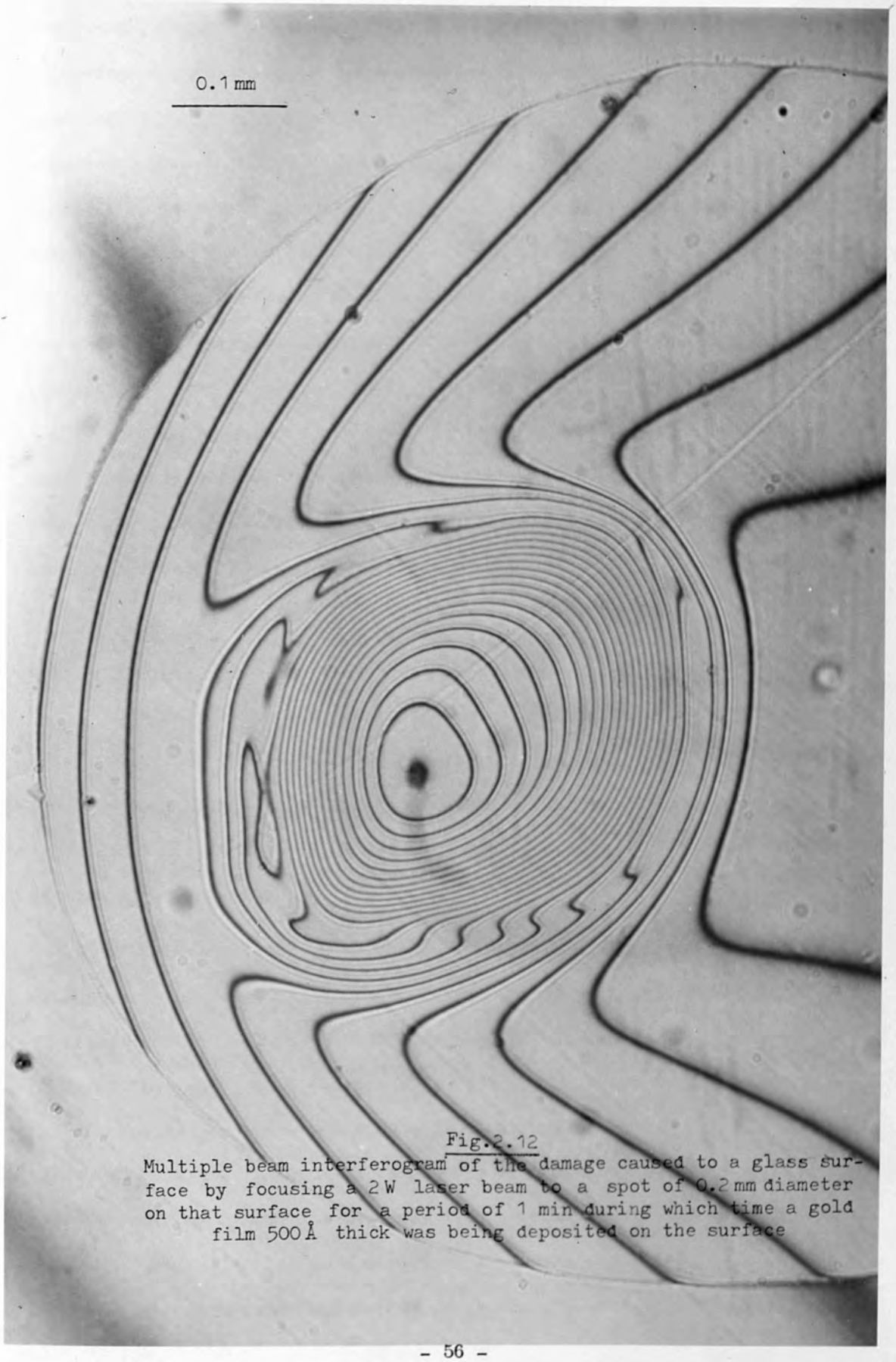

Fig.2.12

Multiple beam interferogram of the damage caused to a glass surface by focusing a 2 W laser beam to a spot of 0.2 mm diameter on that surface for a period of 1 min during which time a gold film 500 Å thick was being deposited on the surface

the damage was viewed with a transmission microscope, a number of regions of different surface colour were revealed. In a central region, having approximately the same diameter as the focal spot, the glass surface had acquired a smooth yellow colouration. This region was surrounded by an almost transparent area with a slight red granulation that became more marked with increasing distance from the centre of the spot. This area, in turn, was surrounded by a red border which extended to the limit of the area of surface deformation. The cracking around the damaged area (indicated by the discontinuity in the interference pattern shown in Fig. 2.12) occurred some hours after the laser illumination, and indicates that extremely high stresses had been induced in the glass as a result of this experiment. All the surface colours could be easily scratched off, but their removal by aqua regia occurred much more slowly than that of the gold film.

2.8 CONCLUSIONS

The results of the damage analysis indicate that the mechanism by which damage was caused to the glass surface was entirely thermal in nature. The intensity of the light was many orders of magnitude too low to induce significant nonlinear optical effects, and no damage was observed in the absence of the absorbing gold film.

The mechanism by which the surface was raised to the very large height could be explained by thermal expansion, since this would cause an increase in height of the correct order of magnitude, but in the absence of glass flow this would disappear on cooling. If the surface structure had been caused by expansion of the glass then the 'hills' and the glass below them would be less dense than the surrounding glass. In this event an interferogram taken from the back side of the microscope slide would not have observed any surface structure, but this was found not to be the case and interferograms from front and back appeared to be identical.

The slow growth of the deformation caused by the larger focal spots and the fact that damage occurred where the surface temperature had reached the melting point of glass, suggests that glass flow plays a crucial role. Such flow would, however, leave another region perceptibly lower than the undisturbed surface, unless very large stresses were frozen into the bulk substrate, no such region was in fact observed.

Similar experiments were performed on fused quartz, where the estimated surface temperature had reached 6900°C but no damage results. Clearly in this case re-radiation of the incident light from the surface must have contributed significantly in reducing the surface temperature to below that of the melting point of gold, otherwise this would have resulted in damage to the 1000 Å gold film.

CHAPTER III

THE TEMPORAL DEVELOPMENT OF OPTICALLY ETCHED GRATINGS

3.1 INTRODUCTION

One of the first methods employed to 'Q' switch lasers was the insertion inside the laser cavity of a semitransparent metallic film[100,101]. This film will cause a significant loss for light propagating along the axis of the laser cavity. During the operation of the laser, the intensity of the light inside the cavity may increase to such an extent that evaporation of the film takes place. This evaporation process will reduce the absorption experienced by the light beam and so effectively switch the 'Q' of the cavity. Using this technique, output powers of 10 MW in a 30 ns pulse have been observed[102]. A detailed study of exploding film 'Q' switches has been reported by Rowley[103].

Due to the Fabry-Perot configuration of laser cavities and the mode selectivity of 'Q' switches, there exist well defined standing waves inside lasers. These standing waves have been experimentally observed by Bragg reflection of a pulsed argon ion laser from the periodic structure inside a lasing ruby crystal[104].

The standing wave also extends into the rest of the laser cavity, its presence was experimentally confirmed by Ledger[105] in 1966 and later by Little et al[102]. Experimental evidence for the existence of the standing wave inside the laser cavity was obtained by inserting inside the laser cavity, at a small angle to the end mirror, a thin metallic film. This metallic film also acted as a 'Q' switch. Since the intense light of the laser is obliquely incident on the thin partially absorbing film simultaneously from two opposite directions, heating occurs much more rapidly at the antinodes than at the nodes of the electric field of the resulting standing wave. If the light is sufficiently intense, this

heating can cause evaporation and ionization of the film, and may also result in the etching of any underlying substrate. Since the film intersects the antinodes of the standing wave in a series of lines, this removal of the film material and substrate etching results in the creation of a diffraction grating. The line separation d of the grating is given by the equation $d = \lambda/(2 \sin \theta)$, where λ is the wavelengths of the incident light and θ the angle between the direction of propagation of the light and the normal to the film.

The phenomenon is of interest both as a means of rapidly producing small diffraction gratings of accurately known spacing, and also because it provides a technique by which the dynamics of surface laser damage may conveniently be studied[21,106].

An extensive investigation of the properties and the manufacture of these gratings has previously been undertaken[103]. In this reported work, microscope slides were coated with 200 Å films of gold and placed in a ruby laser cavity, where gratings with a spatial period of less than 0.4 μm were manufactured. Gratings with spatial periods as small as 0.2 μm were also produced by frequency doubling the ruby laser output and forming the standing wave in a cavity external to the laser cavity.

It was noted in the work reported[103] by Rowley, that the strength of the diffracted orders was too large to be explained solely from the point of view of an amplitude grating. On further investigation, it was found that the transparent substrate had also been etched to a depth of 0.5 μ. This etching had taken place at the antinodes of the standing wave and thus resulted in the formation of a phase grating.

Due to the lack of transverse mode selection in the ruby laser used[103], gratings were uniform only over areas of a few square millimeters and a resolution of 1 Å was obtained for gratings having a spatial period of 0.4 μm.

To improve the diffraction efficiency of the gratings, the substrates were etched a number of times. To achieve this, the substrate was coated in the laser cavity. After each laser shot, the substrate was again coated with a 200 Å film of gold and then periodically evaporated by the laser. Using this procedure, up to twenty subsequent shots were achieved with no observable degradation of the modulation profile. Diffraction efficiencies of 25% for the uncoated substrates were recorded[103] which compared favourably to the theoretical limit of 34%.

In addition to recording the hologram of the two main interfering beams of the laser, the diffraction patterns caused by dust particles and other absorbing centres had also been recorded[103] on the metallic films.

In 1971 the same author reported[107], observing the converse of the periodic evaporation process, namely the spatial periodic inhibition of condensation. This was observed by placing a transparent condenser plate close to the metallic coated substrate. The condenser plate was orientated parallel to the coated substrate and so experienced a similar periodic electric field as the coated substrate. On firing the laser the gold evaporated and subsequently deposited on the condenser plate at the nodes of the standing wave. It was found that in order to obtain a periodic distribution, the plate separation had to be small enough to allow the gold vapour to reach the condenser plate before the end of the laser pulse.

In work reported in this thesis the area of the metallic film illuminated by a ruby laser beam, has been probed by a continuous argon ion laser. This light was itself too weak to damage the metallic films used, but was diffracted by the grating caused by the ruby laser light. The temporal development of this diffracted beam thus gives information concerning the dynamics of the processes involved in the creation of the

grating. A time resolved investigation has been made of the development of such gratings in a number of metallic films, and the effect of film thickness, incident laser intensity, and angular orientation of the film has been studied. In addition the spectral output of the film surface during illumination by the ruby light was studied.

3.2 LASER SYSTEMS USED IN EXPERIMENT

3.2.1 Principles of the Ruby Laser

In any material the electron population is confined to various energy levels. The disposition of the electron populations in ruby is shown in Fig.3.1. Ruby consists of chromium doped Al_2O_3 with the active ingredient being chromium. The most common doping concentration is 0.05% by weight of Cr_2O_3.

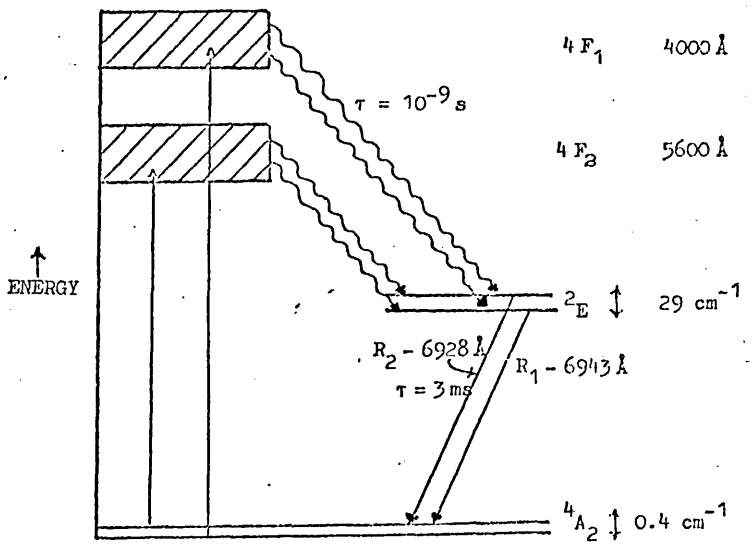

Fig.3.1
Energy levels of chromium ion in Ruby. Radiative and absorptive transitions are shown by solid lines while non-radiative transitions are shown by wavy lines

In the inactivated stage virtually all the electrons are in a degenerate ground level $^4A_2$. Levels $^4F_1$ and $^4F_2$ consist of numerous closely spaced degenerate energy levels which overlap to give two broad absorption bands. Levels ^2E are metastable and have a lifetime of 2.9 ms. As can be seen in Fig.3.1, there exists two possible modes of decay from the ^2E levels to the ground level, that is either by R_1 (6943 Å) or R_2 (6928 Å). The R_1 line is polarised at right angles to the optic axis and travels as the ordinary ray in the birefringent crystal. The R_2 line is polarised along the optic axis in the crystal and travels

as the extraordinary ray. Only the R_1 line oscillates under normal conditions, since it attains inversion before the R_2 line on account of its larger transition probability.

On activation of ruby by irradiation with the intense light pulse created by a flash tube discharge, electrons are excited from the ground level to the levels $^4F_1$ and $^4F_2$ by absorption of energy from the light pulse. The levels $^4F_1$ and $^4F_2$ absorb energy in broad bands centred on 4000 Å and 5600 Å respectively, thus allowing a reasonable amount of the energy radiated by the flash tube to be effective.

In any transition, an incident photon has equal probabilities of exciting by absorption an electron from the lower level to the higher, or of stimulating the decay of an electron from the higher level to the lower, with the emission of a second photon. It is not possible, therefore, even in an ideal system, for the population of levels $^4F_1$ or $^4F_2$ to exceed that of the ground level. However, electrons which are excited to levels $^4F_1$ or $^4F_2$ decay spontaneously, by a fast non-radiative decay process, to level ^2E, so increasing the population of level ^2E. Due to the relative long half life of this metastable level ^2E, the population of this level increases as a result of the pumping of electrons via levels $^4F_1$ and $^4F_2$ and can be made greater than that of the ground level. This condition is known as population inversion.

When population inversion exists, a photon having a wavelength of 6943 Å, corresponding to the $^2E - ^4A_2$ transition, is more likely to stimulate the decay of an electron from level ^2E, with the resultant emission of a second photon, than it is to be absorbed by an electron at the ground level. The second photon released by the stimulation is emitted in the same direction and in phase with the incident photon. Photons travelling along the length of the rod are returned into the ruby by

mirrors situated at each end and in passing to and fro along the rod stimulate further emissions from excited ions in their path, thus building up to a coherent parallel beam of monochromatic light.

Once lasing action occurs, the population of level ^2E reduces rapidly to less than that of the ground level, causing the action to cease until level ^2E again reaches a state of population inversion as a result of the pumping from ground level to the broad absorption bands $^4F_1$ and $^4F_2$. Due to this repeated cessation and restoration of the lasing action, the output consists of a number of short pulses. A typical output is shown in Fig.3.2(a).

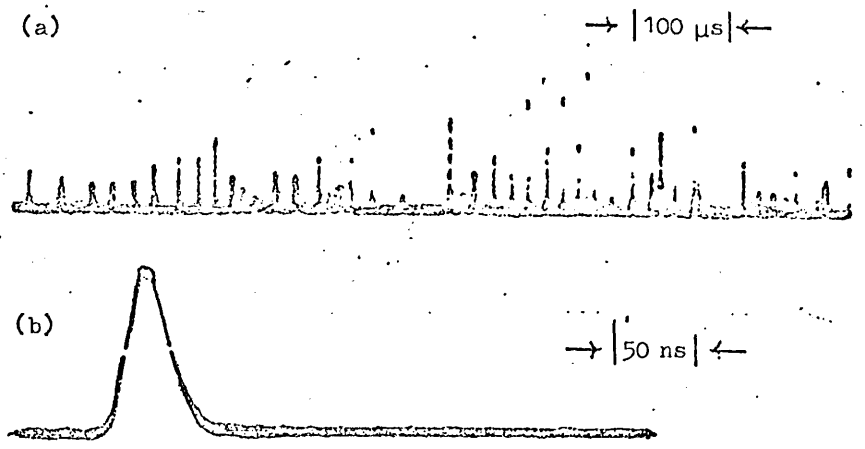

Fig.3.2
(a) Intensity output of a 'free-running' ruby laser
(b) The 10 MW/cm^2 output of a 'Q' switched ruby laser

3.2.2 Construction and Operation of the Ruby Laser

The ruby laser used in the experiments described in this thesis was a type 351, made commercially by G & E Bradley Ltd. A photograph of the laser head is shown in Fig.3.3.

The active medium of the laser is a ruby crystal, $6\frac{1}{2}$" long by $\frac{5}{8}$" diameter, which is positioned along one of the foci of an aluminium

Fig.3.3 - The ruby laser

cylinder of elliptical cross-section. The inner surfaces of the cylinder are highly polished and anodised to form an efficient reflector. Also situated in the laser head is the optical pump, this consists of a quartz cylinder filled with xenon gas at a pressure of 45 cm of mercury and with an arc length of $6\frac{1}{2}$ inches.

Both the ruby crystal and the flash tube are encased in quartz water jackets, through which deionized water circulates. This ensures rapid cooling and allows the ruby to be fired once every few minutes.

The power unit supplied with the laser head consists of a capacitor drive unit, capacitors and two triggering circuits. The capacitor drive unit provides the energy for charging five high voltage 300 μF capacitors to a maximum potential difference of 3 kV. The five capacitors are placed in parallel and thus capable of supplying 6.75 kJ of electrical energy to the xenon flash tube. In practice the capacitors were very rarely charged above 2.5 kV giving an input energy to the flash lamp of 4.7 kJ.

If the ruby is to be pumped efficiently then the pump light must cause inversion in a time comparable to the metastable lifetime (2.9 ms) of the ruby lasing level involved. To satisfy this condition an inductance is placed in series with the flash tube and across the output terminals of the capacitors.

Two trigger circuits are employed in the power unit, see Fig.3.4. One trigger unit supplies 15 kV in a few microseconds to the flash tube terminals, this triggers the discharge of the flash tube. The second trigger circuit supplies a low voltage pulse coincident with the firing of the flash tube. This trigger pulse was used to synchronise the oscilloscopes.

Feedback of light into the ruby crystal was achieved at one end by a 99.7% reflecting mirror supplied by Balzers. The high reflectivity and

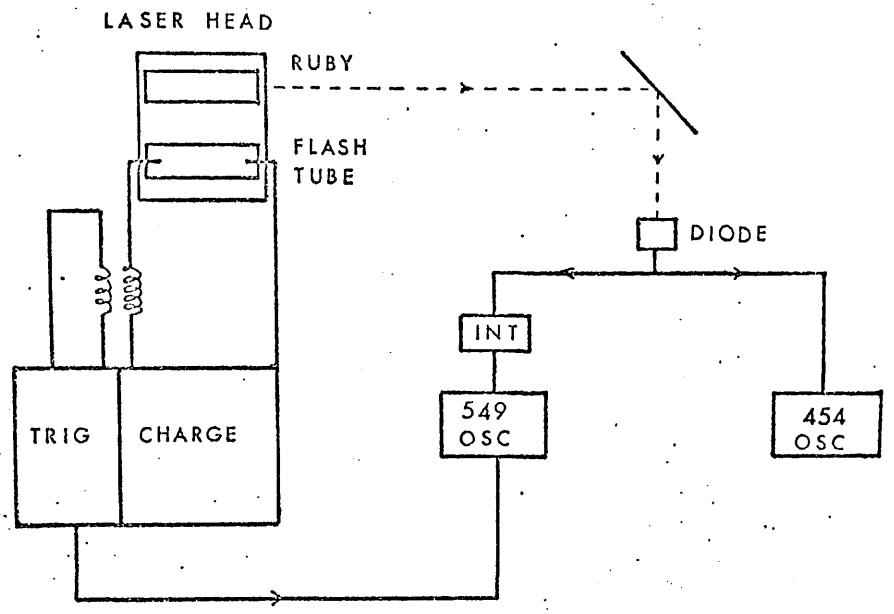

Fig.3.4
The ruby laser triggering circuit.

high damage threshold (300 MW/cm^2) of this mirror is achieved by coating a quartz substrate with alternate $\lambda/4$ layers of dielectric materials of high and low refractive indices.

At the output end of the laser cavity partial reflection was achieved by use of a short uncoated resonant cavity. This produced an effective reflectivity of 16%. The output from the laser consisted of light of a number of different longitudinal modes. By using the resonant reflector, which consisted of two parallel quartz flats, the laser could be made to operate in a limited number of longitudinal modes.

Complete longitudinal mode selection was achieved by inserting inside the laser cavity a 'Q' switch. This consisted of a thin optical cell (1 cm path length), containing cryptocyanine (1,1' - diethyl - 4,4' - carbocyanine iodide) dissolved in pure methanol. A spectrophotometer trace of the density of this dye is shown in Fig.3.5. It can be seen

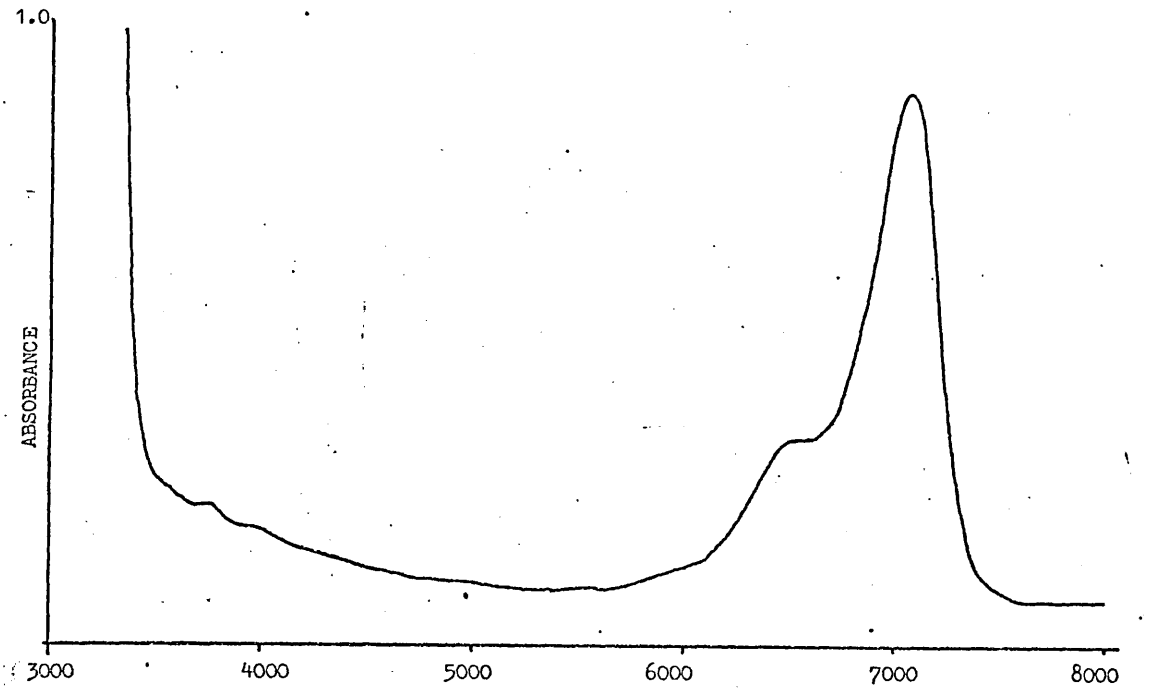

Fig.3.5
Absorption spectrum of cryptocyanine dissolved in acetone

that its optical density has a maximum at approximately 6943 Å, thus efficiently absorbing the ruby output. Absorption of the ruby light by this dye will effectively cease when the population of the ground level approaches that of the upper. At this stage the dye is said to be 'bleached' and transmission of the ruby light ensues. By increasing the concentration of the dye in the cell inside the laser cavity, the number of individual microsecond pulses normally observed in the output light of the laser can be reduced. If the dye concentration is sufficiently high, the lasing action can be limited to one pulse, this resulting pulse is typically a few tens of nanoseconds in duration and has a peak power of around 50 MW. A photograph of a typical 'Q' switched pulse is shown in Fig.3.2(b).

The one big disadvantage of our ruby laser output was that it exhibited poor transverse mode selection. Even by including inside the cavity an aperture to limit the diverging light, no great improvement could be made, in fact the aperture presented so much resistance to the

light that it became impracticable to fire the laser. One probable cause of the poor transverse mode control was that the ruby output passed through a layer of water which was used to cool the ruby crystal. Another possible cause which came to light later when experiments on mode locking were being performed, was that self focusing of the light by the ruby crystal produced a significant deterioration in the spatial intensity profile of the output pulse.

3.2.3 Gas Lasers Used in Experiments

In addition to the ruby laser two other lasers were used. One of these was a simple helium-neon gas laser (Metrologic 360) which was used to align the complicated optical system. This laser had a continuous output of 1 mW at 6328 Å in a single transverse mode. The output from the helium-neon laser was directed normal to the 99.7% reflecting mirror of the ruby laser cavity. By removing this mirror the light from the helium-neon laser traced out the path of the ruby laser beam. This procedure allowed correct alignment of the optical components used in the experiments to be made with ease.

The second gas laser used in the experiments was a Coherent Radiation 52B continuous argon ion laser. This laser was operated solely on the 5145 Å line, giving it a maximum output of 1.4 W. The output occurred in a single TEM_{oo} transverse mode and had a divergence of 1 mrad and an initial beam diameter at the $1/e^2$ intensity points of 1.4 mm. This laser incorporated a power meter into its design and regulated the output power of the laser to within 0.1% of a preselected value. At times a knowledge of the power level of the argon ion laser light was required at points remote from the laser. In these instances a calibrated Spectra Physics photocell and meter were used.

3.3 DETECTION EQUIPMENT

Deflection by beam splitters of approximately 4% of the main laser light into two EMI 9648B photodiodes facilitated the detection of the temporal intensity profile of the forward and backward going ruby light. These two photodiodes had a bismuth silver cathode and an inherent rise time of approximately 1.5ns . Both diodes were fitted with Barr and Stroud narrow band filters, centred on 6943 Å, to eliminate unwanted light. Diffusion screens were also inserted inside the diode casings to eliminate any saturation effect of the photocathode that may have resulted from the high light intensities used.

Detection of the diffracted argon ion light was achieved by using two Mullard 56 AVP's and one EMI 9810QB photomultiplier. All three photomultipliers had identical characteristics, of a 2.4ns risetime and a 45ns transit time. The diffracted signals were attenuated by a diffusion screen and a Grubb and Parsons narrow band filter having a bandwidth of 28 Å centred on 5148 Å. It was also found necessary to use two JENA BG 18 green filters to further attenuate the unwanted ruby light.

Calibration of the photomultipliers and detection of the saturation point was achieved by chopping the argon ion light with a rotating disc.

To ensure that only one 'Q' switched pulse was emitted by the laser, the output from the photodiodes detecting the ruby pulse was fed into a Tektronik 549 storage oscilloscope. This instrument has a bandwidth of 30 MHz and a sensitivity of 5mV/div . Its main advantage though is that it is capable of storing on its screen a picture of the oscilloscope trace. This meant that the oscilloscope did not need to be viewed or the trace photographed to ascertain the number of pulses emitted by the ruby laser. Unfortunately though, even in the enhanced writing mode, the writing speed was only 5 cm/μs . This meant that it was incapable of recording the 20ns

pulses emitted by the photodiodes in response to the detection of the ruby pulse. But by integrating these fast electrical pulses with an R-C circuit having a response time of 10^{-5} s , the resulting slow pulses could be easily detected and displayed even when using the normal writing speed of 0.5 cm/μs.

In addition to the 549 storage oscilloscope, two Tektronix 454's and one Tektronix 7904 were employed. The two 454's had a 150 MHz bandwidth giving them an effective risetime of 2.4 ns . While the 7904 has a bandwidth of 500 MHz resulting in an instrument risetime of 0.8 ns . All three oscilloscopes had sensitivies of 5 mV/cm .

In every instance where these three oscilloscopes were used to record the output from either of the two photodiodes or the three photomultipliers, the signal was conveyed by 50 ohm impedance coaxial cable, and in the case of the two 454's, terminated with a suitable 50 ohm matching piece. (The 7904 had an input impedance of 50 ohm, while the 454's had an input impedance of 1 MΩ.) This ensured that no reflections occurred at the terminals of the oscilloscopes due to impedance mismatches.

Generally the discharge of the ruby laser's capacitors produced so much electromagnetic noise that it triggered the oscilloscopes. This effect was unimportant as far as the 549 was concerned, since the sweep rate was so slow that it displayed both the noise from the capacitors and the individual 'Q' switched pulses. To overcome this problem with the three other oscilloscopes, the double triggering system of these oscilloscopes was employed. This meant that a signal could not be detected until both systems had been triggered. The first triggering system was fired from the electromagnetic noise and after an adjustable delay allowed the second trigger system to be fired from the photodiode pulse. Since the time interval between the electromagnetic noise and the first ruby pulse

was of the order of milliseconds, the second trigger system was never fired by the noise. This approach completely eliminated any spurious triggering.

The two 454's and the 7904 all had two channel inputs, which enabled one to combine two signals of different magnitude on one trace by using different gains and suitable delays. The delays were obtained by using the appropriate length of 50 ohm impedance coaxial cable.

The energy of the laser pulses was measured by use of a calibrated calorimeter (Laser Associates model 42). This calorimeter consisted of a polished cone into which the laser light was directed. The shape of the cone was such that after multiple reflections on its surfaces very little of the incident light escaped from it. The heat produced by absorption of the light was detected by an array of thermocouples on the outer surface of the cone. These were connected to a multivoltmeter calibrated in terms of beam energy and allowed accurate measurements to about one tenth of a joule. By using the calorimeter in conjunction with the photodiodes, an intensity calibration of the photodiodes was made. This procedure also enabled one to determine the intensity saturation point of the photodiodes.

3.4 EXPERIMENTAL ARRANGEMENT

A detailed diagram of the experimental arrangement is shown in Fig. 3.6. The polarization of both the ruby and argon ion lasers lies in a plane perpendicular to the plane of the diagram.

The passively Q-switched ruby laser gave a pulse of up to 50 MW peak power and a duration of 10-20 ns (FWHM). The metallic film which was to be illuminated by the ruby was placed in a cavity external to the laser cavity. This external cavity was formed by a 97.7% reflecting dielectric mirror orientated parallel to the two laser mirrors and positioned approximately two metres away. The metallic film was positioned

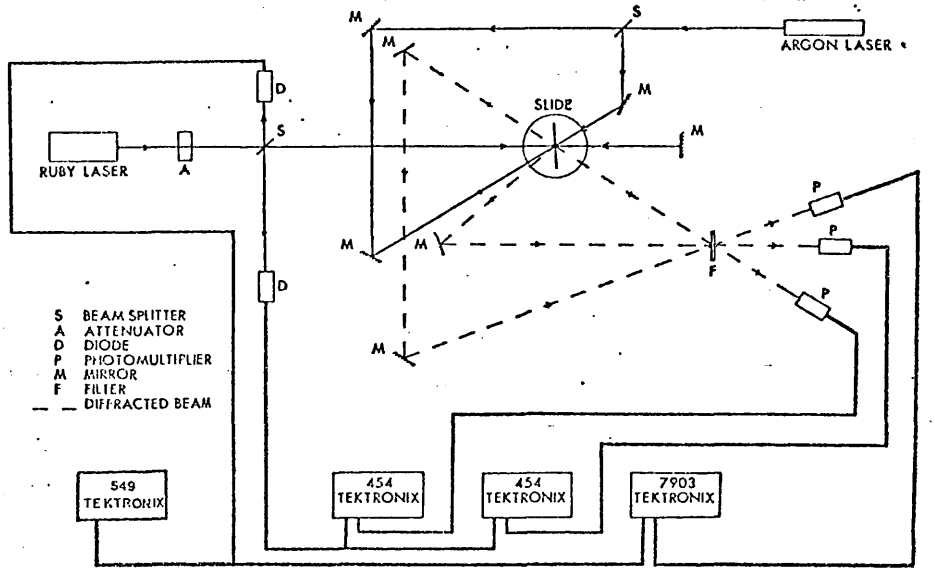

Fig.3.6
Experimental arrangement for the study of the temporal development of the light diffracted from an optically etched grating

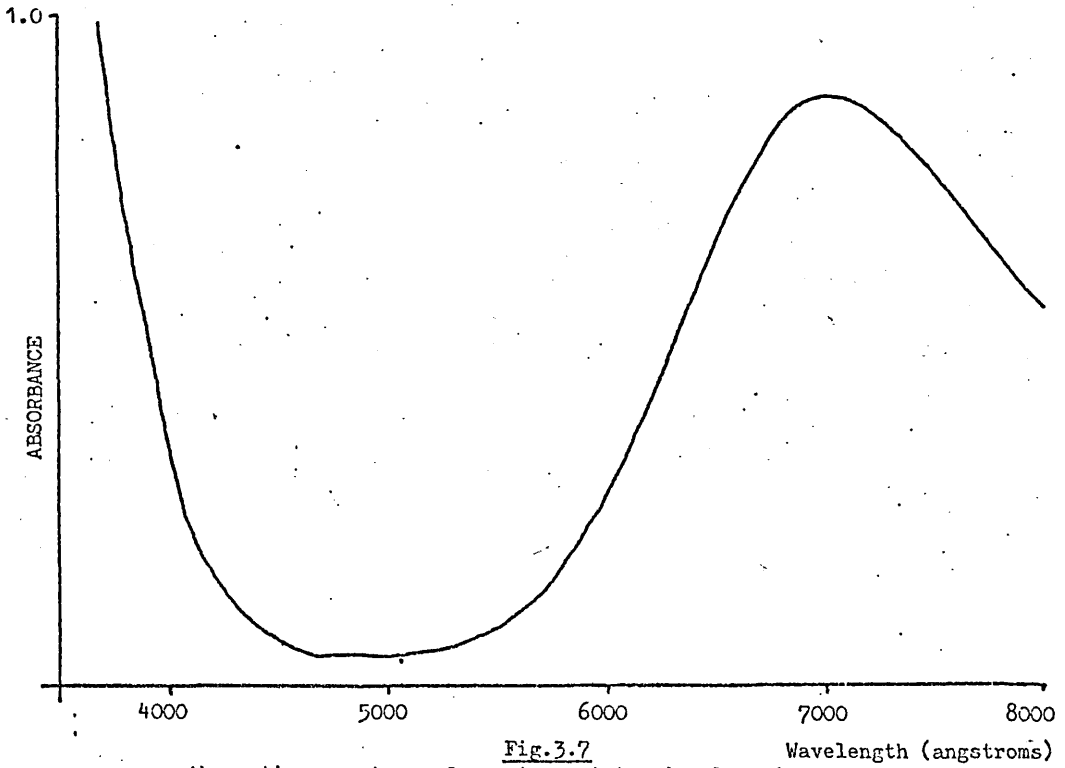

Fig.3.7
Absorption spectrum of cupric acetate dissolved in methanol

within 20 cm of this high reflecting external mirror. The intensity of the light incident on the film was varied from 0.5 mW to 40 mW by an attenuating cell containing cupric acetate dissolved in methanol. A spectrophotometer trace of the density of this solution is shown in Fig.3.7. No absorption saturation of this solution was found with the power levels used. The forward and backward going beams of ruby laser light, which were incident on each side of the film at 5° to the normal, were detected by the fast photodiodes described in the previous section. The signal generated by the forward going beam was displayed on the two Tektronix 454 oscilloscopes, while that generated by the backward beam was displayed on the Tektronix 7904 oscilloscope.

The output of the argon ion laser emitting light of 5145 Å wavelength was split into two beams. These beams were incident, at an angle of $18^{\circ}40'$ to the normal, on opposite faces of that part of the film illuminated by the ruby laser. As the grating was created, by the action of the ruby laser light upon the thin film, the development of three of the first order diffracted beams of argon ion laser light was studied. Two of these originated from the light reflected from each side of the film, while the third arose from the light transmitted through it. These three beams passed through a narrow band filter, transmitting light of 5145 Å to eliminate any blue-green light generated at the surface of the film. Further green filters (JENA BG18) were used to eliminate scattered ruby laser light. The beams were then detected by three photomultipliers (2×56 AVP's, 1×9810 QB). Two of the signals were displayed, using suitable delay lines, on the same Tektronix 454 oscilloscopes as the ruby laser signals, while the third was displayed on the Tektronix 7904 oscilloscope. The Tektronix 549 storage oscilloscope was used to check the occurence of only one Q-switched pulse from the ruby laser.

The absorbing films used were evaporated layers of silver, gold and aluminium of thicknesses from 50 Å to 400 Å on glass microscope slide substrates. The temporal development of the beams diffracted from the gratings formed by the various films was observed over a range of ruby laser intensities. The metallic films were mounted on a rotating table which could be positioned to an accuracy of five minutes. The effect of varying the angle of incidence of the ruby laser beam upon the film was studied.

3.5 GENERAL RESULTS

The main features of the development of the diffracted signals were generally the same for each type of film. At different energies of the incident ruby laser pulse, three main types of development were observed. For pulses of very high energy, the diffracted signal was a pulse with a short duration comparable with that of the incident light. With low incident energy, the diffracted signal resembled a step function rising to a constant level in a time comparable to the rise time of the laser pulse. These two types of signals were present irrespective of the type of film material used. At intermediate energies, both reflected diffraction signals from the aluminium films and the transmitted diffraction signal from the gold and silver films exhibited a more complex structure. This complex structure consisted of a short initial pulse followed by a relatively slow rise and then a decay to a constant level.

The three types of signal can be clearly seen in Figs.3.8 - 3.10. While the slow decaying signal, Fig.3.10, was present in the cases indicated above, the other beams diffracted at the same time displayed the fast pulse type of signal (Fig.3.8).

A time check on the occurrence of the diffracted signal established that in every case a diffraction grating began to develop on the arrival

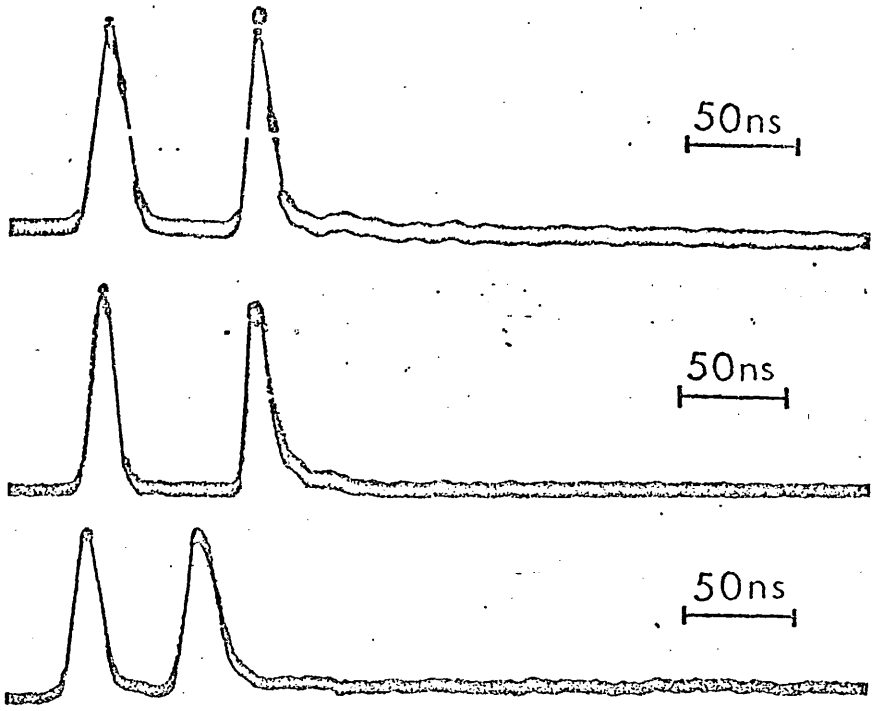

Fig.3.8

Diffracted signals observed using high energy ruby laser pulses. (Traces show the ruby laser output followed by the delayed diffracted signal.) Top Trace: Reflected signal diffracted from front of 200 Å aluminium film illuminated by a 0.9 J/cm^2 ruby laser pulse. Middle Trace: Reflected signal diffracted from front of 200-Å silver film illuminated by a 0.45 J/cm^2 ruby laser pulse. Bottom trace: Reflected signal diffracted from back of 200-Å gold film illuminated by a 0.40 J/cm^2 ruby laser pulse

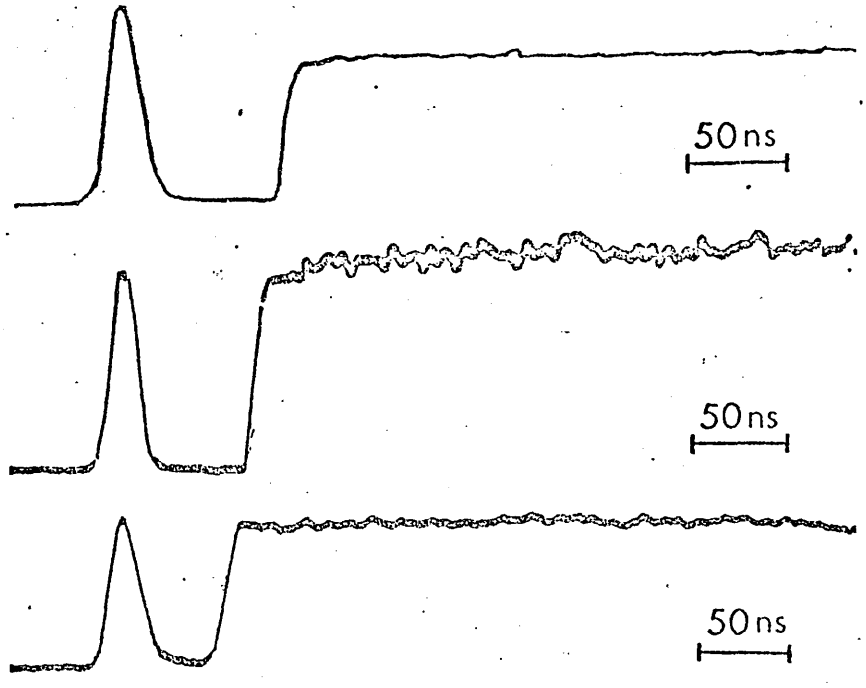

Fig.3.9

Diffracted signals observed using low energy ruby laser pulses. (Traces show the ruby laser pulse followed by the delayed diffracted signal.) Top trace: Reflected signal diffracted from front of 50-Å aluminium film illuminated by a 0.03 J/cm^2 ruby laser pulse. Middle trace: Reflected signal diffracted from front of 100-Å silver film illumiminated by a 0.045 J/cm^2 ruby laser pulse. Bottom trace: Reflected signal diffracted from back of 100-Å gold film illuminated by a 0.045 J/cm^2 ruby laser pulse

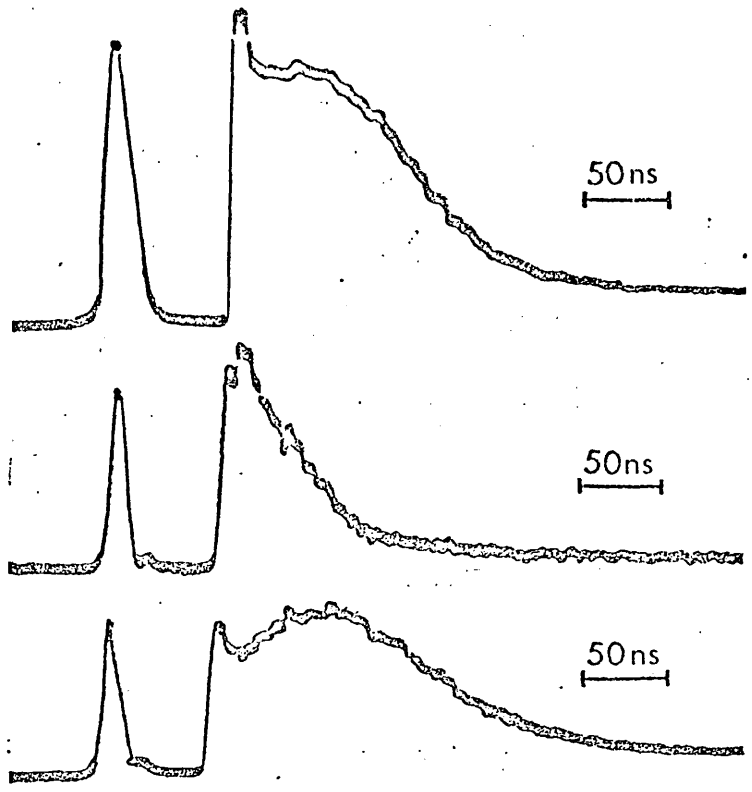

Fig.3.10
Diffracted signals observed using intermediate energy ruby laser pulses. (Traces show ruby laser output followed by the delayed diffracted signal.) Top trace: Reflected signal diffracted from front of 100-Å aluminium illuminated by a 0.2 J/cm^2 ruby laser pulse. Middle trace: Transmitted signal diffracted from 200-Å silver film illuminated by a 0.3 J/cm^2 ruby laser pulse. Bottom trace: Transmitted signal diffracted from 200-Å gold film illuminated by a 0.1 J/cm^2 ruby laser pulse

of the ruby pulse, estimated to within the accuracy of the detection system i.e. 5ns .

Although the conditions of the laser oscillator were kept constant, the duration of the output pulse varied from 10ns to 20ns (FWHM) . Analysis of this effect, of pulses of different widths, showed the crucial factor determining the nature of the diffracted signal to be the energy rather than the power of the laser pulse.

The diffraction efficiency (i.e. intensity ratio of the first to zeroth order diffracted beams) of the grating left after the etching, varied with pulse energy and film thickness. The pulse energy for which this efficiency was a maximum, tended to increase with increasing film thickness. Those gratings exhibiting the highest efficiencies were always those where the step function type of diffraction signal (Fig.3.9) had resulted. In general the diffraction efficiencies were always greatest

for reflected orders rather than the transmitted. This was true both for the transient signals displayed electronically and for the remaining gratings.

3.6 RESULTS FROM DIFFERENT GRATING MATERIALS

3.6.1 Gold

The threshold energy required for the ruby laser beam to etch the gold films varied from 20 mJ/cm^2 in the case of the 50 Å film to 100 mJ/cm^2 for the 400 Å film. The diffraction efficiencies of gratings formed in the 50 Å film were always very low, reaching a maximum of 8×10^{-4}% when the incident energy was 150 mJ/cm^2. Much better gratings were formed in the 100 Å and 200 Å films having maximum efficiencies of 5×10^{-2}% and 8×10^{-3}% at energies of 60 mJ/cm^2, respectively. The gratings formed in the 400 Å film were of comparable efficiency, up to 2×10^{-2}% at 400 mJ/cm^2. These diffraction efficiencies are low since the measurements are averaged over the total area illuminated by the argon ion laser.

At high beam energies all the diffracted signals showed a pulsed development of the type illustrated in Fig.3.8 regardless of the film thickness, but at lower energies the three beams showed different features. The signals from the 50 Å film were too weak to be conveniently studied. In the case of the 100 Å film the transmitted beam began to develop in the slow manner illustrated in Fig.3.10 for input energies of less than 300 mJ/cm^2, but the two reflected beams retained the features shown at the higher energies. These beams never showed the slow development of Fig. 3.10, but at energies of less than 50 mJ/cm^2 the beam reflected from the back of the film (i.e. from the side in contact with the glass slide) lost its pulsed character and developed in the step-function manner shown in Fig. 3.9. The beam reflected from the front of the film retained a partially pulsed character right down to the etching threshold. Using a 200 Å film

similar results were obtained, but the transition from pulsed to slow development of the transmitted beam occurred at 600 mJ/cm^2. The development of the diffracted beams from the 400 Å film was again similar, except that the transmitted beam showed slow development up to the highest available ruby laser energies (1500 mJ/cm^2), while both reflected beams showed pulsed development right down to threshold intensity.

3.6.2 Silver

The threshold energy required to etch the silver films varied from 60 mJ/cm^2 for the 50 Å film to 500 mJ/cm^2 for the 400 Å film. Much more efficient gratings (7×10^{-2}% at 450 mJ/cm^2) were formed in the 50 Å film than in the equivalent gold films. The gratings formed in the 100 Å and 200 Å films were also of greater efficiency (6×10^{-2}% at 100 mJ/cm^2 and 10^{-2}% at 1000 mJ/cm^2, respectively), but those in the 400 Å film were very poor.

The development of the diffracted beams was broadly similar to that of those produced from the gold films but showed much less slow development (Fig.3.10) and more often took the form of a step-function (Fig.3.9). Using the 50 Å film, all three beams showed a development intermediate between Figs.3.8 and 3.9 at the highest available ruby laser energies. At energies of less than 400 mJ/cm^2 all three beams showed purely step function behaviour, but at no stage was there any significant slow development. The beams diffracted from the 100 Å film were very similar, acquiring a purely step function character for energies of less than 150 mJ/cm^2. Using the 200 Å film, however, the transmitted beam showed slow development for energies of less than 450 mJ/cm^2, while the two reflected signals were of the pulsed type shown in Fig.3.8. The very weak signals reflected from the 400 Å film were also of the pulsed type, while the transmitted beam was undetectable.

3.6.3 Aluminium

The threshold for etching the aluminium films varied from 20 mJ/cm^2 for the 50 Å film to 200 mJ/cm^2 for the 400 Å film. The efficiencies of the gratings formed in the 50 Å film were greater than in the case of either the gold or silver films (0.25% at 60 mJ/cm^2). The maximum efficiencies of gratings formed in the 100 Å and 200 Å films were 10^{-2}% at 750 mJ/cm^2 and 3×10^{-2}% at 700 mJ/cm^2, respectively, while the 400 Å film gave gratings with maximum efficiency of 2×10^{-4}% at 600 mJ/cm^2.

The overall features of the development of the diffracted beams were similar to those observed with the other two metals, except that slow development (Fig.3.10) was in this case more prominent in the reflected than in the transmitted beams. At high incident energies all the beams diffracted from the 50 Å film, had a pulsed character (Fig.3.8), but below 250 mJ/cm^2 the two reflected beams showed slow development. At energies below 50 mJ/cm^2 all three beams showed a mainly step function behaviour (Fig.3.9). Using the 100 Å film the transition from pulsed to slow development of the two reflected beams occurred at about 400 mJ/cm^2, while the transmitted beam showed pulsed behaviour down to the etching threshold. Surprisingly this situation was reversed using the 200 Å film when the reflected beams had a pulsed character down to threshold energy, while the transmitted beam showed slow development even at the highest available energy. The signals reflected from the 400 Å film were of pulsed form for high incident energies but became of the step function type for energies below 300 mJ/cm^2. The slowly developing transmitted beam was so weak that it was only observable at the highest available energy.

A summary of the types of diffraction signals observed from the various metallic films at low, medium and high laser pulse energies can be seen in Fig.3.11.

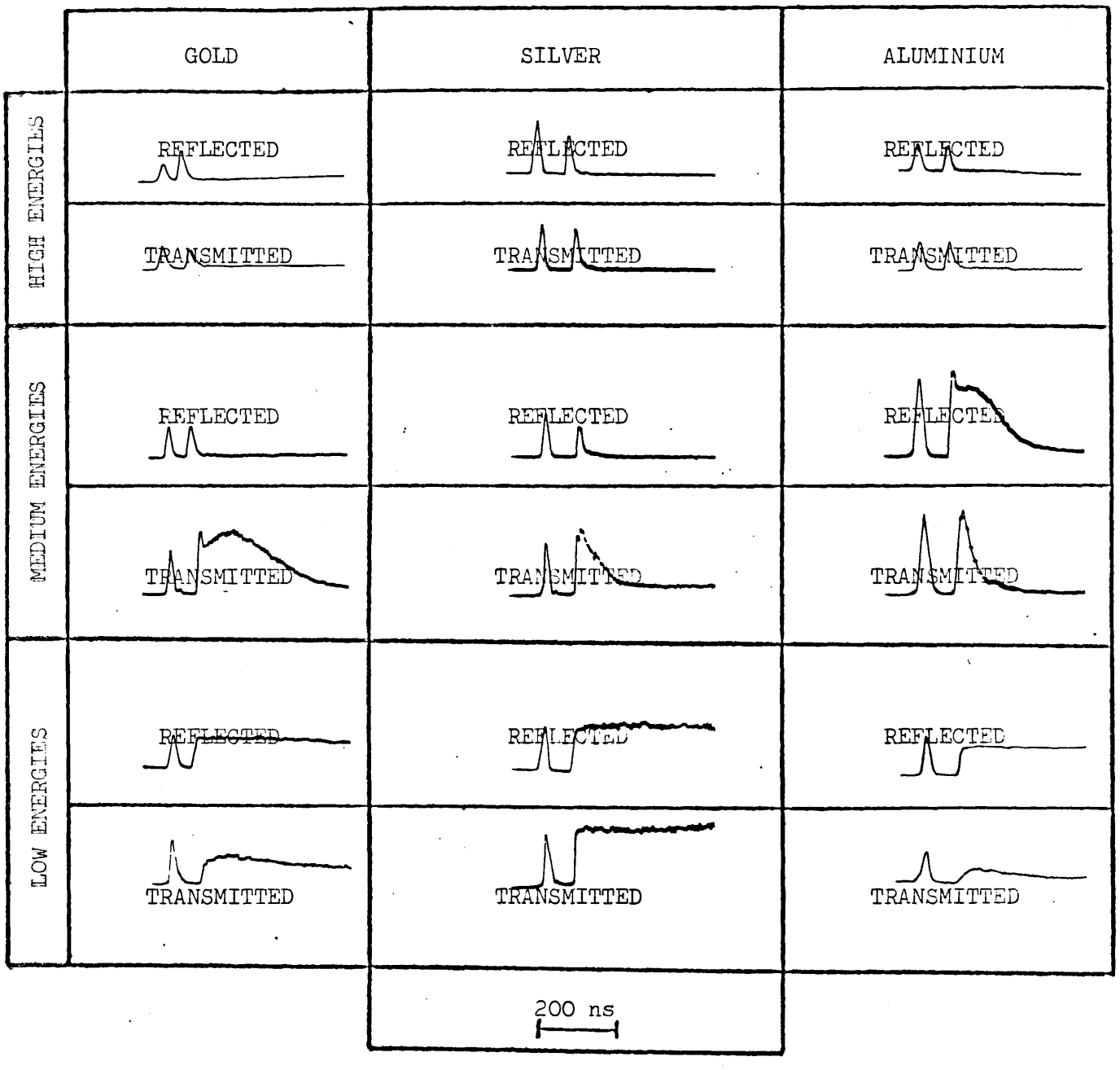

Fig.3.11

Diffracted signals observed, from a variety of film materials, using high (> 0.4 J/cm^2), medium ($0.1 - 0.3$ J/cm^2) and low (< 0.05 J/cm^2) energy ruby laser pulses. The thickness of both the gold and silver films were 200 Å or less, while the aluminium films were 100 Å or less in thickness

3.7 PHYSICAL QUALITY OF THE GRATINGS

The ideal optically etched gratings would consist of a periodic thin metallic film, undamaged at its thickest points and totally absent at its thinnest, on a completely unaffected substrate.

The gratings formed in our experiments were examined under a microscope of up to 1300× magnification. This showed that those gratings formed by illumination of 50–100 Å gold or aluminium films by ruby laser beams of only just sufficient energy to affect the films, approached closest to the ideal (Fig.3.12). These gratings were very small in area but could have diffraction efficiencies of up to 10%. (The much lower efficiencies recorded in section 3.6 were the average efficiencies measured over the whole area illuminated by the argon ion laser.) Higher energy illumination of these films, by the ruby laser, tended to cause total removal of the free metal even at the nodes of the field, leaving a dull reddish layer with little absorption or reflectivity on the substrate surface (Fig.3.13). The resulting grating was of very low diffraction efficiency. Such total removal of the free metal (perhaps involving its penetration into the substrate surface to form the reddish layer) occurred even more frequently using thicker films of gold or aluminium, or with silver films of any thickness.

Correlation of the time resolved diffracted signals with the appearance of the gratings clearly showed that the ideal type of grating was formed when the beam energy was sufficiently low to give the step function type of diffracted signal. Whenever a fast pulse was visible in the diffracted signal, complete removal of the metal film had occurred over at least some part of the grating.

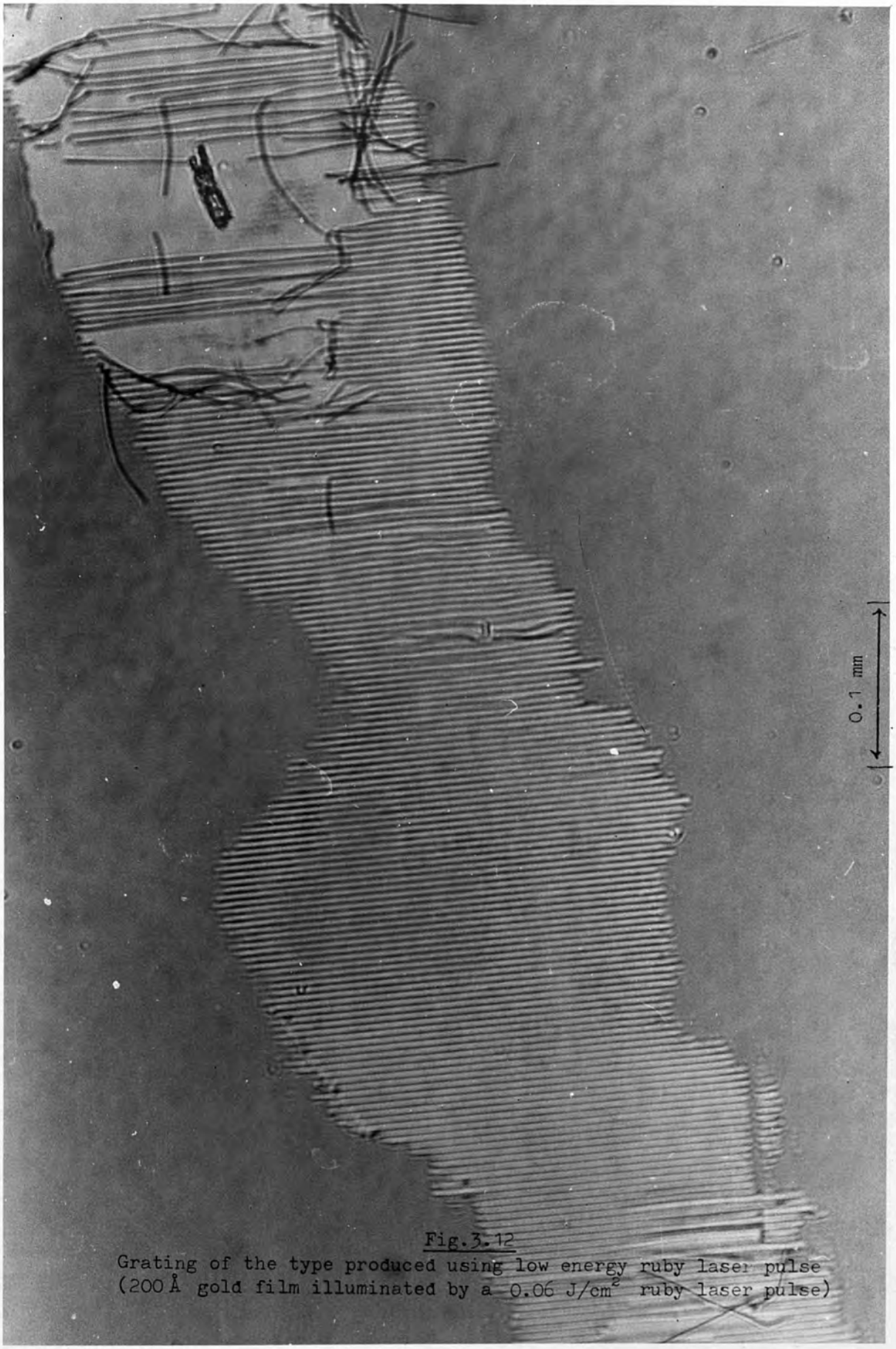

Fig.3.12
Grating of the type produced using low energy ruby laser pulse (200 Å gold film illuminated by a 0.06 J/cm^2 ruby laser pulse)

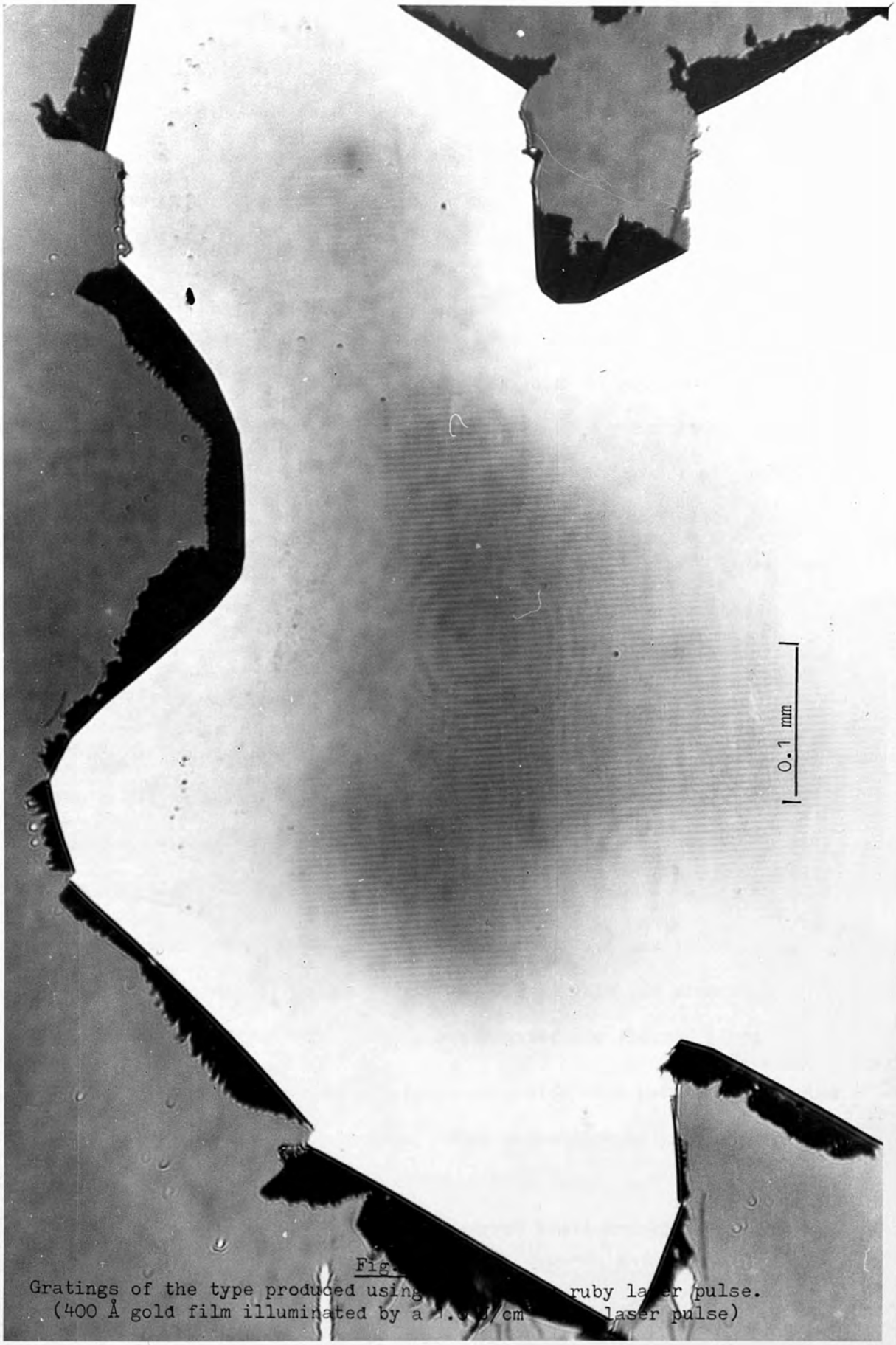

Fig.
Gratings of the type produced using ruby laser pulse.
(400 Å gold film illuminated by a cm laser pulse)

3.8 SPECTROSCOPY OF THE LASER IRRADIATED SURFACES

When the 5145 Å narrow band filter between the photomultipliers and the film was removed, a signal with a decay time of approximately 15 ns was observed even in the absence of the argon ion laser light. Inserting a 50% transmitting 6943 Å narrow band filter between the photomultipliers and the film had the effect of reducing considerably the detected signal. The signal cannot therefore be attributed to scattered ruby light, but probably to light generated by the film during the etching process. This suggested the possible formation of a microplasma as a result of the very rapid heating of the film at the antinodes of the optical standing wave. It was noted that the 15 ns signal was still present, but reduced in intensity by a factor of four, when the backward going beam and hence the standing wave was removed. In an attempt to establish whether or not ionization had taken place, the spectrum of the light emitted by the film was investigated.

The light emitted from the film was collected by a lens and directed into a Hilger medium quartz spectrometer. The spectrum displayed by the spectrometer was recorded on the fastest available photographic plate. This was an Ilford HP 3 plate having a sensitivity of 400 A S A.

An output energy from the ruby laser of 1 J/cm^2 was incident on metallic films having thicknesses of 200 Å. Both gold and aluminium films were irradiated but only aluminium exhibited any ionized lines.

During the recording of the spectrum a wide slit had to be employed since the light intensity was so low. This unfortunately gave a poor resolution of approximately 60 Å in the 5500 - 6500 Å range, over which most of the ionized lines were recorded. The observed lines are listed below.

WAVELENGTH (Å)	ATOMIC STATE
6335.70	Al^+
5971.94	Al^+
5867.81	Al^+
5861.53	Al^+
5853.62	Al^+
4227.98	Al^+
4227.92	Al^+
4227.86	Al^+
4227.40	Al^+
3961.52	Al
3944.06	Al
6530.20	Au
5837.39	Au

Parenthesis is used to group together those lines which may well have appeared within the recorded linewidth.

It can be seen from the list above that a number of singly ionized lines of aluminium have appeared, this is undoubtedly as a consequence of the lower ionization potential.

Using very low resolution a number of spectrograms (Fig.3.14) were taken of a 200 Å gold film irradiated by a 1 J/cm^2 laser pulse. This low resolution was achieved by using a very wide slit setting, so that the whole of the image of the illuminated area entered the instrument. From these spectrograms we were able to establish that the background of the spectrum radiated resembled that of a black body of 6000°K.

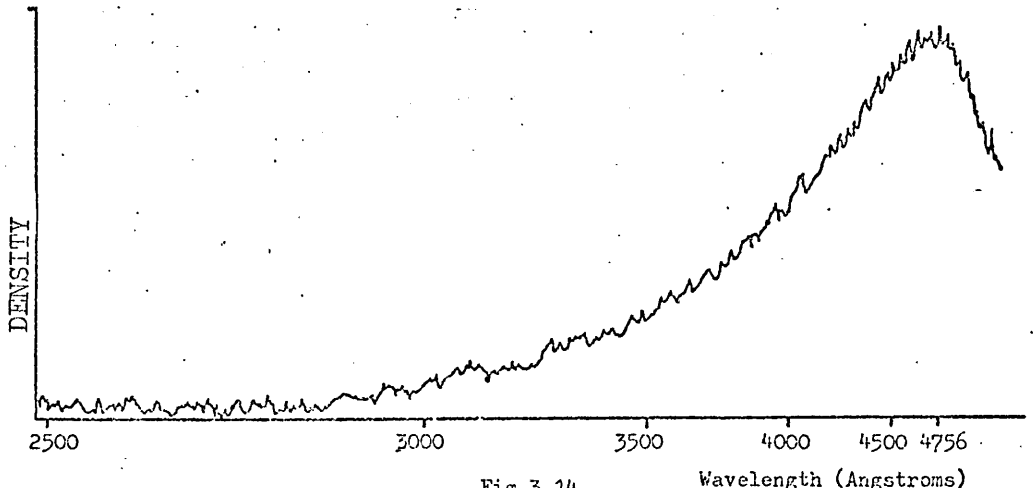

Fig.3.14

Spectrum of the light reradiated from a 200 Å gold film after having been irradiated by a 1 J/cm^2 ruby laser beam

3.9 ANGULAR DEPENDENCE OF DIFFRACTED SIGNALS

The dependence of the temporal development of the beam diffracted from the gratings, formed in a 200 Å gold film, on the angle θ between the normal to the film and the incident ruby laser beams, was studied. The rise and decay times of the slowly varying part of the signal observed with ruby laser beams of intermediate energy were found to depend strongly on this angle (Fig.3.15). Figs.3.16 and 3.17 show graphs of the rise and fall times, respectively, plotted as functions of cosecθ for the case of the transmitted diffracted beam. The straight line in both graphs was derived by using the method of weighed least squares fit[108].

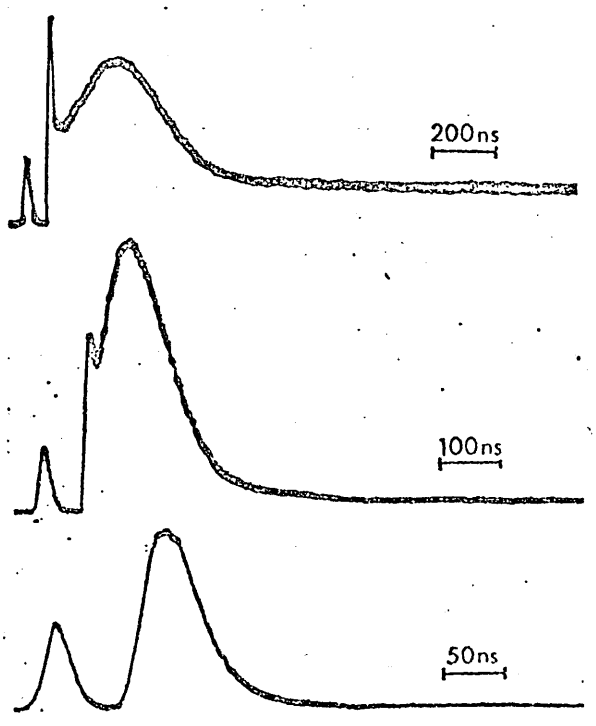

Fig.3.15
Variation of diffracted signal with angle of incidence of the ruby laser light. (Traces show ruby laser output followed by the delayed diffraction signal.) Each trace shows the transmitted signal diffracted from a 200 Å gold film illuminated by a 0.3 J/cm^2 ruby laser pulse. The angle between the ruby laser direction and the normal to the film was 2° for the top trace, 5° for the middle trace, and 16° for the bottom trace

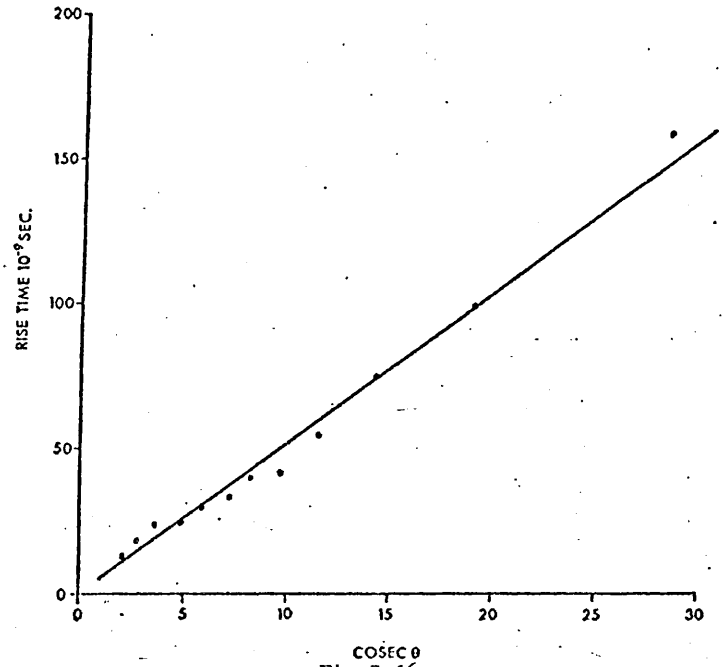

Fig.3.16

Variation of rise time (to maximum) of the diffracted signal with angle of incidence θ of the ruby laser light. (Transmitted signals diffracted from a 200 Å gold film illuminated by a 0.3 J/cm^2 ruby laser pulse.)

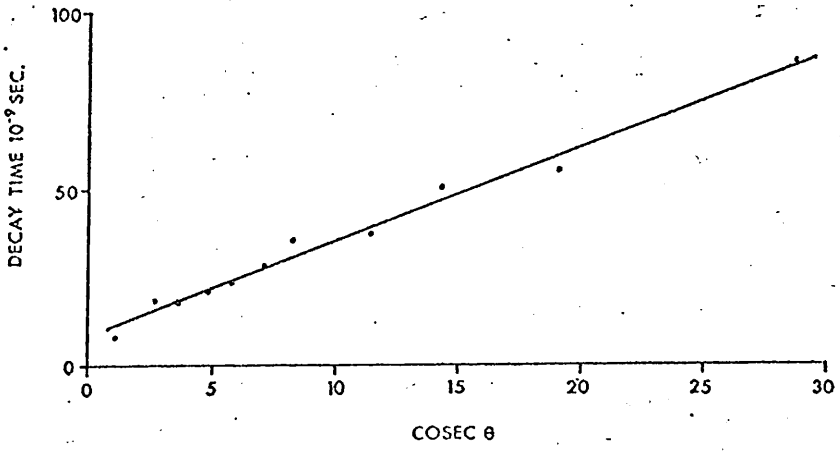

Fig.3.17

Variation of decay time (to half-intensity) of the diffracted signal with angle of incidence θ of the ruby laser light. (Transmitted signals diffracted from a 200 Å gold film illuminated by a 0.3 J/cm^2 ruby laser pulse.)

No angular dependence was observed for either of the diffracted beams reflected from the gold surface. It was also noted that the 15 ns signal, which was attributed to the radiating surface, due to the high temperature that it had attained, was also independent of the angle θ.

The angle of the probing argon ion beam was varied while the angle made by the film with the ruby laser beam was kept constant. This allowed us to establish that the probe beam angle did not in anyway affect the rise and decay times of the slowly decaying signals.

3.10 DISCUSSION OF GRATINGS FORMED AT HIGH ENERGIES

The complexity of the temporal development of the diffracted laser beam under various conditions of film excitation suggests that a number of mechanisms are involved in the formation of the gratings. This fact and the essentially destructive nature of the processes occurring within the film make quantitative analysis of the observations extremely difficult.

Many authors[18,22,26,38,108,110] have reported the formation of a microplasma when a Q switched laser pulse with an intensity of the same order of magnitude as that used in our experiments, impinges on a solid surface. The short pulse of diffracted signal observed using ruby pulses of very high energy (Fig.3.8), may be readily explained on the assumption that lines of plasma were first formed at the antinodes of the standing wave causing a strong diffracted signal. Subsequent heating at the nodes of the wave (owing to the fact that with our experimental arrangement the forward and backward ruby laser beams were never exactly equal) would, however, cause a rapid decrease in this signal by creating a uniform plasma over the whole surface. Complete removal of the film (Fig.3.13) over some part of the grating was always associated with this type of signal.

3.11 DISCUSSION OF GRATINGS FORMED AT LOW ENERGIES

The step function diffracted signals (Fig.3.9) observed using beams of very low energy, may be explained on the assumption that at such energies there was no damage to the film at the nodes of the standing wave and no plasma formation. The development of the signal was in this case caused by vapourisation of the film at the antinodes of the electric field. The remaining film caused diffraction as a result of the induced periodicity in its thickness, but the vapour, being transparent to argon ion laser light, had no effect on the diffracted signal. Hence the constant diffracted signal, once the laser pulse had formed the grating. (Gratings formed under these conditions are shown in Fig.3.12.)

3.12 DISCUSSION OF GRATINGS FORMED AT INTERMEDIATE ENERGIES

The slowly decaying signal observed at intermediate beam energies (Fig.3.10) may be interpreted as a result of the formation at such energies, of a periodically distributed plasma, rather than unionized vapour.

The rise and fall times of the slow signal were proportional to $\mathrm{cosec}\theta$, i.e. proportional to the line separation of the grating. Such a dependence would be expected if the diffraction were governed by the motion of a plasma across the surface, in which the distance to be travelled, and thus the time required to achieve any given ionic distribution, was proportional to the original line separation, i.e. the separation of the plasma clouds.

Apart from the plasma that may be produced, there also exists the question of whether or not the substrate having had a periodically heated surface will, due to the diffusion of the heat in the substrate, affect the optical path length experienced by the light. The temperature distribution of such a surface can be obtained by solving the 2-D differential heat flow equation. It can be shown that the temperature distribution is

of the form (Appendix I):

$$T(x,y,t) = T_0 \pi^{\frac{3}{2}} \sqrt{\frac{\rho_0 c_p}{KT}} \cdot \cos kx \cdot e^{-Kk^2 t/\rho_0 c_p} \cdot e^{-y^2 \rho_0 c_p / 4KT}$$

where T is the temperature as a function of position (x,y) and time t, resulting from an instantaneous periodic distribution of heat $T_0 \delta(y) \cos kx$ at the surface $y = 0$, K is the thermal conductivity, ρ_0 the density, c_p the specific heat at constant pressure, and k is the wave vector of the periodic distribution of heat.

The change in the refractive index μ for light passing through the substrate along the y-axis is

$$\Delta\mu \propto \int_0^\infty T(x,y,t)\, dy .$$

$$\therefore \quad \Delta\mu \propto \cos kx \; e^{-Kk^2 t/\rho_0 c_p}$$

which would result in a signal having a relaxation time:

$$\tau = \frac{\rho_0 c_p}{Kk^2} = \frac{\rho_0 c_p}{K} \cdot \frac{\lambda^2}{16\pi^2} \operatorname{cosec}^2\theta$$

where λ is the wavelength of the periodic distribution. Therefore the distribution of the substrate temperature, or any other parameter controlled by a diffusion law, would show a development with a characteristic time proportional to the square of that separation. This is also true of a critically damped or over-damped standing acoustic surface wave[213]. If, however, the damping is weak, then the acoustic surface wave would have a period proportional to the line spacing, but this would result in a diffracted signal whose intensity would oscillate with a period smaller than the observed decay time.

Decay of the plasma, chemical processes occurring at the surface, or any phenomenon involving transport perpendicular to the surface would on the other hand give a decay time independent of spacing.

3.12.1 Plasma Kinetics

In a plasma of temperature T the ions have velocities whose components in any given direction follows a Gaussian distribution. The median value v of this distribution is given by $v = 0.69(kT/M)^{\frac{1}{2}}$, where k is Boltzmann's constant and M the ionic mass.

Thus, if the plasma ions acquire their energy in a time τ_o, the time required for half of the ions to travel a distance of one line separation d is given by

$$\tau = \tau_o + d/v = \tau_o + 0.735\,\lambda\,(M/kT)^{\frac{1}{2}}\,\mathrm{cosec}\,\theta$$

where λ is the wavelength of the ruby laser light and θ the angle between the ruby laser beam and the normal to the film.

While the exact relationship between plasma distribution and diffraction efficiency is difficult to establish, it seems clear that any signal arising from this process would develop in a time comparable with τ.

Since gold vapour does not absorb ruby laser light, we may assume that the temperature of the plasma, when first initiated from the vapour, was about 2500°K, the boiling point of gold. The duration of the slowly developing part of the diffracted signal did not vary significantly over the range of beam energies under which the phenomenon was observable. This suggests that, at such energies, there was no significant heating by absorption of the ruby laser light in the plasma. We may therefore assume that the temperature of the plasma at intermediate beam energies was still about 2500°K. (The temperature of 6000°K mentioned in section 3.8, occurred using a ruby laser beam of much higher energy.) Given this temperature, the gradients of the graphs shown in Figs.3.16 and 3.17 are of the same order of magnitude as the gradient $0.735\,\lambda\,(M/kT)^{\frac{1}{2}}$ of τ against $\mathrm{cosec}\,\theta$ indicated by the equation above. This provides a reasonable experimental justification for assuming that the slowly varying signal

results from the creation of a microplasma at the antinodes of the standing wave of the ruby laser light.

3.12.2 Thermal Decay of the Irradiated Surface

It is worth noting that the 15 ns light signal observed by the photomultiplier viewing the metallic film and attributed to black body radiation, gives an indication of the decay time τ_T of the temperature of the film.

The spectral energy density $u(\nu)$ of a radiating black body at temperature T as a function of frequency ν is given by

$$u(\nu) = \frac{8\pi h \nu^3}{c^3} \frac{1}{e^{h\nu/kT} - 1}$$

where h is Plank's constant, c the velocity of light, and k is Boltzmann's constant.

Now $$\frac{du(\nu)}{dt} = \frac{8\pi h \nu^3}{c^3} \cdot \frac{e^{h\nu/kT} \cdot h\nu/kT^2}{(e^{h\nu/kT} - 1)^2} \cdot \frac{dT}{dt}$$

hence $$\left(u(\nu)/\frac{du(\nu)}{dt}\right) = \frac{kT}{h\nu} \left\{1 - e^{-h\nu/kT}\right\} \left(T/\frac{dT}{du}\right) .$$

Let $$\tau_T = \left(T/\frac{dT}{dt}\right)$$

and $$\tau_u = \left(u/\frac{du(\nu)}{dt}\right)$$

where τ_u is the decay time of the black body radiation.

$$\therefore \quad \tau_u = \frac{kT}{h\nu} \left\{1 - e^{-h\nu/kT}\right\} \tau_T$$

from which we obtain three separate cases:

(i) $kT < h\nu$ $\quad \therefore \quad \tau_u \approx \frac{kT}{h\nu} \cdot \tau_T$

(ii) $kT \gg h\nu$ $\quad \therefore \quad \tau_u \approx \tau_T$

(iii) $kT = h\nu$ $\quad \therefore \quad \tau_u \approx \frac{2}{3} \tau_T$.

For the situation described in the experiment where the temperature is assumed to be approximately 2500°K the quantity $\frac{kT}{h\nu} = 0.08$, indicating that $\tau_T \approx 180$ ns .

This large value for τ_T adds weight to the argument that the decay of the plasma from its ionic to neutral state is slow compared to the time it takes adjacent plasma clouds to diffuse together. This suggests, therefore, that the characteristic decay time of the slow diffracted signals is not governed by the decay of the plasma. The magnitude of τ_T needs to be interpreted with caution, since the metallic films were vapourized and therefore cannot be expected to follow the same thermal decay as a solid.

3.12.3 An Empirical Model of the Transient Gratings

In order to explain fully the experimental results observed, it is useful to establish an empirical model to describe the evolution of the gratings. First, though, let us discuss the characteristics of laser initiated plasmas.

In general laser initiated plasmas will have three components. One component will consist of electrons travelling with a velocity (10^7 cm/s) governed by the electron mass. The second component will consist of ions travelling at a much slower velocity (10^4 cm/s) and will have resulted from thermionic emission. In addition to these two obvious components, there also exists a third component consisting of electrons travelling at a speed governed by the ionic masses. This slow speed is a result of the space charge effect and has been observed by many research workers[26,111-116].

The extent of ionization due to thermionic emission is generally described by the Langmuir-Saha equation[117];

$$i_+/i_o = \left(g_+/g_o\right) \exp\left[(\Phi - I)/kT\right]$$

where i_+ and i_o are, respectively, the positive ion and neutral molecule fluxes leaving the surface at temperature T, and g_+ and g_o are, respectively, the statistical weights of the ionic and neutral states, I is the ionization potential and Φ the electron work function of the metal.

This equation was derived for equilibrium conditions and does not include collisional ionization. Collisional ionization will become increasingly important as additional kinetic energy is obtained by the electrons through the process of free-free absorption.

The equation, however, gives a reasonable estimate of the relative ionization that will result from different metals irradiated under the same conditions. By application of this equation to the conditions of the experiment, it is estimated that 1% of the total material removed from the aluminium film will undergo thermionic ionization, whereas silver and gold have much lower figures of 0.1% and 0.01% respectively. These figures are further supported by the failure of the spectrogram to record any ionized lines of the gold spectrum. It is not suggested that no ionization of the gold and silver takes place but that aluminium has an ion density much higher than that of gold and silver.

(a) Transient gratings produced from gold and silver films.

Let us now consider the process of grating formation in the case of the gold and silver films. Both metallic films exhibited the slow decaying signal on the transmitted diffraction beam (Fig.3.10) and a pulsed nature (Fig.3.8) on both the reflected beams.

Initially it is assumed that heating takes place more rapidly at the antinodes than at the nodes of the standing wave. This results in the formation of the grating as recorded by the three signals. Unfortunately the power level of the laser is higher than that required to just remove the film at the antinodes. This then leads to the complete removal of the metallic film and the subsequent decrease in the diffracted signal. The metal which was removed at the antinodes, suffers the greatest heating and so reaches a higher plasma density than that material removed from the nodes. Therefore the argon ion probe beam sees a plasma with a spatial periodicity.

Several authors have calculated the rate at which radiation of frequency ν is absorbed by electrons from free-free transitions in a plasma of electrons (number density n_e) and ions (number density n_i, with z units of proton charge) at a temperature $T^{\circ}K$. Allen[118] gives the following expression for the linear absorption coefficient in c.g.s. units:

$$k_o = \frac{4\pi e^6 n_e n_i g z^2}{3^{\frac{3}{2}} h c m^2 \nu^3} \cdot \left(\frac{2m}{\pi kT}\right)^{\frac{1}{2}} \left\{1 - \exp\left(-\frac{h\nu}{kT}\right)\right\}$$

where m is the electron mass, e the electron charge, h is Planck's constant, k is Boltzmann's constant, c is the velocity of light, and g is the Gaunt factor. The term $[1 - \exp(-h\nu/kT)]$ accounts for losses by stimulated emission and is effectively unity for $T \ll 20{,}000^{\circ}K$ where the frequency ν is in the visible region.

This gives a value for the absorption coefficient of a plasma for $T \ll 20{,}000^{\circ}K$ of

$$k_o = 3.69 \times 10^8 (z^2 n_i n_e / T^{\frac{1}{2}} \nu^3) \text{ cm}^{-1} .$$

Free-free absorption will therefore give rise to an absorption grating with a spatial period defined by the original line spacing.

This plasma grating will consist of three components as described earlier, fast electrons, slow electrons and ions. All previous observations of three component plasmas produced by laser irradiation have indicated that there are substantially fewer fast electrons than slow electrons. Also, the fast electrons travelling at such a high velocity (10^7 cm/s) will pass through the argon ion laser beam within 10 ns of being formed. Both these facts suggest that the fast electrons contribute little, if anything, to the slowly decaying diffraction signal.

The slow electrons, however, travel with a velocity governed by the ion masses. It was reported[26] by Henderson et al that the slow electrons travelled 20% faster than the ions. This small difference between the

velocity of the slow electrons and that of the ions suggests that the argon ion light will appear to be affected on a time scale governed by the ionic mass velocity.

We therefore have sitting above the surface of the substrate, a periodic density distributed plasma. The resulting grating will have a decay time comparable with the time it takes the slow electrons to travel from one high density area to the next. That is the destruction of the periodic distribution by diffusion of the plasma. This mechanism results in a decay time proportional to the line spacing $\lambda/2 . \operatorname{cosec} \theta$. It is suggested that the risetime of the slow transmitted diffraction signal is not indicative of the time required to initiate the plasma, but more likely the time required for the plasma to diffuse to the position giving maximum efficiency (i.e. changing the mark-space ratio). Again this will have a dependence proportional to the line spacing $\lambda/2 . \operatorname{cosec} \theta$.

Therefore in the case of gold and silver we observe a slow rise and decaying signal from the transmitted diffraction beam; while the reflected diffraction signal is not observed after the total removal of the metallic film. This situation is totally reversed for the aluminium films.

(b) Transient gratings produced from aluminium films

The alumiunium film like the gold and silver, will initially undergo substantial heating at the antinodes of the standing wave. This gives rise to the initial diffracted signals. Again as in the case for gold and silver, the total removal of the film will ensue due to the high power level of the ruby laser pulse. This results in a sudden decrease in the diffracted signals.

Aluminium, unlike gold and silver, has two important properties both of which dramatically affect the slow diffracted signals.

The first of these properties is that singly ionized aluminium has an absorption line at 5145.65 Å only 0.3 Å away from that of the argon ion probe beam at 5145.36 Å. Doppler broadening of the aluminium line at 2500°K will give it a linewidth at half height of 4×10^{-2} Å. A Lorentzian line with such a linewidth would be 1/100 of its maximum value at such a separation. Thus the resulting absorption will undoubtedly be comparable to or possibly larger than, the free-free absorption.

The second important property of aluminium, one that has already been mentioned, is that it has a much lower work function and ionization potential than either gold or silver. As a consequence a much higher electron and ion density will be established above the surface of the substrate. It is suggested that this high electron density produces the resulting reflected diffraction grating.

It has long been known that the transmission of an electromagnetic wave through a plasma is determined by the magnitude of a quantity called the plasma frequency f_p. If the electromagnetic wave is higher in frequency than the plasma frequency unattenuated transmission will result. If, however, the electromagnetic wave is lower in frequency than that of the plasma, then the wave will be reflected at the plasma boundary. The plasma frequency of a plasma of density N is given by[119] :

$$f_p = \frac{1}{2\pi}\left[\frac{NQ^2}{\epsilon_o m}\right]^{\frac{1}{2}} \text{Hz} ,$$

where Q is the charge of the individual particles of mass m and ϵ_o is the permittivity of free space.

There exists, therefore, two plasma frequencies, one governed by the ions and the other by the electrons. The ion plasma frequency for singly ionized aluminium is given by

$$f_i = 0.04 \times N_i^{\frac{1}{2}} \text{Hz}$$

where N_i is the ionic density per cubic metre. Under normal circumstances

the maximum value for N_i is 6×10^{28} ions/metre^3, that is the density of solid aluminium. This therefore leads to a plasma frequency of 2.4×10^{13} Hz which is much too low to affect visible light.

Electrons on the other hand have a plasma frequency f_e given by

$$f_e = 8.98 \times N_e^{\frac{1}{2}} \text{ Hz} ,$$

where N_e is the electron density per cubic metre. Reflection of visible light by the plasma is therefore possible at very high electron densities and has often been reported[120-123].

In order to explain the slow reflected diffraction signal, we assume that at the antinodes of the standing wave the plasma density is high enough (4.5×10^{27} electrons/m^3) to reflect the argon ion laser beam. This reflection will take place from the slow electrons which disperse according to the velocities of the ions. Again we will have a rise and decay time of the diffracted signals which is determined by the line spacing $\lambda/2 . \operatorname{cosec} \theta$.

The failure to record a transmitted diffraction signal suggests that either the free-free absorption and the absorption by the $A\ell^+$ ions is large at the nodes of the standing wave, which will eliminate the spatial periodic absorption; or the initial diffracted signal, produced prior to the metallic film being totally removed at the nodes, was much larger than that resulting from the periodically distributed plasma. Our results indicate that both facts possibly contribute to the lack of a slow decaying signal in the transmitted beam. In one or two cases a very small, almost indistinguishable, slow decay seems to be present in the transmitted diffraction signal.

The type of transient reflection grating described above existed for both the 50 Å and 100 Å aluminium films, although the 200 Å and 400 Å films reverted back to the original situation as described for the gold and

silver films. This has obviously occurred since the 200 Å film absorbs 50% less light than the 100 Å film, due to the higher reflectivity. Consequently the plasma density at the antinodes of the standing wave is not high enough to reflect the light.

By measuring the rise and decay times of the slowly decaying signals from the aluminium films, it was estimated that the ratio of these times to the corresponding rise and decay times detected from the gold films was 2.3:1 (gold:aluminium). However, the ratio of the velocities of the respective ions is 2.7:1. This suggests that the extent of ionization of the plasma determines to some extent the velocity of the slow electrons with respect to the ions.

3.13 CONCLUSION

The results of the experiment substantially support the phenomological model describing the formation of both transient absorption and reflection gratings. The mechanism for the absorption grating is attributed to a periodically distributed plasma, where absorption occurs from free-free transitions.

A similar periodically distributed plasma, but with a density $\geq 4.5 \times 10^{27}$ electrons/m^3 (i.e. high enough to reflect the probe beam), gives rise to the transient reflected gratings. In addition there exist two other distinct types of gratings, one formed at high laser pulse energies, the other at low laser pulse energies.

The gratings formed at high energies are extremely transient in nature, lasting for a time comparable to the duration of the laser pulse. The short lifetime of these gratings is a consequence of the high energy laser pulse, totally destroying the previously established periodic distribution.

At low energies the laser pulse has only just sufficient energy to remove by vaporization the metallic film sitting at the antinodes of the standing wave. This low energy ensures that the film at the nodes is not removed. We are therefore left with a very efficient grating, the efficiency of which increases with increasing film thickness. These low energy type gratings are established in a time comparable to the rise time of the laser pulse, after which they exhibit characteristics that are independent of time.

CHAPTER IV

STIMULATED SCATTERING OF LIGHT IN LIQUID MEDIA

4.1 INTRODUCTION

The first experiments reporting the observation of stimulated scattering[92,94,95,124-129], involved the use of focused laser beams to obtain the high intensities required to generate the stimulated process from the random fluctuations of the medium. Unfortunately with the discovery of self focusing[39], which requires similar power densities to those required to initiate stimulated scattering, the results previously obtained had to be reinterpreted.

One technique employed by experimentalists to overcome the inadequacies of the previous experiments was to use an amplifier. This involved combining the frequency unshifted laser light with an attenuated portion of the frequency shifted backward going light in a cell containing the liquid under investigation. The frequency shifted light is produced by focusing the laser beam into a cell (known as the generator cell) containing the same liquid as in the amplifier, Fig.4.1. If the backward going beam (signal) has an intensity much smaller than the forward going

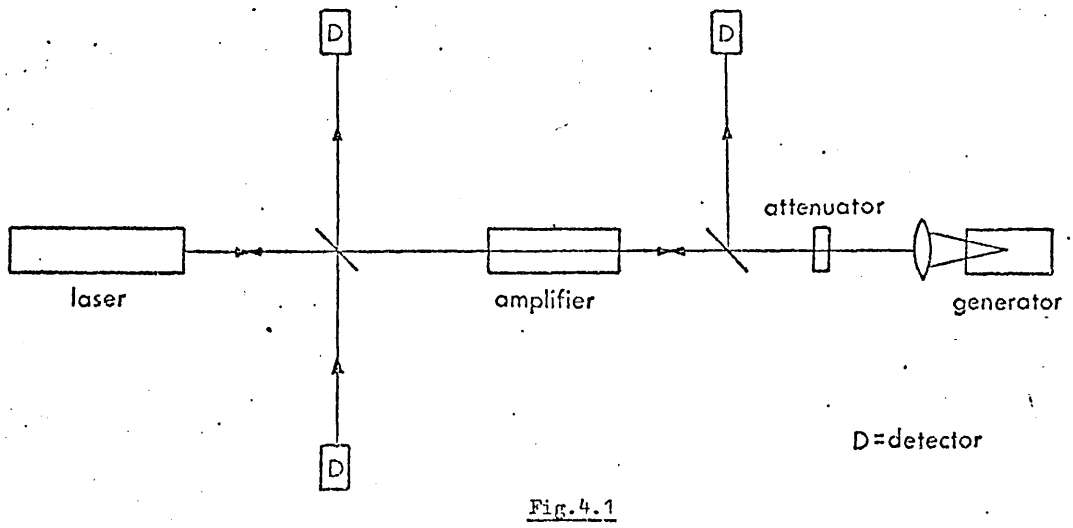

Fig.4.1
Weak amplification of light generated by stimulated scattering in a separate cell

beam (pump) then amplification of the weaker beam will result at the expense of the laser beam, much in the same way as in a parametric amplifier.

It should be noted that there exists no threshold in amplifier experiments, although sufficient power densities are still required to produce the frequency shifted beam in the generator cell.

This technique allowed Denariez and Bret[93] to make the first reliable measurements of the spatial gain associated with stimulated Brillouin and Rayleigh-Wing scattering in liquids, where self-focusing has a very low threshold.

By employing different liquids in the generator to produce a variety of frequency shifts, the amplifier technique enables one to investigate the frequency gain profile of the stimulated scattering process. From a knowledge of the frequency gain profile thus obtained, a measure of the life-time of stimulated scattering processes can be deduced. This technique was successfully used by Pohl et al[130] to investigate the frequency dependence of the gain factor of a number of liquids. The frequency shifts were obtained by varying the concentration of a mixture of two liquids in the generator cell. This produced frequencies shifted from the central frequency of the scattering process by an amount as small as 20 MHz.

Unfortunately 'Q' switched lasers do tend to produce a significant amount of frequency drift. This is typically of the order of 200 MHz across a 20 ns ruby laser pulse[130.131]. Therefore, in order to alleviate any ill effect this might have on the gain measurements, the amplifier and generator cells need to be kept close together.

The chirping effect can in certain circumstances be usefully employed in investigating stimulated Rayleigh scattering. In this

instance the generator cell is replaced by a mirror and placed the appropriate distance away from the amplifier cell, to produce the required frequency shift[130]. As mentioned above a measure of the relaxation time of the scattering process can be deduced from the frequency dependence of the gain profile. This, though, has experimentally two disadvantages: first the presence of the inherent frequency drift of the laser pulse and secondly, the fact that from shot-to-shot the laser pulse profile will change, thus changing the effective gain.

One obvious way around the second problem is to measure the absolute maximum gain factor, knowledge of which allows a direct calculation of the lifetime of the scattering process. Although this technique requires only a single laser pulse to determine the relaxation time, it does rely significantly on the validity of the stimulated scattering theory. It also requires accurate knowledge of the spatial intensity distribution across the laser beam. This situation can be rectified by probing the disturbed medium with an independent laser beam.

The combination of the two light beams, in the medium in which stimulated scattering is taking place, gives rise to a spatial periodicity in refractive index constituting a phase grating. This phase grating is being driven at the difference frequency of the two light beams and has a lifetime characteristic of the particular stimulated scattering process. If a third light beam, of higher frequency and with an intensity low enough not to produce any nonlinear effects, is incident at the Bragg angle, then the intensity of the beam reflected from the grating will indicate the magnitude of the disturbance in the amplifier cell. Also, by recording the temporal duration of the reflected probe beam, a direct measure of the lifetime of the disturbance produced in the medium can be measured, Fig. 4.2.

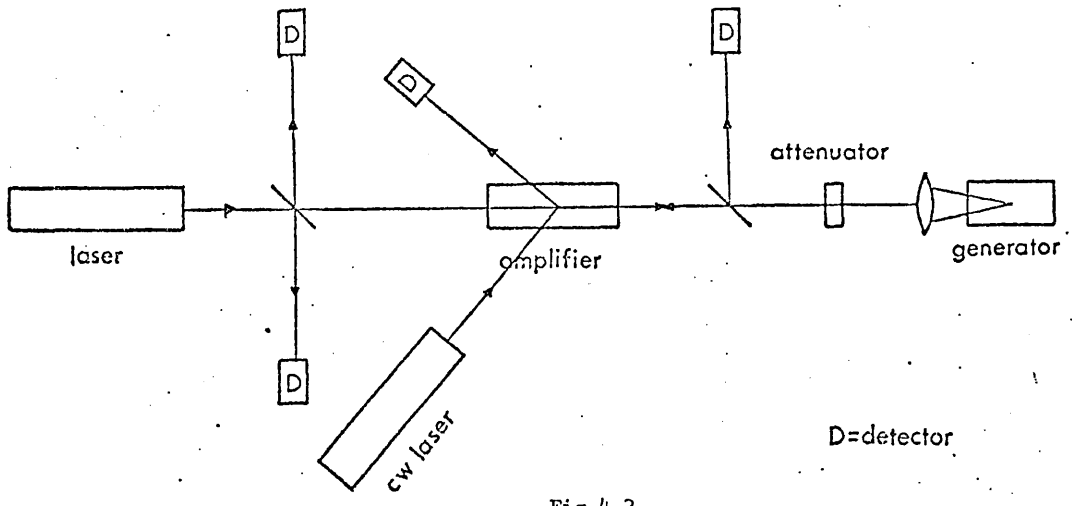

Fig.4.2
Bragg reflection technique for probing an amplifier cell, in a light scattering experiment

Giordmaine and Kaiser[132] in 1966 were the first to employ the Bragg reflection technique to study a stimulated scattering process. They generated lattice vibrations in a calcite sample by use of a 'Q' switched ruby laser. At the same time the excited region of the crystal was illuminated by a frequency doubled portion of the ruby pulse, the probe being of sufficiently low intensity to produce no stimulated Raman scattering. They observed the reflected probe beam to have satisfied the phase matching conditions, and also noted that the Raman scattered light was linear in probe intensity. This effect was predicted by Garmire, Pandarese and Townes[133] and further discussed by Tang[134].

A year later Boersch and Eichler[104] using a similar technique, probed the optical standing wave inside an optically pumped ruby laser. The spatial modulation in the population of the ground and excited state in the ruby crystal was detected by the diffraction of a second light wave from a pulsed argon ion laser. The time necessary for the spatial distribution to decay after the ruby pulse had finished was measured to be 5×10^{-4} s.

The first report of Bragg scattering from a stimulated Brillouin process was made in 1967 by Walder and Tang[135]. Here they generated a hypersonic wave in quartz and detected the disturbance by means of Bragg

diffraction of a probing He-Ne beam at different points in the fused quartz, to estimate the attenuation constant of the 24 GHz sound wave. In 1968 Winterling and Hunick[136] used a delayed portion of the main ruby laser pulse to probe the acoustic wave created by the main laser pulse and determined the phonon lifetime in a quartz crystal at low temperatures.

Later in the same year using the Bragg reflection technique, Harrison et al[137] observed a phase grating in a saturable dye absorber which was 'Q' switching a ruby laser. The same authors later extended this work and made a comprehensive study of the nonlinear optical effects in liquids by the use of the Bragg reflection technique[106,138-141].

4.2 A REVIEW OF THE AMPLIFIER THEORY

The simplicity of the amplifier experiments enabled many authors to theoretically analyse the experimental situation[141-151]. In particular, a number of authors discussed the theory of stimulated Brillouin scattering (SBS) in transparent media. This scattering had resulted from the electrostrictive coupling between the electromagnetic wave and the medium. Up until 1967 only the electrocaloric effect had been suggested as a coupling mechanism for stimulated Rayleigh scattering. The very weakness of the coupling made the observation of stimulated Rayleigh scattering difficult. The first reported observation of stimulated Rayleigh scattering in a transparent liquid was made by Zaitsev et al[95] in 1967. In the same year Herman and Gray[97] suggested absorptive heating as a coupling mechanism. They also introduced the hydrodynamic and heat conduction equations which, together with the nonlinear wave equation, gave a general description of stimulated Brillouin and Rayleigh scattering in transparent and absorbing media. In these equations the additional term due to absorptive heating was included, which gave rise to a strong

anti-Stokes Rayleigh term (stimulated thermal Rayleigh scattering (STRS)) and also modified the Brillouin components (stimulated thermal Brillouin scattering (STBS)).

The steady state solution of the hydrodynamic equations has been derived, for the amplifier situation, by many authors[97,141,146,149,150-153]. From these solutions a description of the modulation of temperature and density within the scattering medium have been obtained, in addition to the frequency-gain profile of the amplifier. The stimulated scattering gain for the steady state regime as a function of frequency is shown in Fig.1.1(b), both for transparent and absorbing media.

The time dependent solution of the differential equations describing the stimulated scattering process has been obtained by a number of different approaches. In 1970 Pohl and Kaiser[154] investigated transient stimulated Brillouin scattering in transparent and absorbing media. They obtained the solution of the differential equations for the transient case by expanding the functions describing the temperature, density and signal amplitude in terms of a power series. From these solutions they were able to show that if the difference in frequency $(\omega_p - \omega_s)$ between the pump and signal waves was not equal to the Brillouin frequency ω_B then the resulting gain would be modulated. This modulation would decay in time and have a frequency $\Delta\omega$ defined by $\Delta\omega = \omega_B - (\omega_p - \omega_s)$, i.e. the mismatch frequency. Using the same method, Rangnekar and Enns[155], the following year, extended the theory to include the second order term of the power series. They showed that the extension was necessary in order to calculate the gain which occurs, for short pulses, when both the pump and signal waves have the same frequency. (This effect had previously been calculated by Rother et al[156].) Additional oscillatory terms were also predicted for both the frequency and time dependent gain of the stimulated thermal Brillouin scattering.

In 1970 Rother[157] also solved the differential equations describing the stimulated scattering of light. His solution was obtained by means of a Fourier transformation. Unfortunately, in his solution, the time-dependent amplification of the signal amplitude is described by a complicated integrodifferential equation. In order to solve this equation analytically for the case of a step function and Gaussian input signal, he introduced a power series and separated out the contributions to the spectrum from the three distinct regions, i.e. the Rayleigh line and Brillouin doublet. His results were therefore similar to those of Pohl et al and Rangnekar et al. Rother did, however, discuss in addition the angular dependence of stimulated scattering, and predicted the appearance of transient induced diffraction effects at small scattering angles.

The solution of the scattering equations for transient stimulated thermal Rayleigh scattering valid for all times and gains, has been obtained by Enns[158]. By use of a suitable transformation, he obtained an analytical solution for the particular case of a constant pump signal and a step function type signal. Unfortunately the final expression is far from simple and involves many terms.

Much more recently Bambini, Vallauri and Zoppi[159] have derived an analytical solution for the signal amplitude. The solution describes the transient behaviour at all frequency differences between the pump and the signal waves. In their derivation they considered a time independent pump wave and a step function signal wave. The solution of the differential equations is obtained by means of a Laplace transformation and subsequent residue calculus.

In this chapter a new approach is used to obtain the time dependent stimulated gain profile. It will be shown that by suitable convolutions this profile can be directly obtained from the steady state results.

4.3 THE STIMULATED SCATTERING EQUATIONS AND THE STEADY STATE SOLUTION

The propagation of an electromagnetic wave E in a medium with a varying dielectric constant, is described by the nonlinear Maxwell wave equation[58]:

$$\nabla^2 E - \frac{n_o^2}{c^2} \frac{\partial^2 E}{\partial t^2} = \frac{1}{c^2} \frac{\partial^2 (\Delta \epsilon . E)}{\partial t^2} \qquad \ldots (4.1)$$

where n_o is the refractive index of the undisturbed medium (owing to dispersion the refractive index for terms of frequencies ω_s will be n_s and for terms of frequency ω_p, n_p), c is the velocity of light, t the time and $\Delta\epsilon$ the variation of the dielectric constant within the medium.

If we apply this equation to the amplifier situation where we have a signal wave of amplitude A_s travelling in the z-direction and a pump wave of amplitude A_p travelling in the opposite direction, then we obtain, for the small signal approximation[139,140], the expression

$$\frac{\partial A_s}{\partial z} = \frac{k_s}{4n_s^2} A_p \epsilon'' \qquad \ldots (4.2)$$

where k_s is the wavevector of the signal, and ϵ'' is the amplitude of that part of the dielectric constant which is one quarter period out of phase with the component of E^2 producing it.

It can be shown[139,140], in the steady state regime, that ϵ'' is proportional to $A_s A_p$. Therefore, provided $A_s \ll A_p$, A_p is almost constant and the forward travelling signal beam undergoes an exponential spatial amplification of intensity, with gain coefficient $G(\omega)$, where

$$G = \frac{k_s}{2n_s^2} \left[\frac{A_p}{A_s} \epsilon'' \right] . \qquad \ldots (4.3)$$

Therefore we need to describe the modulation of the dielectric constant produced by the two light beams, in order to calculate the gain experienced by such a signal.

The variation of the dielectric constant of a medium responsible for stimulated Rayleigh and Brillouin scattering is related to changes $\Delta\rho$ in the density, and ΔT in the temperature, by the equation

$$\Delta\epsilon = \left(\frac{\partial\epsilon}{\partial\rho}\right)_T \Delta\rho + \left(\frac{\partial\epsilon}{\partial T}\right)_\rho \Delta T \quad . \qquad \ldots (4.4)$$

Solving for $\Delta\epsilon$ therefore requires a knowledge of the variation of temperature and density within the scattering medium. The linearised hydrodynamic and conduction equations describing the density ρ and temperature T of a medium which is being driven by electrostriction, absorption and the electrocaloric effect, are given by[99]:

$$\frac{\partial^2\rho}{\partial t^2} - \frac{v^2}{\gamma}\nabla^2\rho - \frac{\eta + \frac{4}{3}\eta'}{\rho_o}\cdot\frac{\partial\nabla^2\rho}{\partial t} - \frac{v^2\beta\rho_o}{\gamma}\nabla^2 T = -\left(\frac{Y}{8\pi}\right)\nabla^2 E^2 \qquad \ldots (4.5)$$

and

$$\rho_o C_v \frac{\partial T}{\partial t} - K\nabla^2 T - \frac{C_v(\gamma-1)}{\beta}\frac{\partial\rho}{\partial t} = \frac{1}{4\pi} nc\alpha E^2 + \frac{T_o}{8\pi}\left(\frac{\partial\epsilon}{\partial T}\right)_\rho \frac{\partial E^2}{\partial t} \qquad \ldots (4.6)$$

where ρ_o and T_o are the density and temperature respectively of the unperturbed medium, v is the adiabatic velocity of sound, η and η' the shear and bulk viscosities, β the coefficient of thermal expansion, K the themal conductivity, C_v the specific heat capacity at constant volume, γ the ratio of the principal specific heat capacities, α the light absorption coefficient, Y the electrostrictive constant $\rho(\partial\epsilon/\partial\rho)_T$, n the refractive index of the unperturbed medium and c is the velocity of light.

Since these equations are linear, $\Delta\rho$ and ΔT will be driven at the same frequency and have the same wavevector as the driving force. The driving force is of course electrostriction, absorptive heating and the electrocaloric effect , all of which are proportional to E^2 (E, the total electric field, is the sum of the fields of the two light waves, so E^2 contains a term at the difference frequency).

To represent the solution of these equations for that component of E^2 with frequency $\omega = \omega_p - \omega_s$, wavevector $k = k_p + k_s$, and amplitude $A_p A_s$

it is convenient to define:

$$\text{the Brillouin frequency, } \omega_B = kv$$

$$\text{the Brillouin linewidth, } \Gamma_B = (\eta + \tfrac{4}{3}\eta')\frac{k^2}{\rho_o}$$

$$\text{the Rayleigh linewidth, } \Gamma_R = \frac{2Kk^2}{\rho_o c_p}$$

and also a dimensionless coefficient proportional to absorption

$$A = \frac{4n c \alpha \beta v^2}{Y \gamma c_p \Gamma_R}$$

where c_p is the specific heat capacity at constant pressure. Hence it may be shown[141] that for most liquids, where $\Gamma_R \ll \Gamma_B \ll \omega_B$ and

$$\left(\frac{\partial \epsilon}{\partial T}\right)_\rho \Big/ \beta Y \ll 1$$

$$\epsilon'' = \frac{Y^2 A_p A_s}{8\pi \rho_o v^2} \left\{ \begin{array}{ll} \underline{\text{Electrostrictive Terms}} & \underline{\text{Absorptive Terms}} \\ + \dfrac{\omega_B}{\Gamma_B}\,[F_1] & - \dfrac{A\gamma^2\Gamma_R^2}{4\omega_B\Gamma_B}\,[F_1] \\ + \dfrac{\gamma-1}{2}\left[\dfrac{\Gamma_B}{2\Gamma_B}\cdot F_{2R}\right] & - \dfrac{A\gamma}{2}\left[\dfrac{\Gamma_R}{2\Gamma_B}\,F_{2R}\right] \\ + \dfrac{\gamma-1}{4}\cdot\dfrac{\Gamma_R}{\Gamma_B}\,[F_{2B}] & - \dfrac{A\gamma}{4}\,\dfrac{\Gamma_R}{\Gamma_B}\,[F_{2B}] \end{array} \right\} \quad (4.7)$$

where each term in square brackets is a function of ω with a maximum of unity. The antisymmetric functions F_1, F_{2R} and F_{2B}, illustrated graphically in Fig.4.3, are defined as:

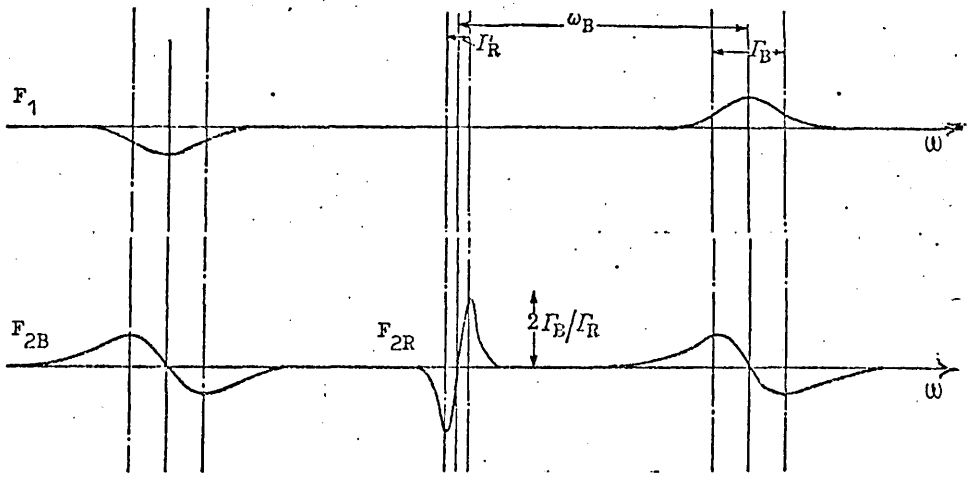

Fig.4.3
The frequency profile governing steady state stimulated scattering in hydrodynamic media

$$F_1 = \frac{(\Gamma_B^2/\omega_B^2)\ (\omega/\omega_B)}{\left(1-\omega^2/\omega_B^2\right)^2 + \left(\Gamma_B\omega/\omega_B^2\right)^2} \qquad \ldots (4.8)$$

$$F_{2R} = \frac{2\Gamma_B}{\Gamma_R} \cdot \frac{4\omega/\Gamma_R}{1+4\omega^2/\Gamma_R^2} \qquad \ldots (4.9)$$

$$F_{2B} = \frac{2\left(1-\omega^2/\omega_B^2\right)\left(\Gamma_B/\omega_B\right)\left(\omega_B/\omega\right)}{\left(1-\omega^2/\omega_B^2\right)^2 + \left(\Gamma_B\omega/\omega_B^2\right)^2} \; . \qquad \ldots (4.10)$$

These functions represent respectively the frequency profile usually associated with stimulated Brillouin, stimulated thermal Rayleigh and stimulated thermal Brillouin scattering.

For media such as fused silica or water at 4°C, where the condition $(\partial\epsilon/\partial T)_\rho/\beta Y \ll 1$ does not hold, the above equations for ϵ'' should then include electrocaloric terms. In the region of stimulated Rayleigh scattering ϵ'' is then approximately given by the expression

$$\epsilon'' = \frac{Y^2 A_p A_s}{8\pi\rho_o v^2} \left\{ \begin{array}{l} \dfrac{\gamma-1}{2} + \dfrac{\gamma^2}{4}\dfrac{\Gamma_R\Gamma_B}{\omega_B^2} - \dfrac{A\gamma}{2} \\ + \dfrac{A\gamma}{2} \cdot \left\{\left(\dfrac{\partial\epsilon}{\partial T}\right)_\rho \Big/ \beta Y\right\} \\ - \dfrac{(\gamma-1)}{2} \cdot \left\{\left(\dfrac{\partial\epsilon}{\partial T}\right)_\rho / \beta Y\right\}^2 \end{array} \right\} \cdot \left[\frac{\Gamma_R}{2\Gamma_B} F_{2R}\right] \qquad \ldots (4.11)$$

We may therefore insert the equations (4.7) and (4.11) describing ϵ'' into equation (4.3) to obtain an expression for the gain coefficient in the steady state regime.

4.4 THE TIME DEPENDENT STIMULATED SCATTERING THEORY

4.4.1 Modulation of the Dielectric Constant

Consider two electromagnetic waves E_s and E_p travelling in opposite directions inside a liquid amplifier cell. Let us define the electric field of the forward travelling beam as:

$$E_s = \frac{1}{2}\left[A_s e^{i(k_s z - \omega_s t)} + A_s^* e^{-i(k_s z - \omega_s t)}\right] \quad \ldots (4.12)$$

and the backward going beam as:-

$$E_p = \frac{1}{2}\left[A_p e^{i(-k_p z - \omega_p t)} + A_p^* e^{-i(-k_p z - \omega_p t)}\right] \quad \ldots (4.13)$$

The total electric field experienced by the scattering medium will therefore be the superposition of these two fields, i.e.

$$E = E_s + E_p = \frac{1}{2}\left[A_s e^{i(k_s z - \omega_s t)} + A_p e^{i(-k_p z - \omega_p t)} + \text{c.c.}\right] \quad \ldots (4.14)$$

(c.c. = complex conjugate)

and

$$E^2 = \frac{1}{4}\left[A_s A_p^* e^{i(kz + \omega t)} + A_s^* A_p e^{-i(kz + \omega t)} + \text{terms of other frequencies} + \text{d.c. term}\right] \quad \ldots (4.15)$$

where $k = k_s + k_p$

$\omega = \omega_p - \omega_s$.

Since the hydrodynamic and heat conduction equations describing the scattering medium are linear, $\Delta\epsilon$ will be driven at the same frequency and have the same wavevector as the driving force. The driving force is of course electrostriction, absorptive heating and the electrocaloric effect all of which are proportional to E^2. The electric intensity will, therefore, modulate the dielectric constant such that:-

$$\Delta\epsilon = \frac{1}{2}\left[\epsilon\, e^{i(kz + \omega t)} + \epsilon^* e^{-i(kz + \omega t)}\right] . \quad \ldots (4.16)$$

In the steady state regime where A_s and A_p are independent of time it can be shown that:

$$\epsilon = \sigma(\omega)\, A_s A_p^* \quad , \qquad \epsilon^* = \sigma^*(\omega)\, A_s^* A_p$$

where $\sigma(\omega)$ and $\sigma^*(\omega)$ are functions describing the frequency shift of the amplitude of the modulation of the dielectric constant.

If, however, A_s and A_p are time dependent, we may write

$$A_s A_p^* = \int_{-\infty}^{+\infty} a(\Omega)\, e^{i\Omega t}\, d\Omega \qquad \ldots (4.17)$$

and

$$A_s^* A_p = \int_{-\infty}^{+\infty} a^*(\Omega)\, e^{-i\Omega t}\, d\Omega \qquad \ldots (4.18)$$

where a is a function of position z and frequency Ω but not time t.

Hence

$$E^2 = \frac{1}{2} \int_{-\infty}^{+\infty} a\, e^{i(kz + (\omega+\Omega)t)}\, d\Omega + \frac{1}{2} \int_{-\infty}^{+\infty} a^*\, e^{-i(kz + (\omega+\Omega)t)}\, d\Omega \quad . \qquad \ldots (4.19)$$

Each term of E^2 will give rise to a modulation of the dielectric constant with the appropriate frequency and amplitude.

$$\therefore \quad \Delta\epsilon = \frac{e}{2}^{i(kz + \omega t)} \int_{-\infty}^{+\infty} a\sigma_{(\omega+\Omega)}\, e^{i\Omega t}\, d\Omega + \frac{e}{2}^{-i(kz + \omega t)} \int_{-\infty}^{+\infty} a^*\sigma^*_{(\omega+\Omega)}\, e^{-i\Omega t}\, d\Omega \quad . \qquad \ldots (4.20)$$

The integrals of $\Delta\epsilon$ are basically Fourier transforms. Now the Fourier transform of the product of two functions is equal to the convolution of the Fourier transform of the two terms taken separately, i.e.

$$\widehat{f\,g} = \hat{f} * \hat{g}$$

where $\hat{f}$ denotes a Fourier transform and $f * g$ denotes a convolution.

$$\therefore \quad \Delta\epsilon = \frac{e}{2}^{i(kz + \omega t)} \left[\left\{ \int_{-\infty}^{+\infty} \sigma_{(\omega+\Omega)}\, e^{i\Omega t}\, d\Omega \right\} * \int_{-\infty}^{+\infty} a(\Omega)\, e^{i\Omega t}\, d\Omega \right] + \frac{e}{2}^{-i(kz + \omega t)} \left[\left\{ \int_{-\infty}^{\infty} \sigma^*_{(\omega+\Omega)}\, e^{-i\Omega t}\, d\Omega \right\} * \int_{-\infty}^{\infty} a^*(\Omega)\, e^{-i\Omega t}\, d\Omega \right] \qquad \ldots (4.21)$$

or

$$\Delta\epsilon = \frac{e}{2}^{i(kz + \omega t)} \left[\hat{\sigma}_{(\omega+\Omega)} * (A_s A_p^*) \right] + \frac{e}{2}^{-i(kz + \omega t)} \left[\hat{\sigma}^*_{(\omega+\Omega)} * (A_s^* A_p) \right] \qquad \ldots (4.22)$$

By suitable substitution we obtain

$$\Delta\epsilon = \frac{e}{2}^{i(kz + \omega t)} \left[(e^{-i\omega t} \widehat{\sigma_{(\Omega)}}) * (A_s A_p^*) \right]$$

$$+ \frac{e}{2}^{-i(kz + \omega t)} \left[(e^{i\omega t} \widehat{\sigma^*_{(\Omega)}}) * (A_s^* A_p) \right] \qquad \ldots (4.23)$$

This expression describes the temporal and spatial development of the magnitude $\Delta\epsilon$ of the modulation of dielectric constant for various values of the frequency difference between the two beams.

4.4.2 The Spatial Intensity Gain of the Signal

The spatial and temporal variation of the amplitude A_s of a small signal travelling within an amplifier is described by the nonlinear wave equation. By inserting the functions describing E and $\Delta\epsilon$ into the wave equation and equating coefficients we get:

$$\frac{dA_s}{dz} = \frac{iA_p \epsilon \omega_s}{4nc} \quad , \qquad \frac{dA_s^*}{dz} = -\frac{iA_p^* \epsilon^* \omega_s}{4nc}$$

$$\frac{dA_p}{dz} = -\frac{iA_s \epsilon^* \omega_p}{4nc} \quad , \qquad \frac{dA_p^*}{dz} = \frac{iA_s^* \epsilon \omega_p}{4nc} \qquad \ldots (4.24)$$

The intensity gain of a signal A_s is described by:

$$\frac{d}{dz}(A_s A_s^*) = A_s^* \frac{dA_s}{dz} + A_s \frac{dA_s^*}{dz}$$

$$\therefore \quad \frac{d}{dz}(A_s A_s^*) = \frac{i\omega_s}{4nc} \left[A_s^* A_p \epsilon - A_s A_p^* \epsilon^* \right] . \qquad \ldots (4.25)$$

In the steady state regime

$$\epsilon = \sigma(\omega) A_s A_p^*$$

$$\epsilon^* = \sigma^*(\omega) A_s^* A_p$$

$$\therefore \quad \frac{d(A_s A_s^*)}{dz} = \frac{i\omega_s}{4nc} \left[\sigma(\omega) - \sigma^*(\omega) \right] A_s A_s^* A_p A_p^* \qquad \ldots (4.26)$$

The dielectric constant can be defined by:-

$$\Delta\epsilon = \epsilon' \cos(kz + \omega t) + \epsilon'' \sin(kz + \omega t) \qquad \ldots (4.27)$$

as is the case in the previous section (4.3), with the steady state solution

where ϵ' and ϵ'' are the amplitude of that part of the modulated dielectric constant in phase and one quarter period out of phase respectively, with that component of E^2 which has the same frequency and wavevector as the modulation.

It can be shown that

$$\epsilon = \epsilon' - i\epsilon'' \qquad \text{similarly} \qquad \sigma = \sigma' - i\sigma''$$
$$\epsilon^* = \epsilon' + i\epsilon'' \qquad\qquad\qquad\quad \sigma^* = \sigma' + i\sigma''$$

where $\sigma' = \epsilon'/A_s A_p$

$\sigma'' = \epsilon''/A_s A_p$

$$\therefore \quad \frac{1}{A_s A_s} \frac{d(A_s A_s)}{dz} = \frac{\omega_s \sigma''}{2cn} A_p A_p \qquad \ldots (4.27)$$

and the corresponding gain factor G is given by

$$G = \frac{\omega_s}{2cn} \left[\epsilon'' \frac{A_p}{A_s} \right] \qquad \ldots (4.28)$$

i.e. the steady state gain coefficient, cf. equation (4.3).

4.5 THEORETICAL PREDICTIONS

To calculate the variation of the intensity of the signal with position, frequency and time, we need to determine the functions ϵ and ϵ^*. In determining these functions it is convenient to consider separately the two distinct scattering regions, i.e. Brillouin and Rayleigh. By doing this we can approximate the steady state frequency profiles $\sigma(\omega)$ and $\sigma^*(\omega)$ to Lorentzian functions and so obtain the Fourier transforms of these functions.

Throughout the analysis we have considered a step function type signal wave of small amplitude A_s travelling in the z-direction and an intense time independent pump wave of amplitude A_p travelling in the opposite direction. The weak electrocaloric term has been ignored and it is assumed that $\omega_B \gg \Gamma_B \gg \Gamma_R$.

We have, therefore, two terms contributing to scattering in the Brillouin region ($\omega \simeq \omega_B$), they are electrostriction and absorption, while in the Rayleigh region ($\omega \simeq 0$) only the strong absorptive term is retained.

4.5.1 Transient Stimulated Brillouin Scattering In Absorbing and Non-Absorbing Liquids

Let us restrict ourselves to the case where A_p and A_s are totally real. This condition is the same as assuming that the effect of the medium on the signal is of the first order.

$$\therefore \quad \frac{d(A_s A_s)}{dz} = \frac{\omega_s A_p^2 A_s}{2nc} \left[\left\{ \sin\omega t \cdot \hat{\sigma}(\Omega) \right\} * A_s \right] \qquad \ldots (4.29)$$

It can be shown that $\hat{\sigma}(\Omega)$ is given by:-

$$\hat{\sigma}(\Omega) = \frac{Y^2 \omega_B}{8\pi v^2 \rho_o} \left[\left(\sin\omega_B t + \mu \cos\omega_B t \right) e^{-t\Gamma_B/2} - \mu\, e^{-t\Gamma_R/2} \right] \qquad \ldots (4.30)$$

where $\mu = \dfrac{\gamma A \Gamma_R}{2\omega_B}$.

$$\therefore \frac{d(A_s A_s)}{dz} = A_s \cdot g(\omega_B, \infty) I_p \frac{\Gamma_B}{2} \left[\left\{ \sin\omega t \sin\omega_B t + \mu \sin\omega t \cos\omega_B t \right\} e^{-t\Gamma_B/2} - \mu \sin\omega t\, e^{-t\Gamma_R/2} \right\} * A_s \Big] \qquad \ldots (4.31)$$

where $g(\omega_B, \infty)$ is the steady state gain factor and is given by:

$$g(\omega_B, \infty) = \frac{\omega_s Y^2 \omega_B}{2c^2 n^2 v^2 \rho_o \Gamma_B}$$

$$I_p = \frac{nc}{8\pi} A_p^2 \ .$$

If we define the transient gain factor as $G(\omega, t)$ where the variation of the signal intensity is given by:

$$I_s = I_{s(z=0,\, t=0)}\, e^{G(\omega, t) z I_p}$$

then

$$\frac{G(\omega\simeq\omega_B,t)}{g(\omega_B,\infty)} = \frac{\Gamma_B}{2}\left[\frac{\Gamma_{B/2}+\mu\omega_-}{\Gamma_{B/4}^2+\omega_-^2}\left\{1-\left[\cos\omega_- t+\frac{(\mu\Gamma_{B/2}-\omega_-)}{(\Gamma_{B/2}+\mu\omega_-)}\sin\omega_- t\right]e^{-\Gamma_B t/2}\right\}\right.$$

$$+\frac{\mu\omega_+-\Gamma_{B/2}}{\Gamma_{B/4}^2+\omega_+^2}\left\{1-\left[\cos\omega_+ t+\frac{(\mu\Gamma_{B/2}+\omega_+)}{(\mu\omega_+-\Gamma_{B/2})}\sin\omega_+ t\right]e^{-\Gamma_B t/2}\right\}$$

$$\left.-\frac{2\omega\mu}{\Gamma_{R/4}^2+\omega^2}\left\{1-\left[\cos\omega t+\frac{\Gamma_R}{2\omega}\sin\omega t\right]e^{-t\Gamma_R/2}\right\}\right] \qquad \ldots (4.32)$$

where $\omega_\pm = \omega \pm \omega_B$.

When $\omega \simeq \omega_B$ the last two terms in the above equation are small and modify the first term with frequency $2\omega_B$ and ω_B. In fact, if we consider a non-absorbing liquid ($\mu = 0$) such as CCl_4, then the second term only modifies the first by 4%. If on the other hand we consider an absorbing liquid with $\mu = 1$, which for coloured CCl_4 represents an absorption coefficient of 0.25 cm^{-1}, then the second term will modify the first term by 4%, while the third term represents a much larger modification of 15%.

It should also be noted that the coefficient $\Gamma_R/2\omega$ of the sine in the last term is small and so we have a pure cosine oscillation decaying slowly with a characteristic time $2/\Gamma_R$. Therefore true steady state conditions are not reached under these circumstances until $t \gg 2/\Gamma_R$. It has been shown by Rangnekar and Enns[155] that the oscillations are only present when the rise time of the signal pulse is less than $1/\omega_B$, for CCl_4 $1/\omega_B \simeq 40$ ps, and so the oscillations would only be present with mode locked pulses.

The first term of the function $G(\omega\simeq\omega_B,t)/g(\omega_B,\infty)$ is plotted against time and frequency in Figs.4.4 - 4.7 for both non-absorbing and absorbing liquids. Dimensionless units are used to make the curves applicable to almost any liquid.

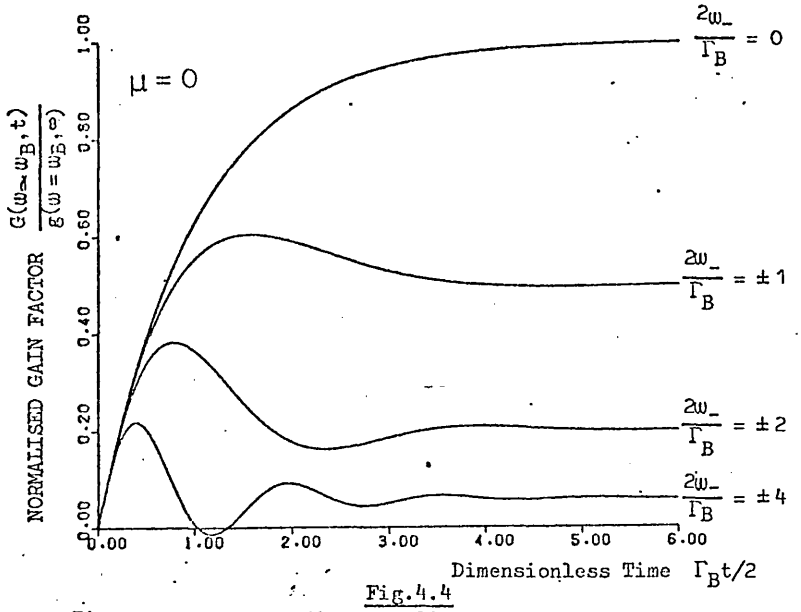

Fig.4.4

Time dependence of the normalised SBS gain factor for various frequency shifts ω_- after the arrival of a step-function type signal

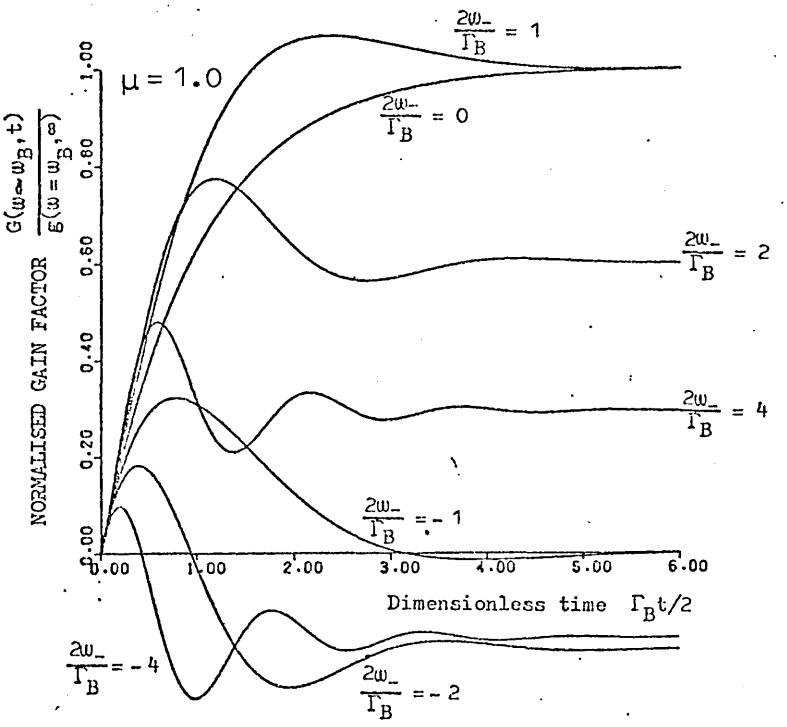

Fig.4.5

Time dependence of the normalised STBS gain factor for various frequency shifts ω_- after the arrival of a step-function type signal

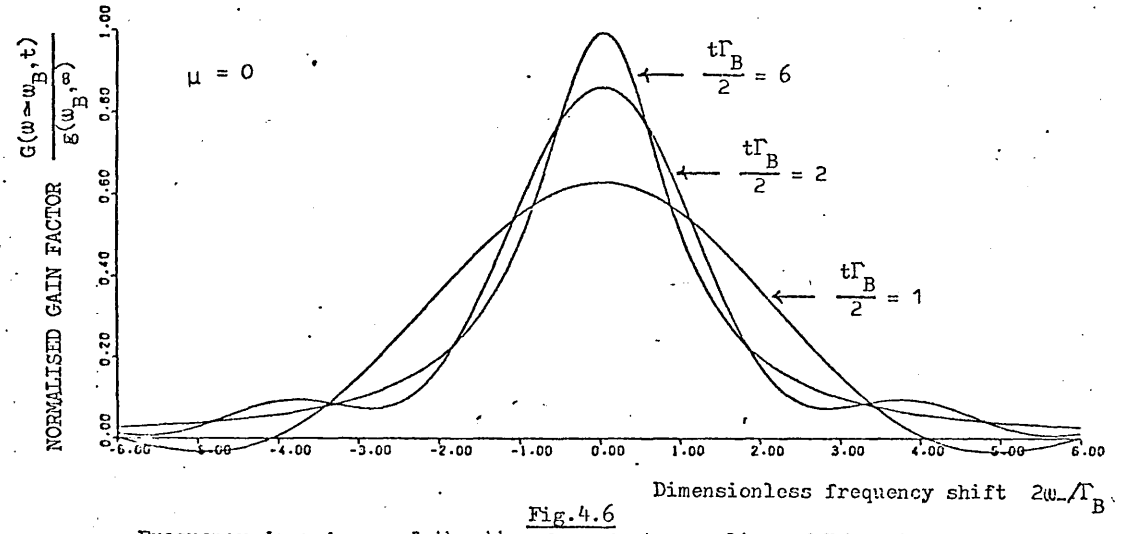

Fig.4.6

Frequency dependence of the time dependent normalised SBS gain factor at various times t after the arrival of a step-function type signal

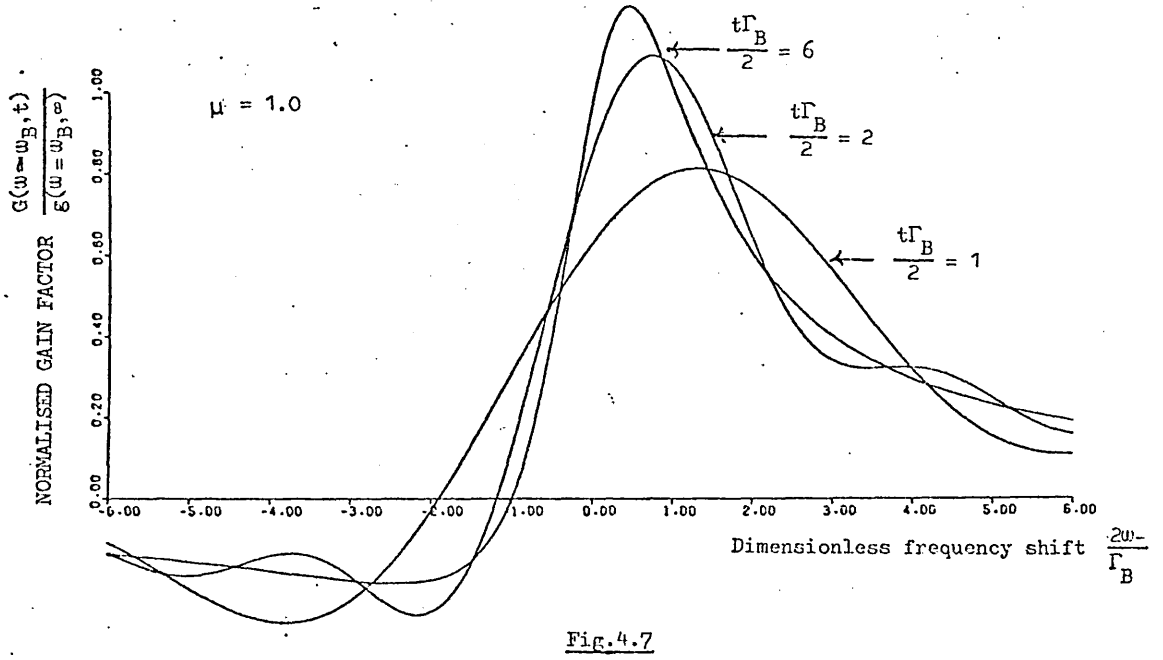

Fig.4.7

Frequency dependence of the time dependent normalised STBS gain factor at various times t after the arrival of a step-function type signal

It is clearly seen in Figs.4.6 and 4.7 that the gain profile sharpens up with increasing time, reaching the steady state width when $t > 6.2/\Gamma_B$.

4.5.2 Transient Stimulated Thermal Rayleigh Scattering

It can clearly be seen from the previous analysis that if $\omega = 0$ then the gain factor is zero (cf. equation (4.29)). We have, however, made the assumption that the effect of the medium on the signal is of the first order. If this assumption is removed then it can be shown that I_s undergoes amplification for short pulses.

Now from equation (4.24)

$$\frac{dA_s(z,t)}{dz} = ig\left(-\frac{\Gamma_R}{2}, \infty\right) I_p \frac{\Gamma_R}{2}\left[\left\{e^{-i\omega t} e^{-t\Gamma_R/2}\right\} * A_s\right] \quad \ldots (4.33)$$

where $A_s(z,t)$ is complex and $g(-\Gamma_R/2, \infty)$ is the steady state Rayleigh gain factor and is given by:

$$g\left(-\frac{\Gamma_R}{2}, \infty\right) = \frac{\omega_s Y^2 A \gamma}{4c^2 n^2 v^2 \rho_o}$$

To solve the above equation it is convenient to introduce

$$A_s(z,t) = \bar{A}_s(z,t)\, e^{i\psi(z,t)}$$

where $\bar{A}_s(z,t)$ represents the absolute magnitude of the signal amplitude and $\psi(z,t)$ the phase.

Inserting $\bar{A}_s(z,t)e^{i\psi(z,t)}$ into equation (4.33) and equating coefficients of the real and imaginary parts we have:

$$\frac{d\bar{A}_s}{dz} = -g\left(-\frac{\Gamma_R}{2}, \infty\right) I_p \frac{\Gamma_R}{2} \int_0^t \bar{A}_s(t')\left\{\sin\Delta\psi \cos\omega\Delta t - \cos\Delta\psi \sin\omega\Delta t\right\} e^{-\Delta t\, \Gamma_R/2}\, dt'$$

$$\ldots (4.34)$$

$$\frac{\bar{A}_s\, d\psi(z,t)}{dz} = g\left(-\frac{\Gamma_R}{2}, \infty\right) I_p \cdot \frac{\Gamma_R}{2} \int_0^t \bar{A}_s(t')\left\{\cos\Delta\psi \cos\omega\Delta t + \sin\Delta\psi \sin\omega\Delta t\right\} e^{-\Delta t\, \Gamma_R/2}\, dt'$$

where $\Delta\psi = \psi(z,t') - \psi(z,t)$ $\quad \ldots (4.35)$

$\Delta t = t - t'$.

If $\omega = 0$ then the term $\frac{d\bar{A}_s}{dz}$ will only be non-zero when the phase varies with time.

For small amplification the above equations can be solved analytically to give:-

$$\psi(z,\omega,t) = -\frac{g(-\Gamma_R/2,\infty)}{\left[\Gamma_R^2/4 + \omega^2\right]} I_p z \frac{\Gamma_R}{2}\left[\frac{\Gamma_R}{2} - e^{-t\Gamma_R/2}\left\{\frac{\Gamma_R}{2}\cos\omega t - \omega \sin \omega t\right\}\right] \quad \ldots (4.36)$$

This function is displayed graphically in Fig.4.8 for various frequency shifts about $\omega = 0$. The curves indicate very little change in $\psi(z,\omega,t)$ when $t > 6.2/\Gamma_R$ which is of the order 50 - 100 ns for most liquids.

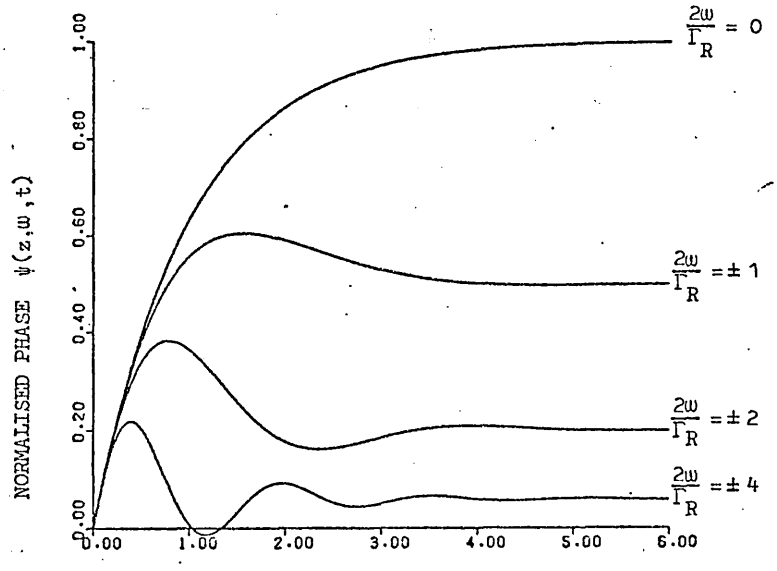

Fig.4.8
Time dependence of the normalised phase for various frequency shifts ω after the arrival of a step-function type signal with $g(-\Gamma_R/2,\infty)\, I_p z = 1.0$

The transient gain can now be obtained by inserting the above expression for $\psi(z,\omega,t)$ into the equation

$$\frac{d(A_s A_s^*)}{dz} = ig\left(-\frac{\Gamma_R}{2},\infty\right) \cdot \frac{\Gamma_R}{2}\left[A_s^*\left\{e^{-\Gamma_R t/2} * A_s\right\} - A_s\left\{e^{-\Gamma_R t/2} * A_s^*\right\}\right] \cdot I_p \quad \ldots (4.37)$$

Solving this for $\omega = 0$ we have:

$$G(\omega = 0, t) = g^2\left(-\frac{\Gamma_R}{2},\infty\right) z\, I_p\left[e^{-t\Gamma_R} - e^{-t\Gamma_R/2}\left(1 - \frac{\Gamma_R t}{2}\right)\right] \quad \ldots (4.38)$$

The equation for $d(A_s A_s^*)/dz$ has also been solved analytically for $\omega \neq 0$ but due to the numerous terms involved, the resulting function is omitted.

The transient gain profile $G(\omega \simeq 0,t)$ is plotted against frequency and time in Figs.4.9 and 4.10 for a value of $g(-\frac{\Gamma_R}{2},\infty)\, z\, I_p = 0.5$. Although it is not strikingly obvious from Fig.4.6, the gain profile does not have equal maxima when $\omega > 0$ and $\omega < 0$. This arises since $G(\omega \approx 0,t)$ contains odd and even terms of ω, in fact the magnitude of the even terms are determined by $g(-\Gamma_R/2,\infty)\, z\, I_p$. Hence with increasing absorption the even terms become more important.

In addition to Fig.4.9 and 4.10 which describe the transient gain profile $G(\omega \simeq 0,t)$ a 3-D surface is displayed in Fig.4.11 which depicts the function $G(\omega \simeq 0,t)$ for ω and t, between $\omega = -6.\Gamma_{R/2} \longrightarrow \omega = 6.\Gamma_{R/2}$ and $t = 0 \longrightarrow t = 6.2/\Gamma_R$. The axes are the corners of the box containing the whole surface and not the origin.

4.6 DISCUSSION

In order to observe the oscillating transient gain, an abrupt input signal is required which has a rise time short compared to $1/\omega_m$ where ω_m is the frequency of the modulation of the gain factor. This fact has precluded the experimental observation of oscillations of SBS with frequency $2\omega_B$ and oscillations of STBS with frequencies $2\omega_B$ and ω_B. To observe these frequencies an input signal with a rise time of less than 40ps would be required[155]. Unfortunately it is experimentally difficult to produce a Brillouin frequency shifted signal with a duration of 40ps. The production of such a signal inside a generator cell is impossible since strong competition exists between the Brillouin and Raman processes, which results in the preclusion of a Brillouin shifted component when the rise time of the laser pulse is less than $2/\Gamma_B$ [160]. This is equal to 0.3 - 2ns for most liquids

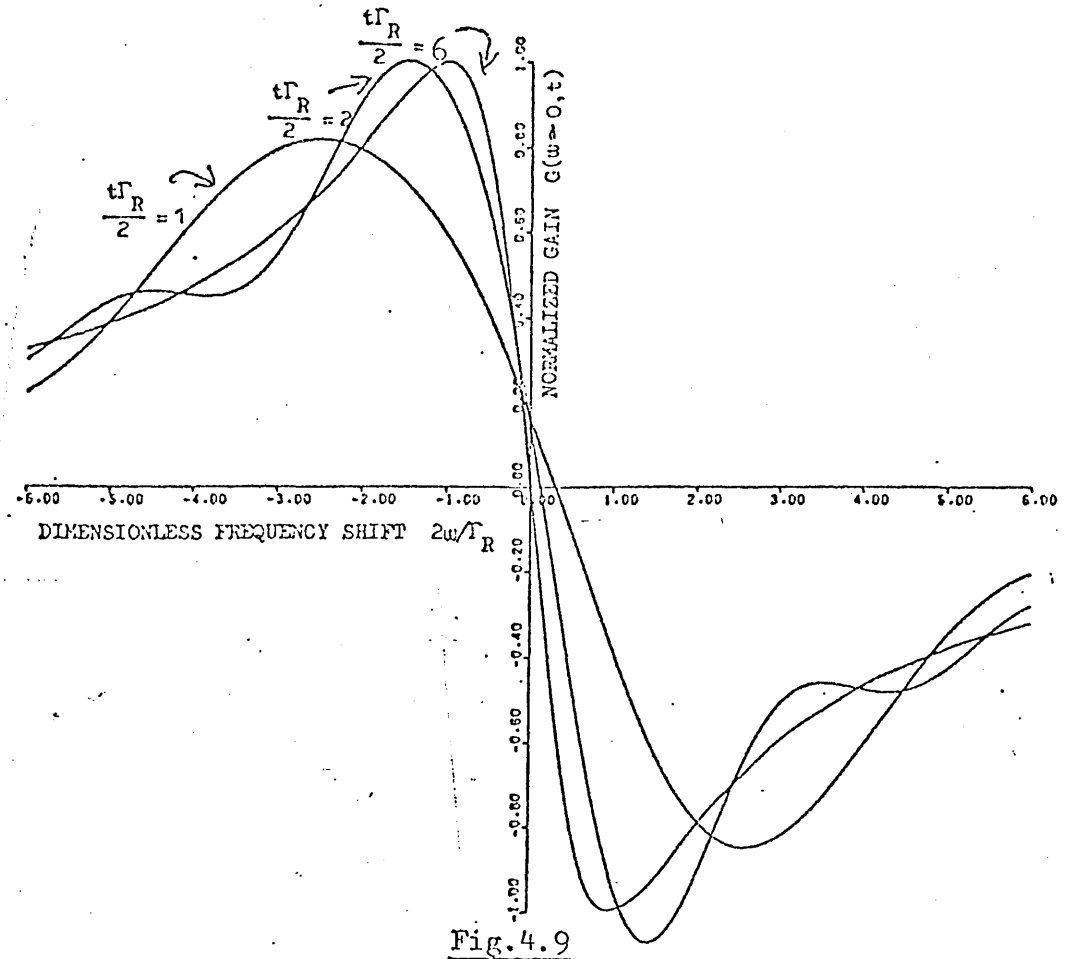

Fig.4.9

Frequency dependence of the time dependent normalised STRS gain factor at various times t after the arrival of a step-function type signal with $g(-\Gamma_R/2,\omega)\ I_p z = 0.5$

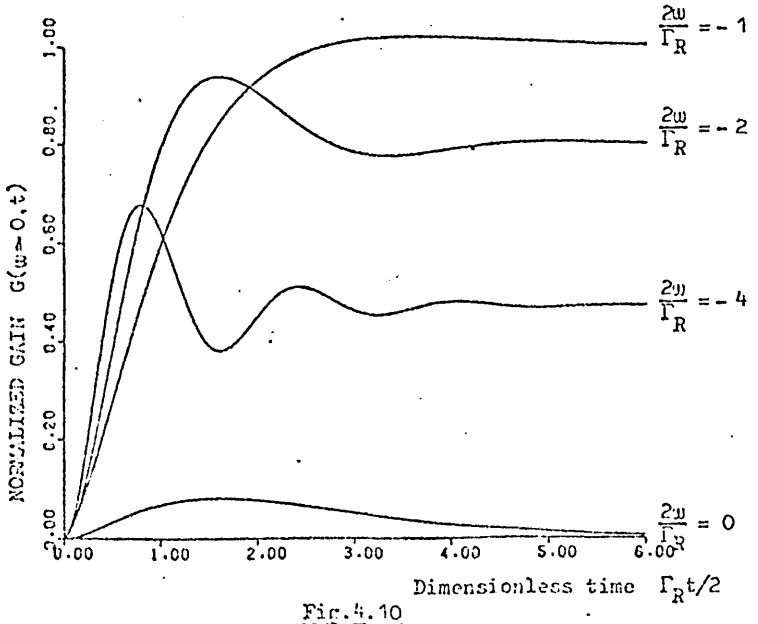

Fig.4.10

Time dependence of the normalised STRS gain factor for various frequency shifts ω after the arrival of a step-function type signal with $g(-\Gamma_R/2,\omega)\ I_p z = 0.5$

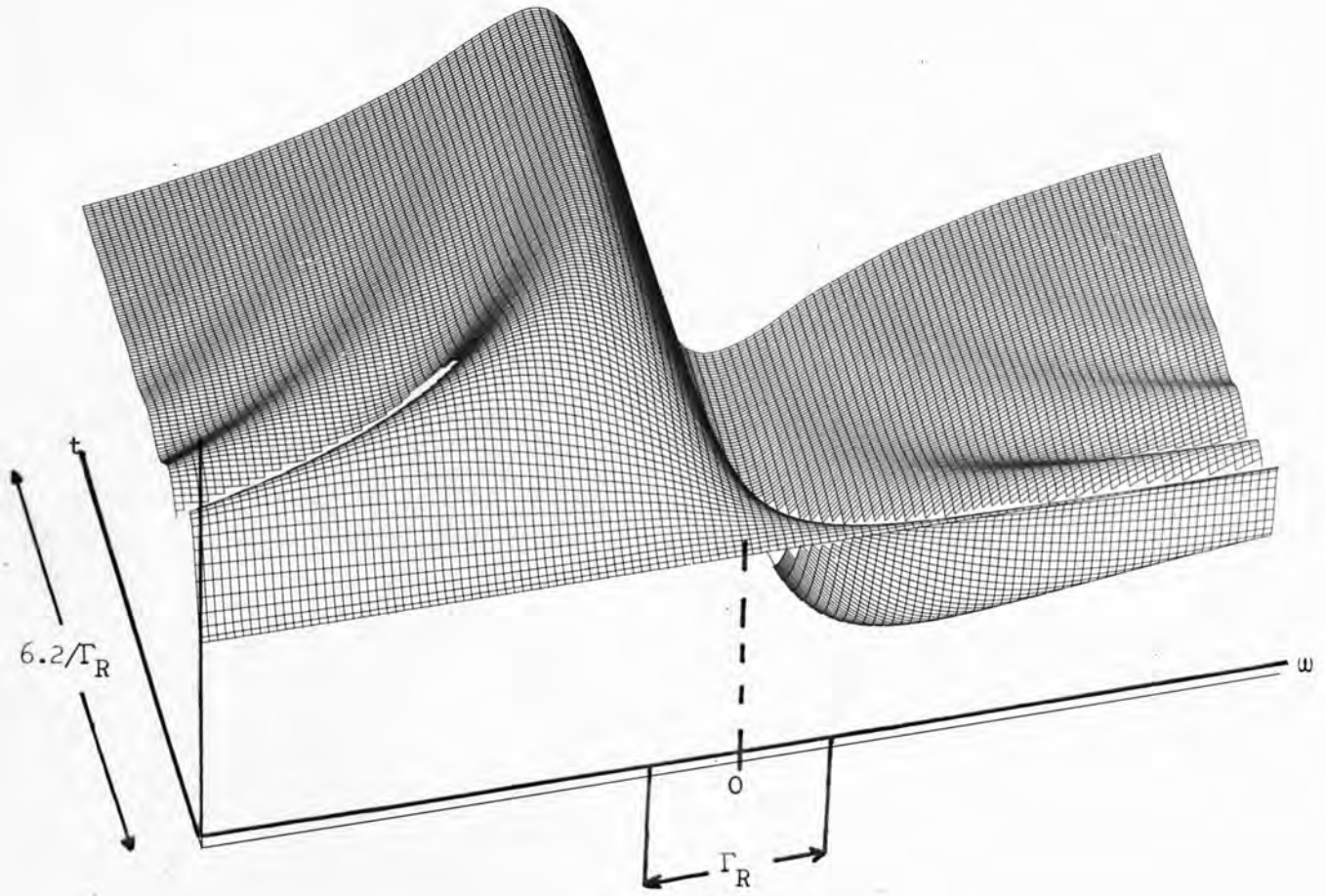

Fig.4.11

A 3-D illustration of the time-dependent STRS gain factor $G(\omega \simeq 0, t)$ The input light signal is a step function and $g(-\Gamma_R/2, \infty)$ $I_p z = 0.5$.

The experimental observation of oscillations of the much smaller mismatch frequency ($\omega_- \equiv \omega - \omega_B$) has, however, been achieved[154]. Observations of the gain at $\omega = 0$ and measurement of the time required for the gain to reach the steady state condition have been made and the results agree closely with the transient theory[154,156,130].

CHAPTER V

A MODE LOCKED RING LASER

5.1 MODE LOCKING

The output of a 'free running' laser will, in general, consists of a number of uncorrelated spikes. In the case of the ruby laser these spikes will be approximately 1 μs in duration and last for a few milliseconds. If the laser cavity contains no mode selecting device apart from the Fabry-Perot configuration of the cavity, then the spectral output will consist of numerous modes of different frequencies. The intensity of the light in each mode is defined by the gain profile of the laser and different modes will attain their peaks at different times, i.e. an independent phase relationship exists between adjacent modes. The frequency separation of these axial modes is $c/2L$, where c is the velocity of light, and L is the optical path length between the two mirrors forming the laser cavity. A 'Q' switch inserted into such a cavity will have the affect of preferentially selecting those modes positioned nearest the centre of the gain profile. Complete mode selection may be achieved by also inserting into the cavity a Fabry-Perot etalon. The temporal output of a strongly 'Q' switched laser will consist of only one smooth pulse, the smoothness of this pulse reflects the mode selectivity of the 'Q' switch. Such pulses are, for solid state lasers, typically a few tens of nanoseconds in duration and have peak powers of a few megawatts.

In order to attain the shortest pulse it is necessary to employ as wide a spectrum as possible. This means that all the axial modes within the gain profile of the laser would be required to oscillate, but unlike the case of the free running laser we require each mode to have some fixed phase relationship between adjacent modes.

To illustrate the effect this has on the temporal profile of the output pulse, let us undertake a Fourier summation over $2N+1$ modes. For

simplicity we shall assume that all modes are of equal amplitude E_0 and that the phase difference between adjacent modes is equal to φ.

The total electric field $E(t)$ at any point can be written as:

$$E(t) = \sum_{k=-N}^{N} E_0 \exp i \left[(\omega_0 + k\omega)t + k\varphi\right]$$

where ω_0 is the centre frequency, and ω is the difference frequency between adjacent modes, i.e. $\omega = \pi c/L$.

The summation can be carried out with the result

$$E(t) = A(t) \exp (i \omega_0 t)$$

where

$$A(t) = \frac{E_0 \sin \left[\frac{1}{2}(2N+1)(\omega t + \varphi)\right]}{\sin \left[\frac{1}{2}(\omega t + \varphi)\right]} .$$

Therefore $E(t)$ consists of a sinusoidal carrier of frequency ω_0 whose intensity changes in time and is proportional to $A^2(t)$; Fig.5.1 illustrates the result for a large number of modes.

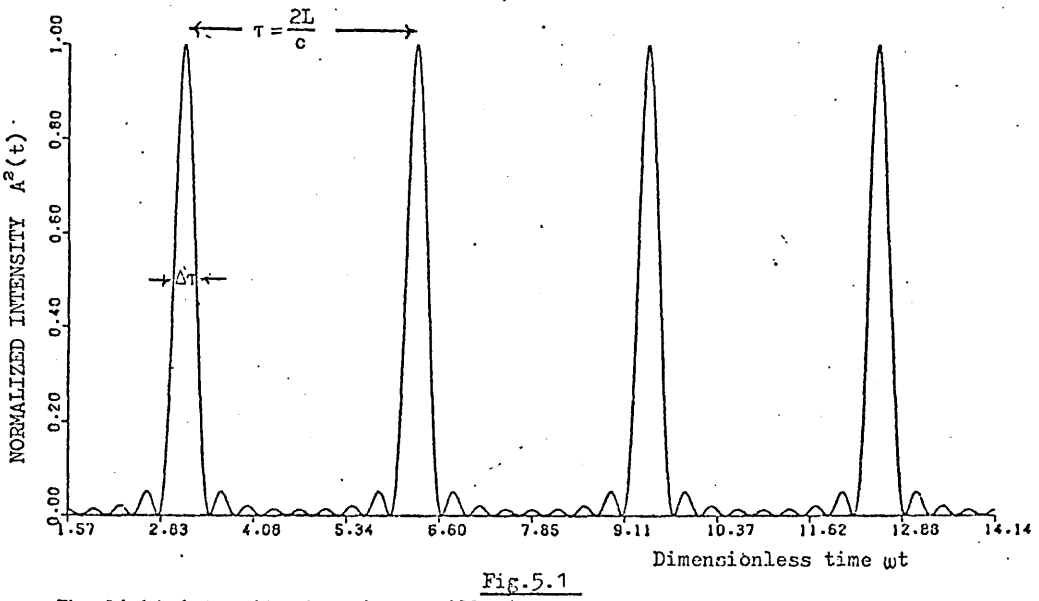

Fig.5.1

The light intensity for nine oscillating modes of equal amplitude and locked phases, where $\Delta\tau = 4\pi/(2N+1)\omega$ and is the width of the pulses at half height

The pulse maxima occur when the denominator of the expression for $A(t)$ vanishes. Successive pulses are thus separated by $\tau = 2L/c$, which is the round trip time of the laser cavity. The width of the individual pulses is inversely proportional to the width $\Delta\omega$ of the excited frequency

spectrum. For a fixed length cavity this is, therefore, inversely proportional to the number of excited modes. For the situation described above, the peak intensity is proportional to $(2N+1)^2E_0^2$, whereas, for random phases the intensity would have been the sum of the intensities in the modes, i.e. proportional to $(2N+1)E_0^2$.

A laser maintaining a constant frequency spacing of the axial modes and well defined mode phases is said to be mode locked.

For solid state lasers there can be $10^3 - 10^4$ modes all existing under a total bandwidth of up to 1000 GHz. This results in powers in excess of a gigawatt and with pulses as short as 1ps.

The methods of achieving mode locking fall into two basic categories, these are:

(i) Active mode locking; (ii) Passive mode locking.

5.1.1 Active Mode Locking

In this method an electro-optic modulator such as a Pockel cell is inserted into the laser cavity and driven by some external signal at a frequency ω. If an electromagnetic wave of frequency ω_0, travelling inside the laser cavity, passes through the modulator, then the sum $(\omega_0 + \omega)$ and difference $(\omega_0 - \omega)$ frequencies of the electromagnetic wave will be created. Since the laser cavity is a feedback device, the electromagnetic wave with its additional sidebands will again pass through the modulator and suffer further frequency modulation, i.e. $\omega_0 + 2\omega$, $\omega_0 + \omega$, ω_0, $\omega_0 - \omega$, $\omega_0 - 2\omega$ frequency components, will be created. This process will continue, coupling numerous frequency modes together all of which are separated from their adjacent modes by a frequency shift ω. A well defined phase shift will also be created between adjacent modes, but this will not be maintained unless we ensure that the light wave stays in phase with the modulator when travelling up and down the cavity. To satisfy this condition we

have the familiar expression $\omega = \frac{\pi c}{L}$ and if this is maintained then we are left with a completely mode locked train of frequency modes.

5.1.2 Passive Mode Locking

To understand the mechanism by which passive mode locking is achieved it is easier to discuss the temporal development of the pulse rather than the spectral output. In this method of mode locking, a saturable absorber is inserted inside the cavity. The transmission characteristics of such an absorber are displayed for different intensity pulses in Fig.5.2.

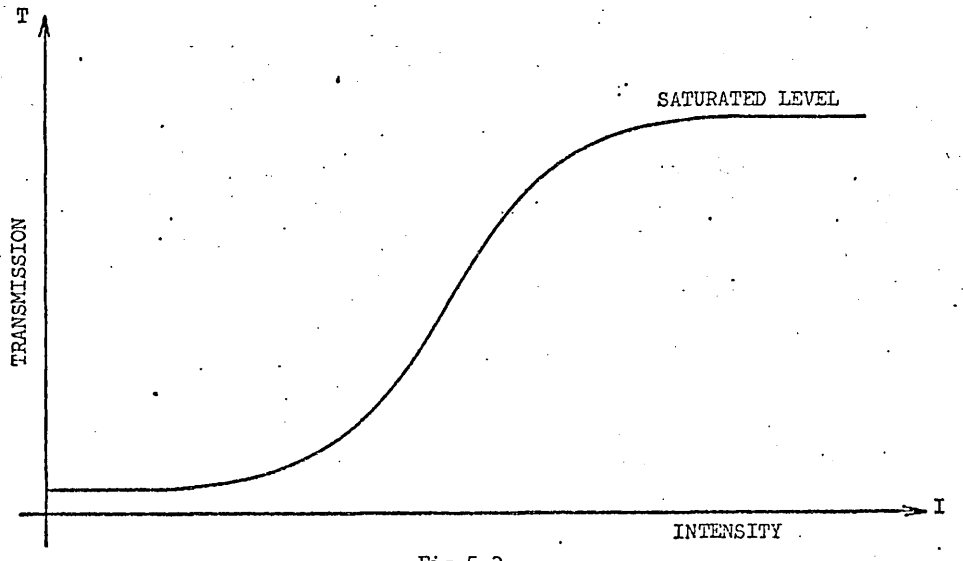

Fig.5.2
The transmission characteristics of a typical saturable absorber for light pulses of incident intensity I

The saturable absorber has the effect of discriminating between light pulses of different intensity, transmitting those of highest intensity with least loss. Since lasing action generally starts from optical noise, the saturable absorber has, therefore, the effect of preferentially transmitting the largest noise spikes. These spikes will subsequently be amplified by the active medium and again pass through the saturable absorber where the largest spikes will be allowed to develop fastest. Continuation of this process will result in a single pulse travelling up and down the cavity. It should be noted, though, that the rise and decay time of the saturable absorber needs to be short compared to the round trip time of the cavity.

The output from the laser will, therefore, consist of a series of pulses separated by the cavity round trip time. The Fourier transform of such a train of pulses is of course a train of frequency modes locked together and separated by frequencies $\omega = \frac{\pi c}{L} . n$ where $n = 1,2,3,\ldots,$.

This method of mode locking is generally the accepted way of mode locking pulsed lasers, since it requires very little apparatus and is relatively simple compared to the active mode locking method.

It should be noted that in practice, when either active or passive mode-locking is employed, additional conditions need to be met in order to obtain good mode locked pulses. These additional conditions include the elimination of all mode selecting elements, the correct positioning of the modulator and choosing a modulator sufficiently thin compared to the duration of the required output pulses.

The elimination of mode selecting elements is achieved by ensuring that most if not all the optical surfaces within the laser cavity are Brewster angled. If a saturable absorber is positioned at a point within the laser cavity other than either end, then there will be a tendency for at least two pulses to exist per cavity round trip time. These two pulses develop in such a way, so as to arrive at the saturable absorber at the same time, but from opposite directions. Arriving at the saturable absorber at the same time ensures that they both suffer the lowest possible attenuation, since together they will reduce the optical density of the saturable absorber more than if they acted independently. A single pulse per round trip time can, however, be obtained by placing the saturable absorber close to one end of the cavity, this ensures that the two pulses are effectively the same pulse.

5.2 REVIEW OF EARLY WORK

One of the first papers on the theory of mode-locking was published in 1964 by Di Domenico[161]. He predicted that modulating the internal losses of a laser at a frequency equal to some multiple of the axial mode spacing, causes all axial modes to couple with a well defined amplitude and phase. A year earlier, Tang et al[162] had discussed the spiking behaviour of solid state lasers and the locking together of frequency modes. Tang et al[162] were, however, more interested in discussing high power single mode operation lasers than pursuing the consequences of mode locking.

The first successful attempts at mode locking came in 1964, with Hargrove et al[163] locking the axial modes of a continuous He-Ne gas laser operating on the 6328 Å line. They obtained 2.5ns pulses by internally modulating the laser with a block of fused quartz vibrating under the influence of a transducer.

In 1965 Deutsch[164] successfully mode locked the output of a pulsed ruby laser. He inserted inside the cavity a KDP (potassium dihydrogen phosphate) Pockel cell and was able to obtain pulses as short as 1ns .

In practice most active modulators have at best a rise time of approximately 1ns , corresponding to a bandwidth of a few GHz. This bandwidth represents only a small fraction of the available bandwidth of a solid state laser, indicating that active modulators are not taking full advantage of the potential of the laser.

This state of affairs was relieved by the introduction of passive modulators for mode locking lasers. These generally employ organic dyes which have relaxation times of a few tens of picoseconds or less.

Mocker and Collins[165] were the first to employ a passive modulator to mode lock a laser. They inserted inside the cavity a cell containing

cryptocyanine dissolved in methanol. This dye had previously been used as a 'Q' switch and was found to act as an efficient mode selector when fast build-up rates were used. Mocker and Collins showed that at slow build up rates, mode selection by the 'Q' switch could be suppressed, allowing the dye to act as a cavity modulator. At these slow build up rates they observed a self locked train of pulses each 1 ns at half-width separated by 10 ns and with peak powers of 5 MW.

In 1966 DeMaria et al[166] successfully mode locked a Nd : glass laser with a passive modulator. This laser has a much larger bandwidth than the ruby (100 Å as compared to 10 Å) and is therefore capable of producing shorter pulses. The actual duration of the pulses in many of these earlier mode locking experiments are uncertain since their detection systems were slow.

5.3 EXPERIMENTAL DETAILS OF MODE LOCKING

In order to obtain reliable mode locking a number of different laser cavity configurations were investigated. The cavities were not only assessed on their ability to produce good mode locked pulses, but also on the cheapness and sensitivity to damage of the optical components.

Throughout the experiments on mode locking, Brewster angled ruby rods were employed to avoid mode selection and to minimise reflections from the end faces.

The laser head described in Chapter III was re-designed in such a way that light passing along the ruby did not pass through the water cooling the rod. This not only ensured that the light could enter and leave at the Brewster angle, but also eliminated the possibility of producing stimulated Brillouin scattering from the water.

The first laser cavity configuration to be tried was that of a linear cavity, Fig. 5.3(a). This cavity consisted of two dielectric mirrors

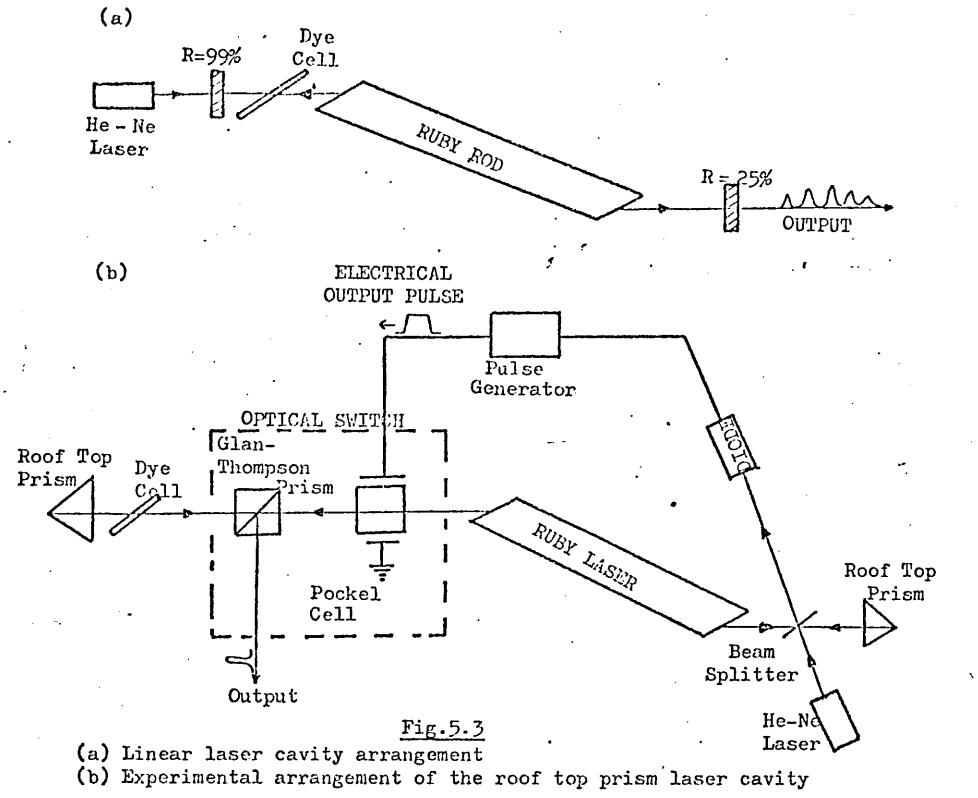

Fig.5.3
(a) Linear laser cavity arrangement
(b) Experimental arrangement of the roof top prism laser cavity

of 99% and 25% reflectivity, a ruby rod 6" × $\frac{5}{8}$" diameter and a dye cell 1 mm thick. A discussion of the dyes used for mode locking can be found in section 5.6.3.

The cavity was aligned by use of a small He-Ne laser placed behind the 99% reflecting mirror. The angle of the ruby rod to the cavity was adjusted until the horizontally polarised He-Ne light at 6328 Å showed no reflections from the Brewster angled end faces of the ruby rod. The angle of the dye cell was adjusted in a similar manner and placed at one end of the cavity so as to ensure that only one pulse was emitted per round trip time[167-170].

This type of cavity occassionally produced good mode locking, although the transverse mode selection of the output was poor. The main disadvantage of this cavity, though, was that the 25% reflecting output mirror suffered considerable damage. The susceptibility to damage of partially reflecting mirrors in laser cavities operating in the mode

locking regime is a general observation made by many authors[165,171]. When damage occurs on a mirror it reduces the reflectivity of the mirror and so effectively increases the lasing threshold. This causes the laser to cease firing until either the mirror is replaced or the flash lamp is fired with a higher input energy. The dielectric mirrors used at the ends of the cavity are expensive, costing more than £20 each and often last no more than a few days.

To overcome the problem of damage to the reflecting surfaces, two roof top prisms were employed, with the intention of introducing into the cavity an optical switch to switch out one of the mode locked pulses, see Fig.5.3(b).

Since the components of the laser cavity are only weakly birefringent, the vertically polarised component of the He-Ne laser light will effectively trace out the same path as taken by the ruby light. Introducing a beam splitter into the cavity at the Brewster angle will, therefore, present no reflection loss to the ruby light, but will allow the vertically polarised portion of the He-Ne laser light to enter the cavity for alignment purposes.

The optical switch consisted of a KDP Pockel cell to switch the polarization of the ruby light and a Glan Thompson prism to select out the light of vertical polarization. Both the KDP crystal and the Glan Thompson prism had entrance and exit faces which were perpendicular to their axes. This meant that these two optical elements had to be slightly tilted to eliminate any mode selection. In addition, the power inside the cavity had to be reduced so as not to exceed the suggested damage threshold of 150 MW/cm^2 of the Glan-Thompson prism as recommended by the manufacturers.

It was found that the laser produced very reliable mode locking when the optical switch was not included in the cavity. Unfortunately the

introduction of the optical switch into the cavity severely limited the possibility of obtaining mode locked pulses. If Brewster angled elements had been available, then the chances are that much more consistent mode locking could have been obtained.

The study of this second laser cavity configuration did, however, highlight two important points which were considered when the third configuration was being chosen. First, the reliability of prism reflectors, since the roof top prisms had been used for more than 1000 shots without any noticeable deterioration or detectable damage. Secondly, the insertion of non-Brewster angled components into the cavity was to be avoided as far as possible, as this would prevent good mode locking.

We were therefore left with the problem of removing the light from the laser cavity without inserting a switch or using a partially reflecting mirror. The obvious answer to this problem was frustrated total internal reflection. This led to the building of a ring laser cavity.

5.4 RING LASER

The third laser cavity configuration chosen was that of a ring laser, the shape of which was based on an equilaterial triangle[172], see Fig.5.4.

Reflection took place at the corners of the triangle by total internal reflection in prisms specially designed so that light entered and left at the Brewster angle. A fourth prism of identical design was placed close to the back of one of the cavity prisms so as to frustrate the total internal reflection process. This method allowed light to be coupled out of the laser cavity. The design of the prisms is also shown in Fig.5.4. These prisms were made of fused quartz and the sides a, b, c were respectively 10 mm, 12 mm and 10 mm long. The prisms were 20 mm in height, the surfaces a, b, c were polished flat to $\lambda/20$, and cost £12.50p each.

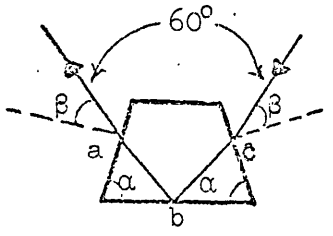

$\alpha = 85^{\circ}\ 30'$
$\beta = \tan^{-1}\mu$
a = c = 10 mm
b = 12 mm
height = 20 mm
μ = refractive index

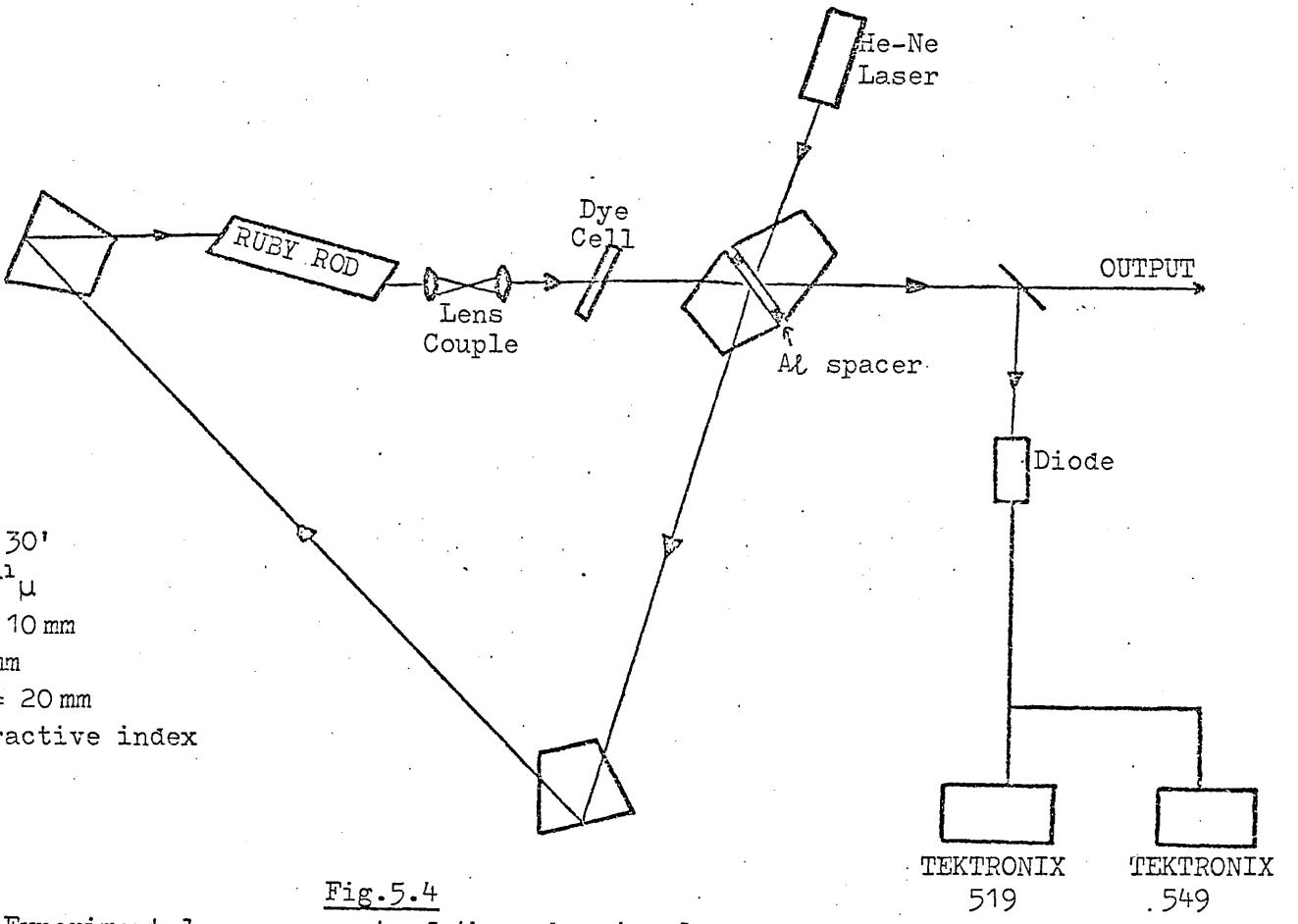

Fig.5.4
Experimental arrangement of the ruby ring laser

The correct spacing between the two prisms forming the output coupler was achieved by vacuum depositing two thin strips of Aℓ along the edge of one of the prisms and then clamping the two prisms firmly together. A harder film such as chromium would have been much more satisfactory. Chromium, though, is difficult to remove and since the thickness of the film deposited with our vacuum system could not be accurately controlled, it was felt that it would be safer to use Aℓ which could be removed with ease if the film was not of the correct thickness.

The transmission of a frustrated total internal reflection system for horizontally polarised light is given by the expression:-

$$T_{\parallel} = \frac{4n^2q^2(n^2p^2-1)}{(n^2-1)^2(n^2p^2-q^2)\sinh^2 u + 4n^2q^2(n^2p^2-1)}$$

where $n = (2\pi d/\lambda)(p^2n^2-1)^{\frac{1}{2}}$

$p = \sin\varphi$

$q = \cos\varphi$

and where φ is the angle of incidence, n the refractive index of the prism material, d the distance between the prisms and λ the wavelength of the light.

$T_{\parallel}$ is displayed graphically in Fig.5.5 for various thicknesses. A transmission of 30% was found adequate for the ring laser, this therefore required the depositing of a 0.35 μm film of Aℓ on the prism.

In ring laser cavities the spurious pulses, associated with the incorrect positioning of the dye cell is avoided, since a pulse will only traverse the dye cell once per round trip time. Therefore the positioning of the dye cell in the ring laser cavity was unimportant.

It has been found[173], however, that whenever a mode locked pulse is formed in a ring laser cavity, a satellite pulse develops travelling in the opposite direction. These two pulses are found to overlap at the dye cell producing a system in which the overall loss is minimised.

The length of the laser cavity is important since it pre-determines the number of possible frequency modes that can lie beneath the gain profile of the active medium. A higher mode density will give rise to higher output intensities. A long cavity will also act as a transverse mode selector allowing only light of a limited divergence to be successively amplified. Unfortunately this also reduces the output energy of the laser and thus a compromise needs to be reached. A cavity length of 300 cm was found to be adequate in order to obtain good mode locked pulses; this represented a round trip time of 10 ns .

To avoid movement of the different optical components relative to each other, the components were mounted on a large 'Dural' table which could be moved in any direction. The table was 3' × 6' × $\frac{5}{16}$" and a matrix of holes were drilled into it within which threaded inserts were fitted. Such a matrix allowed individual optical components to be easily clamped to the table. A photograph of the table with the optical components assembled is shown in Fig.5.6.

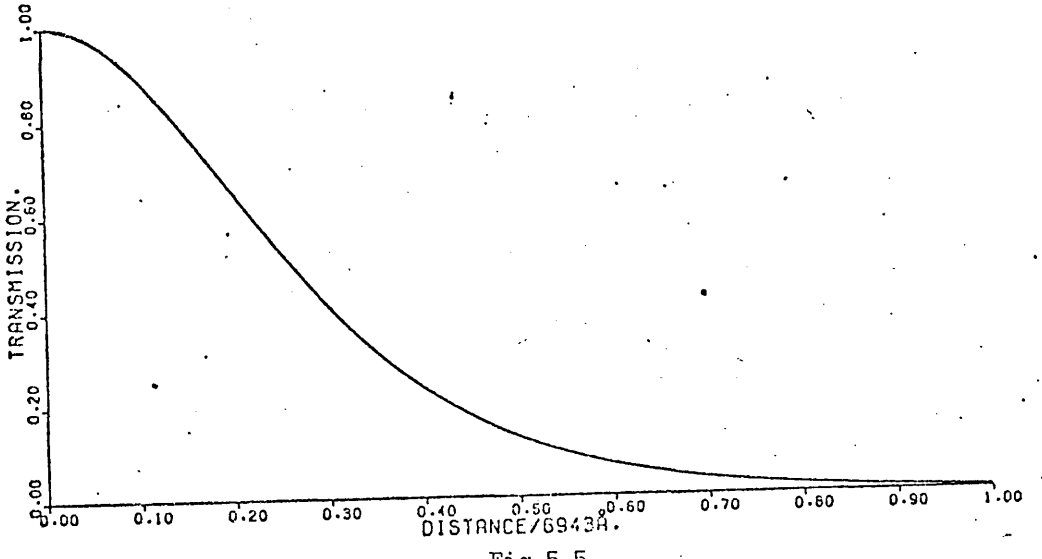

Fig.5.5

The transmission characteristics of the frustrated total internal reflection prism system for various values of the distance between the two prisms

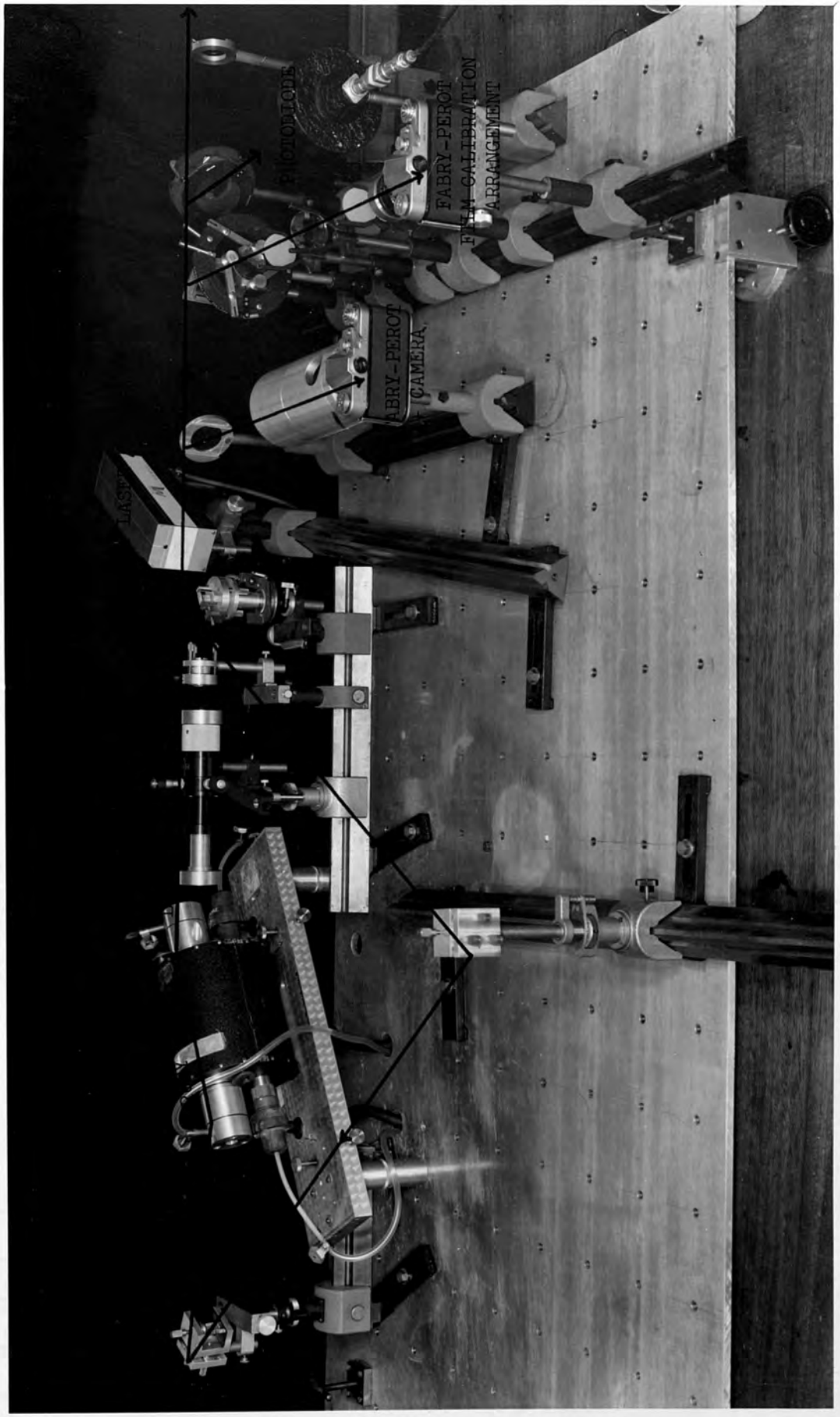

Fig.5.6 - The ruby ring laser

5.5 TRANSVERSE MODE CONTROL OF THE RING LASER OUTPUT

One of the great advantages of this ring laser design, apart from the high damage threshold, was that the beam cross-section reverses at each passage through the ruby rod. This occurs since the beam suffers in a round trip, an odd number of reflections. Any non-uniformity in the amplification of the light across the ruby rod would, therefore, be averaged out after a number of round trips of the light. Unfortunately this did not in itself produce a TEM_{00} output, since severe focusing of the ruby light took place when the light traversed the ruby rod. The focusing mechanism was probably thermal in nature since the ruby rod acted as a diverging lens when the cylindrical surface of the rod was polished, and converging when the surface had a matt finish. A polished rod would allow the flash light to preferentially excite the centre of the rod while the matt finished surface would scatter the light, exciting the rod most strongly at the surface. We therefore have a rod with a high temperature and thus a low refractive index, in the centre when the surface is polished, so effectively producing a diverging lens, while the converse is true of the rod with the matt finish. The temperature change within the rod arises from the non-radiative transitions of the chromium ions after being excited by the flash lamp.

To overcome this problem, a lens couple was inserted into the cavity similar in design to an astronomical telescope of unit magnification. The lens couple consisted of two 10 cm focal length lenses and was adjusted by means of a Hilger Watt autocollimator, so that parallel light which entered the lens couple would also leave it parallel. The lenses were therefore approximately 20 cm apart. Axial mode selection by the lenses was avoided by slightly tilting the lenses and coating them with a $\lambda/4$ film of magnesium fluoride, which acted as an anti-reflection coating. By inserting this lens couple into the laser cavity and adjusting the position of the

lens nearest to the laser, the light leaving the lens couple could be correctly collimated.

The correct collimation or minimum divergence of the laser light is generally determined by measuring the spot size of the output pulse on photographic film at different positions from the laser. This method is very tedious since the output has to be recorded on film which has been correctly calibrated.

A much less accurate method commonly used, is to note the size of the burnt mark produced by the laser on a piece of polaroid film at various distances from the laser. This method, although giving a good picture of the cross-section of the beam profile, is unfortunately too insensitive to be used to adjust the lens couple.

The method adopted was that of measuring the output energy of the laser. If the laser beam is incorrectly collimated, some of the light travelling around the laser will eventually, after a number of round trips, diverge or converge enough to bring it outside the cross-sectional area covered by the ruby. Therefore a loss of energy will result. Correct collimation is therefore expected to coincide with the maximum output energy of the laser. The output energy was measured with a sensitive calorimeter. This technique was found to be sufficiently sensitive to allow us to adjust the lens couple to give TEM_{00} output.

A graph of energy output against lens couple position is shown in Fig.5.7 for the case when the flash lamp capacitors were being charged to 2200V and pumping a $6" \times \frac{3}{8}"$ diameter polished ruby rod. This graph indicates that the ruby rod is equivalent to a diverging lens of 4.2cm focal length, placed at the exit face of the ruby rod. By using the polaroid burn mark method, the beam output divergence was estimated as < 1.5 mrad.

A series of apertures were inserted between the lenses but these had the effect of increasing the lasing threshold and did not noticeably affect the transverse modes.

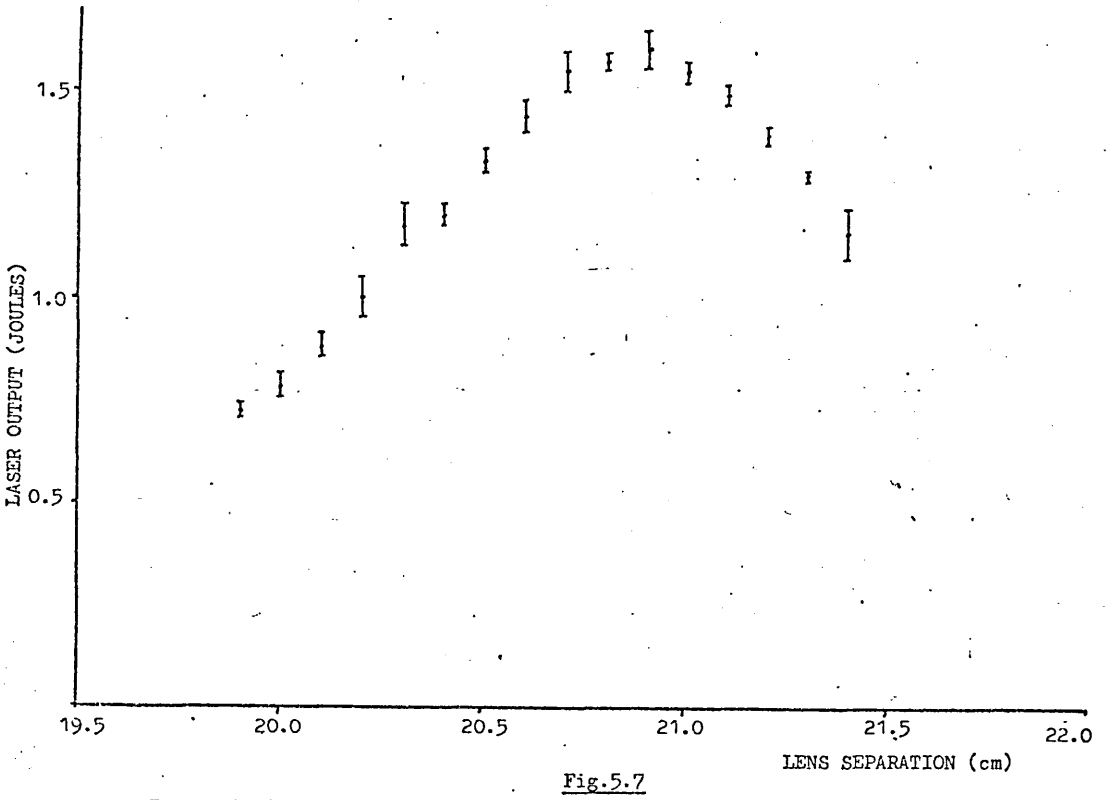

Fig.5.7
The variation of laser output for different separations of the two 10 cm focal length lenses which form the lens couple. The capacitors supplying the electrical energy to the flash lamp were charged to 2.2 kV

5.6 SATURABLE ABSORBER DYES

The choice of dye is important in determining the duration of the individual mode locked pulses, and it also determines the ease with which mode locking can be repeated.

The most important requirement of the dye is that it should have a short relaxation time. This relaxation time is the time it takes the dye to return to an unbleached state after the passage of an infinitesimally short optical pulse. The importance of the short relaxation time is that it allows the dye to suppress pulses following the main laser pulse.

Other requirements of the dye are that it should have: a strong absorption at the lasing wavelength, a high solubility and stability to optical radiation especially ultra violet.

5.6.1 Energy Level System of Saturable Absorbers

The group of dyes generally employed to mode lock ruby lasers are the polymethine cyanine dyes of which cryptocyanine (1,1' - diethyl - 4, 4' - dicarbocyanine iodide) and DDI (1',1' - diethyl - 2,2' - dicarbocyanine iodide) are two.

A simplified form of the energy level diagram for these dyes is shown in Fig.5.8.

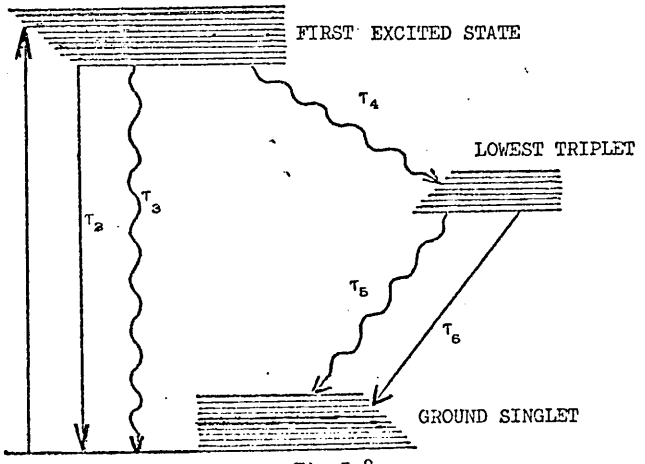

Fig.5.8

Energy level diagram for saturable absorbers. Radiative and absorptive transitions are shown by solid lines while non-radiative transitions are shown by wavy lines. Vibronic sublevels are included for each electronic level

After being optically excited by the laser the dye is left in one of its vibrational levels within the first excited singlet, from here it will decay down into a lower vibrational energy level, via a process known as thermalization. The characteristic time τ_1 of this process for dyes dissolved in organic fluids is generally[174] $< 10^{-13}$ s. Thermalization will also take place within other electronic levels.

From the first excited singlet state the dye can decay by one of three modes. First, it may decay back to the ground state by a radiative transition with a characteristic time τ_2. This fluorescent life time τ_2 lies between $10^{-9} - 10^{-8}$ s, and its value is not thought to be a strong function of the environment of the molecule. Secondly, it may decay by a direct non-radiative transition of a singlet-singlet nature. For many organic materials the lifetime τ_3 of this process is thought to be large.

Spaeth and Sooy[175] have found evidence, however, that this is an important decay mode for cryptocyanine. Thirdly, decay of the first excited singlet state may take place via a nonradiative intersystem transition to the lowest lying triplet level. According to Porter[176-179] and others, τ_4, the characteristic time of this process, is not sensitive to the environment.

From the triplet level the dye molecules can decay by a nonradiative transition. The lifetime τ_5 of this process is often affected in an important manner by solvent-solute interactions, the presence of impurities, dissolved oxygen, temperature, and viscosity or phase of the solvent. The other alternative decay mechanism from triplet to ground state singlet is via a radiative transition. This is generally slower than the nonradiative transition and therefore unimportant.

The lifetime of the first excited singlet is therefore

$$\tau^{-1} = \tau_2^{-1} + \tau_3^{-1} + \tau_4^{-1} .$$

Spaeth and Sooy[175] calculate this to be approximately 40 ps for cryptocyanine dissolved in propanol, with

$$\tau_2 \simeq 4 \times 10^{-9} \text{ s}$$
$$\tau_3 \simeq 4 \times 10^{-11} \text{ s}$$
$$\tau_4 \simeq 5.6 \times 10^{-10} \text{ s} .$$

It can be seen, therefore, that the lifetime of this dye dissolved in alcohol is determined by the rate of internal conversion between the two singlet states involved.

The lifetimes listed above were obtained by Spaeth and Sooy on the basis of quantum efficiency measurements. Other measurements by Schuller and Puell[180] suggest that the singlet lifetime of cryptocyanine dissolved in methanol is 25 ps. This lower value is substantiated by the results of Duguay and Hansen[181], who measured the lifetime to be 22 ps when dissolved in either acetone or methanol. It was also found by Duguay and

Hansen[181] that DDI dissolved in either methanol or acetone has a shorter lifetime of 14ps. It should be noted that DDI/methanol, and cryptocyanine/acetone combination are best suited for mode locking since with these solvents the absorption peak of the dye lies closest to the ruby line.

As mentioned earlier, the three energy level system of the dyes is only a simplification of the actual situation. For instance a number of authors[180,182-184] have observed a blue fluorescence from saturable absorbers when they are excited by ruby laser light. This they have attributed to the result of excited state absorption to the second singlet state. The lifetime of this second excited singlet state for the dyes used is about 10^{-12} s [180]. This transition therefore, produces a residual absorption after the saturation of the first excited singlet state at very high light intensities.

5.6.2 Decomposition of Saturable Absorbers

It has been shown[185,186] that ultraviolet radiation in a band of wavelengths near 3000 Å, produced by the flashlamps used to pump a ruby rod, is responsible for nearly all the photochemical decomposition (irreversible bleaching) of cryptocyanine dissolved in methanol, when the dye was being used as a 'Q' switch in a high peak power ruby laser. The laser beam itself has little or no irreversible effect upon cryptocyanine.

To check the stability of DDI to laser and flash lamp radiation, a sample of DDI dissolved in methanol which had an absorption of 55% at the laser wavelength was inserted into the laser cavity. It was found even after 10 laser shots that no change had occurred in the absorption coefficient of the dye. In a similar check on cryptocyanine dissolved in acetone, it was found that the transmission increased by 1%, a figure much smaller than that reported by Hollier et al[185].

In addition to the above check, the two dye samples were exposed to daylight (which is strong in UV) for five minutes. Again no change was recorded in DDI, but the cryptocyanine's absorption had decreased from 55% to 30%. The above results were obtained when the dyes were contained in quartz cells, no change in the absorption of the dyes being recorded when the dyes were contained in glass cells.

A trace of the two dyes absorption profile from a spectrophotometer clearly shows that cryptocyanine, Fig.3.5, has a high absorption below 3250 Å while DDI, Fig.5.9, shows similar characteristics below 2250 Å. Unfortunately a high UV absorption is usually associated with chemical decomposition of the dye, leading to a lowering of the absorption of the dye and thus to instability during lasing. Much of the UV radiation can of course be avoided by using glass dye cells, although these have lower damage thresholds than quartz cells.

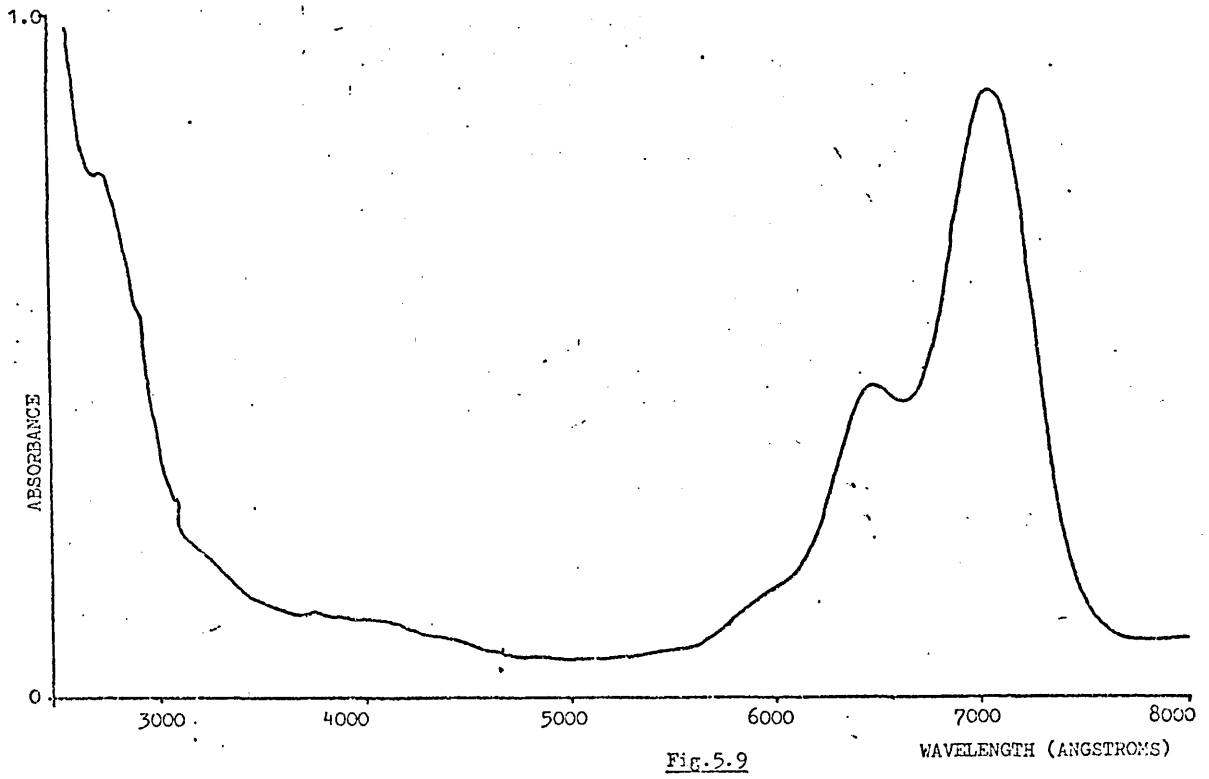

Fig.5.9
Absorption spectrum of DDI dissolved in methanol

5.6.3 Choice of Dye Cell Length and Dye

It has been found by Bradley et al[187] that there is a strong relationship between saturable absorber cell length and pulse duration in passively mode locked lasers.

They investigated the dependence both experimentally and theoretically and found that it is very advantageous to use a dye cell which is shorter than the required pulse length. With this in mind a dye cell of 1 mm was employed in the ring laser cavity which represents a transit time of 4 ps to the ruby light.

From the information presented concerning relaxation times and stability, it would appear that DDI/methanol would produce the best mode locked pulses; this was found to be true. When cryptocyanine is used, a higher probability of producing unwanted satellite pulses was observed. An additional advantage of using DDI is that when the laser is operated at the same level there is generally four times more output energy with DDI than there is with cryptocyanine.

Having correctly adjusted the lens couple, chosen the appropriate dye and cell length, all that remained to be done, therefore, was to judiciously adjust the dye concentration until a single train of mode locked pulses was emitted after each firing of the flash lamps. Throughout the use of the ruby ring laser the contents of the dye cell were replenished after each laser shot to ensure that deterioration of the dye did not hinder mode locking.

5.7 DETECTION SYSTEM

5.7.1 Photodiode/Oscilloscopes

In general the very short optical pulses emitted by mode locked ruby lasers (10 - 40 ps) are much shorter than the intrinsic risetime of the available photodiodes or oscilloscopes. This means that such detection systems can only serve as a crude method of detecting the presence of mode locked pulses.

The photodiode used to detect the optical pulses was an HCBI (S-20) type diode supplied by ITL. The diode was always used in conjunction with a 6943 Å narrow band filter to eliminate flash lamp light and a diffusion screen to preclude saturation of the photocathode. This diode had an intrinsic rise time of 0.2 ns, and supplied sufficient current in the electrical output pulse so as to be easily detected on a Tektronix 519 oscilloscope. The Tektronix 519 is a travelling wave oscilloscope having no amplification stages and a rise-time of 0.3 ns. These two instruments used together, resulted in an overall instrumental risetime of approximately 0.5 ns.

In addition to the 519 oscilloscope a Tektronix 549 storage oscilloscope was employed to ensure that only one train of mode locked pulses was emitted by the laser. This oscilloscope was supplied half of the electrical signal from the HCBI(S-20) photodiode by means of a matched 'T' piece.

5.7.2 Calorimeter

The calorimeter described in Chapter III, was found to be far too insensitive to measure the output energy of the mode locked laser. To measure the energy output of the laser an ITL laser calorimeter was used; this was capable of measuring energies over a range 30 J - 0.2 mJ without attenuators. By using the calorimeter, together with the diode, the calibration of the photodiode was made.

5.7.3 Fabry-Perot Interferometer

A schematic diagram of the arrangement of the Fabry-Perot interferometer employed to measure the spectral width of the mode locked laser is shown in Fig.5.10. This consisted of two optical flats, flat to $\lambda/100$ and separated by 1 mm. The flats were housed in a thick stainless steel cylinder, the inclination of which could be adjusted by three bolts which formed part of an adjustment mechanism.

The surface of the flats were vacuum coated with a 500 Å layer of silver to give a reflectivity of better than 95%. The interference rings formed by the ruby laser were photographed with a Zenith camera, focused on infinity. Kodak 2475 recording film was used to record the image which was later developed in Kodak DK-50 developer.

The short focal length lens displayed in Fig.5.10 was used to increase the angular inclination of the incident light upon the Fabry-Perot plates. This is essential since the short spacing of the plates implies a large angular separation of the rings.

In order to calibrate the photographic film correctly, part of the ruby light was channelled off along a separate line, Fig. 5.10. A series of lenses and diffusion screens were employed as shown in Fig.5.10 to form a uniformly illuminated area which was to act as a source to a series of neutral density filters. The neutral density (ND) filters had been previously calibrated at 6943 Å on a spectrophotometer. The ND filters were then photographed, as was the illuminated area without the ND filters, on the same film as the previously recorded Fabry-Perot interference rings. Each film taken in such a way contained all the information necessary for the determination of the width and shape of the interference rings. These films were then studied on a Joyce Lobel microdensitometer and analysed to determine the spectrum of the mode locked pulses.

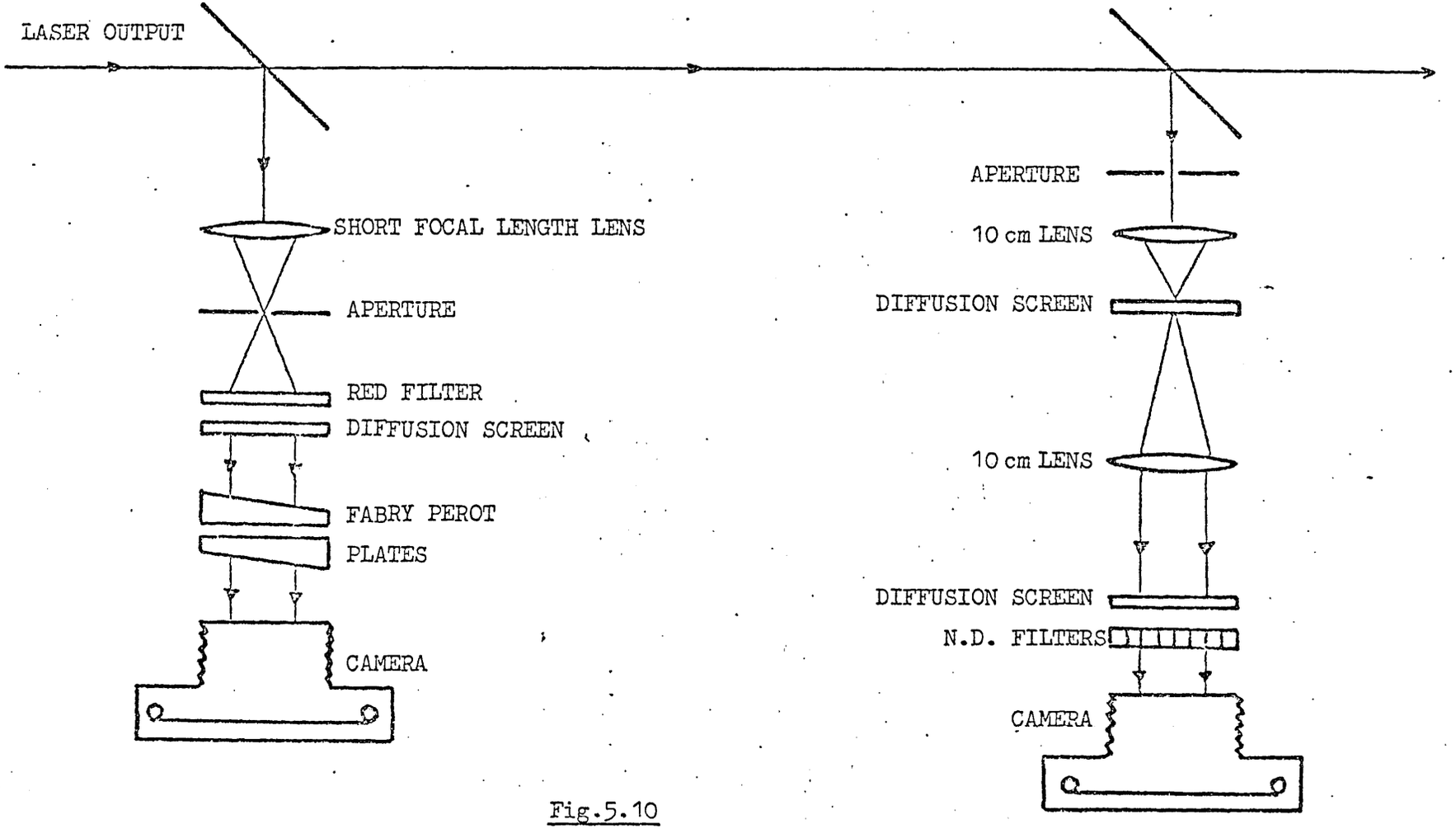

Fig.5.10

Schematic diagram of the Fabry-Perot interferometer including the arrangement used to calibrate the photographic film

5.7.4 Two Photon Fluorescence Pulse Width Measurement Technique

The two photon fluorescence technique (TPF) used to measure pulse width was first developed by Giordmaine et al[79] in 1967. In this technique two equal portions of a high intensity laser pulse travelling in opposite directions, cross in a cell containing a two photon absorption liquid. Enhanced fluorescence results at the points were the two beams overlap. By photographing the fluorescence track, a record of the shape of the enhanced fluorescence pattern is obtained. The photograph can be analysed by a microdensitometer to give an indication of the pulse duration.

In practice one of two folded optics configurations are used to obtain the TPF profile. The first configuration used was simply to reflect the laser light normally from a mirror immersed in a TPF liquid, Fig.5.11(a). Unfortunately the autocorrelation profile of the pulse in this method is immediately adjacent to the mirror which is therefore difficult to photograph. Additional TPF profiles can be found a distance away from the mirror, but these arise from the cross-correlation of the pulse with other pulses in the mode locked train, and will, therefore, not necessarily give a good indication of the pulse width.

The second configuration and the one most often employed in experiments is that of the triangular arrangement, Fig.5.11(b). Here the light from the laser is split by means of a beam splitter into two equal portions which traverse a triangular path in opposite directions, and overlap in a TPF cell placed in one arm of the triangle. This method has the added advantage over that of the first configuration, in that if the TPF cell is placed a distance from the beam splitter which is equal for both portions of the pulse, then the autocorrelation profile is always observed.

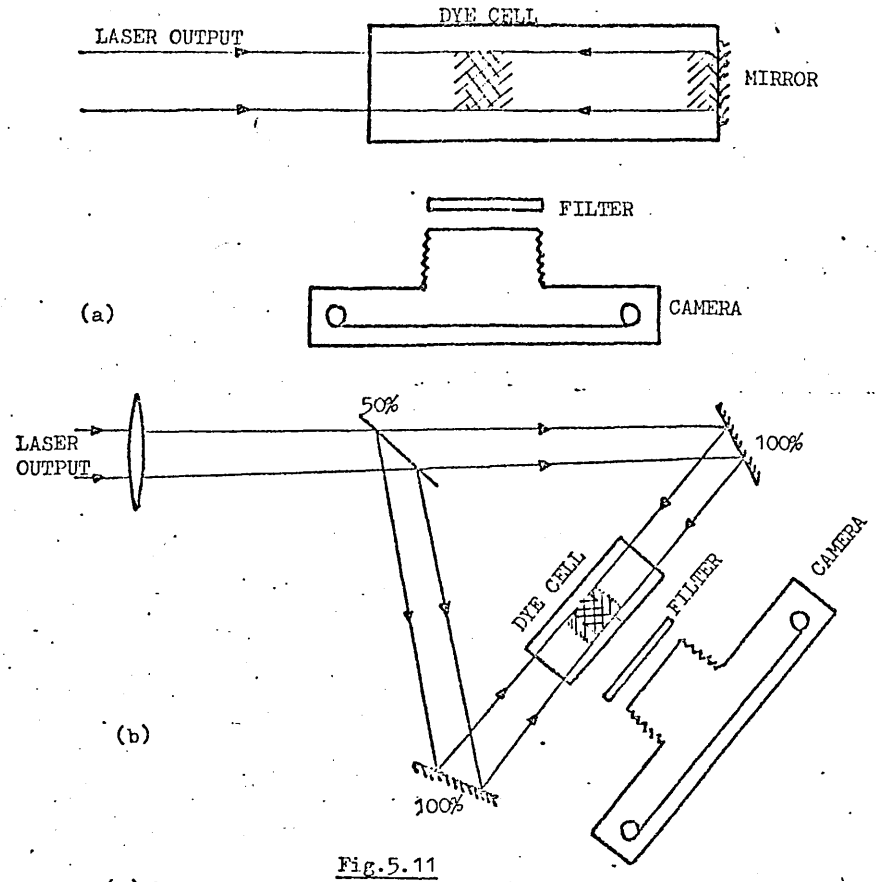

Fig.5.11
(a) Linear two photon fluorescent arrangement
(b) Triangular two photon fluorescence arrangement

The width Δz of the fluorescence trace at half height, above the background, is related to the pulse duration τ_p by:

$$\tau_p = \frac{2 \Delta z n}{c k}$$

where n is the refractive index of the TPF liquid, c the velocity of light, and k a constant dependent on the pulse shape. For Gaussian pulses $k = \sqrt{2}$ (see Appendix II).

Unfortunately it was found that the short structures recorded may easily arise from noise fluctuations as well as mode locked pulses[188]. To be able to distinguish the noise from a record of truly mode locked pulses, a measure of the contrast ratio has to be made. The contrast ratio is the ratio of the peak intensity to background intensity. It can be shown (see Appendix II), from a theoretical analysis of the TPF process, that the maximum contrast ratio is 3, and that if the recorded structure

has arisen from the overlapping of a mode locked pulse with itself, then the contrast ratio should be greater than 1.5.

The configuration adopted to measure the widths of the mode locked pulses from the ring laser was that of the triangular arrangement. To obtain two equal portions of each pulse, a TiO_2 coated beam splitter was incorporated. This was produced by vacuum coating an optical flat with a $\lambda/2$ layer of TiO and then baking the surface in an oven at 400°C to oxidise it. This resulted in a beam splitter with 45/55 percent reflection/transmission characteristics. Inserting a clean microscope slide into the arm of the triangle transmitting the largest portion of light, resulted in the two light beams being identical in intensity to within 4%. A considerable inequality in the strength of the overlapping pulses can be tolerated[190-191] (see Appendix II). Neutral density filters had been found to be incapable of correctly attenuating the light at such high intensities (> 1 MW/cm^2). The reflection/transmission characteristics quoted above only existed when the ruby light is vertically polarised. Since the laser output is in fact horizontally polarised, a $\lambda/2$ quartz retardation plate was employed to rotate the polarization by 90°.

The triangular arrangement was placed three metres away from the laser and misaligned by 2 mrad so that the light returning from the triangle did not disrupt the process of mode locking. The alignment of the two beams in the TPF cell is critical[190-194] and so the triangle does need to be placed a good distance away from the laser. To increase the intensity of the light in the TPF cell a 100 cm focal length lens was used. The resulting fluorescent pattern was photographed with a Zenith camera with a short focal length lens and wide aperture. Kodak 2475 recording film was used to record the image which was subsequently developed in Kodak DK-50 developer.

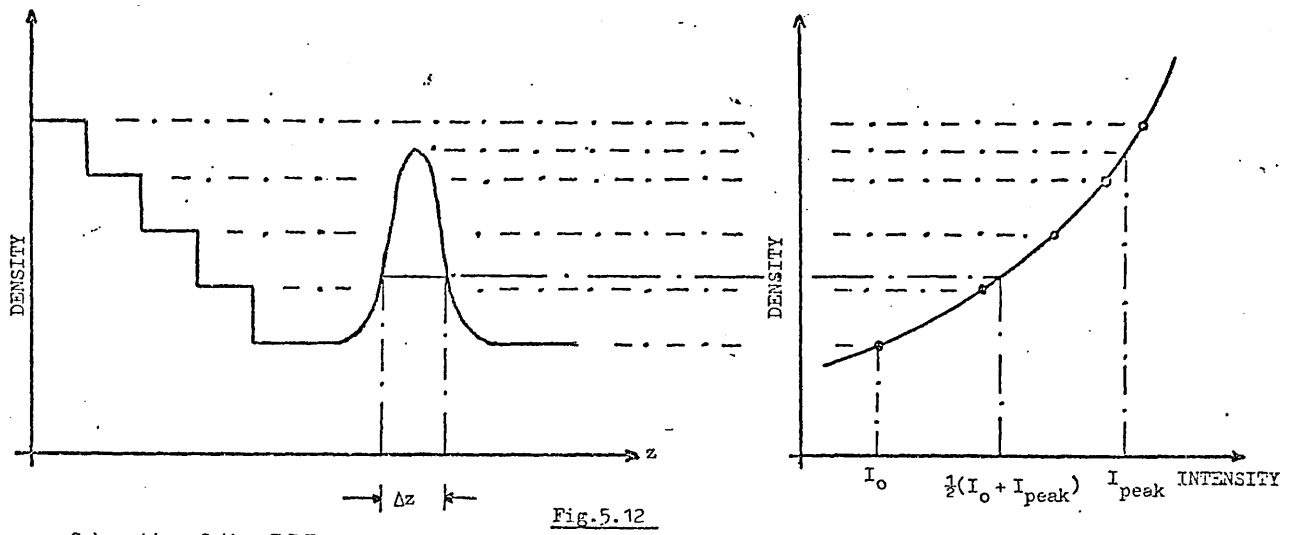

Fig.5.12

Schematic of the TPF measurement. The characteristic curve of the photographic film is obtained from the microdensitometer trace on the left. The density steps are produced by placing calibrated neutral density filters over the image of the fluorescence trace. Using the characteristic curve the halfwidth Δz and the contrast ratio I_{peak}/I_o are obtained

To measure the contrast ratio of the TPF pattern, a series of calibrated neutral density filters were inserted between the TPF cell and the camera, as well as a BG 18 JENA (green-blue) filter to cut out the unwanted scattered ruby light. The inclusion of the neutral density filters meant that each frame of the film had its own calibration steps recorded on it and could easily be interpreted by using a microdensitometer (see Fig.5.12).

A number of dyes were investigated to find the liquid most suitable for the recording of the TPF traces. Basically there exists three main problems. First, some dyes exhibit quenching[195,196] and so produce a low contrast ratio. Secondly, the fluorescent output of the dyes is often too low to be easily recorded. Lastly, to overcome this last problem one would increase the concentration of the dye, but often many of the available organic dyes which show the correct frequency response have low solubilities.

The problem of two photon fluorescence quenching has been investigated by a number of authors[195,196] and it is true to say that one needs first to assess the situation with relation to each individual laser. Five different liquids were tested for their suitability as TPF dyes, these are listed below.

DYE/SOLVENT	MOLAR CONCENTRATION	QUENCHING INTENSITY
DPA/CYCLOHEXANE	5×10^{-3}	$\gg 10$ GW/cm^2
DIMETHYL POPOP/TOLUENE	5×10^{-3}	≥ 5 GW/cm^2
POPOP/TOLUENE	5×10^{-3}	≥ 1 GW/cm^2
α-NPO/TOLUENE	10^{-2}	≥ 1 GW/cm^2
RHODAMINE 6G/METHANOL	5×10^{-3}	≥ 1 GW/cm^2

DPA - [9, 10, Diphenyl-anthracene]

DIMETHYL POPOP - [2,2' - p - Phenylenebis(4-methyl-5-phenyl) oxazole]

POPOP - [2,2' - p - Phenylenebis (5 - phenyl oxazole)]

α - NPO - [2 - (1 - Naphthyl) - 5 - phenyloxazole] .

It would appear from the list that DPA dissolved in cyclohexane is the most suitable dye, unfortunately this yields the least fluorescence and could not be detected even with the high speed 2475 recording film.

The next best dye was dimethyl POPOP dissolved in toluene; this in fact gave the highest fluorescent output. This dye was used for most of the pulse width measurements and to be doubly sure that no quenching occurred, the concentration of the dye was increased to 10^{-2} mole. This meant that the dye cell had to be slightly heated since the concentration of the dye lay close to its maximum solubility at room temperature (20°).

5.8 SINGLE PULSE SELECTION

In order to spectrally resolve a single mode locked pulse, as opposed to a train of pulses, a single pulse was switched out by means of a Pockel cell. The details of the experimental apparatus are shown in Fig.5.13.

The horizontally polarized output from the ruby laser passed through a KDP Pockel cell which was kinematically mounted so that it could be correctly aligned. The mounting mechanism also allowed the Pockel cell to be rotated with very little backlash, Fig.5.14.

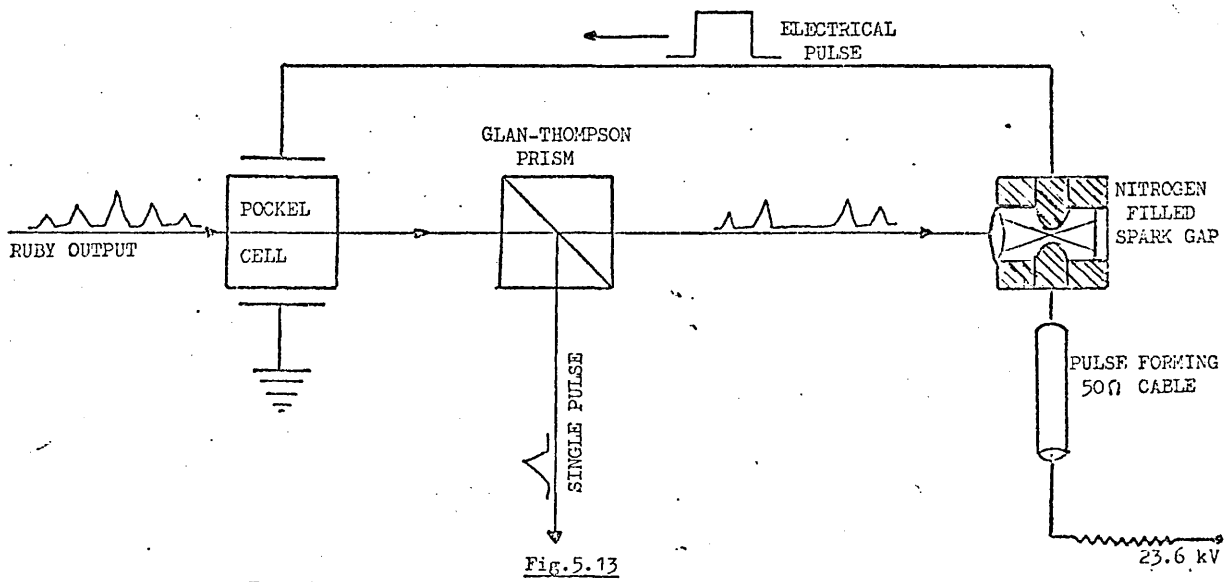

Fig.5.13
Experimental arrangement for switching out a single pulse from a train of mode locked pulses

The polarization of the light passing through the Pockel cell was rotated through 90° by applying a voltage pulse of 11.8 kV. This voltage pulse was supplied by means of a nitrogen filled spark gap (Fig.5.15), filled to a pressure of ≃100 p s i and with a gap of 2 mm. The electrical circuit of the spark gap is shown in Fig.5.16. The light from the laser

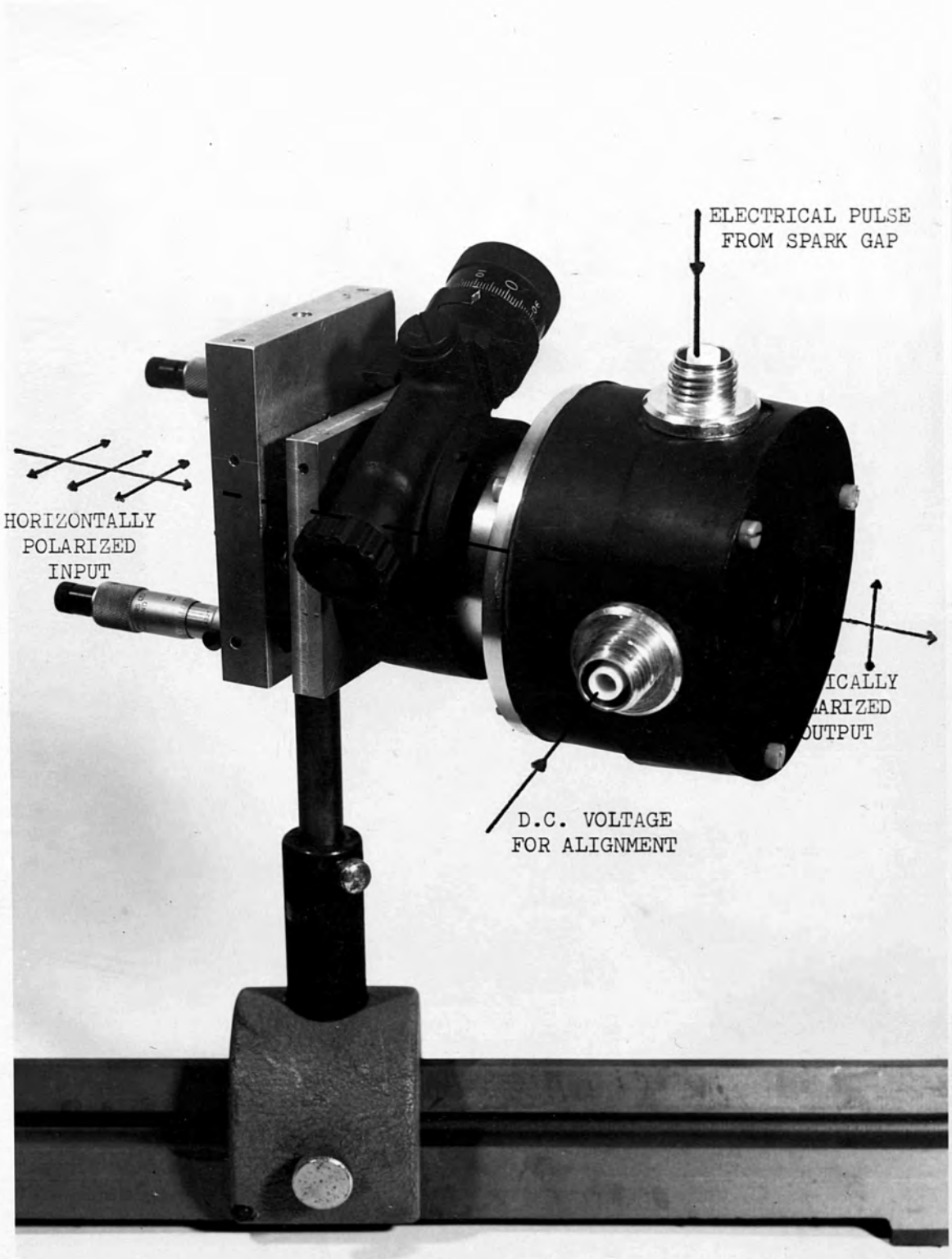

Fig.5.14
Pockel cell and mounting mechanism

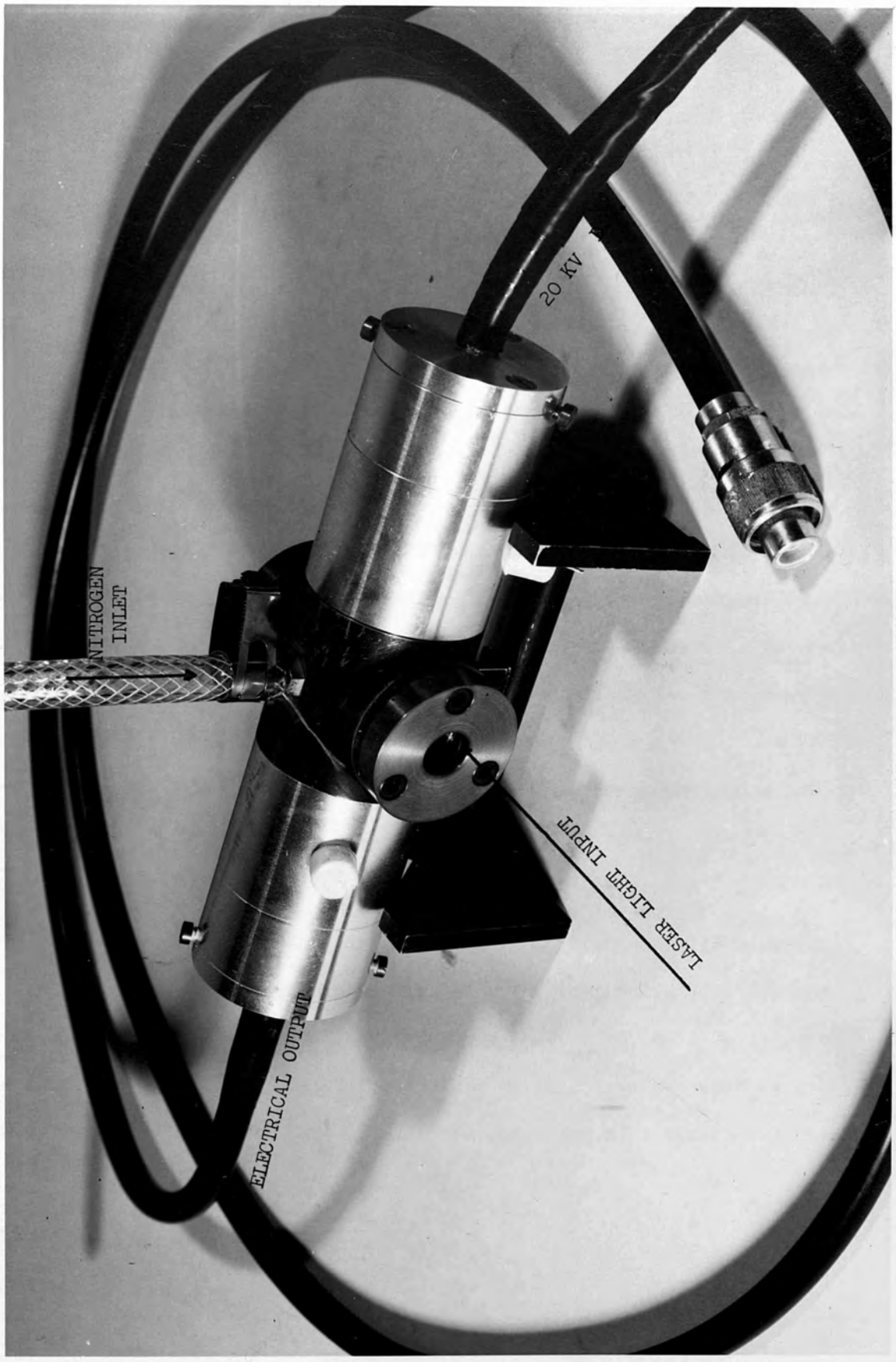

Fig.5.15
Laser triggered spark gap

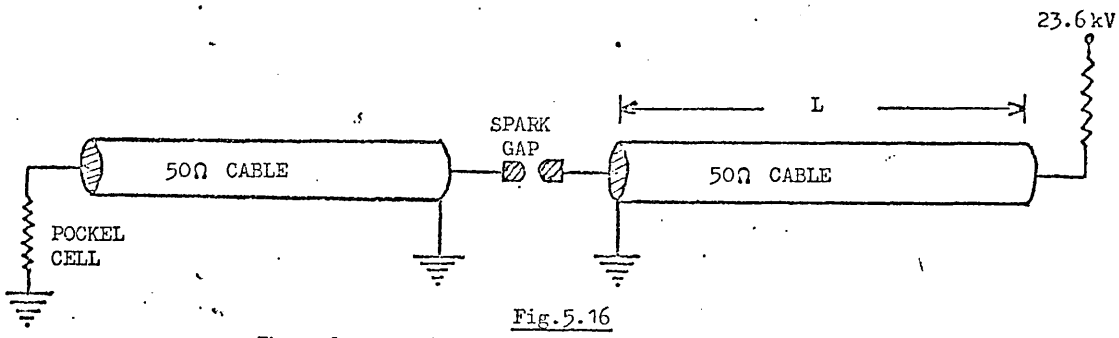

Fig.5.16
The pulse forming network for the Pockel cell. The pulse duration $\tau = 2L/v$, where v is the velocity of the electrical pulse

was focused down into the spark gap which was holding off 23.6 kV. Ionization of the nitrogen occurred allowing a current to flow across the spark gap. The pulse forming cable was adjusted in length so that an 8 ns voltage pulse resulted, Fig.5.17(b). The fast risetime (< 0.6 ns) of this pulse is attributed to the careful design of the spark gap; designed so as to present an impedance of 50 Ω to the electrical pulse and thus matched to the input and output cables. By judiciously adjusting the pressure inside the spark gap and the length of cable between the spark gap and Pockel cell, the Pockel cell could be made to rotate the polarization of one of the mode locked pulses. The pulse with the vertically polarised electric vector was then selected by the Glan Thompson prism.

It was found that the Pockel cell and Glan Thompson prism arrangement could, under static conditions, give an extinction ratio of 370:1 and even with the expected reduction under dynamic conditions, this was found to be adequate. A discussion of the extinction ratio can be found in a paper by Okado and Ieiri[197]. An oscilloscope trace of a train of pulses with a missing pulse is shown in Fig.5.17(a).

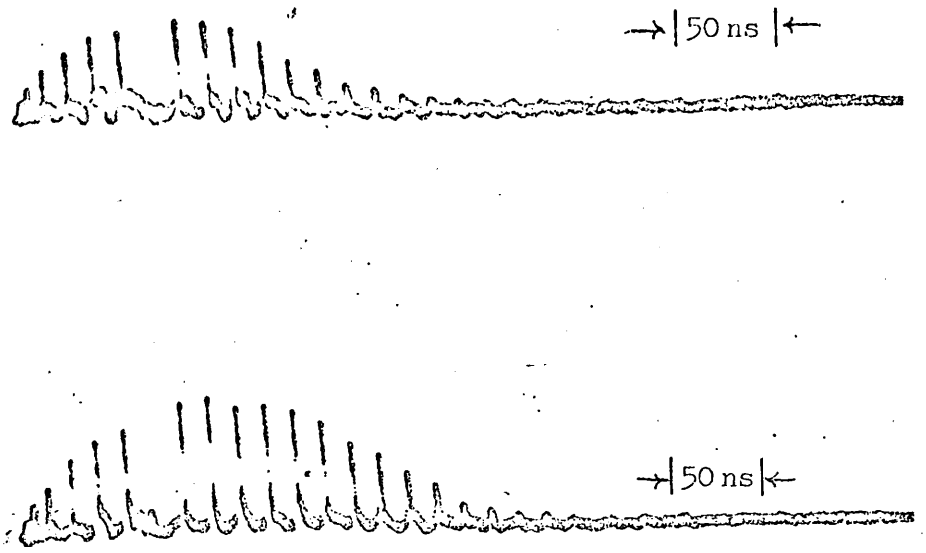

Fig.5.17(a)

Laser output showing the absence of the switched out pulse
Intensity of the largest pulse is approximately 50 MW/cm^2

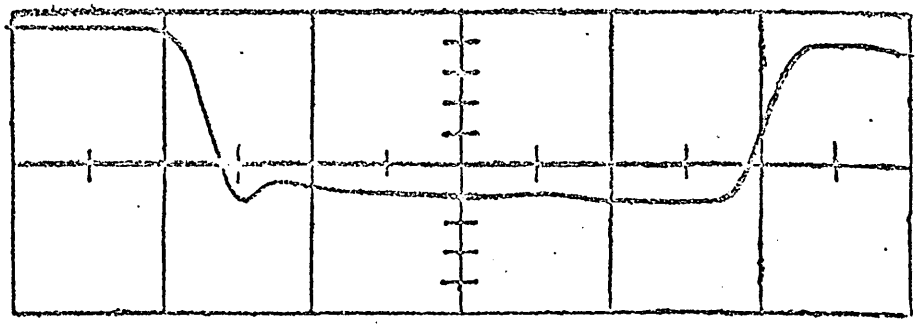

Fig.5.17(b)

Electrical output of the laser triggered spark-gap 2 ns/Div ; 10 kV/Div

5.9 LASER OUTPUT

The output from the ring laser varied in length from 80 - 600 ns (FWHM). This figure is indicative of the width of each frequency mode. If the frequency modes and the envelope of the train of pulses follow a Gaussian profile, then a 400 ns train from the ring laser represents a frequency mode width of approximately 1 MHz with each mode separated by 100 MHz.

A series of oscillograms showing the regular output from the ring laser, when DDI dissolved in methanol is used as the 'Q' switch, are shown in Fig.5.18. To ensure that the output from the laser was reproducible the laser had to be fired at regular intervals. This ensured that the temperature of the ruby rod and thus the extent of the thermal focusing was always the same. If the laser flash lamps were driven approximately 5% or more above threshold, then lasing was restricted to a few dominant frequency modes. The intensity of the output from the laser then had a distorted sinusoidal modulation, Fig.5.18. Similar results of poor mode locking were also recorded from the output of the other two laser cavity configurations when driven above threshold.

Two photon fluorescent analysis of the ring laser output revealed a variation of pulse width from 20 - 32 ps with an average duration of 26 ps. This was accompanied by a variation in contrast ratio of 2.9 - 2.0 with the largest contrast ratios having been recorded with the shortest pulses.

A theoretical analysis[198] of the TPF process clearly indicates that the higher contrast ratios are representative of the larger fraction of the oscillating modes which are phase locked. Many oscillating modes implies a large oscillating bandwidth and thus the possibility of obtaining shorter pulses.

The highest contrast ratios were always obtained when the TPF profile exhibited a narrow spike, Fig.5.19. Many authors[189,199,200]

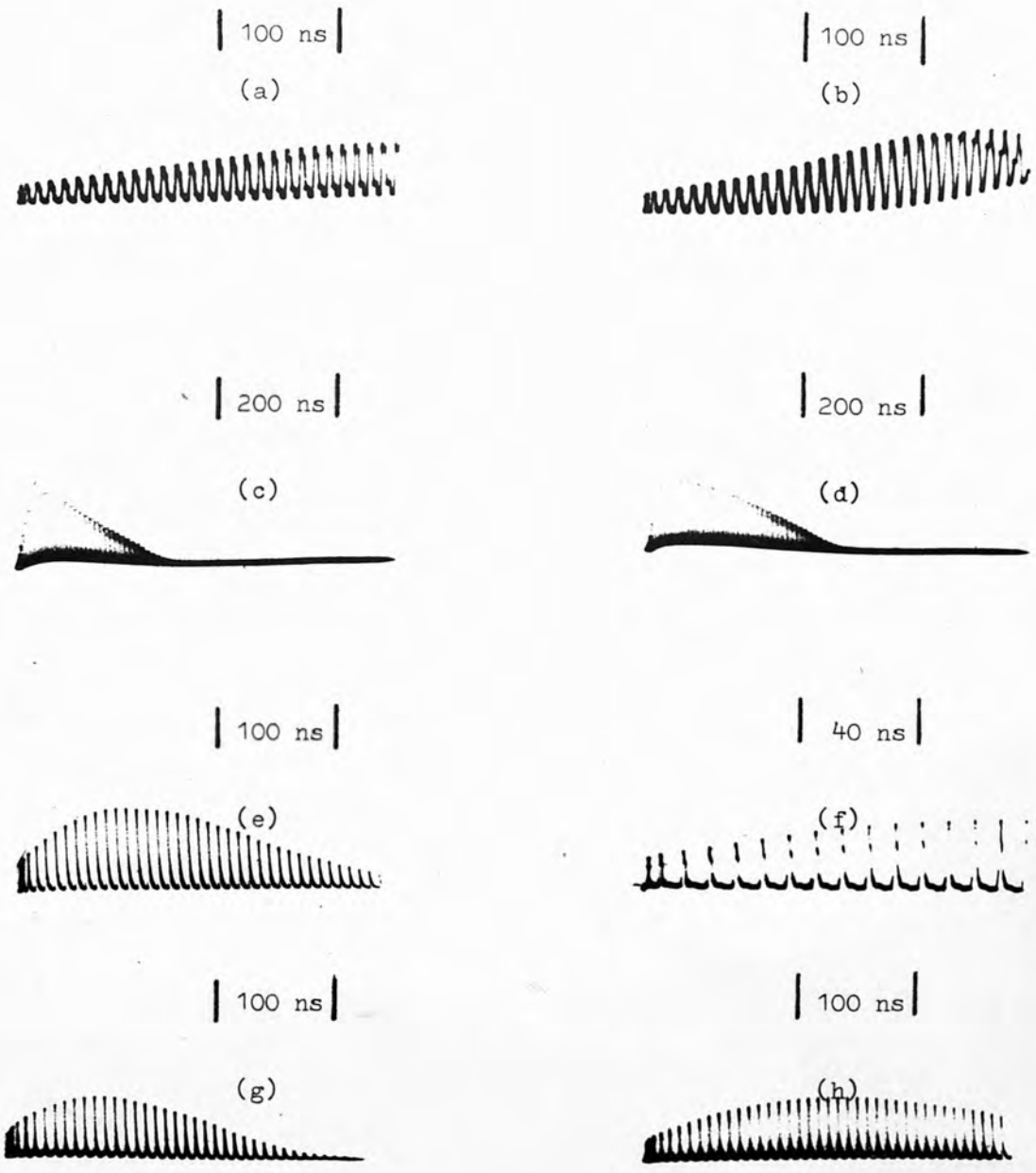

Fig.5.18
Oscillograms of the output of the ruby ring laser. The oscillograms (a) and (b) illustrate the output produced when only a few dominant frequency modes oscillate. The oscillograms (c)-(h) illustrate the 50 MW/cm^2 output of the mode locked ruby ring laser

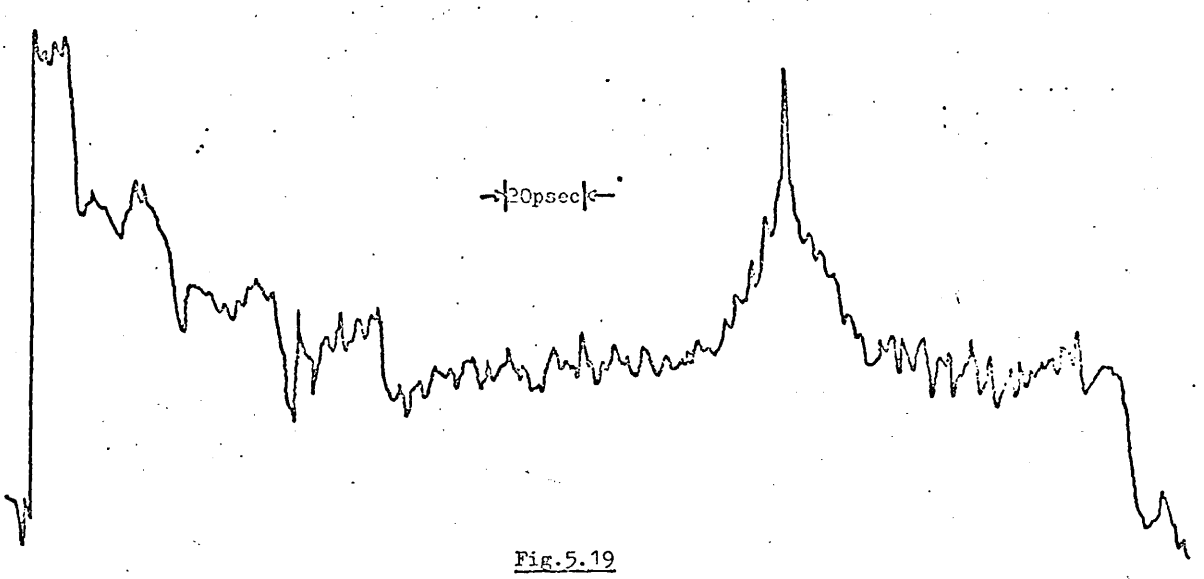

Fig.5.19

A two photon fluorescence trace of a 22 ps (FWHM) ruby ring laser pulse, taken in a 10^{-2} molar solution of dimethyl POPOP. The neutral density steps on the trace correspond from right to left to contrast ratios of 1.25, 1.65, 2.3 and 3.0 respectively. The pulse on this trace has a contrast ratio of ≃2.9

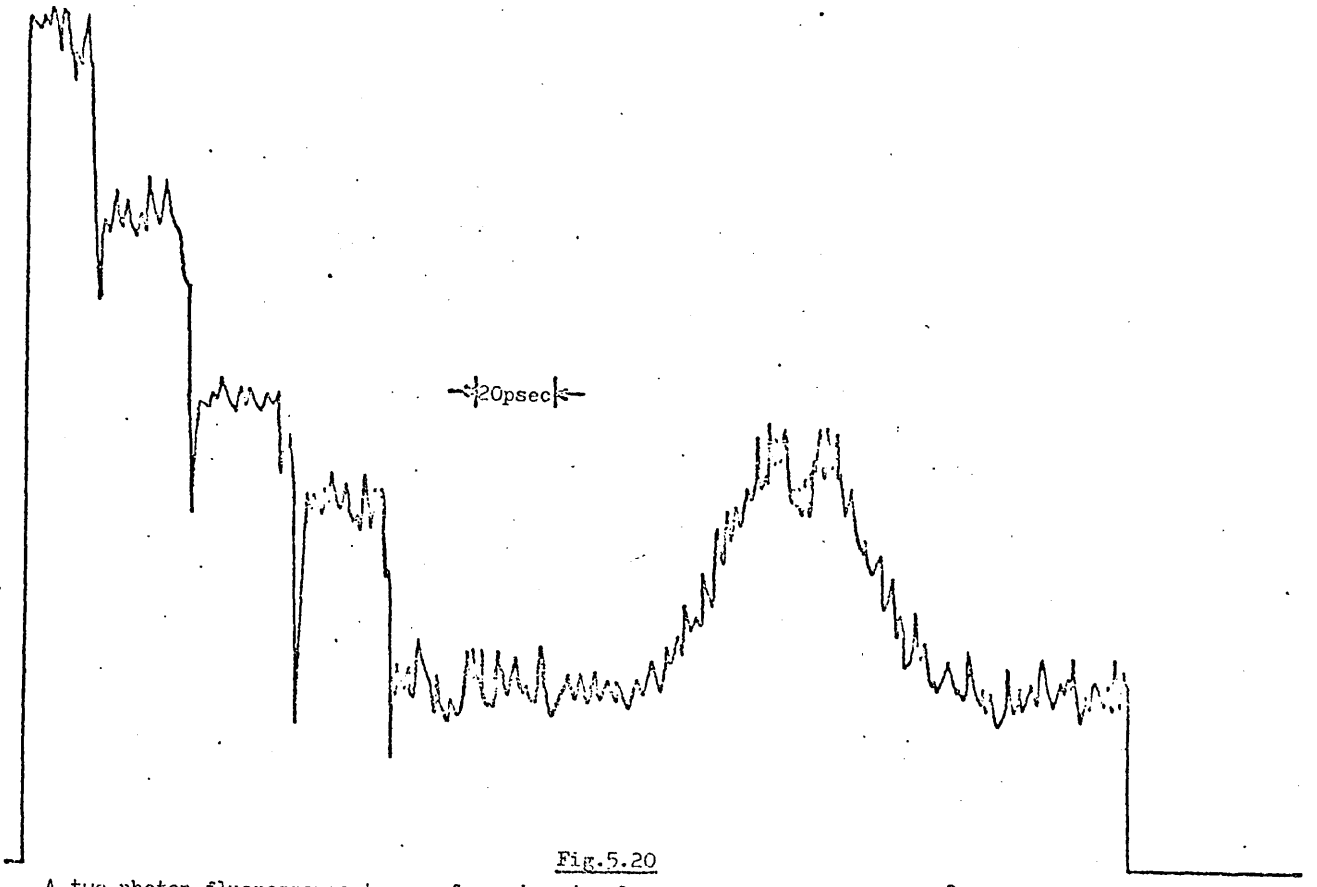

Fig.5.20

A two photon fluorescence trace of a ruby ring laser pulse, taken in a 10^{-2} molar solution of α-NPO. Quenching of the TPF process can be seen in the centre of the profile

have suggested that the TPF profile should include a fine central spike. Unfortunately poor recording techniques and TPF quenching, Fig.5.20, have probably resulted in the failure by many researchers to record this spike. The presence of this spike was confirmed by Shapiro and Duguay[190,201,202] who scanned the overlap region with a very thin dye cell and recorded the subsequent fluorescence with a photomultiplier.

The output energy of a single pulse varied from 1 - 2 mJ, with an intensity of between 10 and 100 MW/cm^2. This meant that the TPF profile of a single pulse could not be recorded because of the weak fluorescence from the TPF liquid.

Obtaining Fabry-Perot interferograms from a single pulse was much less of a problem and photographs of interferograms from both a train of pulses and a single pulse can be seen in Fig.5.21. The average spectral width of a pulse train was approximately 0.62 Å, while single pulses had spectral widths as large as 1.1 Å.

If we assume the laser pulses to be Gaussian, then the uncertainty relationship for a transform limited pulse is given by:

$$\Delta\nu\,\Delta t = \frac{2\log_e 2}{\pi} = 0.44$$

where $\Delta\nu$ and Δt are respectively the FWHM of the spectral and temporal intensity profiles of the pulse.

The spectral and temporal measurements of the laser output indicates a $\Delta\nu\,\Delta t \simeq 0.97$, a figure twice that of the transform limited case. This discrepancy is not at all surprising once the spectral shape of the laser pulse is determined, Fig.5.22. Fig.5.22 clearly shows a strong asymmetry which would probably be reflected in the temporal profile of the laser. Unfortunately the TPF profile measurement technique

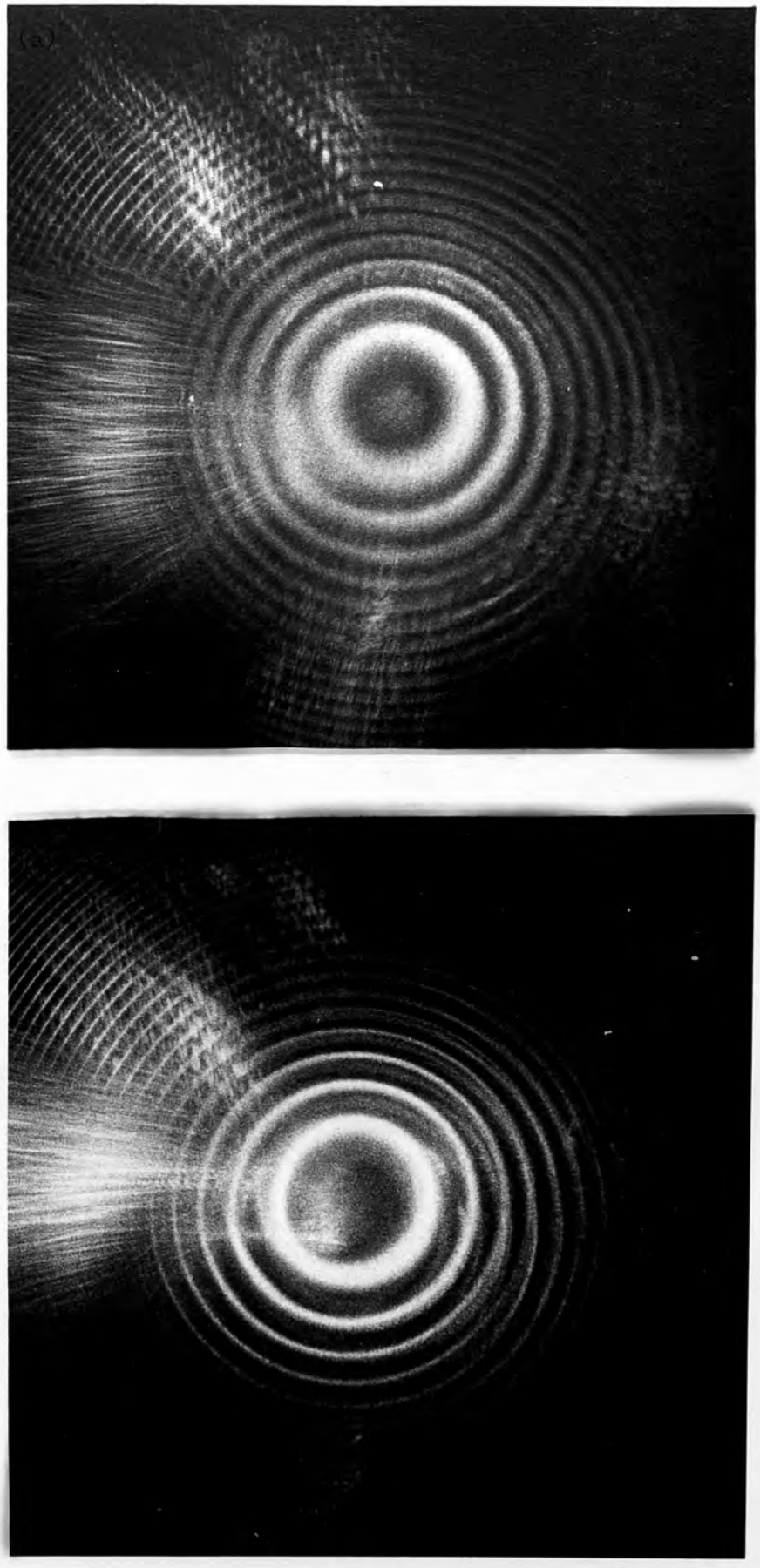

Fig.5.21
Fabry-Perot interferogram of (a) a single pulse, and (b) a train of pulses from a mode locked ruby laser

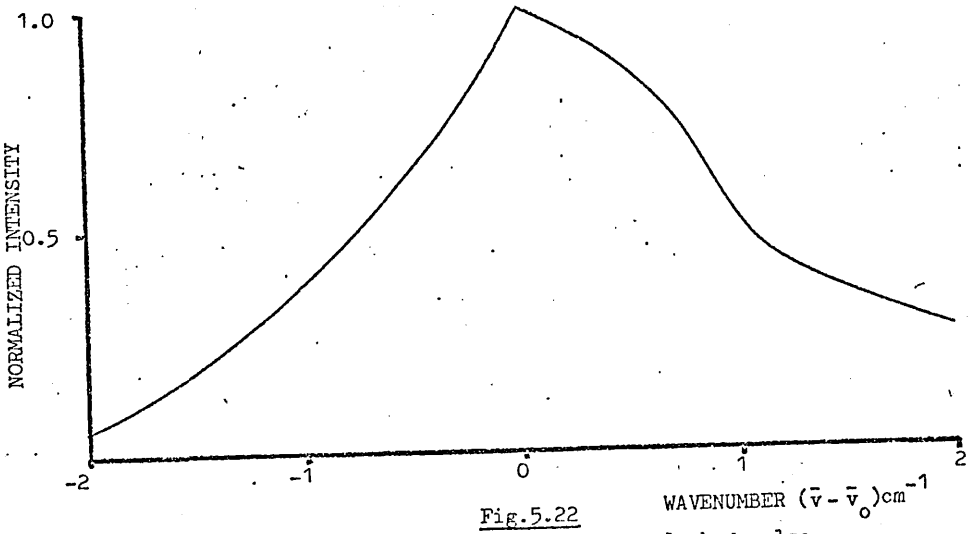

Fig.5.22
Frequency profile of a single mode locked pulse, recorded from a Fabry-Perot interferometer

produces the autocorrelation function of the pulse, which is symmetrical even if the pulse is asymmetrical. The lack of pulse shape information from the TPF technique is one of its main disadvantages.

The strong asymmetry in the spectral profile of the laser output suggests a possible positive frequency sweep, which could be a prelude to the break-up of the profile as described by Eckardt et al[203]. This type of frequency sweep or chirping is common to Nd:Glass lasers[173,190,204,205] but rarely observed with ruby. It is generally attributed to self-phase modulation[173,190,204] resulting from an intensity-dependent refractive index change in the laser rod.

CHAPTER VI

CONCLUSION AND SUGGESTIONS FOR FUTURE WORK

The results of the damage analysis of Chapter II indicate that the problem of the deterioration of a coated glass surface, irradiated by low power laser light, is far from simple.

It was shown for power levels as low as 0.1W and intensities of less than 5 KW/cm^2, that irreversible damage occurred to the glass substrate. It is reasonable to conclude that the mechanism of the damage process is thermal in nature, although the actual reason why the glass should flow against gravity to form small 'hillocks' is unclear. The extent of the damage can to some extent be deduced from the solution of the heat conduction equation; however, a comprehensive formulation of the processes involved requires taking into consideration not only the phase of the material but also its mechanical properties. The task of formulating such a problem is immense, and a more fruitful approach may be that of undertaking a time dependent interferometric study of the surface during the initial stages of hillock development before any vaporization takes place.

In Chapter III a study of the temporal development of optically etched gratings was undertaken. It was shown that during the creation of these gratings, small microplasmas may form above the surface of the glass substrate. The density of some of these plasmas is estimated to be greater than 4.5×10^{27} electrons/m^3. This figure represents the critical density above which the argon ion probe beam, used to investigate the formation of the gratings, will be reflected from the plasma.

This technique is useful in determining not only the point at which the plasma density is above the critical density, but also the kinetics, over small distances, of the laser initiated plasma.

One of the main problems with this technique is that the recorded diffraction signal represents a summation of the diffraction signals from different points on the surface of the grating. If the grating were completely uniform no problem would exist, but this is generally not the case. A further improvement of the technique would, therefore, be to improve the transverse profile of the ruby laser beam. This could be done by including lenses to compensate for thermal focusing, or the use of apodizers[214] to reduce the high order transverse modes. Once uniformity has been established across the laser beam, then such hardware as streak cameras could be used to clarify the kinetics of the laser initiated plasma.

A new approach has been adopted in Chapter IV to determine the time-dependent stimulated scattering frequency-gain profile, for both absorbing and non-absorbing liquids. This new technique has been applied to the particular case of Rayleigh and Brillouin scattering. Although this technique gives identical results to the methods previously used, it does simplify considerably the mathematics involved, and it is possible from a cursory inspection to understand the physics of the problem without becoming confused by the mathematics.

This approach has recently been extended[215] to calculate the time dependent gain profile for other types of scattering, some of which have not previously been solved by any other method.

In Chapter V the design of a ruby ring laser is described. This laser, although not the ultimate design for a mode locked laser, is far more reliable and inexpensive than many other systems. This laser is capable of supplying pulses of approximately 26 ps in duration with peak intensities of 100 MW/cm^2. In the same chapter the techniques used to measure the temporal and spectral width of the laser output are described.

In addition, a simple method for determining the adjustment necessary for minimum divergence is also detailed. This method involves measuring the output energy of the laser for various positions of a lens couple. The lens couple is used to compensate for thermal focusing.

By incorporating a ruby amplifier into the system, the laser could be used to investigate, on a picosecond time scale, both damage and non-linear optical processes. The additional power of the system would also allow the duration of the individual pulses to be determined from a two photon fluorescence arrangement.

APPENDIX I

THE SOLUTION OF THE 2-D HEAT FLOW EQUATION FOR AN INSTANTANEOUS PERIODIC DISTRIBUTION OF HEAT AT THE SURFACE OF A SEMI-INFINITE SOLID

The 2-D heat flow equation is given by:

$$\frac{\partial^2 T(x,y,t)}{\partial y^2} + \frac{\partial^2 T(x,y,t)}{\partial x^2} - \frac{\rho_o c_p}{K} \frac{\partial T(x,y,t)}{\partial t} = 0 \qquad \ldots (A1.1)$$

Taking the Laplace transform of equation (A1.1) with respect to time, we get:

$$\beta \frac{\partial^2 \bar{T}(x,y,p)}{\partial y^2} + \beta \frac{\partial^2 \bar{T}(x,y,p)}{\partial x^2} - p\bar{T}(x,y,p) = - T(x,y,0) \qquad \ldots (A1.2)$$

where

$$\bar{T}(x,y,p) = \int_0^{+\infty} T(x,y,t)\, e^{-pt}\, dt$$

$$\beta = K/\rho_o c_p$$

and $T(x,y,0) = T_o\, \delta(y) \cos kx$ Initial condition .

Now let us take the Fourier transform of the spatial coordinates of equation (A1.2), where

$$\hat{T}(k_x,k_y,p) = \int_0^{\infty} dy \int_{-\infty}^{+\infty} \bar{T}(x,y,p)\, e^{i(k_x x + k_y y)}\, dx$$

$$\therefore \quad \hat{T}\left[\beta k_y^2 + \beta k_x^2 + p\right] = T_o \int_{-\infty}^{+\infty} \cos kx\, e^{ik_x x}\, dx$$

or

$$\hat{T}(k_x,k_y,p) = \frac{T_o \int_{-\infty}^{+\infty} \cos kx\, e^{ik_x x}\, dx}{\left[\beta(k_y^2 + k_x^2) + p\right]}$$

Taking the inverse Laplace transform we get

$$\hat{T}(k_x,k_y,t) = T_o\, e^{-\beta(k_x^2 + k_y^2)t} \int_{-\infty}^{+\infty} \cos kx \,.\, e^{ik_x x}\, dx \,.$$

Taking the inverse Fourier transform w.r.t. k_y we get

$$\hat{T}(k_x,y,t) = T_o\, e^{-\beta k_x^2 t} \int_0^{+\infty} e^{-\beta k_y^2 t} \,.\, e^{-ik_y y}\, dk_y \int_{-\infty}^{+\infty} \cos kx\, e^{+ik_x x}\, dx \qquad \ldots (A1.3)$$

Now let

$$I = \int_0^\infty e^{-\beta k_y^2 t - i k_y y} dk_y$$

By completing the square we get

$$I = e^{-y^2/4\beta t} \int_0^\infty \exp\left\{-\left[(\beta t)^{\frac{1}{2}} k_y + iy/2(\beta t)^{\frac{1}{2}}\right]^2\right\} dk_y$$

Let

$$z = (\beta t)^{\frac{1}{2}} k_y + iy/2(\beta t)^{\frac{1}{2}}$$

then

$$dz = (\beta t)^{\frac{1}{2}} dk_y$$

and

$$I = \frac{e^{-y^2/4\beta t}}{\sqrt{\beta t}} \int_0^\infty e^{-z^2} dz$$

Now

$$\int_0^\infty e^{-z^2} dz = \tfrac{1}{2}\sqrt{\pi}$$

$\therefore$

$$I = \tfrac{1}{2}\sqrt{\frac{\pi}{\beta t}} \cdot e^{-y^2/4\beta t}$$

Substituting this result back into equation (A1.3) we get

$$\hat{T}(k_x,y,t) = T_o \tfrac{1}{2}\sqrt{\frac{\pi}{\beta t}}\, e^{-\beta k_x^2 t} \cdot e^{-y^2/4\beta t} \int_{-\infty}^{+\infty} \cos kx \cdot e^{ik_x x} dx .$$

Now taking the inverse Fourier transform of $\hat{T}(k_x,y,t)$

$$T(x,y,t) = T_o \tfrac{1}{2}\sqrt{\frac{\pi}{\beta t}} \cdot e^{-y^2/4\beta t} \int_{-\infty}^{+\infty} e^{-\beta k_x^2 t} \left\{ \int_{-\infty}^{+\infty} \cos kx \cdot e^{+ik_x x} dx \right\} e^{-ik_x x} dk_x$$

The Fourier transform of the product of two functions is equal to the convolution of the product of the Fourier transforms of the two functions taken separately, i.e.

$$\widehat{FG} = \hat{F} * \hat{G}$$

$$\therefore T(x,y,t) = T_o \tfrac{1}{2}\sqrt{\frac{\pi}{\beta t}} \cdot e^{-y^2/4\beta t} \left[\left\{ \int_{-\infty}^{+\infty} e^{-\beta k_x^2 t} e^{-ik_x x} dk_x \right\} * \cos kx \right]$$

$$= T_o \tfrac{1}{2}\sqrt{\frac{\pi}{\beta t}} \cdot e^{-y^2/4\beta t} \left[\left\{ \sqrt{\frac{\pi}{\beta t}} \cdot e^{-x^2/4\beta t} \right\} * \cos kx \right]$$

$$= T_o \frac{\pi}{2\beta t} \cdot e^{-y^2/4\beta t} \int_{-\infty}^{+\infty} e^{-u^2/4\beta t} \cos\{k(x-u)\}\, du$$

$$= T_o \frac{\pi}{4\beta t} \cdot e^{-y^2/4\beta t} \int_{-\infty}^{+\infty} \left\{ e^{-(u^2/4\beta t + iku)} \cdot e^{ikx} + e^{-(u^2/4\beta t - iku)} e^{-ikx} \right\} du$$

Completing the squares we get :

$$\therefore \quad T(x,y,t) = T_o \frac{\pi}{4\beta t} \cdot e^{-y^2/4\beta t} \cdot e^{-\beta t k^2} \int_{-\infty}^{+\infty} \left\{ \exp\left[-\left\{ \frac{u}{2(\beta t)^{\frac{1}{2}}} + i(\beta t)^{\frac{1}{2}} k \right\}^2 \right] e^{ikx} + \exp\left[-\left\{ \frac{u}{2(\beta t)^{\frac{1}{2}}} - i(\beta t)^{\frac{1}{2}} k \right\}^2 \right] \cdot e^{-ikx} \right\} du$$

which reduces to :

$$T(x,y,t) = T_o \frac{\pi}{\sqrt{\beta t}} \cos kx \cdot e^{-y^2/4\beta t} \cdot e^{-\beta t k^2} \int_{-\infty}^{+\infty} e^{-z^2} dz$$

$$\therefore \quad T(x,y,t) = T_o \pi^{\frac{3}{2}} \sqrt{\frac{\rho_o c_p}{Kt}} \cdot \cos kx \cdot e^{-y^2 \rho_o c_p / 4Kt} \cdot e^{-K k^2 t / c_p \rho_o} \quad \ldots (AI.4)$$

Equation (AI.4) therefore describes the temperature of a semi-infinite solid due to an instantaneous periodic distribution of heat at its surface, the surface being defined by the plane $y = 0$.

APPENDIX II

AN ANALYSIS OF THE TWO PHOTON FLUORESCENCE PROFILE

The procedure[79] adopted for measuring pulse widths from two photon fluorescence profiles has been described in Chapter V. In such an arrangement two portions of a laser beam overlap in a cell containing a two photon absorption liquid. Fluorescence is induced in the liquid by simultaneously absorbing two photons at the fundamental laser frequency from the field, resulting from the overlap of the two light beams.

A2.1 THE CONTRAST RATIO

Let us assume that the laser oscillates in many of its axial modes and that the electric field of the beams in the two arms of the triangular folded optics configuration are given by $E_1(z,t)$ and $E_2(z,t)$. The total field at a point z is therefore

$$E(z,t) = E_1(z,t) + E_2(z,t+\tau) \qquad \ldots (A2.1)$$

where τ represents the time delay between the two portions of the laser beam.

The intensity F of the fluorescence recorded in a TPF experiment is proportional to the square of the intensity of the two interacting beams or to the fourth power of the total electric field, i.e.

$$F = k\int\left[E(z,t)E^*(z,t)E(z,t)E^*(z,t)\right]dt \ldots \qquad \ldots (A2.2)$$

where the integral extends over the duration of the optical pulse and k is a constant which takes into consideration the characteristics of the dye and the photographic recording process.

Substituting equation (A2.1) into (A2.2) and multiplying out we get:

$$F(\tau) = k\int E_1(t)\ E_1(t)\ E_1^*(t)\ E_1^*(t)\ dt$$

$$+ k\int E_2(t+\tau)\ E_2^*(t+\tau)\ E_2^*(t+\tau)\ E_2(t+\tau)\ dt$$

$$+ 4k\int E_1(t)\ E_2(t+\tau)\ E_1^*(t)\ E_2^*(t+\tau)\ dt$$

$$+ 2k\int \left\{E_1(t)E_1^*(t) + E_2(t+\tau)E_2^*(t+\tau)\right\}\left\{E_1(t)E_2^*(t+\tau) + E_1^*(t)E_2(t+\tau)\right\} dt$$

$$+ k\int \left[\left\{E_1(t)\ E_2^*(t+\tau)\right\}^2 + \left\{E_1^*(t)\ E_2(t+\tau)\right\}^2\right] dt$$

The slow response time of the TPF dye and the low resolution of the photographic recording technique ensures that the interval dt of the integrals extends over several optical periods. The last two terms of $F(\tau)$ will, therefore, tend to zero since these describe interference effects which are proportional to oscillatory terms and will cancel out over many optical periods.

Apart from the magnitude, the first two terms of F are identical, since no cross products occur and they describe the same function.

$$\therefore \quad F(\tau) = (\alpha^2 + \beta^2)k\int E^2(t)E^{*2}(t)dt + 4\alpha\beta k\int E(t)E^*(t)E(t+\tau)E^*(t+\tau)\,dt$$

where $E_1(t) = \sqrt{\alpha}\,E(t)$

$E_2(t) = \sqrt{\beta}\,E(t)$

The two integrals in the above equation are proportional to the normalised intensity autocorrelation function $G^{(2)}$, this is also known as Glaubers second order coherence function[205] and is given by:

$$G(\tau) = \frac{\int E(t+\tau)E^*(t+\tau)E(t)E^*(t)\,dt}{\int E^2(t)\,E^{*2}(t)\,dt}$$

$$\therefore \quad F(\tau) = F_o\left[(\alpha^2 + \beta^2)\ G^{(2)}(0) + 4\alpha\beta\ G^{(2)}(\tau)\right]$$

where F_o is the fluorescence produced by a single pulse.

Let us define the contrast ratio (CR) as the ratio of the intensity peak of the fluorescence to that of the background, where the background is taken at some point remote from the overlap region.

Then

$$CR = \frac{(\alpha^2 + \beta^2 + 4\alpha\beta)G^{(2)}(0)}{(\alpha^2 + \beta^2)G^{(2)}(0) + 4\alpha\beta\, G^{(2)}(\tau)}$$

We shall now discuss the value of the contrast ratio for both a mode locked laser pulse (i.e. bandwidth limited), and the output of a free running laser in which the modes are randomly phased.

(a) A Mode Locked Laser Pulse

For a well defined laser pulse which is frequency mode locked, the value of the coherence function $G^{(2)}(\tau)$ at some point remote from the overlap region is zero, since no correlation exists between the two pulses.

$$\therefore \quad CR = \frac{\alpha^2 + \beta^2 + 4\alpha\beta}{\alpha^2 + \beta^2}$$

If both beams are of equal intensity, then $\alpha = \beta$ and $CR = 3.0$.

(b) A Free Running Laser

For a free running laser or chaotic light, the coherence function $G^2(0)$ is equal to two. The value of this function was first measured by Hanbury-Brown and Twiss[206] in 1954. They showed that the correlation function $G^{(2)}(\tau)$ exhibits a well defined structure even though the incoming light is thermal or chaotic (i.e. without any regular structure). For the same reasons the TPF experiments record a structure, with a maximum at $\tau = 0$, when the laser is free running. The value of the correlation decreases from two to become equal to one when $G^{(2)}(\tau)$ is sampled at a point remote from the overlap region[207-209].

$$\therefore \quad CR = \frac{\alpha^2 + \beta^2 + 4\alpha\beta}{\alpha^2 + \beta^2 + 2\alpha\beta}$$

If both beams are equal then, $CR = 1.5$.

It can clearly be seen that an estimate of the CR is needed from a TPF experiment before the validity of the results can be confirmed; this was originally pointed out by Weber[188] in 1968.

A computational study of the TPF profile resulting from a low number of oscillating modes and a free running laser have been reported by Rowe et al[210] and Weber, et al[211].

It is interesting to note that with a well made locked laser pulse where the two interacting beams differ in intensity by 4% (as in the TPF experiments described in Chapter V), the contrast ratio hardly changes from 3.0. In fact a gross inequality in the intensity of the two beams is needed before any significant change is seen in the recorded contrast ratio (see Fig.AII.1).

The recorded contrast ratio is also dependent on the fraction of the oscillating modes that are phase locked. The effect of partial mode locking has been treated by Picard and Schweitzer[200] and by Harrach[198]. Harrach[198] shows that the contrast ratio will be reduced to approximately 2.5 if only 50% of the oscillating modes are phase locked.

A2.2 CALCULATION OF THE TPF PROFILE FOR GAUSSIAN PULSES

Consider a TPF experiment in which two equal portions of a laser beam having a Gaussian temporal profile overlap in a TPF cell at a position z. Let the electric field of the two laser beams be described by:

$$E(t) = E_0 \exp\left[-a t^2/2\right] e^{i(\omega_0 t + kz)} + c.c.$$

$$E(t+\tau) = E_0 \exp\left[-a(t+\tau)^2/2\right] e^{i(\omega_0 (t+\tau) + kz)} \quad c.c.$$

c.c. = complex conjugate.

where τ represents the delay between the two portions of the original laser beam, i.e. $\tau = 2zn/c$, n being the refractive index of the dye, and c the velocity of light.

As we have seen in the previous section, the fluorescence recorded at z is given by:

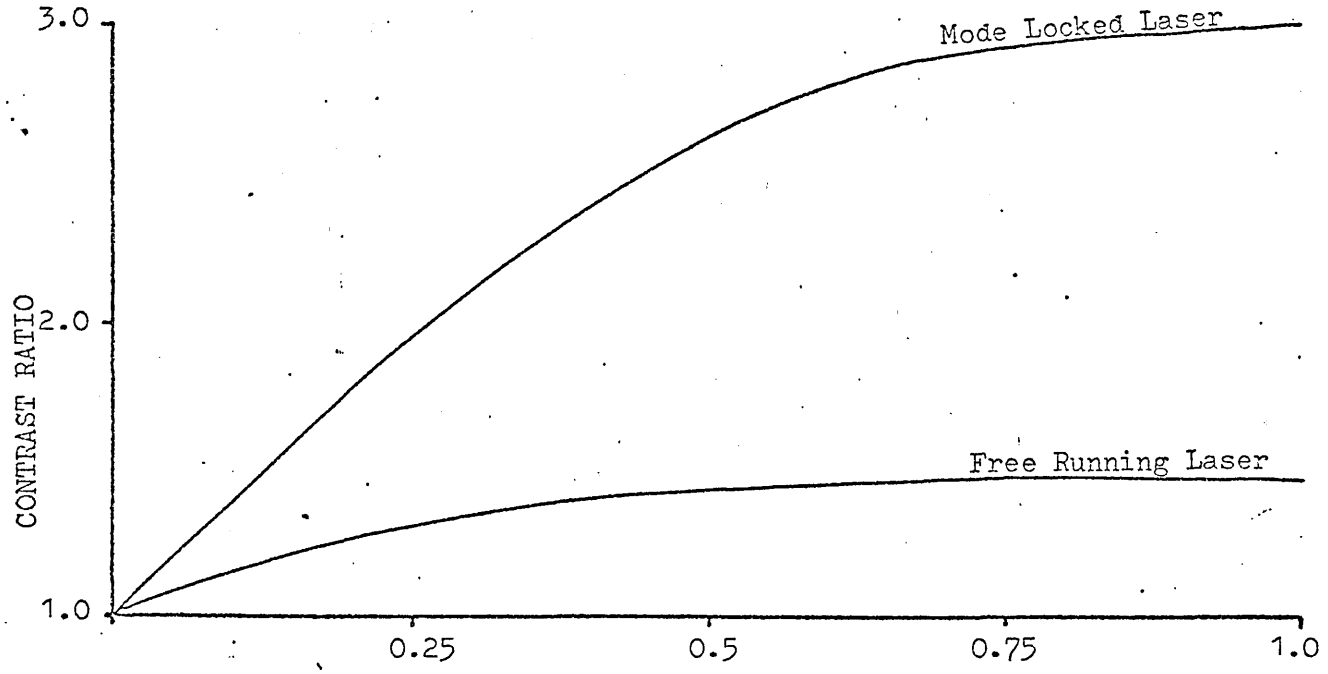

Fig.AII.1

The variation of contrast ratio with the intensity ratio of the two beams in a two photon fluorescence experiment

$$F(\tau) = 2F_o\left[G^{(2)}(0) + 2\,G^{(2)}(\tau)\right] .$$

Since experimentally the recording technique is low in both temporal and spatial resolution, the high frequency components of $E(t)$ will cancel out over many optical periods. This means that only the envelope of the pulse, the duration of which we assume is large compared to $(\omega_o)^{-1}$, will be of any importance.

$$\therefore \qquad F(\tau) = 2F_o \left[1+ \frac{2E_o^4 \int_{-\infty}^{\infty} e^{-a(t+\tau)^2}\, e^{-at^2} dt}{E_o^4 \int_{-\infty}^{\infty} e^{-2at^2}\, dt} \right]$$

which reduces to:

$$F = 2F_o\left[1 + 2e^{-a\tau^2/2}\right] .$$

A Gaussian light pulse will, therefore, give rise to a Gaussian fluorescence profile sitting on a background.

If we define $\tau_{\frac{1}{2}}$ as the full width at half maximum (FWHM) of the fluorescence profile above the background, and $t_{\frac{1}{2}}$ as the FWHM of the intensity profile of the Gaussian laser pulse, then it can be seen that

$$\tau_{\frac{1}{2}} = \sqrt{2}\; t_{\frac{1}{2}} .$$

The spatial width Δz of the TPF profile is what one normally measures in an experiment, and since $\tau = \frac{2zn}{c}$, the width of the laser pulse is, therefore, given by:

$$t_{\frac{1}{2}} = \frac{2\Delta z\, n}{\sqrt{2}\, c} .$$

In general the ratio of $\tau_{\frac{1}{2}}/t_{\frac{1}{2}}$ will depend on the shape of the laser pulse, but in practice it is found to lie, for most types of pulses, between one and two.

REFERENCES

(1) EINSTEIN, A., Physik, 18, (7), 121 (1917).

(2) PURCELL, E. and POUND, R., Phys. Rev., 81, 279 (1951).

(3) GORDON, J., ZEIGER, H., and TOWNES, C., Phys. Rev., 95, 282 (1954).

(4) SCHAWLOW, A. and TOWNES, C., Phys. Rev., 112, 1940 (1958).

(5) MAIMAN, T., Nature, 187, 493 (1960).

(6) McCLUNG, F. and HELLWARTH, R., J. Appl. Phys., 33, 828 (1962).

(7) SOROKIN, P., LUZZI, J., LANKARD, J. and PETTIT, G., IBM J. Research and Development, 8, 182 (1964).

(8) KAFALAS, P., MASTERS, J. and MURRAY, E., J. Appl. Phys., 35, 2349 (1964)

(9) PENNEY, A. and HEYNAU, H., Appl. Phys. Lett., 9, 257 (1966).

(10) BRADLEY, D., NEW, G. and CAUGHEY, S., Phys. Lett., 30A, 78 (1969).

(11) JAVAN, A., BENNETT, W. and HERRIOTT, D., Phys. Rev. Lett., 6, 106 (1961).

(12) READY, J.F., J. Appl. Phys., 36, (2), 462 (1965).

(13) READY, J.F., Appl. Phys. Lett., 3, (1), 11 (1963).

(14) DABBY, F.W. and PAEK, U., IEEE J. Quant. Elect., QE-8, (2), 106 (1972).

(15) STEVERDING, B., J. Phys. D. Appl. Phys., 3, 358 (1970).

(16) ANISIMOV, S.I., JETP, 31, (1), 181 (1970).

(17) MEAD, S.W., Phys. Fluids, 13, (6), 1510 (1970).

(18) PARKS, J.H. and ALYASSINI, N., 'Laser Induced Damage in Optical Materials', Eds. A.J. Glass and A.H. Guenther, NBS Special Pub., 372 (U.S. Govt. Printing Office, Washington, D.C. p.104 (1972).)

(19) DAWSON, J.M., Phys. Fluids, 7, (7), 981 (1964).

(20) BLISS, E.S., MILAM, D. and BRADBURY, R.A., Appl. Opt., 12, 677 (1973).

(21) CUTTER, M.A., KEY, P.Y, LITTLE, V.I., Appl. Opt., 13, (6), 1399 (1974).

(22) ARCHBOLD, E., HARPER, D.W. and HUGHES, T.P., Brit. J. Appl. Phys., 15, 1321 (1964).

(23) GIBSON, A.F., HUGHES, T.P. and KIMMETT, M.F., Phys. Lett., 27A, (8), 470 (1968).

(24) LICHTMAN, D. and READY, J.F., Phys. Rev. Lett., 10, 342 (1963).

(25) GIORI, F., MACKENZIE, L.A., McKINNEY, E.J., Appl. Phys. Lett., 3, 25 (1963).

(26) HENDERSON, B., GETTY, R., LEROI, G. and ROUSSEAU, D., 'Damage in Laser Materials', Eds. A.J. Glass and A.H. Guenther NBS Special Pub. 356 (U.S. Govt. Printing Office, Washington, D.C., p.31 (1971))

(27) ALLINGHAM, C.O., CUTTER, M.A., KEY, P.Y. and LITTLE, V.I., J. Phys. D., 6, 1 (1973).

(28) BRILLOUIN, L., Ann. Phys. (Paris), 17, 88 (1922).

(29) GROSS, E., Nature, 126, pp.201, 400, 603 (1930).

(30) CHIAO, R., TOWNES, C. and STOICHEFF, B., Phys. Rev. Lett., 12, 592 (1964).

(31) CHIAO, R., Ph.D. Thesis, M I T Cambridge, (1965).

(32) CHIAO, R., TOWNES, C. and STOICHEFF, B., Phys. Rev. Lett., 12, 592 (1964).

(33) BLISS, E., Opto—Electronics, 3, 99 (1971).

(34) WASSERMAN, A., Appl. Phys. Letts., 10, (4), 132 (1967).

(35) ZVEREV, G., MIKHAILOVA, T., PASHKOV, V and SOLOVEVA, N., J E T P , 26, (6), 1053 (1968).

(36) BASS, M., BARRETT, H., 'Damage in Laser Materials', Eds. A.J. Glass and A.H. Guenther, N B S Special Pub. 356 (U.S. Govt. Printing Office, Washington, D.C. p.76 (1971))

(37) BELIKOVA, T., SAVCHENKO, A. and SVIRIDENKOV, E., J E T P , 27, (1), 19 (1968).

(38) BLISS, E., MILAM, D. and BRADBURY, R., Appl. Optics, 12, (4), 677 (1973).

(39) CHIAO, R., GARMIRE, E. and TOWNES, C., Phys. Rev. Lett., 13, 479 (1964).

(40) BUDIN, J., and RAFFY, J., Appl. Phys. Lett., 9, (8), 291 (1966).

(41) ZVEREV, G., MIKHAILOVA, T., PASHKOV, V. and SOLOVEVA, N., J E T P , 5, (11), 319 (1967).

(42) GIULIANO, C., 'Damage in Laser Materials', Eds. A.J. Glass and A.H. Guenther, N B S Special Pub. 356, (U.S. Govt. Printing Office, Washington D.C., p.44 (1971)).

(43) AKHMANOV, S., SUKHOROKOV, A. and KHOKHLOV, R., Sov. Phys. Usp. 10, 609 (1968).

(44) MARBURGER, J., 'Damage in Laser Materials', Eds. A.J. Glass and A.H. Guenther, N B S Special Pub. 356, (U.S. Govt. Printing Office, Washington D.C., p.51 (1971)).

(45) GIULIANO, C.R. and MARBURGER, J.H., Phys. Rev. Lett., 27, (14), 905 (1971).

(46) BREWER, R. and LEE, C., Phys. Rev. Letts., 21, (5), 267 (1968).

(47) ALFANO, R. and SHAPIRO, S., Phys. Rev. Lett., 24, (11), 592 (1970).

(48) POLLONI, R., SACCHI, C. and SVELTO, O., Phys. Rev. Lett., 23, (13), 690 (1969).

(49) CARMAN, R., MOORADIAN, A., KELLEY, P. and TUFTS, A., Appl. Phys. Lett., 14, 136 (1969).

(50) ZVEREV, G. and PASHKOV, V., Sov. Phys. J E T P , 30, 616 (1970).

(51) LITVAK, A., J E T P Letts., 4, 230 (1966).

(52) KERR, E.L., 'Damage in Laser Glass', Philadelphia, Pa, American Society for Testing and Materials, A S T M , S T P 469, p.23 (1969)

(53) ISUMATANI, T., HOSAKA, K. and YAMANAKA, C., 'Laser Induced Damage in Optical Materials', Eds. A.J. Glass and A.H. Guenther. N B S Special Pub. 372 (U.S. Govt Printing Office, Washington, D.C. p.3 (1972).

(54) YOUNG, C., WOODCOCK, R., 'Damage in Laser Glass', Eds. A.J. Glass, A.H. Guenther, C.M. Stickley and J.D. Myers. A S T M , S T P 469 (1969).

(55) HOPPER, R. and UHLMANN, D., J. Appl. Phys., 41, (10), 4023 (1970).

(56) ESHELBY, J.D., In 'Solid State Physics' , Eds. D. Turnbull and F. Seitz, (Academic, New York, vol.3, 1956).

(57) LANDAU, L. and LIFSHITZ, E., 'Electrodynamics of Continuous Media', Pergamon Press, London, 1960.

(58) BLOEMBERGEN, N., 'Nonlinear Optics', Benjamin Press, New York, 1965.

(59) ARMSTRONG, J., BLOEMBERGEN, N., DUCUING, J. and PERSHAN, P., Phys. Rev., 127, (6), 1918 (1962).

(60) FRANKEN, P. and WARD, J., Rev. Mod. Phys., 35, 23 (1963).

(61) BASS, M., FRANKEN, P., WARD, J. and WEINREICH, G., Phys. Rev. Lett., 9, 446 (1962).

(62) FRANKEN, P., HILL, A., PETERS, C. and WEINREICH, G., Phys. Rev. Lett., 7, 118 (1961).

(63) BASS, M., FRANKEN, P., HILL, A., PETERS, C. and WEINREICH, G., Phys. Rev. Lett., 8, (1), 18 (1962).

(64) MAKER, P., TERHUNE, R., NISENOFF, M. and SAVAGE, C., Phys. Rev. Lett., 8, (1), 21 (1962).

(65) GIORDMAINE, J., Phys. Rev. Lett., 8, (1), 19 (1962).

(66) MILLER, R., Phys. Rev., 131, 95 (1963).

(67) FRANKEN, P. and WARD, J., Rev. Mod. Phys., 35, (1), 23 (1963).

(68) SMITH, A. and BRASLAU, N., I B M J. Res. and Development, 6, 361 (1962).

(69) MILLER, R., and SAVAGE, A., Bull. Am. Phys. Soc., 7, 329 (1962).

(70) WANG, C. and RACETTE, C., Appl. Phys. Lett., 8, 169 (1965).

(71) GIORDMAINE, J. and MILLER, R., Phys. Rev. Lett., 14, (24), 973 (1965).

(72) NIEBUHR, K., Appl. Phys. Lett., 2, (7), 136 (1963).

(73) PETERSON, G. and YARIV, A., Appl. Phys. Lett., 5, 184 (1964).

(74) TERHUNE, R., MAKER, P. and SAVAGE, C., Phys. Rev. Lett., 8, 404 (1962).

(75) DUNNINGTON, F., Phys. Rev., 38, 1506 (1931).

(76) KAISER, W. and GARRETT, C., Phys. Rev. Lett., 7, 229 (1961).

(77) RENTZEPIS, P. and DUGUAY, M., Appl. Phys. Lett., 11, (7), 218 (1967).

(78) SINGH, S. and BRADLEY, L., Phys. Rev. Lett., 12, 612 (1964).

(79) GIORDMAINE, J., RENTZEPIS, P., SHAPIRO, S. and WECHT, K., Appl. Phys. Lett., 11, (7), 216 (1967).

(80) RENTZEPIS, P., MITSCHELE, C. and SAXMAN, A., Appl. Phys. Lett., 17, (3), 122 (1970).

(81) RAYLEIGH, Lord, Phil. Mag., 12, 81 (1881).

(82) EINSTEIN, A., Ann. Physik, 33, 1275 (1910).

(83) DEBYE, P., Ann. Physik, 39, 789 (1912).

(84) MANDELSHTAM, L., J. Russian Soc. Phys. Chem., 58, 381 (1926).

(85) LANDAU, L. and PLACZEK, G., Phys. Z. Sov., 5, 172 (1934).

(86) CUMMINS, H., KNABLE, K. and YEH, Y., Phys. Rev. Lett., 12, 150 (1964).

(87) GREYTAK, T. and BENEDEK, G., Phys. Rev. Lett., 17, 179 (1966).

(88) LASTOVKA, J. and BENEDEK, G., Phys. Rev. Lett., 17, 1039 (1966).

(89) FORD, N. and BENEDEK, G., Phys. Rev. Lett., 15, 649 (1965)

(90) RAMAN, C. and KRISHNAN, K., Phil. Mag., 5, 498 (1928).

(91) RAMAN, C., Ind. J. Phys., 2, 387 (1928).

(92) WOODBURY, E., and NG, W., Proc. I R E , 50, 2367 (1962).

(93) DENARIEZ, M. and BRET, G., Phys. Rev., 171, 161 (1968).

(94) MASH, D., MOROZOV, V., STARUNOV, V., TIGANOV, E. and FABELINSKII, I. J E T P Lett., 2, 157 (1965).

(95) ZIATSEV, G., KYZYLASOV, Y., STARUNOV, V. and FABELINSKII, I. J E T P Lett., 6, 255 (1967).

(96) BESPALOV, V. and KUBAREV, A., J E T P Lett., 6, 31 (1967).

(97) HERMAN, R. and GRAY, M., Phys. Rev. Lett., 19, 824 (1967).

(98) RANK, D., CHIAO, C., FOLTZ, N. and WIGGINS, T., Phys. Rev. Lett., 19, 828 (1967).

(99) POHL, D., REINHOLD, I. and KAISER, W., Phys. Rev. Lett., 20, 1141 (1968).

(100) MASTERS J., WARD, J. and HARTOUNI, E., Rev. Sci. Instrum., 34, 365 (1963).

(101) GRANT, D., Proc. I E E E , 51, 604 (1963).

(102) LITTLE, V., ROWLEY, D. and WILTSHIRE, R., Nature, 228, (5266), 49 (1970).

(103) ROWLEY, D., Ph.D. Thesis, London University, (1971).

(104) BOERSCH, H. and EICHLER, H., Z. Fur. Ang. P., 22, 378 (1967).

(105) LEDGER, A., Appl. Opt., 5, 476 (1966).

(106) LITTLE, V.I., CUTTER, M.A., KEY, P.Y. and HARRISON, R.G., Contemp. Phys., 15, (3), 271 (1974).

(107) LITTLE, V.I., KEY, P.Y., WILTSHER, R. and ROWLEY, D.M., Nature Phys. Sci., 232, 165 (1971).

(108) SQUIRES, G., 'Practical Physics', McGraw-Hill, London, (1968)

(109) ALYASSINI, N., PARKS, J., and DeSHAZER, L., University of Southern California: Private communication.

(110) GIULIANO, C.R., IEEE J. Quant. Electron., QE-8, 749 (1972).

(111) ISENOR, N.R., J. Appl. Phys., 36, 316 (1965).

(112) KNECHT, W.L., Appl. Phys. Letts., 6, 99 (1965).

(113) KNECHT, W.L., Appl. Phys. Letts., 8, 254 (1966).

(114) KHAN, S., RICHARDS, F. and WALSH, D., IEEE J. Quant. Electron., QE-1, 359 (1965).

(115) KNECHT, W.L., IEEE J. Quant. Electron., QE-2, 103 (1966)

(116) IANNUZZI, M. and WILLIAMSON, R., Nuovo Cimento, 36, 1130 (1965).

(117) KINGDON, K. and LANGMUIR, I., Phys. Rev., 21, 380 (1923).

(118) ALLEN, C., 'Astrophysical Quantities', Athlone Press: London, (1955).

(119) CORSON, D. and LORRAIN, P., 'Electromagnetic Fields and Waves', W.H. Freeman & Co., London (1962).

(120) CARION, A., LANCELOT, J., de METZ, J. and SALERES, A., Phys. Lett. A (Netherlands), 45A, (6), 439 (1973).

(121) GOLDMAN, L.M., SOURES, J. and LUBIN, M.J., Phys. Rev. Lett.,(USA) 31, (19), 1184 (1973).

(122) SOURES, J., GOLDMAN, L.M. and LUBIN, M., Nucl. Fusion (Austria), 13, (6), 829 (1973).

(123) VOROBEVA, N., ORLOV, V. and ROVINSKII, R., Soviet J. Quant. Electron., (USA), 3, (2), 138 (1973).

(124) McCLUNG, F. and WEINER, D., J. Opt. Soc. Am., 54, (5), 641 (1964).

(125) JONES, W. and STOICHEFF, B., Phys. Rev. Lett., 13, (22), 657 (1964).

(126) WEINER, D., SCHWARZ, S. and McCLUNG, F., J. Appl. Phys., 36, (8), 2395 (1965).

(127) SHIMIZU, T. and SHIMIZU, F., Jap. J. Appl. Phys., 5, (10), 948 (1966).

(128) ZAITSEV, G., KYZYLASOV, Y., STARUNOV, V. and FABELINSKII, I., JETP Lett., 6, 35 (1967).

(129) WIGGINS, T., WICK, R. and RANK, D., Appl. Opt., 5, 1069 (1966).

(130) POHL, D., MAIER, M. and KAISER, W., Phys. Rev. Lett., 20, (8), 366 (1968).

(131) POHL, D., Phys. Lett., (Netherlands), 26A, 357 (1968).

(132) GIORDMAINE, J. and KAISER, W., Phys. Rev., 144, (2), 676 (1966).

(133) GARMIRE, E., PANDARESE, F. and TOWNES, C., Phys. Rev. Lett., 11, 160 (1963).

(134) TANG, C., Phys. Rev., 134A, 1166 (1964).

(135) WALDER, J. and TANG, C., Phys. Rev. Letts., 19, (11), 623 (1967).

(136) WINTERLING, G. and HEINICKE, W., Phys. Letts., 27A, (6), 329 (1968).

(137) HARRISON, R., KEY, P., LITTLE, V., MAGYAR, G. and KATZENSTEIN, J., Appl. Phys. Letts., 13, (8), 253 (1968).

(138) KEY, P., HARRISON, R., LITTLE, V. and KATZENSTEIN, J. IEEE J. Quant. Electron, QE-6, 641 (1970).

(139) KEY, P., 'The scattering of light from light induced structures in liquids', Ph.D. Thesis, London University, (1970).

(140) HARRISON, R., 'Nonlinear optical effects in liquids', Ph.D. Thesis, London University, (1970).

(141) HARRISON, R., KEY, P. and LITTLE, V., Proc. Roy. Soc., London, A 334, 193 (1973).

(142) SHEN, Y. and BLOEMBERGEN, N., Phys. Rev., 137 A, 1787 (1965).

(143) TANG, C., J. Appl. Phys., 37, 2945 (1966).

(144) BAROCCI, F., J. Appl. Phys., 40, (1), 178 (1969).

(145) BOBROFF, D., J. Appl. Phys., 36, 1760 (1965).

(146) GROB, K., Z. Physik, 201, 59 (1967).

(147) LAMBROPOULOUS, P., KERN, S. and MUELLER, R., IEEE J. Quant. Electron. QE-2, (9), 649 (1966).

(148) CORRE, Y. and CACHIER, G., J. de Physique, 28, (2), 1 (1967).

(149) STARUNOV, V., Phys. Lett., 26 A, (9), 428 (1968).

(150) STARUNOV, V., Sov. Phys. JETP, 30, (3), 553 (1970).

(151) BESPALOV, V. and PASMANIK, G., Sov. Phys. JETP, 31, (1), 168 (1970).

(152) BATRA, I. and ENNS, R., Can. J. Phys., 47, 1283 (1969).

(153) BATRA, I. and ENNS, R., Phys. Rev., 185, (1), 396 (1969).

(154) POHL, D. and KAISER, W., Phys. Rev. B, 1, (1), 31 (1970).

(155) RANGNEKAR, S. and ENNS, R., Can. J. Phys., 49, (18), 2307 (1971).

(156) ROTHER, W., POHL, D. and KAISER, W., Phys. Rev. Lett., 22, (18), 915 (1969).

(157) ROTHER, W., Z. Naturforsch, 25a, 1120 (1970).

(158) ENNS, R., Can. J. Phys., 48, 710 (1970).

(159) BAMBINI, A., VALLAURI, R. and ZOPPI, M., Phys. Rev., A 12, 1713 (1975).

(160) Von der LINDE, D., MAIER, M. and KAISER, W., Phys. Rev., 178, 11 (1969).

(161) Di DOMENICO, M. Jr., J. Appl. Phys., 35, (10), 2870 (1964).

(162) TANG, C., STATZ, H. and DeMARS, G., J. Appl. Phys., 34, (8), 2289 (1963).

(163) HARGROVE, L., FORK, R. and POLLACK, M., Appl. Phys. Lett., 5, (1), 4 (1964).

(164) DEUTSCH, T., Appl. Phys. Lett., 7, (4), 80 (1965).

(165) MOCKER, H. and COLLINS, R., Appl. Phys. Lett., 7, (10), 270 (1965).

(166) DeMARIA, A., STETSER, D. and HEYNAU, H., Appl. Phys. Lett., 8, 174 (1966).

(167) SACCHI, C., SONCINI, G. and SVELTO, O., Il Nuovo. Cimento. 48, 58 (1967).

(168) GARMIRE, E. and YARIV, A., IEEE J. Quantum Elect., QE-3, 222 (1967).

(169) FLECK, J., Appl. Phys. Lett., 12, 178 (1968).

(170) FLECK, J., J. Appl. Phys., 39, 3318 (1968).

(171) MACK, M., IEEE J. Quantum Elect., QE-4, (12), 1015 (1968).

(172) POLLONI, R., IEEE J. Quantum Elect., QE-8, 4, Correspondence, 428 (1972).

(173) ECKARDT, R., LEE, C. and BRADFORD, J., Appl. Phys. Lett., 19, (10), 420 (1971).

(174) KASHA, M., Radiation Res., Suppl. 2, 243 (1960).

(175) SPAETH, M. and SOOY, W., J. Chem. Phys., 48, (5), 2315 (1968).

(176) PORTER, G. and WINDSOR, M., Discussions Faraday Society, 17, 178 (1954).

(177) PORTER, G., and WRIGHT, F., Trans. Faraday Soc., 51, 1205 (1955).

(178) GILMORE, E., GIBSON, G. and McCLURE, D., J. Chem. Phys., 20, 829 (1952).

(179) LIVINGSTON, B., PORTER, G. and WINDSOR, M., Nature, 173, 485 (1954).

(180) SCHULLER, H. and PUELL, H., Optics Comm., 3, (5), 352 (1971).

(181) DUGUAY, M. and HANSEN, J., Optics. Comm., 1, (5), 254 (1969).

(182) GIBBS, W., Appl. Phys. Lett., 11, (4), 113 (1967).

(183) MULLER, A. and PFLUGER, E., Chem Phys. Lett., 2, 155 (1968).

(184) HARRISON, R., KEY, P. and LITTLE, V., J. Phys. D. Appl. Phys., 3, 758 (1970).

(185) HOLLIER, R. and MACOMBER, J., Appl. Optics., 11, 1360 (1972).

(186) BOOTH, B., Appl. Opt., 8, 2559 (1969).

(187) BRADLEY, D., NEW, G. and CAUGHEY, S., Opt. Comm., 2, (1), 41 (1970).

(188) WEBER, H., Phys. Lett., 27A, (5), 321 (1968).

(189) DREXHAGE, K., Appl. Phys. Lett., 14, 318 (1969).

(190) DUGUAY, M., HANSEN, J. and SHAPIRO, S., IEEE J. Quantum Elect., QE-6, 725 (1970).

(191) CAUGHEY, S., 'A study of mode-locked giant pulse lasers', Ph.D. Thesis, The Queen's University of Belfast, (1970).

(192) Von der LINDE, D., BERNECKER, O. and KAISER, W., Opt. Comm., 2, 149 (1970).

(193) WEBER, H. and DANIELMEYER, H., Phys. Rev. A, 2, 2074 (1970).

(194) McGEOCH, M., Opt. Comm., 7, 116 (1973)

(195) BRADLEY, D., MORROW, T. and PETTY, M., Optics. Comm., 2, (1), 1 (1970).

(196) BRADLEY, D., HUTCHINSON, M. KOESTER, H., MORROW, T., NEW, G. and PETTY, M., Proc. Roy. Soc., London, A 328, 97 (1972).

(197) OKADA, M. and IEIRI, S., IEEE J. Quant. Elect., QE-6, (8), 526 (1970).

(198) HARRACH, R., Appl. Phys. Letts., 14, (5), 148 (1969).

(199) KLAUDER, J., DUGUAY, M., GIORDMAINE, J. and SHAPIRO, S., Appl. Phys. Lett., 13, 174 (1968).

(200) PICARD, R. and SCHWEITZER, P., Phys. Rev. A., 1, 1803 (1970).

(201) SHAPIRO, S. and DUGUAY, M., Phys. Lett., 28 A, 698 (1969).

(202) DUGUAY, M. and SHAPIRO, S., Bull. Amer. Phys. Soc., ser. II, 14, 618 (1969).

(203) ECKARDT, R., LEE, C. and BRADFORD, J., Opto-Elect., 6, 67 (1974).

(204) KOROBKIN, V., MALYUTIN, A. and PROKHOROV, A., JETP Letts., 12, 150 (1970).

(205) GLAUBER, R., Phys. Rev., 131, 2766 (1963).

(206) HANBURY-BROWN, R. and TWISS, R., Proc. Roy. Soc. (London), A 242, 300 (1957); A243, 291 (1958).

(207) TWISS, R. and LITTLE, A., Australian J. Phys., 12, 77 (1959).

(208) MORGAN, B. and MANDEL, L., Phys. Rev. Lett., 16, 1012 (1966).

(209) ARECCHI, F., GATTI, E. and SONA, A., Phys. Lett., 20, 27 (1966).

(210) ROWE, H. and LI, T., IEEE J. Quant. Elect., QE-6, (1), 49 (1970).

(211) WEBER, H. and DANDLIKER, R., IEEE J. Quant. Elect., QE-4, (12), 1009 (1968).

(212) STARUNOV, V., Sov. Physics Doklady, 8, 1205 (1964).

(213) KATYL, R. and INGARD, U., Phys. Rev. Letts., 20, (6), 248 (1968).

(214) SPECK, D.R. and BLISS, E.S., Lawrence Livermore Laboratory Laser Fusion Programme Semi-Annual Report - July-December 1972, UCRL-50021-72-2, pp.18-19.

(215) CUTTER, M.A., KEY, P.Y. and LITTLE, V.I., Proc. Roy. Soc., (to be published).

(216) STARUNOV, V.S., TIGANOV, E.V. and FABELINSKII, I.L., JETP Letts., 5, 260 (1967).

ACKNOWLEDGEMENTS

I should like to acknowledge the guidance and constant enthusiasm of Dr V.I. Little under whose supervision this work was carried out.

I am also greatly indebted to Dr P.Y. Key with whom I collaborated on many aspects of the work reported in this thesis.

Additional gratitude goes to many other colleagues at Royal Holloway College, especially the workshop staff for their excellent technical support.

In undertaking this research I have been supported financially by the Science Research Council.

This thesis has been typed by Ina Godwin to whom I am most grateful.

Lastly I should like to thank my parents for their support and my wife Sheila for her patience and constant encouragement.

PUBLICATIONS

J. Phys. D: Appl. Phys., Vol. 6, 1973. Printed in Great Britain.

Damage to a transparent substrate by laser light absorption in a thin film

C O Allingham, M A Cutter, P Y Key and V I Little
Royal Holloway College, Egham Hill, Egham, Surrey, TW20 0EX

MS received 10 July 1972, in revised form 7 September 1972

Abstract. Experiments have been performed in which the light output of an argon-ion laser was focused onto a thin film of gold deposited on a glass substrate. In addition to evaporation of the gold film, damage to the substrate surface has been observed for power levels as low as 0·1 W and for intensities of less than 5 kW cm^{-2}. The nature and extent of the damage have been found to vary dramatically with the illumination conditions and film thickness.

1. Introduction

Laser instrumentation very often incorporates components that involve transparent substrates coated with thin metallic or dielectric films. Damage to such films is itself a serious problem which has been the subject of considerable investigation (Kuznetsov *et al* 1970, Turner and Arlin 1970). Even more serious, however, is damage to the substrate material, which, in the presence of an absorbing film, may occur at intensities very much less than those required to damage the uncoated material. Such damage, reported elsewhere by this group (Little *et al* 1970, Rowley 1972, Wiltsher 1973, to be published), has previously been investigated with a pulsed ruby laser. The present paper reports a comprehensive investigation of the damage caused to a glass surface bearing a gold film when illuminated by an argon-ion laser.

2. Experimental details

In the majority of our experiments, the output of a CRL 52B argon-ion laser was focused, in air, onto the surface of a glass microscope slide bearing a thin film of gold previously deposited by evaporation *in vacuo*. The light output, of wavelength 5145 Å, occurred in a single TEM_{∞} transverse mode, and had a divergence of about 1 mrad and a controllable power of up to 3 W. The duration of the illumination was determined by a conventional mechanical shutter, while the use of lenses of 5, 10 and 25 cm focal length gave focal spots whose diameters were 0·05, 0·1 and 0·25 mm respectively. (Throughout this paper the diameter of an illuminated area will refer to the diameter of that region within which the light intensity was greater than $1/e^2$ times the intensity at the centre of the area.) The resulting damage to the substrate surface was analysed interferometrically (Tolansky 1960). The glass slide was placed so that the gold surface formed the mirror of one arm of a Michelson interferometer, and also lay in the focal plane of a microscope receiving the

light from the interferometer. The instrument was illuminated by a sodium lamp, so that adjacent fringes indicate a difference in surface height of 2925 Å. In obtaining the interferograms of figure 1 (plate), the undisturbed surface bearing the gold film was set perpendicular to the interferometer axis, so that the fringes in these pictures indicate the contours of the surface deformation. The interferograms of figure 2 (plate), however, were obtained by setting the glass slide in such a position that the normal to the undisturbed surface made a small angle to the axis of the instrument. This technique, which shows up the relief rather than the contours of the damaged area, was necessary to illustrate unambiguously the complex structure of the surface deformations shown in figure 2.

To test whether the presence of air had any effect on the reported observations, we repeated some of the measurements *in vacuo*; these gave essentially similar results. A further variation of our technique was to focus the laser beam onto the glass surface during the actual deposition of the gold film. The very extensive damage caused in this way is described in §6. When other transparent vitreous substrates were used, the resulting damage was very similar in nature. The extent of the surface damage was, however, much greater for substrates, such as Perspex, which soften at a low temperature, and much less for such refractory substrates as fused silica. More complicated effects on crystal surfaces are still being studied.

3. Theoretical considerations

The intensity I of the light incident at any point in the focal spot of a gaussian laser beam is given by

$$I=I_0 \exp(-8r^2/d^2) \tag{1}$$

where d is the diameter of the focal spot, I_0 the light intensity at its centre, and r the distance of the point from the centre.

The total power P incident on the focal spot is given by

$$P=\int_0^\infty 2\pi r I \, dr. \tag{2}$$

Hence

$$I_0=8P/\pi d^2. \tag{3}$$

If P_T and I_T are respectively the threshold power and intensity for surface damage,

$$I_T=8P_T/\pi d^2. \tag{4}$$

Hence the diameter d_T of the region in the focal spot of a beam of power P, where $I>I_T$, is given by

$$d_T=d\{\tfrac{1}{2}\ln(P/P_T)\}^{1/2}. \tag{5}$$

Now the temperature at the centre of a gaussian focal spot on the surface of a semi-infinite slab which absorbs a fraction a of the light incident upon it is given by (Ready 1971)

$$T=\frac{a\sqrt{2}}{K\sqrt{\pi}}\frac{P}{d} \tag{6}$$

where K is the thermal conductivity of the slab material. Thus the threshold temperature T_T for laser damage is given by

$$T_T=\frac{a\sqrt{2}}{K\sqrt{\pi}}\frac{P_T}{d} \tag{7}$$

and the diameter d_T may be written in the form

$$d_T = d\{\tfrac{1}{2} \ln (a\sqrt{2P/K\sqrt{\pi d T_T}})\}^{1/2}. \tag{8}$$

The temperature indicated by equation (6) is not achieved instantaneously, but is approached asymptotically over a period comparable to τ, where

$$\tau = \frac{d^2 \rho_0 C_p}{32K} \tag{9}$$

ρ_0 and C_p being the density and specific heat of the slab material.

4. Damage caused under various conditions of laser illumination

Figure 1 shows interferograms of the damage caused to the surface of a glass slide bearing a 200 Å gold film by focusing laser beams of the indicated powers and durations to spots with diameters of 0·05, 0·1 and 0·25 mm respectively. Further interferometric tests showed that, in every case, the illuminated region had been raised above the level of the undisturbed surface. The surface distortion caused is clearly very large, rising to a height of 2 μm above the surrounding region in the case of the 3 W, 100 s, 0·25 mm focal spot. The minimum power indicated in each figure is the threshold power below which no surface damage could be detected. Clearly the power P_T is approximately proportional to the focal spot diameter d. Hence equation (7) indicates, in each case, the same threshold temperature T_T: about 1500 °C. At higher powers the diameters of the damaged regions correspond approximately to the value of d_T given by equation (5), although this value is strictly only the diameter of that region where $I > I_T$, and is not necessarily the same as that of the region where $T > T_T$.

The height to which the damaged surface has been raised increases rapidly with increasing light intensity and also with spot diameter. The latter factor is so important that the deformation caused by the 3 W beam when it was focused to a spot of 0·25 mm diameter is much greater than that caused when it was focused to 0·05 mm, in spite of the much higher intensity and temperature indicated by equations (3) and (7) for the smaller spot. (The temperature achieved in focal spots of above-threshold intensity cannot be reliably estimated, since the gold film is destroyed during the illumination, leaving a reddish deposit of unknown absorption coefficient.) Equation (9) indicates that the time τ during which thermal equilibrium was achieved is much less than 0·01 s in all cases. The interferograms show, however, that while all the damaged regions appeared within 0·01 s, none had reached their equilibrium condition within this time. Deformation caused by the 0·25 mm spots continued to grow for more than 10 s, starting as tabular regions with flat tops and steeper sides, but becoming much higher and more rounded with increasing illumination time.

5. Laser damage caused to glass surfaces bearing gold films of various thicknesses

The nature of the damage to the glass surface was found to be strongly dependent on the thickness of the gold film. Interferograms showing the distortion caused to surfaces bearing films of (*a*) 200 Å and (*b*) 1,000 Å are shown in figure 2.

The damage caused to the surface bearing the 200 Å film consisted of a raised region. This region was somewhat depressed in the centre when illuminated for a short period, but

became distinctly domed when the illumination was of longer duration. When the damaged area was examined with a transmission microscope, it could be seen that the gold film had been removed from the raised region, leaving a layer of reddish material. This layer, which was of about the same thickness as the original film, was very soft and could easily be scratched off or dissolved in aqua regia. It was formed even when the surface was illuminated *in vacuo*.

The surface bearing the 1000 Å film was hardly affected by the focal spots of 0·05 mm diameter, whatever the intensity or duration of the illumination. The gold film was entirely removed from the illuminated region, leaving no red deposit, but the only disturbance caused to the surface of the glass was a slight ridge at the boundary of that region. A much higher ridge was generated at the edge of those regions from which the gold had been removed by light focused to a spot of 0·25 mm diameter. In this case the boundary was raised to a height of up to 2 μm, though the surface in the central region was again left undisturbed (except for a 'moat' developed just inside the boundary ridge). This type of damage took from 10 to 100 s to develop fully, and was so severe that it could be examined not only interferometrically but also by direct photography (figure 3, plate).

The diameters of the damaged regions again suggest a threshold temperature for surface damage of about 1500 °C, while total removal of the gold without surface damage appears to have occurred for regions where the temperature exceeded about 2500 °C. This process, however, only occurred in the case of the thicker film, although equation (6) indicates that the temperature of the 200 Å film at the centre of the 3 W spot of 0·25 mm diameter would have approached 4000 °C had the film not been destroyed.

6. Surface damage during inhibition of deposition

When the laser was focused onto the glass surface during the actual deposition of the gold film (Little *et al* 1971), very extensive damage could be caused. Figure 4 (plate) shows an interferogram of the damage caused to the glass surface by a 2 W laser beam focused to a spot of 0·2 mm diameter for a period of 1 min, during which time a gold film 500 Å thick was being deposited on the surface.

The interferogram shows that the damaged region has a domed surface, the centre of which has risen about 6 μm above the surrounding area. When the damage was viewed with a transmission microscope, a number of regions of different surface colour were revealed. In a central region, having approximately the same diameter as the focal spot, the glass surface had acquired a smooth yellow coloration. This region was surrounded by an almost transparent area with a slight red granulation that became more marked with increasing distance from the centre of the spot. This area, in turn, was surrounded by a red border which extended to the limit of the area of surface deformation. The cracking around the damaged area (indicated by the discontinuity in the interference pattern shown in figure 4) occurred some hours after the laser illumination, and indicates that extremely high stresses had been induced in the glass as a result of this experiment. All the surface colours could be easily scratched off, but their removal by aqua regia occurred much more slowly than that of the gold film.

7. Conclusions

Our observations indicate that the mechanism by which damage was caused to the glass surface was entirely thermal in nature. The intensity of the light was many orders of

magnitude too low to induce significant nonlinear optical effects, and no damage was observed in the absence of the absorbing gold film.

The threshold temperature for surface damage was of the same order as that of the melting point of gold, but the exact mechanism by which the surface was raised to the very large heights observed is unclear. Thermal expansion would cause an increase in height of the correct order of magnitude, but in the absence of glass flow this would disappear on cooling. The slow growth of the deformation caused by the larger focal spots also suggests that glass flow plays a crucial role. Such flow would, however, leave another region perceptibly lower than the undisturbed surface, unless very large stresses were frozen into the bulk substrate. No such region was in fact observed, and the cracking that occurred in extreme cases confirms that the increase in volume required for the raised surface arose from extension of the surrounding glass under extreme tension.

The interferograms of the damage caused in the presence of the 1000 Å film show that, in addition to the area of surface damage, there is an inner region, free from deformation, from which the gold has been totally removed. The threshold temperature of this inner region was approximately equal to that of the boiling point of gold, suggesting rapid evaporation from this area. The absence of any such region for the 200 Å film was probably due to the formation of the absorbing red deposit left behind when that film was destroyed. The nature of this deposit is not fully understood. It was left on the surface even when the experiment was performed *in vacuo*, and probably arises from some slight penetration of the glass surface by the gold atoms. Why it only occurred on evaporation of the thinner film is, however, unknown.

Acknowledgment

We would like to acknowledge the financial support of the SRC.

References

Kuznetsov *et al* 1970 *Sov. Phys.-Tech. Phys.* **15** 123–5
Little V I, Key P Y, Wiltsher R and Rowley D M 1971 *Nature Phys. Sci.* **232** 165–6
Little V I, Rowley D M and Wiltsher R 1970 *Nature, Lond.* **228** 49–50
Ready J F 1971 *Effects of High Power Laser Radiation* (New York: Academic Press)
Rowley D M 1972 *PhD Thesis* London University
Tolansky S 1960 *Microtopography of Surfaces and Films* (London: Longmans)
Turner A F and Arlin E M 1970 *US Govt Res. Develop. Rep.* **70** no. 10

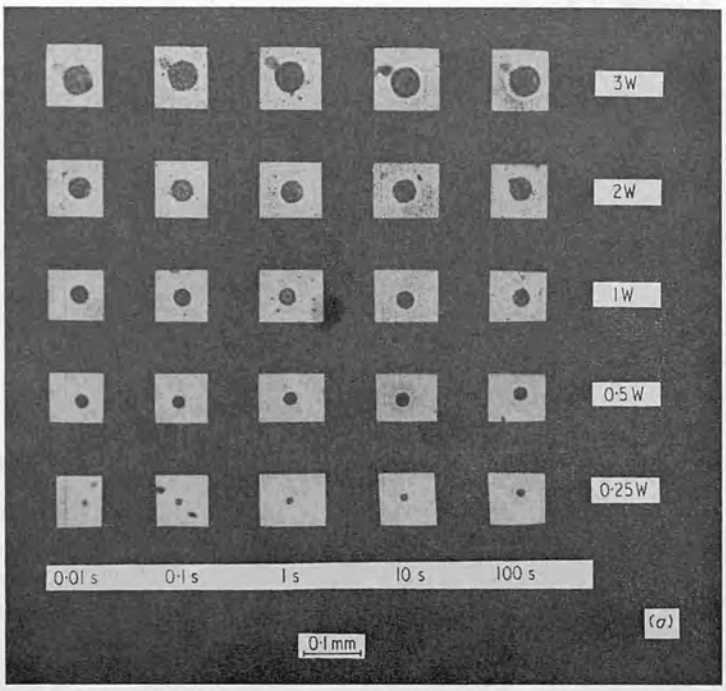
3W
2W
1W
0·5W
0·25W
0·01 s
0·1 s
1 s
10 s
100 s
0·1 mm
(a)

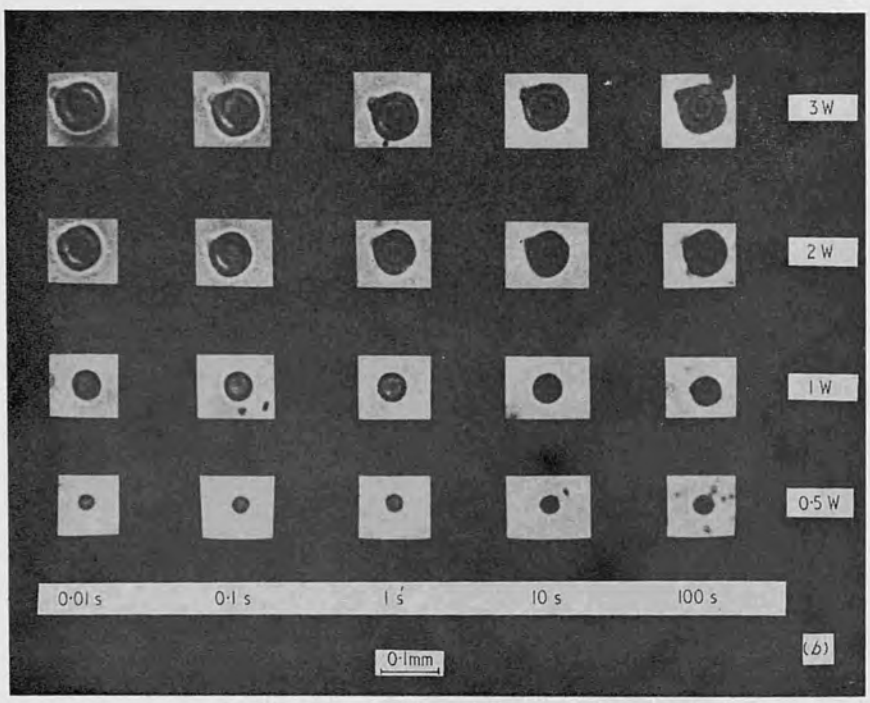
3W
2W
1W
0·5W
0·01 s
0·1 s
1 s
10 s
100 s
0·1mm
(b)

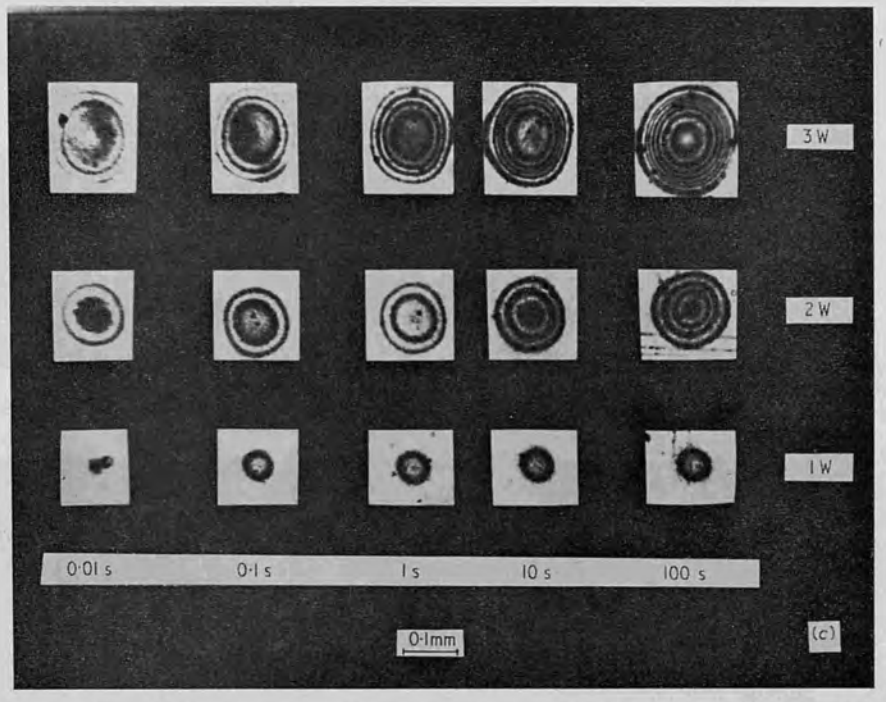

Figure 1. Interferograms of the deformation caused to a glass surface bearing a 200 Å gold film by laser illumination of the indicated power and duration. The laser beam of 1 mrad divergence was focused onto the surface by a lens of focal length (*a*) 5, (*b*) 10 and (*c*) 25 cm.

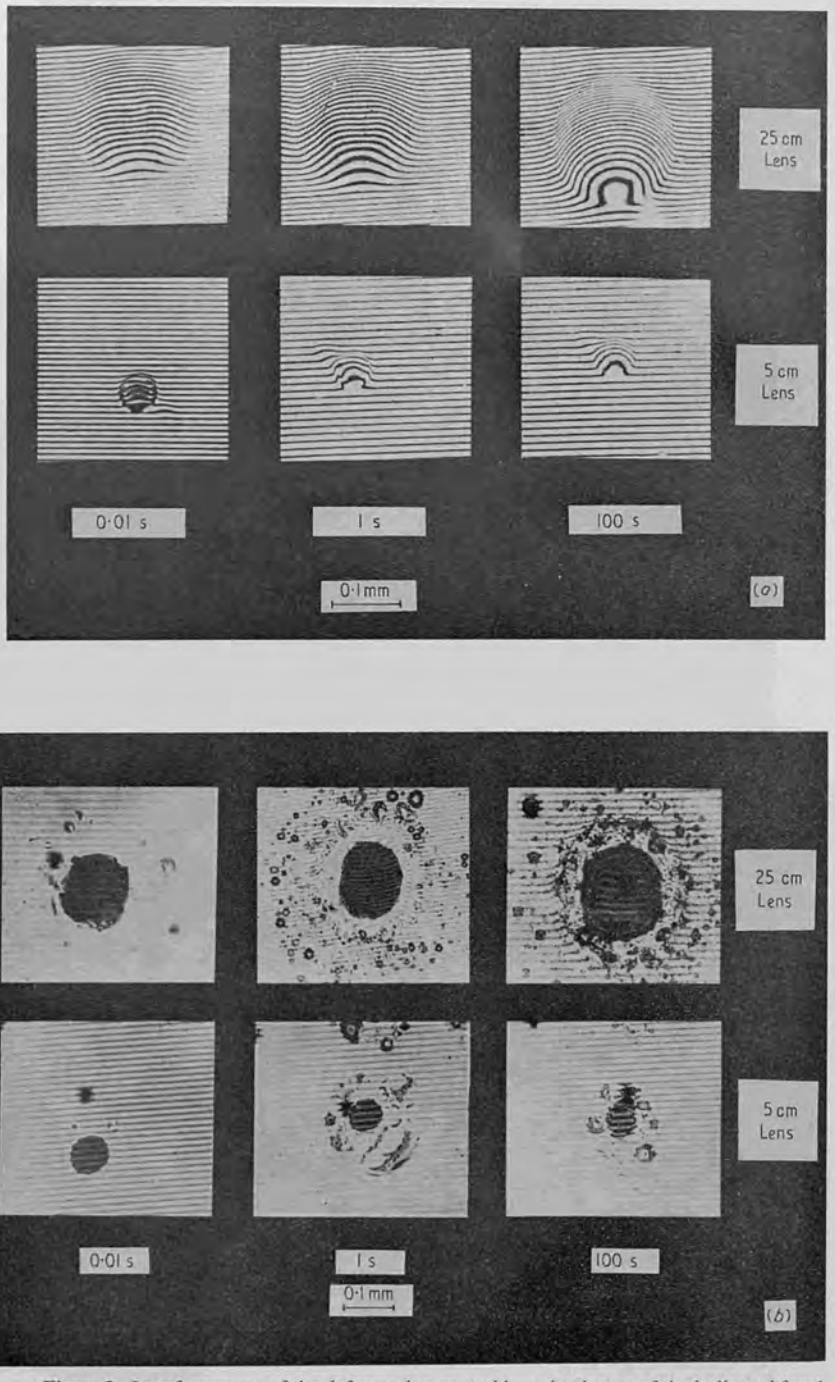

Figure 2. Interferograms of the deformation caused by using lenses of the indicated focal length to focus (*a*) a 3 W laser beam onto a glass surface bearing a 200 Å gold film, and (*b*) a 2 W laser beam onto a glass surface bearing a 1000 Å gold film, for periods of the indicated duration.

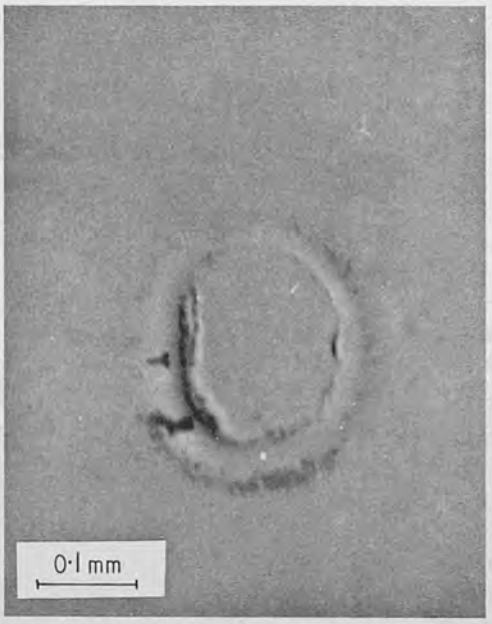

Figure 3. Direct photograph of the damage caused to a glass surface bearing a 1000 Å gold film by using a lens of 25 cm focal length to focus a 2 W laser beam onto the surface for a period of 1 s.

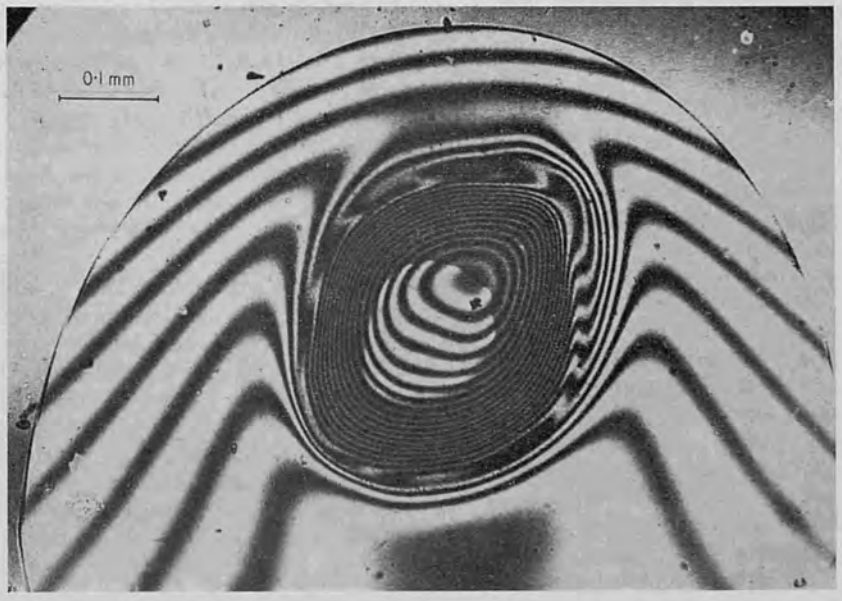

Figure 4. Interferogram of the damage caused to a glass surface by focusing a 2 W laser beam to a spot of 0·2 mm diameter on that surface for a period of 1 min, during which time a gold film 500 Å thick was being deposited on the surface.

Temporal Development of Optically Etched Gratings: a New Method of Investigating Laser-Induced Damage

M. A. Cutter, P. Y. Key, and V. I. Little

An optical etching technique for producing small diffraction gratings, in which a thin metallic film set at an angle to the axis of a ruby laser cavity acted as a Q-switch in the operation of that laser, was previously reported. Here we report a comprehensive investigation of the formation of such etched gratings by the effect of laser light on a thin film external to the laser cavity. A time resolved investigation has been made of the development of such gratings in a number of metallic films, and the effect of film thickness, incident laser intensity, and angular orientation of the film has been studied.

I. Introduction

When the intense light of a Q-switched ruby laser is obliquely incident on a thin partially absorbing film, simultaneously from two opposite directions, heating occurs much more rapidly at the antinodes than at the nodes of the electric field of the resulting standing wave.[1-3] If the light is sufficiently intense, this heating can cause evaporation and ionization of the film[4-16] and may also result in the etching of any underlying substrate. Since the film intersects the antinodes of the standing wave in a series of lines, this removal of film material and substrate etching results in the creation of a diffraction grating. The line separation d of the grating is given by the equation $d = \lambda/2 \sin\theta$, where λ is the wavelength of the incident light and θ the angle between the direction of propagation of the light and the normal to the film.

The phenomenon is of interest both as a means of rapidly producing small diffraction gratings of accurately known spacing and also because it provides a technique by which the dynamics of surface laser damage may conveniently be studied. In our previously reported work[2,3,17] we showed that this was a viable technique for the production of gratings of up to 10% diffraction efficiency although the lack of transverse mode selection in our ruby laser system resulted in gratings that were uniform only over areas of a few square millimeters. In the present work we have probed the area of the film illuminated by the ruby laser beam with the continuous output of an argon ion laser. This light was itself too weak to damage the metallic films used but was diffracted by the grating caused by the ruby laser light. The temporal development of this diffracted beam thus gives information concerning the dynamics of the processes involved in the creation of the grating.

The authors are with the Department of Physics, Royal Holloway College, University of London, Egham Hill, Egham Surrey, U.K.

Received 10 September 1973.

II. Experimental Arrangement

A detailed diagram of the experimental arrangement is shownn Fig. 1. The passively Q-switched ruby laser gave a pulse of up to 50-MW peak power and a duration of 10–20 nsec width at half-power. The intensity of the light incident on the film was varied from 0.5 MW to 40 MW by an attenuating cell containing aqueous copper sulfate solution. The forward and backward going beams of ruby laser light, which were incident on each side of the film at 5° to the normal, were detected by fast photodiodes. The signal generated by the forward going beam was displayed on two Tektronix 454 oscilloscopes of 2-nsec rise time, while that generated by the backward beam was displayed on a Tektronix 7904 oscilloscope (rise time ~1 nsec).

The 300-mW output of a CRL 52B argon ion laser emitting light of 5145-Å wavelength was split into two beams. These beams were incident, at an angle of 18°40′ to the normal, on opposite faces of that part of the film illuminated by the ruby laser. As the grating was created, by the action of the ruby laser light upon the thin film, the development of three of the first order diffracted beams of argon ion laser light was studied. Two of these originated from the light reflected from each side of the film, while the third arose from the light transmitted through it. These three beams passed through a narrow band filter, transmitting light of 5145 Å, to eliminate any blue-green light generated at the surface of the film. Further green filters were used to eliminate scattered ruby laser light. The beams were then detected by three photomultipliers of

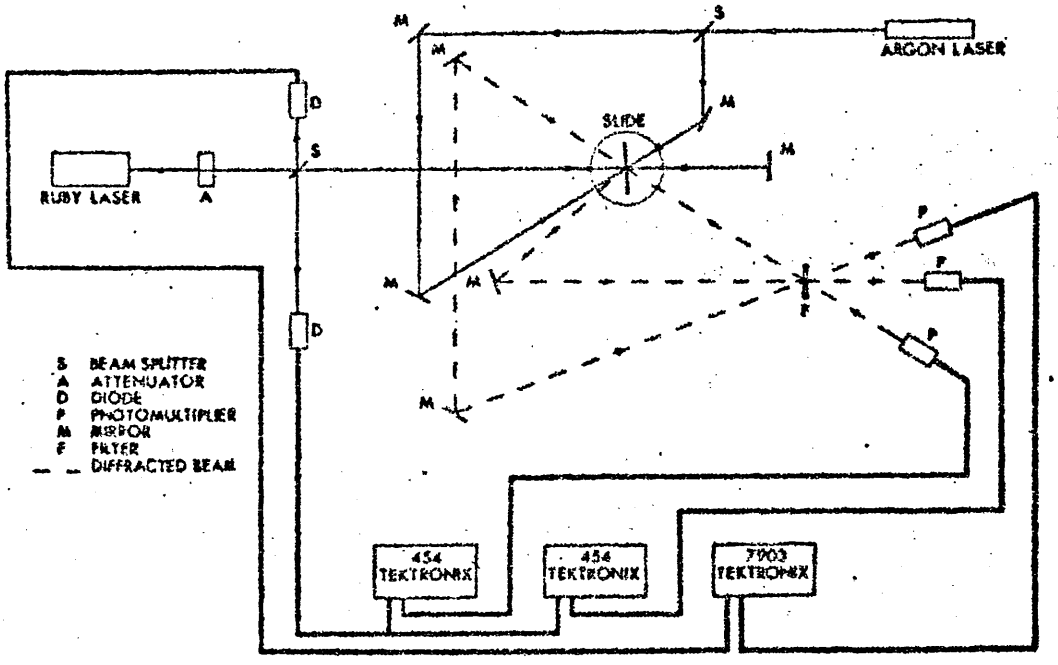

Fig. 1. Experimental arrangement for the study of the temporal development of the light diffracted from an optically etched grating.

about 2-nsec rise time. Two of the signals were displayed, using suitable delay lines, on the same Tektronix 454 oscilloscopes as the ruby laser signals, while the third was displayed on the Tektronix 7904 oscilloscope.

The absorbing films used were evaporated layers of silver, gold, and aluminum of thicknesses from 50 Å to 400 Å on a glass microscope slide substrate. The temporal development of the beams diffracted from the gratings formed by the various films was observed over a range of ruby laser intensities, and the effect of varying the angle of incidence of the ruby laser beam upon the film was also studied.

III. Results

A. General

The main features of the development of the diffracted signals were the same for each type of film. At different energies of the incident ruby laser pulse three main types of development were observed. For pulses of very high energy the diffracted signal was a pulse with a short duration comparable with that of the incident light. With low incident energy the diffracted signal resembled a step function rising to a constant level in a time comparable with the duration of the laser pulse. At intermediate energies the signal had a more complex structure. A short initial pulse was followed by a relatively slow rise and then a decay to a constant level. The three types of signal can be clearly seen in Figs. 2–4.

Although the conditions of the laser oscillator were kept constant, the duration of the output pulse varied from 10 nsec to 20 nsec. Analysis of the effect of pulses of different widths showed the crucial factor determining the nature of the diffracted signal to be the energy rather than the power of the laser pulse.

The diffraction efficiency of the grating, left after etching, varied with pulse energy and film thickness. The pulse energy for which this efficiency was a maximum tended to increase with increasing film thickness.

When the narrow band filter between the photomultipliers and the film was removed, a signal with a decay time of about 15 nsec was observed even in the absence of the argon ion laser light. This light was generated by the film during the etching pro-

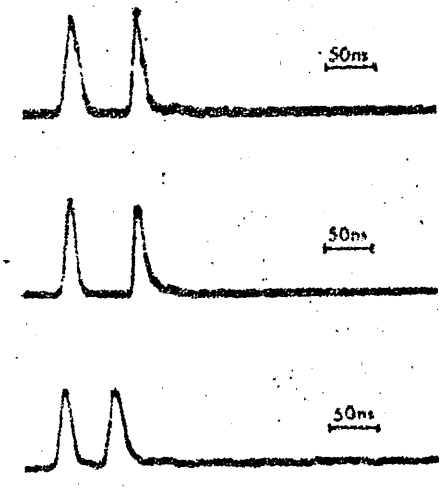

Fig. 2. Diffracted signals observed using high energy ruby laser pulses. (Traces show the ruby laser output followed by the delayed diffracted signal.) *Top trace:* Reflected signal diffracted from front of 200-Å aluminum film illuminated by a 0.9 J/cm² ruby laser pulse. *Middle trace:* Reflected signal diffracted from front of 200-Å silver film illuminated by a 0.45 J/cm² ruby laser pulse. *Bottom trace:* Reflected signal diffracted from back of 200-Å gold film illuminated by a 0.40 J/cm² ruby laser pulse.

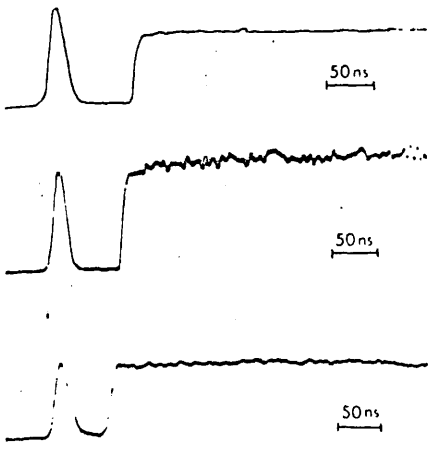

Fig. 3. Diffracted signals observed using low energy ruby laser pulses. (Traces show the ruby laser pulse followed by the delayed diffracted signal.) *Top trace:* Reflected signal diffracted from front of 50-Å aluminum film illuminated by a 0.03 J/cm² ruby laser pulse. *Middle trace:* Reflected signal diffracted from front of 100-Å silver film illuminated by a 0.045 J/cm² ruby laser pulse. *Bottom trace:* Reflected signal diffracted from back of 100-Å gold film illuminated by a 0.045 J/cm² ruby laser pulse.

less, suggesting the probable formation of a microplasma;[6,10,12,13,15,16] as a result of the very rapid heating of the film at the antinodes of the optical standing wave. An attempt to investigate the spectrum of this light, in order to determine whether ionization did in fact occur, proved inconclusive because of the weakness of the signal. Using very low resolution we were, however, able to establish that the background of the spectrum generated, when the incident laser pulses were of the highest energies used in our experiments, resembled that of a blackbody of 5000 K.

B. Gold Films

The threshold energy required for the ruby laser beam to etch the gold films varied from 20 mJ/cm² in the case of the 50-Å film to 100 mJ/cm² for the 400-Å film. The diffraction efficiencies of gratings formed in the 50-Å film were always very low, reaching a maximum of 8×10^{-4}% when the incident energy was 150 mJ/cm². Much better gratings were formed in the 100-Å and 200-Å films having maximum efficiencies of 5×10^{-2}% and 5×10^{-3}% at energies of 60 mJ/cm², respectively. The gratings formed in the 400-Å film were of comparable efficiency: up to 2×10^{-3}% at 1000 mJ/cm².

At high beam energies all the diffracted signals showed a pulsed development of the type illustrated in Fig. 2 regardless of the film thickness, but at lower energies the three beams showed different features. The signals from the 50-Å film were too weak to be conveniently studied. In the case of the 100-Å film the transmitted beam began to develop in the slow manner illustrated in Fig. 4 for input energies of less than 300 mJ/cm², but the two reflected beams retained the features shown at the higher energies. These beams never showed the slow development of Fig. 4, but at energies of less than 50 mJ/cm² the beam reflected from the back of the film (i.e., from the side in contact with the glass slide) lost its pulsed character and developed in the step-function manner shown in Fig. 3. The beam reflected from the front of the film retained a partially pulsed character right down to the etching threshold. Using a 200-Å film, similar results were obtained, but the transition from pulsed to slow development of the transmitted beam occurred at 600 mJ/cm². The development of the diffracted beams from the 400-Å film was again similar except that the transmitted beam showed slow development up to the highest available ruby laser energies (1500 mJ/cm²), while both reflected beams showed pulsed development right down to threshold intensity.

C. Silver Films

The threshold energy required to etch the silver films varied from 60 mJ/cm² for the 50-Å film to 500 mJ/cm² for the 400-Å film. Much more efficient gratings (7×10^{-2}% at 450 mJ/cm²) were formed in the 50-Å film than in the equivalent gold film. The gratings formed in the 100-Å and 200-Å films were also of greater efficiency (6×10^{-2}% at 100 mJ/cm² and 10^{-2}% at 1000 mJ/cm², respectively), but those in the 400-Å film were very poor.

The development of the diffracted beams was broadly similar to that of those produced from the gold films but showed much less slow development (Fig. 4) and more often took the form of a step-function (Fig. 3). Using the 50-Å film, all three beams

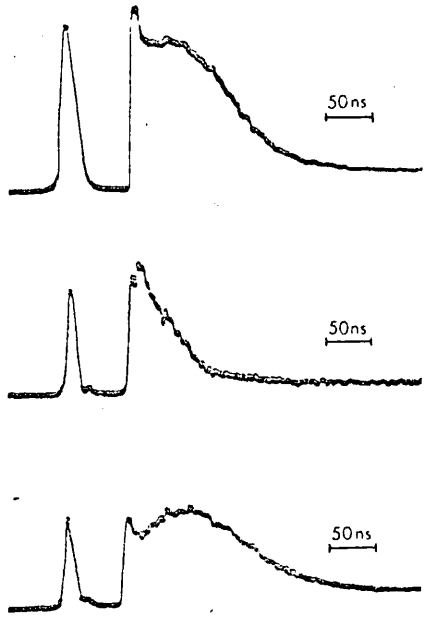

Fig. 4. Diffracted signals observed using intermediate energy ruby laser pulses. (Traces show ruby laser output followed by the delayed diffracted signal.) *Top trace:* Reflected signal diffracted from front of 100-Å aluminum illuminated by a 0.2 J/cm² ruby laser pulse. *Middle trace:* Transmitted signal diffracted from 200-Å silver film illuminated by a 0.3 J/cm² ruby laser pulse. *Bottom trace:* Transmitted signal diffracted from 200-Å gold film illuminated by a 0.1 J/cm² ruby laser pulse.

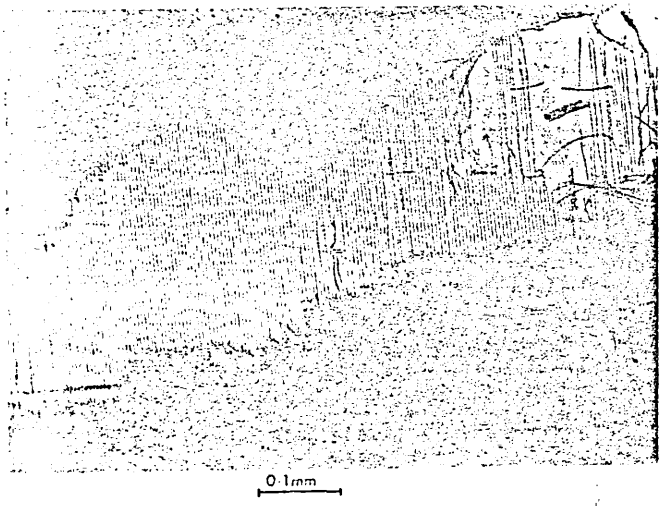

Fig. 5. Grating of the type produced using low energy ruby laser pulse. (200-Å gold film illuminated by a 0.06 J/cm² ruby laser pulse.)

showed a development intermediate between Figs. 2 and 3 at the highest available ruby laser energies. At energies of less than 400 mJ/cm² all the beams showed purely step function behavior, but at no stage was there any significant slow development. The beams diffracted from the 100-Å film were very similar, acquiring a purely step function character for energies of less than 150 mJ/cm². Using the 200-Å film, however, the transmitted beam showed development for energies of less than 450 mJ/cm², while the two reflected signals were of the pulsed type shown in Fig. 2. The very weak signals reflected from the 400-Å film were also of the pulsed type, while the transmitted beam was undetectable.

D. Aluminum Films

The threshold for etching the aluminum films varied from 20 mJ/cm² for the 50-Å film to 200 mJ-cm² for the 400-Å film. The efficiencies of the gratings formed in the 50-Å film were greater than in the case of either the gold or silver films (6.25% at 60 mJ/cm²). The maximum efficiencies of gratings formed in the 100-Å and 200-Å films were 10^{-2}% at 750 mJ/cm² and 3×10^{-2}% at 700 mJ/cm², respectively, while the 400-Å film gave gratings with maximum efficiency of 2×10^{-4}% at 600 mJ/cm².

The over-all features of the development of the diffracted beams were similar to those observed with the other two metals except that slow development (Fig. 4) was in this case more prominent in the reflected than in the transmitted beams. At high incident energies all the beams diffracted from the 50-Å film had a pulsed character (Fig. 2), but below 250 mJ/cm² the two reflected beams showed slow development. At energies below 50 mJ/cm² the transmitted beam showed a mainly step function behavior (Fig. 3). Using the 100-Å film the transition from pulsed to slow development of the two reflected beams occurred at about 400 mJ/cm², while the transmitted beam showed pulsed behavior down to the etching threshold. Surprisingly this situation was reversed using the 200-Å film when the reflected beams had a pulsed character down to threshold energy, while the transmitted beam showed slow development even at the highest available energy. The signals reflected from the 400-Å film were of pulsed form for high incident energies but became of the step function type for energies below 300 mJ/cm². The slowly developing transmitted beam was so weak that it was only observable at the highest available energy.

IV. Physical Quality of the Gratings

The ideal optically etched grating would consist of a periodic thin metallic film, undamaged at its thickest points and totally absent at its thinnest, on a completely unaffected substrate.

The gratings formed in our experiments were examined under a microscope of up to 1300× magnification. This showed that those gratings formed by illumination of 50–100-Å gold or aluminum films by ruby laser beams of only just sufficient energy to affect the films approached closest to the ideal (Fig. 5). These gratings were very small in area but could have diffraction efficiencies of up to 10%. (The much lower efficiencies recorded in Sec. III were the average efficiencies measured over the whole area illuminated by the argon ion laser.) Higher energy illumination of these films tended to cause total removal of the free metal even at the nodes of the field, leaving a dull reddish layer with little absorption or reflectivity on the substrate surface (Fig. 6). The resulting grating was of very low diffraction efficiency. Such total removal of the free metal (perhaps involving its penetration into the substrate surface to form the reddish layer) occurred even more frequently using thicker films of gold or aluminum or with silver films of any thickness.

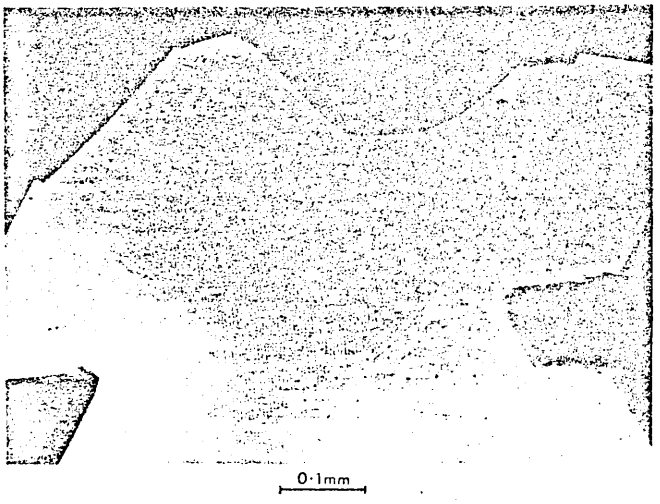

Fig. 6. Grating of the type produced using high energy ruby laser pulse. (400-Å gold film illuminated by a 1.0 J/cm² ruby laser pulse).

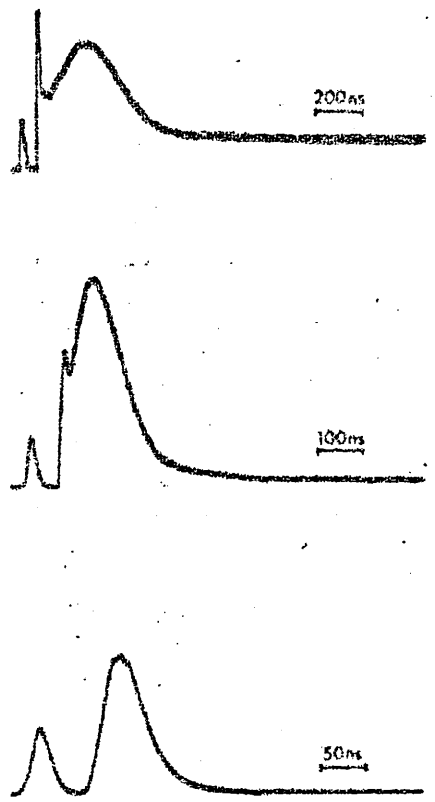

Fig. 7. Variation of diffracted signal with angle of incidence of the ruby laser light. (Traces show ruby laser output followed by the delayed diffracted signal.) Each trace shows the transmitted signal diffracted from a 200-Å gold film illuminated by a 0.3 J/cm² ruby laser pulse. The angle between the ruby laser direction and the normal to the film was 2° for the top trace, 5° for the middle trace, and 15° for the bottom trace.

Correlation of the time resolved diffracted signals with the appearance of the gratings clearly showed that the ideal type of grating was formed when the beam energy was sufficiently low to give the step function type of diffracted signal. Whenever a fast pulse was visible in the diffracted signal, complete removal of the free metal had occurred over at least some part of the grating.

V. Angular Dependence of Diffracted Signals

The dependence of the temporal development of the beam diffracted from the grating formed in a 200-Å gold film on the angle θ between the normal to the film, and the incident ruby laser beams, was studied. The rise and fall times of the slowly varying part of the signal observed with ruby laser beams of intermediate energy were found to depend strongly on this angle (Fig. 7). Figures 8 and 9 show graphs of the rise and fall times, respectively, plotted as functions of $\csc\theta$. The results clearly show that these times depend linearly on $\csc\theta$.

VI. Discussion

The complexity of the temporal development of the diffracted laser beam under various conditions of film excitation suggests that a number of mechanisms are involved in the formation of the grating. This fact and the essentially destructive nature of the processes occurring within the film make quantitative analysis of the observations extremely difficult.

Many authors[8,10,12,13,15,16] have reported the formation of a microplasma when a Q-switched laser pulse with an intensity of the same order of magnitude as that used in our experiments impinges on a solid surface. The short pulse of diffracted signal observed using ruby laser pulses of very high energy (Fig. 2) may be readily explained on the assumption that lines of plasma were first formed at the antinodes of the standing wave causing a strong diffracted signal. Subsequent heating at the nodes of the wave (owing to the fact that with our experimental arrangement the forward and backward ruby laser beams were never exactly equal) would, however, cause a rapid decrease in this signal by creating a uniform plasma over the whole surface. Complete

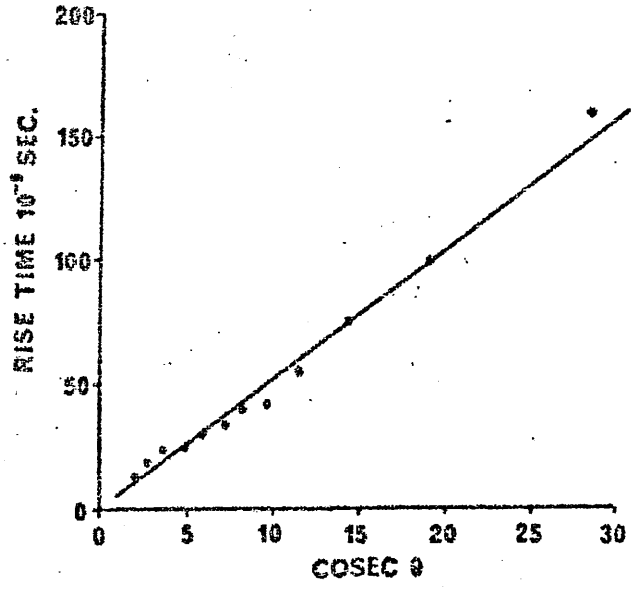

Fig. 8. Variation of rise time (to maximum) of the diffracted signal with angle of incidence θ of the ruby laser light. (Transmitted signals diffracted from a 200-Å gold film illuminated by a 0.3 J/cm² ruby laser pulse.)

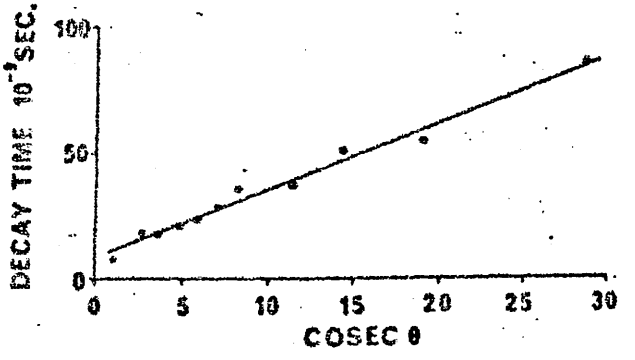

Fig. 9. Variation of decay time (to half-intensity) of the diffracted signal with angle of incidence θ of the ruby laser light. (Transmitted signals diffracted from a 200-Å gold film illuminated by a 0.3 J/cm² ruby laser pulse.)

removal of the film (Fig. 6) over some part of the grating was always associated with this type of signal.

The step-function diffracted signals (Fig. 3) observed using beams of very low energy may be explained on the assumption that at such energies there was no damage to the film at the nodes of the standing wave and no plasma formation. The development of the signal was in this case caused by vaporization of the film at the antinodes of the electric field. The remaining film caused diffraction as a result of the induced periodicity in its thickness, but the vapor, being transparent to argon ion laser light, had no effect on the diffracted signal. Hence the constant diffracted signal, once the laser pulse had formed the grating. (Gratings formed under these conditions are sown in Fig. 5.)

The slowly decaying signal observed, in addition to a constant background, at intermediate beam energies (Fig. 4) may now be interpreted as a result of the formation of plasma, rather than unionized vapor, at such energies. (The additional presence of a sharp pulse in some cases is again due to destruction of the film in the vicinity of nodes in at least some areas of the grating.) The rise and fall times of the slow signal were proportional to $\mathrm{cosec}\theta$, i.e., proportional to the line separation of the grating. Such a dependence would be expected if the diffraction were governed by the motion of a plasma across the lines of the grating in which the distance to be travelled, and thus the time required, to achieve any given ionic distribution would be proportional to the line separation. The distribution of the substrate temperature, or any other parameter controlled by a diffusion law, would show a development with a characteristic time proportional to the square of that separation. Decay of ths plasma, chemical processes occurring at the surface, or any phenomenon involving transport perpendicular to the surface would on the other hand give a decay time independent of spacing. An acoustic surface wave would have a period proportional to the line spacing, but this would result in a diffracted signal whose intensity would oscillate with a period smaller than the observed decay time.

In a plasma of temperature T the ions have velocities whose components in any given direction follow a Gaussian distribution. The median value v of this distribution is given by $v = 0.68\,(kT/M)^{1/2}$, where k is Boltzmann's constant and M the ionic mass.

Thus, if the plasma ions acquire their energy in a time τ_0, the time required for half of the ions to travel a distance of one line separation d is given by

$$\tau = \tau_0 + (d/v) = \tau_0 + 1.47\lambda(M/kT)^{1/2}\ \mathrm{cosec}\theta$$

where λ is the wavelength of the ruby laser light and θ the angle between the ruby laser beam and the normal to the film.

While the exact relationship between plasma distribution and diffraction efficiency is difficult to establish, it seems clear that any signal arising from this process would develop in a time comparable with τ.

Since gold vapor does not absorb ruby laser light we may assume that the temperature of the plasma, when first initiated from the vapor, was about 2500 K, the boiling point of gold. The duration of the slowly developing part of the diffracted signal did not vary significantly over the range of beam energies under which the phenomenon was observed. This suggests that, at such energies, there was no significant heating by absorption of the ruby laser light in the plasma. We may therefore assume that the temperature of the plasma at intermediate beam energies was still about 2500 K. (The temperature of 6000 K mentioned in Sec. III.A occurred using a ruby laser beam of much higher energy.)

Given this temperature, the gradients of graphs shown in Figs. 8 and 9 are of the same of magnitude as the gradient, $1.47\,(M/kT)^{1/2}$, of τ against $\mathrm{cosec}\theta$ indicated by the equation above. This provides a reasonable experimental justification for assuming that the slowly varying signal results from the creation of a microplasma at the antinodes of the standing wave of the ruby laser light.

We would like to acknowledge the technical assistance of J. Williams, who prepared the thin films, and the financial support of the Science Research Council.

References

1. A. M. Ledger, Appl. Opt. 5, 476 (1966).
2. V. I. Little, D. M. Rowley, and R. Wiltsher, Nature 228, 49 (1970).
3. D. M. Rowley, PhD Thesis, London University (1972).
4. J. F. Ready, Appl. Phys. Lett. 3, 11 (1963).
5. J. F. Ready, J. Appl. Phys. 36, 462 (1964).
6. E. Archbold, D. W. Harper, and T. P. Hughes, Brit. J. Appl. Phys. 13, 1321 (1964).
7. Y. V. Afanasev and O. N. Krokhin, Sov. Phys. JETP 25, 639 (1967).
8. S. I. Anasimov, Sov. Phys. JETP 27, 182 (1968).
9. A. M. Bonch-Bruevich, Y. A. Imas, M. N. Libenson, and B. N. Spiridinov, Sov. Phys. Tech. Phys. 15, 512 (1970).
10. B. E. Henderson, R. R. Getty, G. E. Leroi, and D. L. Rousseau, *Damage in Laser Materials*, A. J. Glass and A. H. Guenther, Eds., NBS Special Pub. 356 (U.S. Govt. Printing Office, Washington, D.C., 1971), p. 31.
11. F. W. Dabby and U. C. Paek, IEEE J. Quantum Electron. QE-8, 106 (1972).
12. J. H. Parks and N. Alyassini, *Laser Induced Damage in Optical Materials*, A. J. Glass and A. H. Guenther, Eds., NBS Special Pub. 372 (U.S. Govt. Printing Office, Washington, D.C., 1972), p. 104.
13. N. Alyassini, J. H. Parks, and L. G. De Shazer, University of Southern California; private communication.
14. C. O. Allingham, M. A. Cutter, P. Y. Key, and V. I. Little, J. Phys. D 6, 1 (1973).
15. C. R. Giuliano, IEEE J. Quantum Electron. QE-8, 749 (1972).
16. E. S. Bliss, D. Milam, and R. A. Bradbury, Appl. Opt. 12, 677 (1973).
17. V. I. Little, P. Y. Key, R. Wiltsher, and D. M. Rowley, Nature (Physical Science) 232, 165 (1971).

CONTEMP. PHYS., 1974, VOL. 15, NO. 3, 271–298

Scattering of Light from Light Induced Periodic Structures

V. I. LITTLE, M. A. CUTTER, P. Y. KEY
Department of Physics, Royal Holloway College, University of London.
and
R. G. HARRISON
Department of Physics, University of Bath

SUMMARY. When a beam of high intensity laser light is scattered by the fluctuations spontaneously existing within a fluid medium a spatial modulation of the dielectric constant may be induced. The role of such a modulation in causing stimulated scattering of the intense laser beam or Bragg reflection of any weak independent probe beam is discussed and theoretically analyesd. It is shown that such Bragg reflection provides a convenient technique for the study of the modulation. Experimental observation and investigation of Bragg reflection from such a modulation is described. A related technique has been used to investigate the development of light induced periodic structures on surfaces.

1. Introduction

The first scientific studies of light scattering were made in the second half of the 19th Century, particularly by Lord Rayleigh. He showed that the scattering of light from small particles is essentially unshifted in frequency and proportional to the inverse fourth power of the wavelength of the illuminating light, thus explaining the blue colour of the sky.

The next major development was achieved by Brillouin in 1922 who used Debye's method of analysing the random fluctuations of a medium into its acoustic modes to show that the light scattered from such a medium is shifted up or down in frequency by a Doppler shift due to the velocity of the acoustic waves. This splitting was detected by Gross in 1930. The theory was developed in more detail by Mandelshtam (1926) and Landau and Placzek (1934) who showed that in addition to the ' Brillouin doublet ' there exists scattering, due to non propagating entropy fluctuations, which is unshifted in frequency. This is usually known as the ' Rayleigh line '. Scattering from induced ultrasonic waves was also demonstrated (Debye and Sears 1932) and theoretically analysed.

In the meantime Raman in 1928 had discovered an entirely new type of molecular scattering (Raman scattering). Like the fluorescence investigated earlier by Stokes it was predominantly down-shifted in frequency but unlike fluorescence it was strongly polarized. Furthermore the spectrum of the scattered light consisted of sharp lines reduced in frequency (Stokes shifted) from the illuminating lines by integral multiples of certain fixed frequencies characteristic of the medium. There were also much fainter lines of increased frequency (anti-Stokes shifted). This scattering he correctly explained in terms of the quantum theory, the frequency shifts being determined by the difference between energy levels of the molecule.

At the same time Raman and Krishnan considered the problem of scattering from anisotropic molecules and showed that, as distinct from the case of Rayleigh

line and Brillouin doublet, a depolarization of the scattered light occurs. Further work showed that the depolarized light contributes a broad wing to the light scattering spectrum (the Rayleigh wing) with a frequency spread which is the inverse of the molecular re-orientation time. (Frenkel 1946). This wing was very difficult to observe, the results obtained often being contradictory. The first definite observation was probably that of Gross in 1940.

The general features of the light scattering spectrum had already been worked out before the development of the laser (Fabelinskii 1965). This has however increased the accuracy of measurement by many orders of magnitude and led to the discovery of some entirely new details.

The general characteristics of the polarized component of the spontaneous scattering spectrum are shown in the upper curve of fig. 1 (Denariez and Bret 1968). The spectrum can be analysed as the sum of components due to Rayleigh line, Rayleigh wing, Brillouin doublet and Raman scattering. These are due to fluctuations in refractive index associated with variations of temperature, anisotropy, density and molecular polarizability, respectively. Each resulting component of the curve represents the solution (in terms of the frequency dependence of amplitude) of the equation of a damped resonant system. These components are of the form:

$$I \propto \frac{1}{\left(1-\frac{\omega^2}{\Omega^2}\right)^2+\left(\frac{2\Gamma\omega}{\Omega^2}\right)^2}$$

where I is the intensity at a particular frequency of spontaneously scattered light, ω is the difference in frequency between the incident and scattered light, and Ω and Γ are the frequency shift and width characteristic of a particular scattering process and medium.

The central peaks occur for processes where $\Omega/\Gamma < \sqrt{2}$, and the double peaks where $\Omega/\Gamma > \sqrt{2}$. In the depolarized spectrum the sharp peaks due to the Rayleigh line, Brillouin doublet and Raman scattering are absent leaving a broad band centred on ω_L.

While the spectral purity of the continuous gas laser has made it the main experimental tool for spontaneous scattering studies, the very high intensities available from solid state lasers have led to the discovery of the entirely unforseen phenomenon of stimulated scattering. Every type of spontaneous scattering occurs as a result of spatial variations of dielectric constant arising from statistical fluctuations in a particular property of the medium. In stimulated scattering these properties (and therefore the dielectric constant) are spatially modulated by the effect of the laser and spontaneously scattered beams. This can result in a very intense scattered beam, the first example of which was discovered accidentally in 1962 by Woodbury and Ng, but was soon understood and investigated by Eckhardt *et al.* and other workers (Bloembergen 1967). This phenomenon was stimulated Raman scattering. The very weak wave produced by Raman scattering beats with the main laser wave at the difference frequency. This frequency is, of course, the characteristic frequency of the atom which gave rise to the Raman scattering in the first place. A very strong interaction can therefore occur with the Raman scattered wave and the atomic excitation being amplified at the expense of the laser beam.

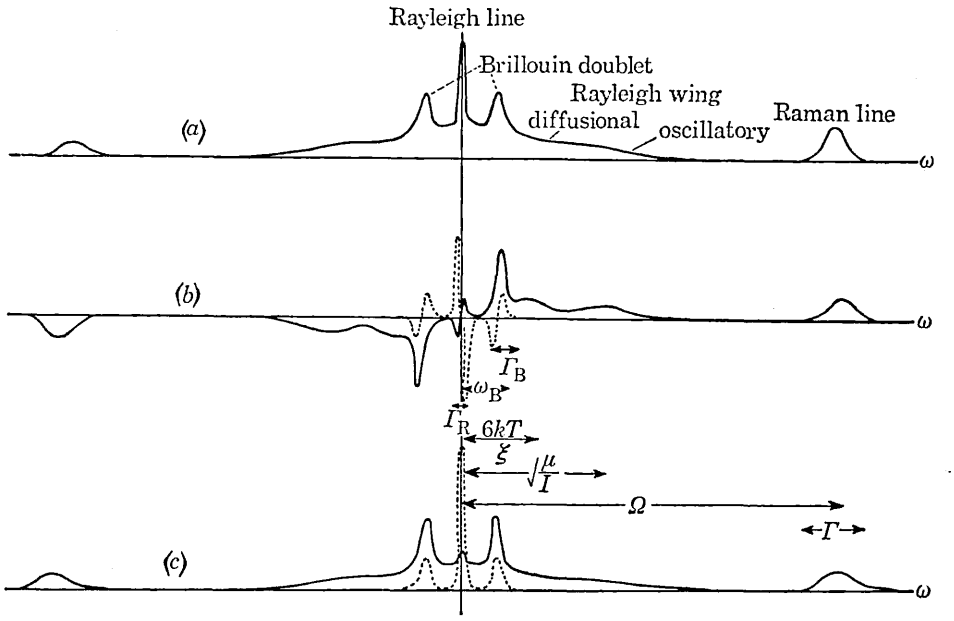

Fig. 1. Spectra of: (*a*) spontaneous scattering intensity, (*b*) stimulated scattering gain, and (*c*) Bragg reflectivity, as a function of frequency shift. The continuous line shows the spectrum of a transparent medium and the dotted line the additional contribution in the presence of absorption. (These spectra must be convolved with that of the laser line to give the experimentally observed spectra.)

It is now accepted that each of the contributions to the spontaneous scattering curve can, under appropriate conditions, give rise to stimulated scattering (though this may be obscured by competition between the possible processes). The gain contributed by each process is a function of the difference in frequency between the amplified light and pump light of the form:

$$G \propto \frac{\frac{2\Gamma\omega}{\Omega^2}}{\left(1-\frac{\omega^2}{\Omega^2}\right)^2+\left(\frac{2\Gamma\omega}{\Omega^2}\right)^2}$$

where the constants are the same as those in the appropriate spontaneous scattering equation. The overall gain curve (Bret and Denariez 1968) shown in fig. 1 is a sum of such terms. The gain curve for a signal polarized perpendicularly to the pump of course, contains only those terms which exist in the depolarized scattering spectrum.

Stimulated Brillouin scattering was observed by Chiao *et al.* in 1964. In this process a hypersonic wave is generated by the laser and spontaneously scattered beams as a result of electrostriction; the tendency of a dielectric medium to move into the regions of high electric field. In 1965 another stimulated scattering process was observed by Mash *et al.* This was stimulated Rayleigh wing scattering in which the molecular orientations are affected by the electric field of the light waves.

The last type of stimulated scattering to be observed was that associated with the Rayleigh central line. The reason for this was that coupling of the light wave to the temperature wave is normally provided by the very weak electrocaloric effect (Landau and Lifshitz 1960), (a change in the temperature of the medium caused by the presence of an electric field) resulting in very small gains. It was observed by Zaitsev *et al.* in 1967, but they were unable to measure the very small Stokes frequency shifts predicted by theory. At the same time Herman and Gray predicted a very strong coupling between the light and temperature waves in absorbing media. This type of scattering and its very small frequency shift was immediately detected by Rank *et al.* in 1967.

In all these experiments a powerful scattered light beam was generated by very strong amplification of extremely weak spontaneously scattered light. This technique allowed measurement of the frequency shifts involved in the various stimulated scattering processes, and also of the threshold intensity required for such scattering to be observed. Direct measurement of the gain coefficient experienced by the scattered light was, however, not possible in these experiments. A convenient arrangement for measuring this gain coefficient is illustrated in fig. 2 (Denariez and Bret 1968). The amplification in cell 1 of the frequency shifted, backward-going beam generated in cell 2 and reduced in intensity by the attenuator is measured directly by the ratio of the signals on the two detectors. This technique has two other important advantages.

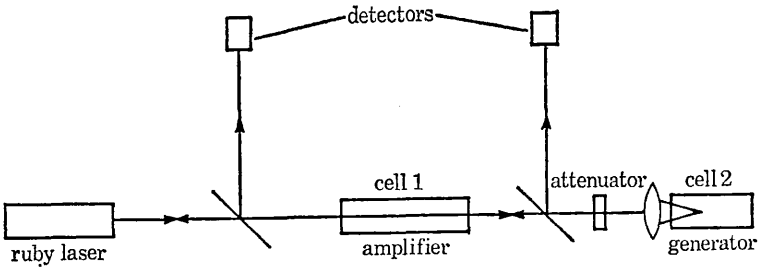

Fig. 2. Weak amplification of light generated by stimulated scattering in a separate cell.

First, the laser intensities in cell 1 can be much lower than the threshold intensity required to generate stimulated scattering directly and avoids interference from other nonlinear effects. Secondly, by varying the medium in cell 2, the gain coefficient of the medium in cell 1 may be measured over a range of frequency shifts, whereas the generation of stimulated scattering only occurs at that frequency shift which gives maximum gain. Thus the complete frequency profile of the gain coefficient (fig. 1) may in principle be experimentally verified.

This technique has, however, two serious limitations. First, as will be shown, measurement of the stimulated scattering gain gives information only about the out-of-phase part of the modulation of dielectric constant which occurs in the scattering process. Secondly, since the backward-going beam is itself responsible for the existence of the modulation, it would be desirable to have an independent source of information about the modulation rather than to measure its effect on the backward beam. We have developed a Bragg reflexion technique which overcomes these problems (Harrison *et al.* 1968, Key *et al.* 1970). In this technique the region in cell 1, where amplification occurs, is probed by a weak, independent laser beam incident on the modulations at the Bragg angle.

Analysis of the reflexion of this beam gives independent information about the total magnitude of the modulation, and allows convenient investigation of its variation with position and time. Our theoretical analysis has shown (Harrison *et al.* 1973) that the Bragg profiles of the Bragg reflectivity as a function of frequency shift (fig. 1) is described for each scattering process by an equation of the form

$$R \propto \frac{1}{\left(1-\frac{\omega^2}{\Omega^2}\right)^2+\left(\frac{2\Gamma\omega}{\Omega^2}\right)^2}.$$

This profile resembles that of spontaneous scattering intensity rather than that of stimulated scattering gain. It will be seen in the theoretical section that this arises directly from the fact that the Bragg reflectivity depends only on the amplitude of the modulations of dielectric constant while the scattering gain depends also on its phase. Simultaneous measurement of both Bragg reflectivity and stimulated scattering gain coefficient can therefore be used to give a complete description of the amplitude and phase of the modulation as a function of frequency shift, position and time.

We have used this technique to demonstrate the existence of modulations involved in a number of stimulated scattering processes, and have made a comprehensive investigation of the thermal modulation associated with stimulated Rayleigh line scattering in absorbing media. (Harrison *et al.* 1973; Key 1970; Harrison 1970).

We have also used a related probe scattering technique to study periodic structures generated by oppositely directed light beams on the surface, rather than in the bulk of the media (Cutter *et al.* 1974). These structures which are generated by the same processes as those that cause the bulk modulation—but have a wavelength determined by the angle between the surface and the laser beam—cause diffraction rather than Bragg reflection of the incident probe beam. In particular, we have studied the effect of two beams of equal frequency impinging on a surface bearing a thin absorbing film. If the light is of sufficient intensity the resultant heating can cause evaporation and ionization of the film material and may also result in the etching of any underlying substrate. Since the electric field resulting from the two light beams is a standing wave whose antinodes intersect the film in a series of lines, this removal of film material and substrate etching may result in the creation of a permanent diffraction grating. (Little *et al.* 1970).

2. Theory

2.1. *General considerations*

Changes in the entropy, pressure, molecular orientation and molecular deformation of a medium are all described by diffusion or damped harmonic equations. Even in the absence of any electric field these parameters undergo small statistical fluctuations. The associated fluctuations of dielectric constant give rise to spontaneous Rayleigh line, Brillouin, Rayleigh Wing and Raman light scattering, respectively. (Fabelinskii 1965). In the presence of an electric field these parameters undergo changes proportional, at equilibrium, to the square of that field—electrostriction, the electrocaloric effect and the Kerr effect (Landau and Lifshitz 1960). As a result of spontaneous scattering the

electric field E in a medium traversed by a powerful laser beam is the sum of a large sinusoidal term with the frequency ω_1 of the laser light and a small term with the frequency ω_2 of the scattered radiation. E^2 thus contains terms of frequency $(\omega_1+\omega_2)$, $(\omega_1-\omega_2)$, $2\omega_1$, $2\omega_2$ and zero.

For light spontaneously scattered at 180° the component of E^2 with frequency $(\omega_1-\omega_2)$ has a wavevector (k_1+k_2) and the resulting change of dielectric constant is a sinusoidal modulation with the same frequency and wavevector (but not necessarily the same phase), travelling through the medium with velocity $(\omega_1-\omega_2)/(k_1+k_2)$. This modulation now acts as a moving phase grating which reflects the laser light incident upon it, Doppler shifting its frequency by the amount $(\omega_1-\omega_2)$; the shift in frequency of the spontaneously scattered light originally responsible for the modulation. The reflected beam, having the same frequency and direction as the spontaneously scattered beam, increases the amplitude of the modulation. This produces a more powerful reflected beam which in turn increases the modulation still further. A cumulative situation thus exists in which, although the light initially backscattered is exceedingly weak, it may trigger the generation of a powerful backscattered beam which has been observed to have an intensity of up to 90 per cent of that of the incident laser beam (Maier, Rother and Kaiser 1967). Each type of spontaneous scattering, arising from fluctuation of a particular parameter of the medium, can thus give rise to a corresponding stimulated scattering in which that parameter is modulated by the electric fields of the incident and scattered waves.

This situation, in which the stimulated scattering builds up from the spontaneously scattered light is in practice difficult to investigate in detail. The amplifier arrangement described in the introduction and shown in fig. 2 is both experimentally and theoretically more convenient to analyse.

The intensity of the light in the unfocused laser beam is insufficient to cause stimulated scattering in cell 1. In cell 2 the stimulated scattering of the focused light results in a beam of slightly shifted frequency propagating in the opposite direction to the laser beam. This beam is strongly attenuated so that when it enters cell 1 it is very much weaker than the laser beam. Under these conditions the reflexion of the laser beam, from the modulation of dielectric constant, results in exponential spatial amplification of the backward-going beam (Bloembergen 1967; Bloembergen and Shen 1964). As shown by eqn. (2.2.4) below, this stimulated scattering gain is determined not by the whole amplitude of the modulation of dielectric constant, but solely by the amplitude of that part of the modulation which is one quarter period out of phase with the component of E^2 producing it (Key 1970). Thus the frequency profile of the gain, shown in fig. 1, is also that of the out of phase part of the modulation.

Consider a weak independent beam crossing the region of modulated dielectric constant. When incident on the modulations at the appropriate angle (fig. 3) such a beam, of frequency ω_3 is Bragg reflected to form another beam of Doppler-shifted frequency $\omega_4=\omega_3-(\omega_1-\omega_2)$. The angle giving maximum Bragg reflectivity is such that the light reflected from successive layers of the modulation should add exactly in phase. The profile of the Bragg reflectivity, as a function of the frequency shift $(\omega_1-\omega_2)$, is shown in fig. 1. Eqn. (2.2.10) below shows that this reflectivity depends on the whole amplitude of the modulation. Eqns. (2.3.3) and (2.3.8) show that the resulting frequency profile resembles that of the

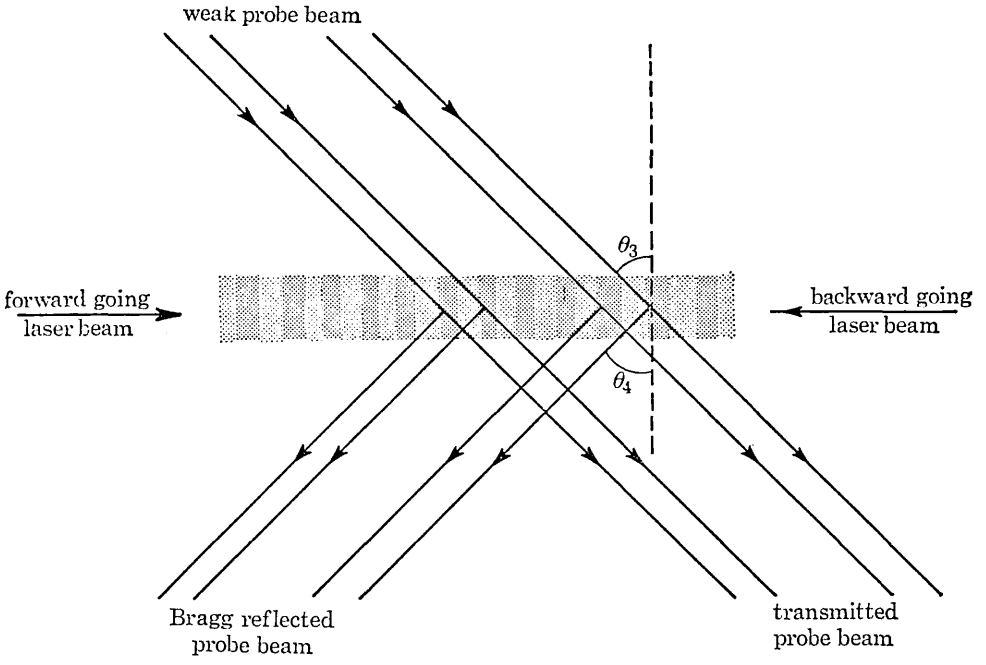

Fig. 3. Bragg reflexion for an induced modulation of dielectric constant.

spontaneous scattering intensity rather than that of the stimulated scattering gain. Thus if the Bragg reflectivity experienced by a weak laser beam traversing the modulations and the amplification of the backward going beam causing the modulation are measured, the amplitudes both of the whole modulation and of its out of phase part can be determined. The amplitude and phase of the modulation can then be specified whereas conventional stimulated scattering experiments give information only about its out of phase part. Furthermore, when a continuous laser is used to generate the weak independent beam, the variation in time of the intensity of the Bragg reflected light gives a direct measurement of the development and decay of the modulation.

2.2 *Effects of a modulation of dielectric constant*†

Consider the effect, on the light beams propagating through a medium, of a modulation of dielectric constant with angular frequency $\omega=(\omega_1-\omega_2)$, wavevector $k=(k_1+k_2)$ and amplitude proportional to $A_1\times A_2$; ω_1, k_1, A_1 and ω_2, k_2, A_2 are the angular frequencies, wavevectors and amplitudes of the electric fields of the forward and backward going beams, respectively.

Let $\Delta\epsilon$ be the difference between the dielectric constant at any point and its value in the undisturbed medium. Let $|\Delta\epsilon|$ be the amplitude of the modulation of dielectric constant and ϵ' and ϵ'' be the amplitudes of that part of the modulation in phase and one quarter period out of phase, respectively, with that component of E^2 which has the same frequency and wavevector as the modulation. (E, the total electric field, is the sum of the fields of the two light waves, so E^2 contains a term at the difference frequency.)

†This term is used throughout to denote relative permittivity.

(i) *Stimulated scattering*

The propagation of light in a medium with varying refractive index is described by the nonlinear Maxwell wave eqn. (Bloembergen 1965).

$$-\nabla^2 E+\frac{n^2}{c^2}\frac{\partial^2 E}{\partial t^2}=-\frac{1}{c^2}\frac{\partial(\Delta\epsilon\,.\,E)}{\partial t^2}, \tag{2.2.1}$$

where n is the refractive index of the undisturbed medium; owing to dispersion, the refractive index for terms of frequency ω_1 will be n_1 and for terms of frequency ω_2, n_2, c is the velocity of light, and t the time.

Substituting the appropriate expressions for E and $\Delta\epsilon$ in the above eqn. and equating the coefficients of those terms on the right- and left-hand sides which have the same dependence on position and time, it follows in the steady state, small signal approximation (Key 1970; Harrison 1970) that

$$\frac{1}{A_1}\frac{\partial A_1}{\partial x}=\frac{k_1}{4n_1^2}\frac{A_2}{A_1}\epsilon'', \tag{2.2.2}$$

$$\frac{1}{A_2}\frac{\partial A_2}{\partial x}=\frac{k_2}{4n_2^2}\frac{A_1}{A_2}\epsilon'', \tag{2.2.3}$$

where x is the distance along the direction of propagation of the beams.

As shown in Section 2.3.7, ϵ'' is, for all interaction mechanisms, proportional to A_1A_2. Therefore, provided $A_2 \ll A_1$, A_1 is almost constant, and the backward going beam (negative X-direction) undergoes an exponential spatial amplification of intensity, with gain coefficient G, where

$$G=-\frac{k_2}{2n_2^2}\left(\epsilon''\frac{A_1}{A_2}\right). \tag{2.2.4}$$

(This expression is adequate to describe amplification of a weak backward going beam by stimulated scattering, as occurs in cell 2 (fig. 2), but does not describe the generation of a scattered beam for which $A_2 \ll A_1$ is not valid.)

(ii) *Bragg reflexion*

When a weak probe beam traverses the region of modulated dielectric constant, $\Delta\epsilon$ is still determined by the interaction of the two powerful beams and is unaffected by the fields of angular frequencies ω_3 and ω_4, wavevectors k_3 and k_4, arising from the incident and reflected probe beams. Substituting expressions describing these fields and the refractive index change into eqn. (2.2.1), and equating coefficients with the same dependence on position and time, it follows that

$$\frac{\partial A_3}{\partial y}\cos\theta_3+\frac{\partial A_3}{\partial x}\sin\theta_3=\frac{|\Delta\epsilon|}{4n_3^2}k_3A_4\cos\delta, \tag{2.2.5}$$

and

$$-\frac{\partial A_4}{\partial y}\cos\theta_4+\frac{\partial A_4}{\partial y}\sin\theta_4=\frac{|\Delta\epsilon|}{4n_4^2}k_4A_3\cos\delta, \tag{2.2.6}$$

where n_3 and n_4 are the refractive indices experienced by beams of angular frequencies ω_3 and ω_4; x, y, θ_3 and θ_4 are as shown in fig. 4 and

$$\delta=(k_3\sin\theta_3+k_4\sin\theta_4-k)x+(k_3\cos\theta_3-k_4\cos\theta_4)y-(\omega_3-\omega_4-\omega)t,$$

where $\omega=(\omega_1-\omega_2)$ and $k=(k_1+k_2)$ are the angular frequency and wavevector of the modulation. When $\delta=0$ for all x, y, and t the interaction is a maximum.

For all types of scattering except stimulated Raman scattering, $\omega/k \ll c$ so $\partial = 0$ when

$$\theta_3 = \theta_4 = \arcsin(k/2k_3), \tag{2.2.7}$$

the usual condition for Bragg reflection.

Eqns. (2.2.5) and (2.2.6) describe the field amplitudes at any point within the Bragg reflecting region. To find the overall reflectivity of the region (Harrison *et al.* 1973) the boundary conditions relevant to a particular geometry of the interaction region must be imposed.

To treat the scattering situation shown in fig. 4 it is convenient to define new variables a and b along the incident and Bragg reflected beams respectively.

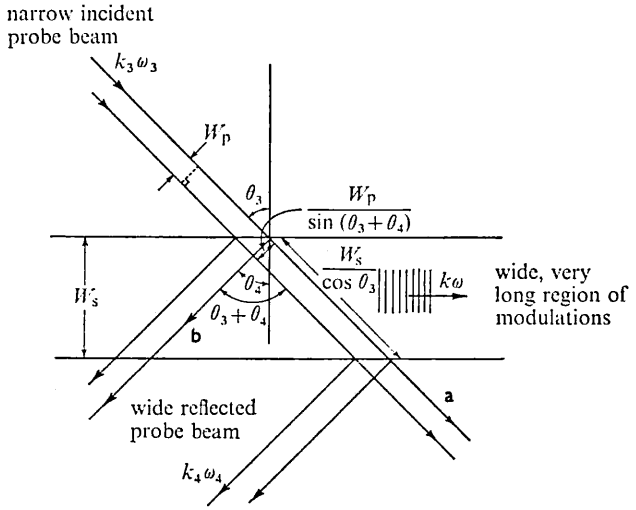

Fig. 4. Bragg reflexion geometry

Written in terms of these variables eqns. (2.2.5), (2.2.6) become

$$\frac{\partial A_3}{\partial a} = \frac{|\Delta\epsilon|}{4n_3^2} k_3 A_4 \cos\delta, \tag{2.2.8}$$

$$\frac{\partial A_4}{\partial b} = -\frac{|\Delta\epsilon|}{4n_4^2} k_4 A_3 \cos\delta. \tag{2.2.9}$$

Hence, for any process other than stimulated Raman scattering involving a very large frequency shift it may be shown that

$$R_B = \left(\frac{k_3}{4n_3^2}\right)^2 \frac{|\Delta\epsilon| W_s W_p}{\cos\theta_{3M} \sin 2\theta_{3M}}, \tag{2.2.10}$$

and

$$\frac{R}{R_B} = \left(\frac{\sin(k_3 W_p \delta\theta_3)}{k_3 W_p \delta\theta_3}\right)^2 \tag{2.2.11}$$

where W_p and W_s are respectively the width of the probe beam and the width of the region of modulated dielectric constant, and θ_{3M} is the angle at which Bragg reflectivity is a maximum. R_B is the reflectivity experienced by light incident at the Bragg angle and R that for light incident at an angle differing from the Bragg angle by a small angle $\delta\theta_3$. Thus, given the modulation of dielectric constant produced in a liquid by two oppositely directed light beams

of high intensity, the effect of that modulation on those beams or on any other weak beam traversing the medium can be calculated.

2.3. *Description of the modulation of dielectric constant*

(i) *Modulations arising from the changes in the polarizability of individual molecules.*

The modulation of dielectric constant responsible for stimulated Raman and Rayleigh wing scattering arises from the Kerr effect (Bloembergen 1967; Shen and Shaham 1967). The Kerr effect is caused by the change in polarizability of individual molecules due to their deformation and change of orientation under the influence of an electric field (Landau and Lifshitz 1960). The deformation, which is responsible for stimulated Raman scattering, can only be fully described quantum mechanically, but is often well represented by an equation of damped harmonic motion with a force term proportional to E^2 from which it follows that the change of dielectric constant is described by

$$\frac{\partial^2 \Delta\epsilon}{\partial t^2} + 2\Gamma \frac{\partial \Delta\epsilon}{\partial t} + \Omega^2 \Delta\epsilon = \Omega^2 K E^2, \tag{2.3.1}$$

where Ω and Γ are the angular frequency and line-width of the excited states responsible for a particular Raman line and K is that part of the Kerr coefficient which arises from the molecular deformation responsible for this line. (K is equal to the difference in the Kerr coefficient for electric fields of frequencies below and above that of the Raman shift.)

Substituting into (2.3.1) the expression describing that component of E^2 with frequency $\omega = \omega_1 - \omega_2$ (the amplitude of which is $A_1 A_2$) we find

$$\epsilon'' = -K \frac{2\Gamma\omega/\Omega^2}{(1-\omega^2/\Omega^2)^2 + (2\Gamma\omega/\Omega^2)^2} \Lambda, \tag{2.3.2}$$

and

$$|\Delta\epsilon|^2 = K^2 \frac{1}{(1-\omega^2/\Omega^2)^2 + (2\Gamma\omega/\Omega^2)^2} \Lambda. \tag{2.3.3}$$

The change of orientation, which is responsible for stimulated Rayleigh wing scattering in liquids with polar molecules, is governed by the same eqn. but, in this case there are two separate mechanisms (Fabelinskii and Starunov 1967). Firstly there is an angular oscillation of the molecule in the electric field of its neighbours. For this oscillation

$$\Omega = \sqrt{\left(\frac{\mu}{I}\right)} \text{ and } = \Gamma \frac{\xi}{2I}$$

where μ is a constant determined by the dipole moment of the molecule and the value of the local field, I is the moment of inertia of the molecule and ξ the effective viscosity damping the molecular oscillations. Secondly, the equilibrium position of this oscillation is not constant but, as a result of Brownian motion, will tend to ' jump ' to a new position after an average lifetime, τ.

The eqn. describing this oscillation is thus only valid for components of E^2 in which $\omega \gg 1/\tau$. Since, for most liquids $\sqrt{(\mu/I)} > \xi/I$ eqn. (2.3.1) implies a resonant interaction when $\omega \approx \mu/I$. For most liquids $\sqrt{(\mu/I)} > 1/\tau$, so the eqn. adequately describes the far part of the Rayleigh wing.

When $\omega \ll \tau$, however, the above oscillations are not significantly excited, and the molecular polarizability is determined by the thermal diffusion of the equilibrium positions of the orientation. For such diffusion $\Omega = \sqrt{(4kT/I)}$ and $\Gamma = \xi/3T$ where k is the Boltzmann constant and T the absolute temperature. This is valid for the near part of the Rayleigh wing.

(ii) *Modulations arising from changes in the density and temperature of the medium.*

The modulation of dielectric constant responsible for stimulated Rayleigh line and stimulated Brillouin scattering is related to changes $\Delta\rho$ in the density and ΔT in the temperature of the medium by the eqn.

$$\Delta\epsilon = \left(\frac{\partial\epsilon}{\partial\rho}\right)_T \Delta\rho + \left(\frac{\partial\epsilon}{\partial T}\right)_\rho \Delta T. \tag{2.3.4}$$

But the density ρ and the temperature T of the medium are governed by the following linearized hydrodynamic and heat conduction equations driven by terms proportional to E^2 representing electrostriction, absorption and the electrocaloric effect (Herman and Gray 1967)

$$\frac{\partial^2\rho}{\partial t^2} - \frac{v^2}{\gamma}\nabla^2\rho - \frac{\eta + \frac{4}{3}\eta'}{\rho_0}\frac{\partial}{\partial t}\nabla^2\rho - \frac{v^2}{\gamma}\beta\rho_0\nabla^2 T = -(Y/8\pi)\nabla^2 E^2 \tag{2.3.5}$$

and

$$\rho_0 c_v \frac{\partial T}{\partial t} - K\nabla^2 T - \frac{c_v(\gamma-1)}{\beta}\frac{\partial\rho}{\partial t} = \frac{1}{4\pi}n_1 c\alpha E^2 + \frac{1}{8\pi}T_0\left(\frac{\partial\epsilon}{\partial T}\right)_\rho \frac{\partial E^2}{\partial t}, \tag{2.3.6}$$

where ρ_0 and T_0 are the density and temperature respectively of the unperturbed medium, v is the adiabatic velocity of sound, η and η' the shear and bulk viscosities, β the coefficient of thermal expansion, K the thermal conductivity, c_v the specific heat capacity at constant volume, γ the ratio of the principal specific heat capacities, α the light absorption coefficient, Y the electrostrictive constant $\rho(\partial\epsilon/\partial\rho)_T$ n_1 the refractive index of the unperturbed medium and c is the velocity of light.

To represent the solution of these eqns. for that component of E^2 with frequency $\omega = \omega_1 - \omega_2$, wave vector $k = k_1 + k_2$, and amplitude $A_1 A_2$ it is convenient to define:-

the Brillouin frequency, $\omega_B = kv$,

the Brillouin linewidth $\Gamma_B = (\eta + \frac{4}{3}\eta')k^2/\rho_0$,

the Rayleigh linewidth $\Gamma_R = 2Kk^2/\rho_0 c_p$, and also

a dimensionless coefficient proportional to absorption $\mathscr{A} = \dfrac{4n_1 c\alpha\beta v^2}{Y\gamma c_p \Gamma_R}$.

where c_p is the specific heat capacity at constant pressure.

Hence it may be shown that for most liquids, where $\Gamma_R \ll \Gamma_B \ll \omega_B$. and $\dfrac{(\partial\epsilon/\partial T)_\rho}{\beta Y} \ll 1$ (Key *et al.* 1972)

$$\epsilon'' = -\frac{Y^2 A_1 A_2}{8\pi\rho_0 v^2}\left\{\begin{array}{ll} \text{electrostrictive terms} & \text{absorptive terms} \\ +\dfrac{\omega_B}{\Gamma_B}[F_1] & -\dfrac{\mathscr{A}\gamma^2\Gamma_R^2}{4\omega_B\Gamma_B}[F_1] \\ +\dfrac{\gamma-1}{2}\left[\dfrac{\Gamma_R}{2\Gamma_B}F_{2R}\right] & -\dfrac{\mathscr{A}\gamma}{2}\left[\dfrac{\Gamma_R}{2\Gamma_B}F_{2R}\right] \\ +\dfrac{(\gamma-1)}{4}\dfrac{\Gamma_R}{\Gamma_B}[F_{2B}] & -\dfrac{\mathscr{A}\gamma}{4}\dfrac{\Gamma_R}{\Gamma_B}[F_{2B}] \end{array}\right\}, \tag{2.3.7}$$

and

$$|\Delta\epsilon|^2 = \left(\frac{Y^2 A_1 A_2}{8\pi\rho_0 v^2}\right)^2\left\{\begin{array}{l} +\dfrac{\Gamma_R^2}{4\Gamma_B^2}\left(\gamma^2(1-\mathscr{A})^2+\dfrac{4\omega_B^2}{\Gamma_R^2}\right)\left[F_1\dfrac{\omega_B}{\omega}\right] \\ +\gamma^2(1-\mathscr{A})^2\left[\dfrac{\Gamma_R^2}{8\Gamma_B\omega_B}F_{2R}\dfrac{\omega_B}{\omega}\right] \\ +\gamma^2(1-\mathscr{A})^2\dfrac{\Gamma_R^2}{8\Gamma_B\omega_B}\left[F_{2B}\dfrac{\omega_B}{\omega}\right] \end{array}\right\}, \tag{2.3.8}$$

where each term in square brackets is a function of ω with a maximum of unity. The antisymmetric functions F_1, F_{2R} and F_{2B}, illustrated graphically in fig. 5, are defined as

$$F_1 = \frac{(\Gamma_B^2/\omega_B^2)(\omega/\omega_B)}{(1-\omega^2/\omega_B^2)^2+(\Gamma_B\omega/\omega_B^2)^2},$$

$$F_{2R} = \frac{2\Gamma_B}{\Gamma_R}\left(\frac{4\omega/\Gamma_R}{1+4\omega^2/\Gamma_R^2}\right),$$

$$F_{2B} = \frac{2(1-\omega^2/\omega_B^2)(\Gamma_B/\omega_B)(\omega_B/\omega)}{(1-\omega^2/\omega_B^2)^2+(\Gamma_B\omega/\omega_B^2)^2}.$$

These functions represent respectively the frequency profiles usually associated with stimulated Brillouin, stimulated Rayleigh and stimulated thermal Brillouin scattering. The symmetric functions $[F_1\omega_B/\omega]$, $[F_{2R}\omega_B/\omega]$ and $[F_{2B}\omega_B/\omega]$, which determine $|\Delta\epsilon|^2$ and hence control the Bragg reflexion, are also illustrated in fig. 5. These represent frequency profiles resembling those of spontaneous Brillouin and Rayleigh line scattering (fig. 1).

2.4. *Stimulated scattering and Bragg reflexion*

Using the results of sections 2.2 and 2.3, the gain coefficient for each type of stimulated scattering and the Bragg reflectivity of the associated modulation may be calculated. The frequency profiles of the reflectivity and gain, indicated by these calculations, are illustrated in fig. 1.

(i) *Stimulated Raman scattering*

For most Raman transitions, $\Gamma \ll \Omega$, and the expressions obtained by combining eqns. (2.2.4) with (2.3.2) and (2.2.9) with (2.3.3) indicate sharp maxima in the regions $\omega \sim \pm\Omega$. The gain is positive for positive ω, i.e. Stokes-shifted, backward-going beams undergo amplification while anti-Stokes-shifted beams are absorbed (see fig. 1). These results apply only for the amplifier arrangement described, and assume that no other processes are competing with the stimulated

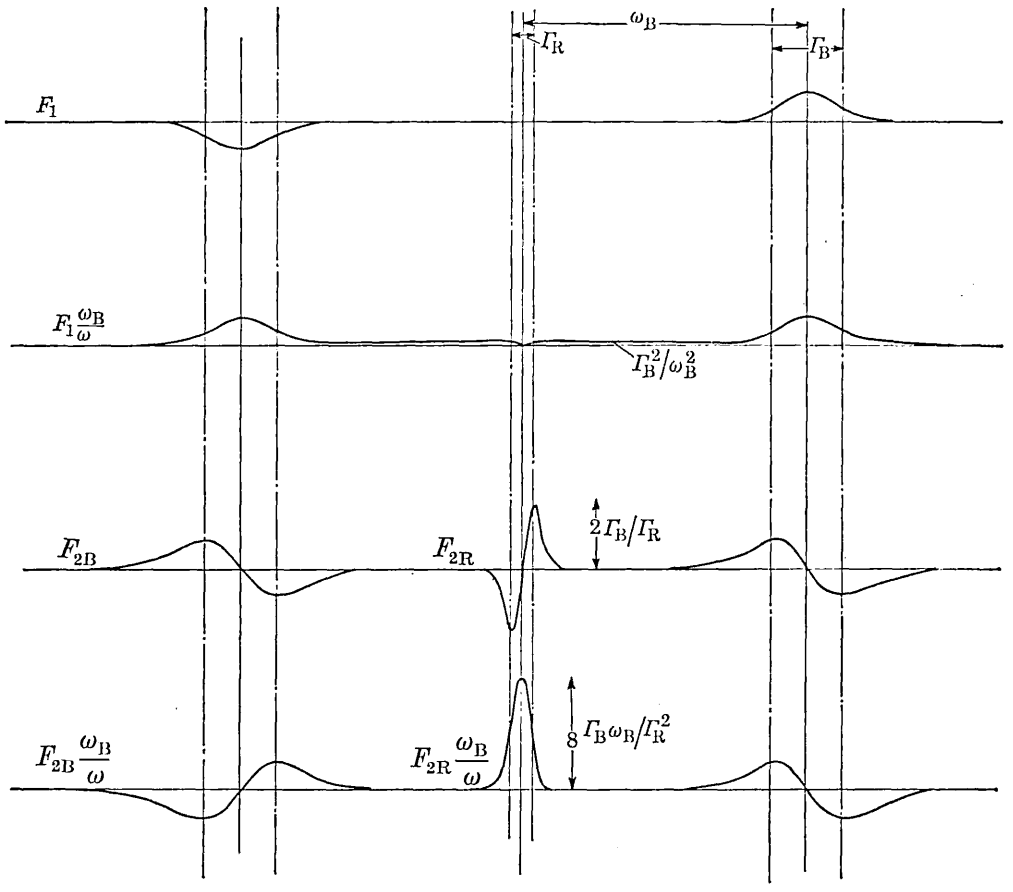

Fig. 5. The frequency profiles governing stimulated scattering and Bragg reflexion in hydrodynamic media.

Raman scattering. At higher intensities more complex interactions can cause generation of cones of light of anti-Stokes shifted frequency, (Bloembergen 1967).

(ii) *Stimulated Rayleigh wing scattering*

The gain and reflectivity which result from the oscillation of the molecules of the medium in the fields of their neighbours (i.e. the gain and reflectivity in the far part of the wing from 20 to 200 cm^{-1}) are governed by the same eqns. but for this process $\Gamma \sim \Omega$ because the viscous damping of molecular rotations is very strong though not necessarily critical for these oscillations. The resulting maxima of the gain profile and of the reflectivity profile are therefore very broad. For the gain and reflectivity existing in the near part of the wing out to about 20 cm^{-1}, which are determined by the diffusional mechanism, $\Gamma \geqslant \Omega$ because the viscous damping of this process is usually greater than critical. The gain profile therefore has diffuse maxima while the reflectivity profile is a single broad peak with a maximum at the laser frequency.

In general the oscillatory and diffusional parts of the wing are not strictly separable, so a more sophisticated theory is required to describe the intermediate region (Starunov 1964).

(iii) *Stimulated Rayleigh line and Brillouin scattering*

For media in which $(\partial\epsilon/\partial T)\rho \ll \beta Y$ we may combine eqns. (2.2.4) with (2.3.2) and (2.2.9) with (2.3.8) (Key and Harrison 1972) to give expressions describing the gain and reflectvity arising from changes of density and temperature. The total profile of the gain, as a function of the frequency shift ω, is a sum to which electrostriction and absorption each make contributions with all three types of profile F_1, F_{2R} and F_{2B}.

The term $(\omega_B/\Gamma_B)[F_1]$ gives the usual expression for stimulated Brillouin scattering in a non-absorbing medium (Herman and Gray 1967; Starunov and Fabelinskii 1970). The terms $-\frac{1}{2}\mathscr{A}\gamma[(\Gamma_R/2\Gamma_B)F_{2R}]$ and $-\frac{1}{4}\mathscr{A}\gamma(\Gamma_R/\Gamma_B)[F_{2B}]$ describe the stimulated Rayleigh scattering and stimulated thermal Brillouin scattering due to absorption first predicted by Herman and Gray (1967).

The terms $\frac{1}{2}(\gamma-1)[(\Gamma_R/2\Gamma_B)F_{2R}]$ and $\frac{1}{4}(\gamma-1)(\Gamma_R/\Gamma_B)[F_{2B}]$ describe, respectively stimulated Rayleigh scattering in non-absorbing media and a slight modification of the profile of stimulated Brillouin scattering in such media. The remaining absorptive term $-(\gamma^2\Gamma_R^2/4\omega_B\Gamma_B)[F_1]$ slightly affects the magnitude of the stimulated Brillouin scattering gain in absorbing media, but is negligible under normal conditions. The profile of the Bragg reflectivity is not readily separable into terms arising from different physical effects. (Harrison *et al.* 1973).

The term $\omega_B^2/\Gamma_B^2[F_1\omega_B/\omega]$ shows however that electrostriction gives rise to a profile similar to that of spontaneous Brillouin scattering. The smaller term $(\Gamma_R^2/4\Gamma_B^2)\gamma^2(1-\mathscr{A})^2[F_1\omega_B/\omega]$ shows that, in an absorbing medium, the reflectivity in this part of the frequency profile is slightly increased.

The term $\gamma^2(1-\mathscr{A})^2[(\Gamma_R^2/8\omega_B\Gamma_B)F_{2R}\omega_B/\omega]$ shows that electrostriction also gives rise to a weak contribution to reflectivity with the same profile as that of spontaneous Rayleigh scattering. In an absorbing medium, however, $\mathscr{A}$ may greatly exceed unity and in such a medium that part of the reflectivity with this profile may be very large.

The term $\gamma^2(1-\mathscr{A})^2(\Gamma_R^2/8\omega_B\Gamma_B)[F_{2B}\omega_B/\omega]$ indicates a very small electrostrictive modification of the Brillouin line-shape which is also somewhat increased in absorbing media.

3. Experiments

3.1. *Bragg reflection from light induced periodic structures in bulk media*

(i) *Experimental arrangement*

The experimental arrangement used for the observation of Bragg reflection from a modulation of dielectric constant induced in a liquid is illustrated in fig. 6 and shown schematically in fig. 7. (Key *et al.* 1970; Key 1970; Harrison 1970).

The output of a passively Q switched ruby laser (duration 15 ns, intensity up to 100 MW/cm^2 in a single longitudinal mode) passed through a quartz cell containing the liquid under investigation and was reflected back through the cell in the opposite direction by a dielectric mirror. The action of the forward and backward going beams on the liquid produced a spatial modulation of its dielectric constant. This modulation was traversed by the 1W continuous output of an argon ion laser operating at 488 nm. This beam, which was continuously recorded on a power meter, was directed into the cell by the mirror M_1 which could be sensitively adjusted to make the beam incident on the

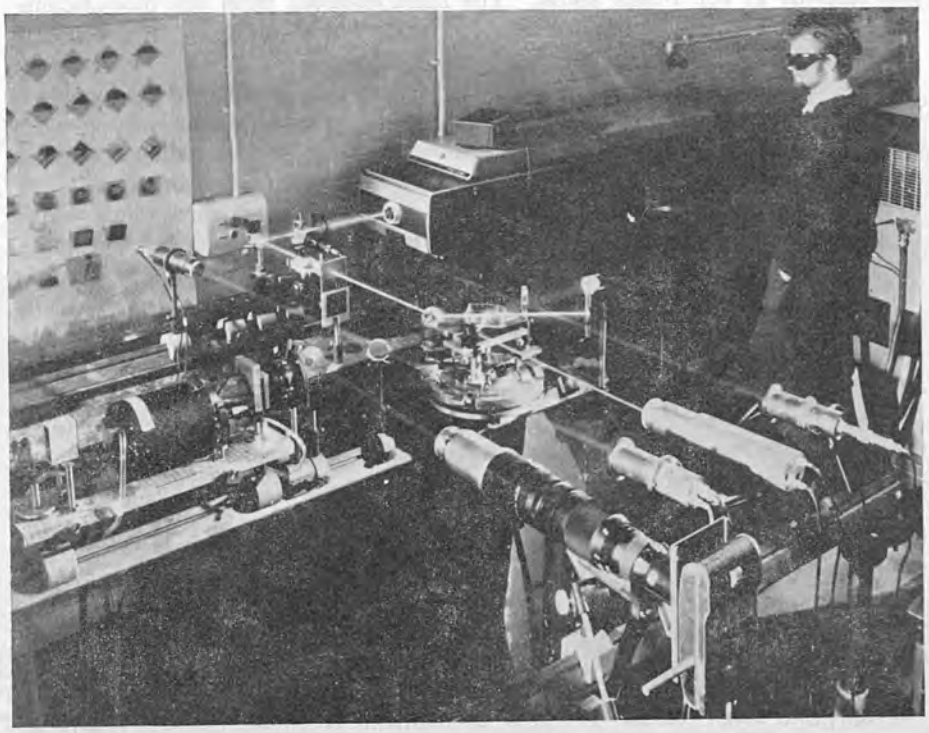

Fig. 6. Experimental arrangement for Bragg reflexion of argon laser light.

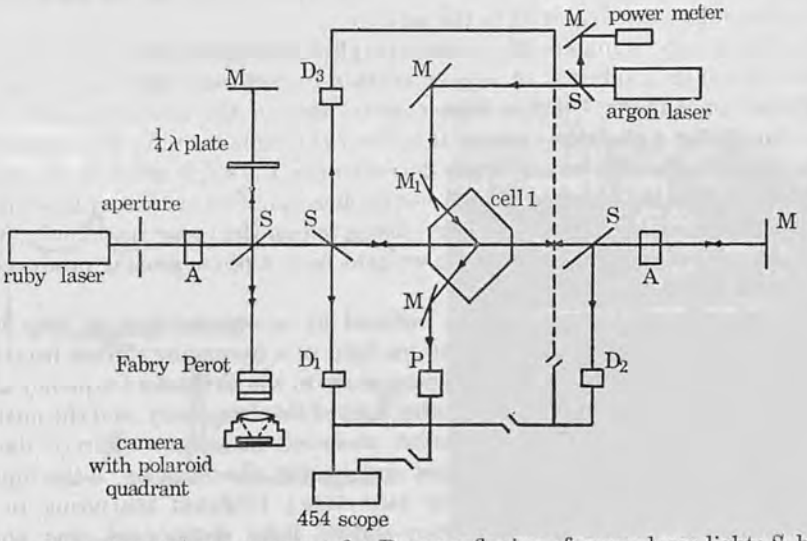

Fig. 7. Experimental arrangement for Bragg reflexion of argon laser light: S, beam splitter; M, mirror; A, attenuator; D, diode; P, photomultiplier; ⌇, delay line.

modulations at the Bragg angle. The light reflected from the modulations was directed onto the photomultiplier, P, from which the signal was recorded on an oscilloscope.

This oscilloscope could also record the signals generated by the ruby laser light incident on photodiodes, D_1, D_2 and D_3. D_1 and D_2 measured the powers of the forward and backward going beams arriving at the cell, while P and D_3 simultaneously measured the light reflected by the modulation in the cell and the amplification which the modulation caused in the backward going beam. By use of appropriate cable delays all four signals could be displayed on a single trace of the oscilloscope.

A Fabry-Pérot interferometer was used for spectral analysis of the light in the forward and backward going beams. Discrimination between these beams could be achieved by using a quarter wave plate and a disc of polaroid with adjacent quadrants oppositely orientated.

The intensities of the forward and backward beams were controlled (and feedback into the laser minimized) using attenuators consisting of aqueous solutions of copper sulphate.

(ii) *Qualitative investigation of Bragg reflexion arising from various interaction mechanisms*

The principal contributions to Bragg reflexion arise from absorption, electrostriction, the electrocaloric effect and the Kerr effect. Under suitable experimental conditions, Bragg reflexion arising from each separate effect may be identified.

Absorption is the easiest of these mechanisms to identify. The resulting Bragg reflexion has a maximum when the backward going and forward going beams are of the same frequency. This reflexion though absent when the beams intersect in a pure non-absorbing solvent, can be much greater than the contribution arising from any other effect when there is but a small amount of an absorbing substance dissolved in the solvent.

Fig. 8 shows the signals on the diodes and photomultiplier when pure methanol (upper trace) or a solution of copper acetate in methanol with an absorption coefficient of $0{\cdot}15\ \mathrm{cm}^{-1}$ (lower trace), were used in the scattering cell. The photomultiplier signal disappeared if either ruby light beam or the argon laser beam was cut off and it was critically dependent on the angle between the beams. These facts, and the absence of photomultiplier signal on the upper trace imply that the signal on the photomultiplier, displayed on the lower trace of fig. 8 was due to Bragg reflexion of the argon laser light from a phase grating produced by absorption of the ruby laser light.

The refractive index modulation induced by electrostriction is very small unless the backward going beam contains light of a frequency shifted from that of the forward going beam by an amount close to the Brillouin frequency shift. When the backward going beam contains light of this frequency, and the medium is non-absorbing, any Bragg reflexion observed is almost entirely due to electrostriction. To obtain the traces and spectra shown in fig. 9 the light of shifted frequency was generated by stimulated Brillouin scattering in the laser Q-switch. When the frequency-shifted light component was absent (upper trace) there was no Bragg reflected signal, but in the presence of this component (lower trace) such a signal was clearly visible. The electrocaloric

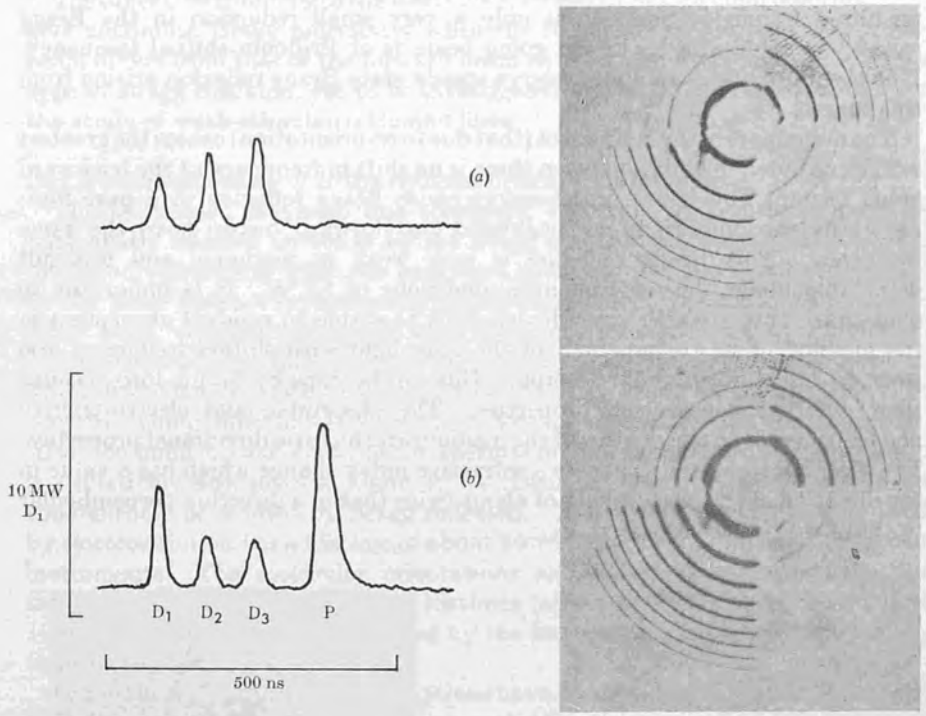

Fig. 8. Comparison of Bragg reflexion in a non-absorbing liquid (methanol) (upper trace), with an absorbing solution of copper acetate in methanol (lower trace).

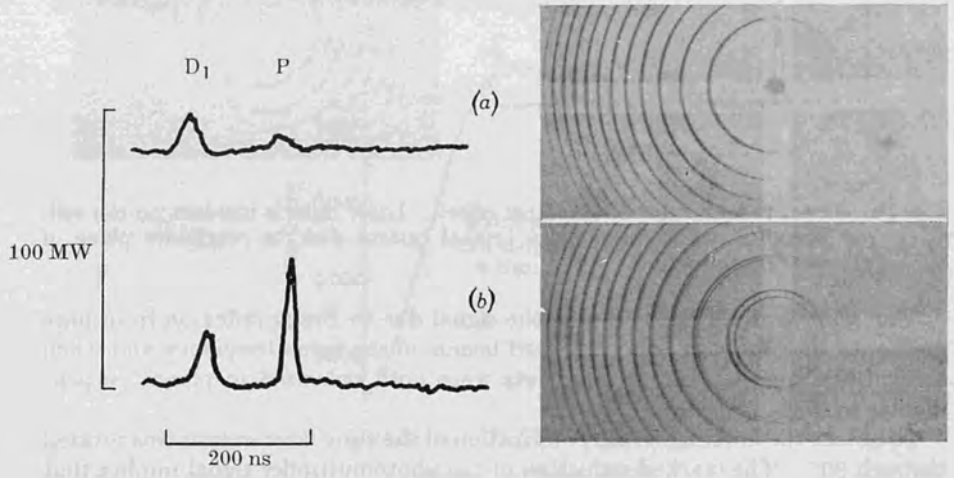

Fig. 9. Bragg reflexion due to electrostriction.

effect has no influence on Bragg reflexion when the backward going beam is of unshifted frequency and causes only a very small reduction in the Bragg reflectivity when the backward going beam is of Brillouin-shifted frequency. It is therefore not possible to observe steady state Bragg reflexion arising from this source.

The major part of the Kerr effect (that due to re-orientation) causes the greatest refractive index modulation when there is no shift in frequency of the backward going beam. This effect can therefore cause Bragg reflexion in a pure non-absorbing medium when the backward and forward beams have the same frequency. This Bragg reflexion is very weak in methanol and was not detectable under the experimental conditions of fig. 8. It is important to distinguish this weak Bragg reflexion from that due to residual absorption in the medium or to a component of the laser light with shifted frequency, too weak to detect on the Fabry-Pérot. This can be done by taking into account their different polarization properties. The absorptive and electrostrictive mechanisms act on the density of the medium and have no directional properties. The Kerr effect, however, causes a refractive index change which has a value in the direction of the electric field of about twice that in a direction perpendicular to that field (Havelock's law).

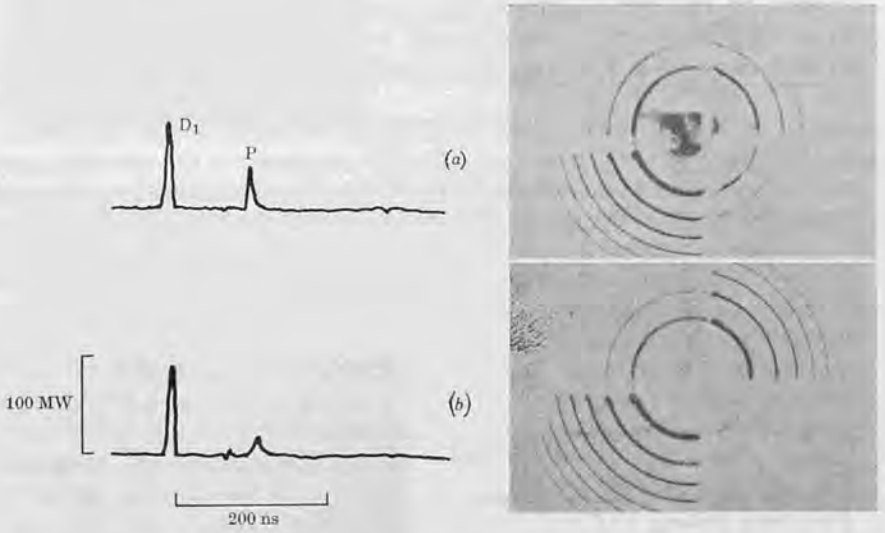

Fig. 10. Bragg reflexion due to the Kerr effect. Laser light is incident on the cell: (*a*) directly, and (*b*) through a crystal quartz disk to rotate its plane of polarization through 90°.

The upper trace of fig. 10 shows the signal due to Bragg reflexion from pure methanol with forward and backward beams of the same frequency and when the ruby and argon ion laser outputs were both polarized in planes perpendicular to that of fig. 9.

To obtain the lower trace the polarization of the ruby laser output was rotated through 90°. The marked reduction of the photomultiplier signal implies that the Kerr effect was the mechanism responsible for the Bragg reflexion observed.

The other contributions to the Kerr effect, arising from molecular deformations, give maximum Bragg reflectivity when the frequency of the backward going beam differs from that of the forward beam by a Raman frequency shift. This type of Bragg reflexion, yet to be investigated, might provide a useful tool for the study of weak stimulated Raman lines.

(iii) *Quantitative study of Bragg reflexion arising from absorption.*

The stimulated Rayleigh line scattering occurring in absorbing media is particularly suitable for study by the Bragg reflexion technique, since it gives maximum reflectivity when the backward going beam is of the same frequency as the laser beam. Investigation of the electrostrictive mechanism, on the other hand, requires generation of a frequency shifted beam by stimulated Brillouin scattering which can result in rapid uncontrolled intensity fluctuations. The reflectivity generated as a result of the Kerr effect has its maximum at zero frequency shift but is very much weaker than that due to absorption. Also, the build-up and decay of the thermal modulation induced by absorption is a relatively slow process, about 10^{-8} s (Denariez and Bret 1968), which can conveniently be studied by Bragg reflexion. The density modulation induced by electrostriction has a lifetime of about 10^{-10} s; too short for resolution by our instruments. The molecular orientations and deformations responsible for the Kerr effect have much shorter lifetimes (about 10^{-12} s) (Denariez and Bret 1968) which are more easily studied by the broadening of the associated spontaneous scattering lines.

In the theory, a number of assumptions have been made and it must be ensured that the experimental conditions are such that these remain valid or can be suitably modified. First, it has been assumed that I_1 and I_2 are uniform over any cross-section of the ruby laser beam. In practice, however, the transverse mode composition of the ruby laser output was erratic and the resulting intensity distribution was non-uniform and variable. This situation was somewhat improved by using an aperture to transmit only the most consistently uniform part of the beam. It remained, however, the most serious source of error in these experiments and accounts for the ' scatter ' of the points in figs. 11 and 12.

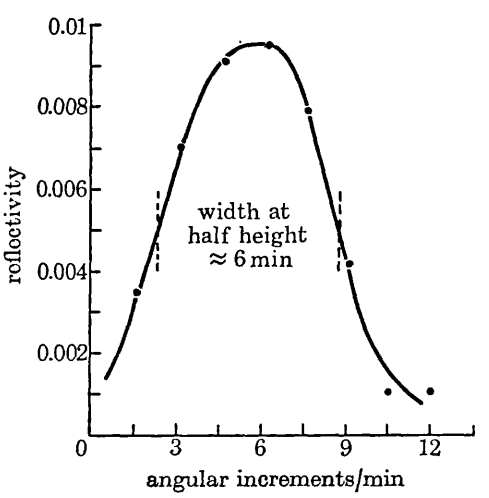

Fig. 11. Variation of reflectivity with the angle between the beams.

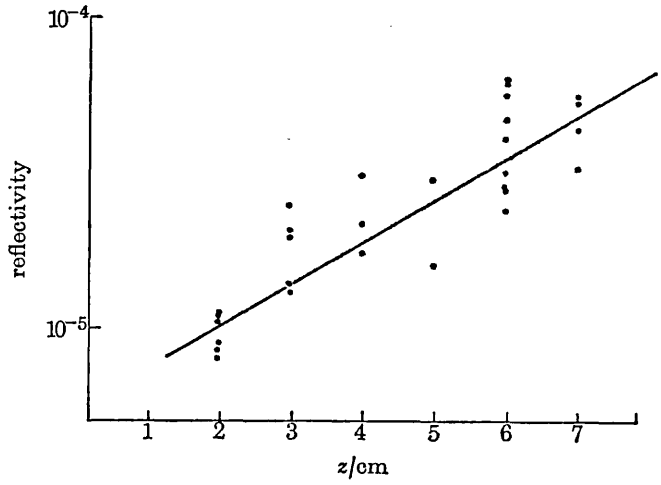

Fig. 12. Variation of reflectivity with position of the interaction region.

It has, throughout, been assumed that the intensity I_1 of the forward going ruby laser beam is very much greater than I_2, the intensity of the backward beam. This condition was ensured by use of the attenuators shown in fig. 1. It has also been assumed, in calculating the reflectivity, that the magnitude of the modulation remains constant over the length of the reflecting region. This requires that $I_1 \times I_2$ remains constant over that region. Since the beams are travelling in opposite directions this remains true for any linear absorption of the beams but is not true when the backward going beam is significantly amplified in this distance, by stimulated scattering. For the experimental situation in this investigation that amplification remained insignificant provided $I_1 < 70$ MW cm^{-2}.

The theory also assumes that the ruby laser output is of a defined angular frequency ω_1. In practice, the output, and the reflected beam, had a finite spread of frequency of approximately Lorenzian profile with width Γ_L. Convolution with these profiles results in a broadening of the width of the Lorenzian Bragg reflectivity profile from Γ_R to $(\Gamma_R + 2\Gamma_L)$, and a reduction of its maximum by a factor $\Gamma_R/(\Gamma_R + 2\Gamma_L)$.

It has also been assumed that the probing laser beam is of an exact frequency and direction. The argon ion laser beam has an output which is a Gaussian function of angle and a Lorenzian function of frequency. Both these distributions cause a broadening of the angle over which Bragg reflexion can be observed, but the effect of the frequency spread is negligible compared with that of the divergence. To take the divergence of the beam into account the reflexion of that fraction of the beam which propagates in each particular direction must be considered separately. The total reflected intensity is then the sum of the intensities of the separately calculated components.

Hence it may be shown that the total reflectivity experienced by the probe beam is given by

$$R_{\text{tot}} = \left(\frac{\alpha\beta Y}{2Kn_3^2k^2}\right)^2 \frac{W_s k_3}{\cos\theta_3 \sin 2\theta_3} \frac{\Gamma_R}{\Gamma_R + 2\Gamma_L} \frac{\sqrt{\pi}\exp -[(\theta_M - \theta_0)/\Delta\theta]^2}{\Delta\theta} I_1 I_2. \tag{3.1.1}$$

The lower trace of fig. 9 was obtained when the intensity I_1 of the forward-going ruby laser beam was 20 MW cm^{-2}, while the intensity I_2 of the backward going beam was a third of this value. The height of the photomultiplier pulse indicates a reflectivity of about 0·01 per cent in reasonable agreement with the value predicted by eqn. (3.1.1) for the experimental conditions. In view of the unknown spatial and spectral distributions of the ruby laser output, exact agreement with the experimental value cannot be expected. For this reason the variation of the reflectivity with the experimental parameters appearing in the eqn. provides a better test of the theory than does its absolute magnitude.

Eqn. (2.2.7) indicates that the argon ion laser beam should experience maximum reflectivity when incident on the ruby laser induced modulations at a glancing angle of 44·5°. Fig. 11 shows the reflectivity observed when the angle was varied about this value. The results confirm this estimate of θ_M.

Fig. 11 indicates an angular distribution of reflectivity with a width at half height of 2 mrad. This graph approximately follows the Gaussian distribution of the intensity of the argon ion laser beam (eqn. (3.1.1)).

When the logarithm of the reflectivity R was plotted against the logarithm of the forward-going intensity I_1, maintaining the second attenuator constant so that $I_2 = I_1/3$, the resulting graph showed that

$$R \propto I_1^2.$$

On the other hand, when I_1 was kept constant, and the logarithm of R was plotted against the logarithm of I_2, the slope of the resulting graph showed that

$$R \propto I_2.$$

These two results confirmed the behaviour predicted by eqn. (3.1.1), namely that

$$R \propto I_1 I_2$$

A simple experiment in which the incident power in the argon-ion laser probe beam was compared with the Bragg reflected power, showed that the argon-ion beam was contributing no non-linear optical effects of its own.

When R was measured as a function of the optical attenuation coefficient α, it was observed that

$$R \propto \alpha^2.$$

This too was in agreement with eqn. (3.1.1).

Fig. 12 shows a log-linear plot of the reflectivity observed when the probe beam intersects the ruby laser beam at a distance z from the back face of the scattering cell. Absorption in the cell results in the relations $I_1 \propto \exp(\alpha z)$, $I_2 \propto \exp(-\alpha z)$. Thus $I_1 I_2$ is constant in the absence of nonlinear effects. Any variation in the reflectivity is therefore due to gain in the backward beam caused by stimulated thermal Rayleigh scattering.

The gain indicated by these results is about 0·2 cm^{-1}. This is in reasonable agreement with the theoretical value predicted under the experimental conditions.

(iv) *Decay of the thermal modulation induced in a liquid*

When two oppositely directed light beams of the same frequency traverse an absorbing medium, more energy is absorbed at the antinodes than at the nodes of the resulting standing wave. It is the temperature modulation caused by such absorption which is responsible for the modulation in density and dielectric constant investigated here.

Such a temperature modulation does not arise or disappear instantly with the electric field of the light wave, but its amplitude tends exponentially towards an equilibrium value for any constant field amplitude. In general when the field amplitude is a function of time the behaviour of the temperature modulation may be deduced by consideration of the heat conduction eqn. (2.3.6). Since we are dealing with a strongly absorbing medium the electro-caloric effect may be neglected. Also, since the frequencies of the forward and backward beams are in this case equal, the temperature modulation is stationary and can have no out of phase component. Thus, provided the fields are varying slowly compared with the time required for sound to propagate over a wavelength of the modulation (10^{-10} s), it may be shown that

$$\frac{\partial|\Delta\epsilon|}{\partial t}+\frac{1}{\tau}|\Delta\epsilon|\propto I, \tag{3.1.2}$$

Where $\tau=(2/\Gamma_R)$ is the relaxation time of the thermal grating.
Hence

$$|\Delta\epsilon|\propto\exp(-t/\tau)\int_{t'=0}^{t} I_1\exp(+t/\tau)\,dt', \tag{3.1.3}$$

The diode-detected laser pulses indicate the value of I_1 as a function of time. Eqn. (3.1.3) allows a numerical calculation of the time dependence of $|\Delta\epsilon|$ for the observed pulse I_1 and any assumed value of τ. Now the grating reflectivity is proportional to $|\Delta\epsilon|^2$ so the assumed value of τ allows calculation of the time dependence of the resulting Bragg reflected pulse. The value of τ giving the best fit to the observed Bragg reflected pulse is the best estimate of the relaxation time of the thermal modulation in the liquid. In fig. 13, points calculated assuming $\tau=16{\cdot}5$ ns are superimposed on the experimentally observed Bragg reflected pulse.
These points are in good agreement with the experimental trace obtained using a solution of copper acetate in methanol in the scattering cell. Significant misfit occurs when it is assumed that $\tau<14$ ns or $\tau>18$ ns. Further results are listed in the table.

Relaxation times of the thermal modulation generated by stimulated Rayleigh scattering of ruby laser light

Solvent	τ/ns	
	Theoretical	Experimental
Methanol	17·0	16·5 ± 2
Water	12·1	12·0 ± 2
Acetone	17·9	17·0 ± 2

3.2. *Diffraction from light-induced periodic structures on surfaces*
(i) *Experimental arrangement*

The experimental arrangement used to investigate the diffraction of light from periodic structures generated in thin films is illustrated in fig. 14. (Cutter *et al.* 1974). The passively Q-switched ruby laser gave a pulse of up to 50 MW peak power and a duration of 10–20 ns width at half power. The intensity of the light incident on the film was controlled by an attenuating cell containing

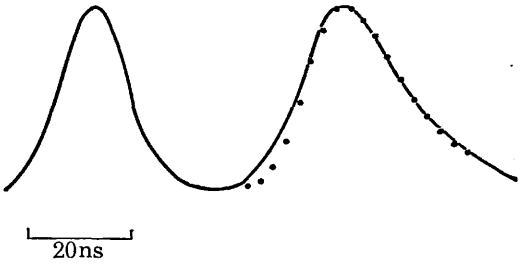

Fig. 13. Time profile of the ruby laser pulse and the resulting Bragg reflected pulse. The points marked are those calculated given the theoretical relaxation time.

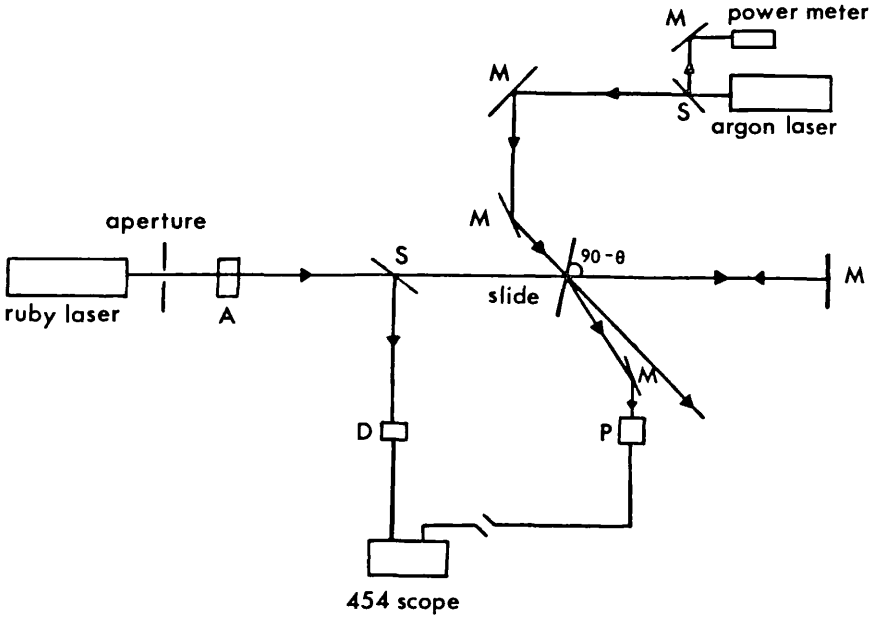

Fig. 14. Experimental arrangement for the study of the temporal development of the light diffracted from an optically induced grating.

aqueous copper sulphate solution. The ruby laser light, which was incident on each side of the film was detected by a fast photodiode and displayed on the oscilloscope.

The output of the argon ion laser was incident on that part of the film illuminated by the ruby laser. As the grating was created by the action of the ruby laser light upon the thin film, the first order diffracted beam of argon ion laser light was detected by a photomultiplier of about 2 ns rise time. The signal was displayed, using a suitable delay line, on the same oscilloscope trace as the ruby laser signal. The absorbing films used were evaporated layers of silver, gold and aluminium of thicknesses from 50Å to 400Å on a glass microscope slide substrate.

(ii) *Results.*

The temporal development of the beams diffracted from the gratings formed by the various films was observed over a range of ruby laser intensities, and the

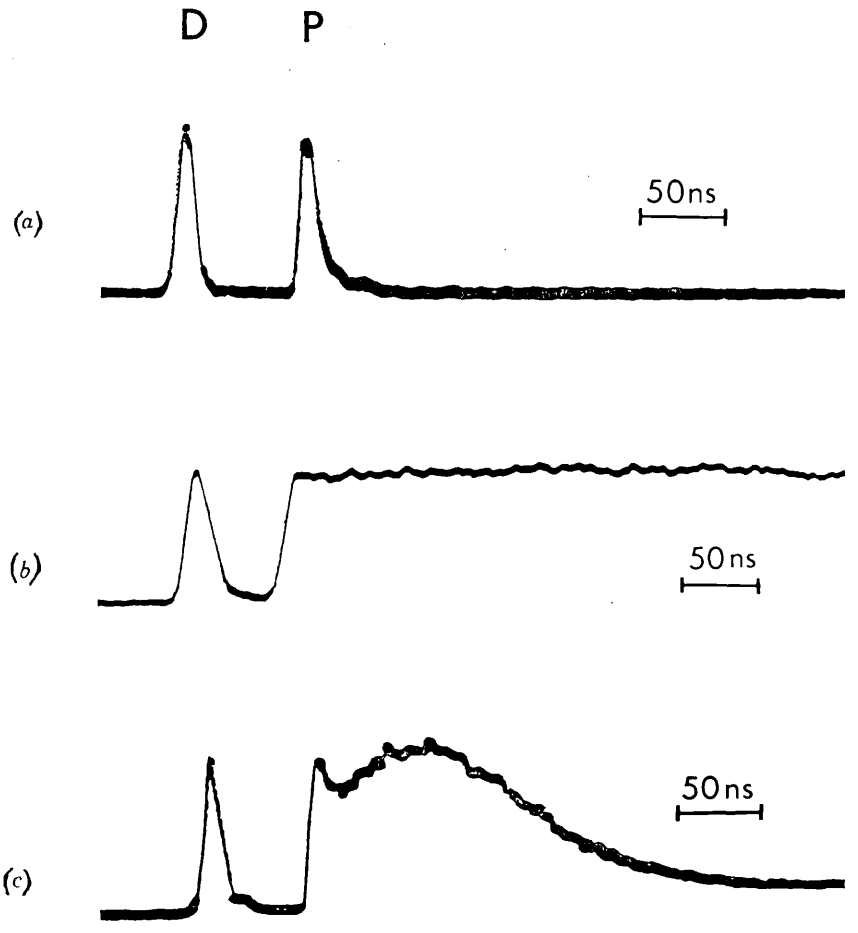

Fig. 15. Signal diffracted from (*a*) 200 Å silver film illuminated by a ' high energy ' 0·45 J/cm^2 ruby laser pulse, (*b*) 100 Å gold film illuminated by a ' low energy ' 0·045 J/cm^2 ruby laser pulse, (*c*) 200 Å gold film illuminated by an ' intermediate energy ' 0·1 J/cm^2 ruby laser pulse.

effect of varying the angle of incidence of the ruby laser beam upon the film was also studied.

The main features of the development of the diffracted signals were the same for each type of film. At different energies of the incident ruby laser pulse three main types of development were observed. For pulses of very high energy the diffracted signal was a pulse with a short duration comparable to that of the incident light. With low incident energy the diffracted signal resembled a step function rising to a constant level in a time comparable to the duration of the laser pulse. At intermediate energies the signal had a more complex structure. A short initial pulse was followed by a relatively slow rise and then a decay to a constant level. The three types of signal can be clearly seen in fig. 15. The rise and fall times of the slowly varying part of the signal observed using a ruby laser beam of intermediate energy were found to depend strongl on the angle between the film and this laser beam. Fig. 16 shows a graph of the decay time of the signal, plotted as a function of cosec θ. The graph clearly shows that this time depends linearly on cosec θ.

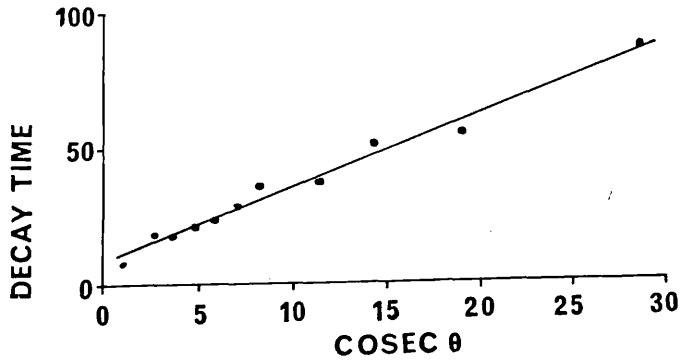

Fig. 16. Variation of decay time to a half intensity (in ns) of the diffracted signal with the angle of incidence of the ruby laser light, (signals diffracted from a 200 Å gold film illuminated by a 0·3 J/cm^2 ruby laser pulse).

Although the conditions of the laser oscillator were kept constant, the duration of the output pulse varied from 10–20 ns. Analysis of the effect of pulses of different widths showed the crucial factor determining the nature of the diffracted signal to be the energy rather than the power of the laser pulse. The diffraction efficiency of the grating left after etching, varied with pulse energy and film thickness. The pulse energy for which this efficiency was a maximum tended to increase with increasing film thickness.

The ideal optically etched grating would consist of a periodic thin metallic film, undamaged at its thickest points and totally absent at its thinnest, on a completely unaffected substrate. Those gratings formed by illumination of 50–100 Å gold or aluminium films by ruby laser beams of only just sufficient energy to affect the films, approached closest to the ideal (fig. 17). These gratings were very small in area, but could have diffraction efficiencies of up to 10 per cent.

Correlation of the time resolved diffracted signals with the appearance of the gratings clearly showed that the ' ideal ' type of grating was formed when the beam energy was sufficiently low to give the ' step function ' type of diffracted signal. Whenever a fast pulse was visible in the diffracted signal, complete removal of the free metal had occurred over at least some part of the grating.

(iii) *Discussion.*

The complexity of the temporal development of the diffracted laser beam under various conditions of film excitation suggests that a number of mechanisms are involved in the formation of the grating. This fact and the essentially destructive nature of the processes occurring within the film make quantitative analysis of the observations extremely difficult.

Many authors (Henderson *et al.* 1971 ; Parks *et al.* 1972 ; Alyassini *et al.* 1972) have reported the formation of a microplasma when a Q-switched laser pulse with an intensity of the same order of magnitude as that used in our experiments impinges on a solid surface. The short pulse of diffracted signal observed using ruby laser pulses of very high energy (fig. 15 (a)) may be readily explained on the assumption that lines of plasma were first formed at the antinodes of the standing wave causing a strong diffracted signal. Subsequent heating at the nodes of the

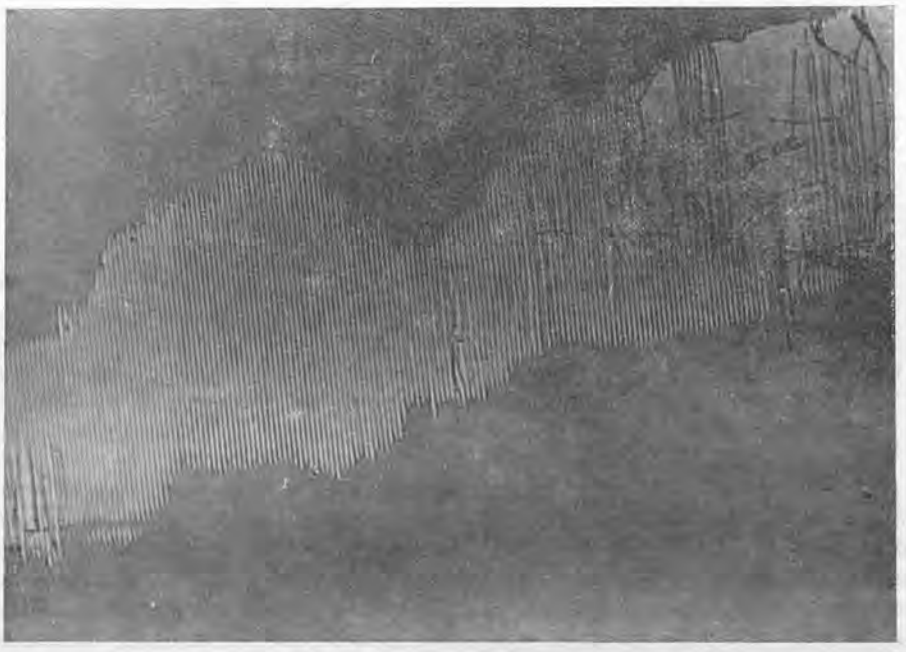

Fig.17. Grating of the type produced using a ' low energy ' ruby laser pulse (200 Å gold film illuminated by a 0·06 J/cm^2 ruby laser pulse).

wave (owing to the fact that with our experimental arrangement the forward and backward ruby laser beams were never exactly equal) would, however, cause a rapid decrease in this signal by creating a uniform plasma over the whole surface. Complete removal of the film over some part of the grating was always associated with this type of signal.

The ' step-function ' diffracted signals (fig. 15 (*b*)) observed using beams of very low energy may be explained on the assumption that at such energies there was no damage to the film at the nodes of the standing wave and no plasma formation. The development of the signal was in this case caused by vaporization of the film at the antinodes of the electric field. The remaining film caused diffraction as a result of the induced periodicity in its thickness, but the vapour, being transparent to argon ion laser light, had no effect on the diffracted signal. Hence the constant diffracted signal, once the laser pulse had formed the grating.

The slowly decaying signal observed, in addition to a constant background, at intermediate beam energies (fig. 15 (*c*)) may now be interpreted as a result of the formation of plasma, rather than un-ionized vapour, at such energies.

Now the decay time of this slow signal was directly proportional to $\operatorname{cosec}\theta$ i.e. proportional to the line separation d of the grating since (Little *et al.* 1970)

$$d = \frac{\lambda}{2}\operatorname{cosec}\theta \qquad (3.2.1)$$

where λ is the wavelength of the ruby laser light.

The distribution of the substrate temperature, or any other parameter controlled by a diffusion law, would show a development with a characteristic

time proportional to the square of that separation. Decay of the plasma, chemical processes occurring at the surface, or any phenomenon involving transport perpendicular to the surface would on the other hand give a decay time independent of spacing.

An acoustic surface wave would have a period proportional to the line spacing, but this would result in a diffracted signal whose intensity would oscillate with a period over an order of magnitude smaller than the observed decay time. A linear dependence of decay time on separation would, however, be expected if the diffraction were governed by the motion of a plasma across the lines of the grating in which the distance to be travelled, and thus the time required, to achieve any given ionic distribution would be proportional to the line separation.

Calculation of the velocities of the ions formed in the plasma (Cutter *et al.* 1974) indicates that they cross one grating spacing in a time comparable to the decay time of the diffracted signal. While the exact relationship between plasma distribution and diffraction efficiency is difficult to establish this provides a reasonable justification for assuming that the slowly varying signal results from the creation of a micro-plasma at the antinodes of the standing wave of the ruby laser light.

3.3. *Further developments of the experimental technique.*

Given optical detectors of better time resolution our Bragg reflection technique could be extended to the measurement of shorter modulation lifetimes. The fastest photomultipliers available have a time resolution of about 100 ps and would allow direct measurement of acoustic phonon lifetimes. The picosecond lifetimes of the optical phonons involved in stimulated Rayleigh wing and Raman scattering (Von der Linde, Laubereau and Kaiser 1971) could be resolved using a streak camera.

Our observations have been made only for backward going light of unshifted frequency or a frequency shift equal to that generated by stimulated Brillouin scattering in the medium under study. A full investigation of the Bragg reflectivity profile would require very precise tuning over a wide range of frequency shifts. It is possible that this could be achieved by using the tunable output of a dye laser as the backward going beam.

The diffraction technique could similarly be developed for a more general investigation of laser generated periodic structures. This phenomenon is of interest both as a means of rapidly producing small diffraction gratings of accurately known spacing and also because it provides a technique by which the dynamics of surface laser damage may be studied.

ACKNOWLEDGMENTS

This article contains in shortened form, much of the material which appeared in two papers by Harrison, R. G., Key, P. Y., and Little, V. I., on ' *Stimulated scattering and induced Bragg reflexion of light in liquid media* '. These papers are contained in *Proc. R. Soc. Lond.* A, **334,** 193–214 and 215–229 (1973). Reference should be made to this work for fuller practical and theoretical detail, and the authors make due acknowledgement to the Royal Society for the use of this material. A more complete and detailed account of the work on the time resolution of optically etched gratings has been accepted for publication in *Applied Optics* and should appear in 1974.

References

Alyassini, N., Parks, J. H., and De Shazer, L. G., (Private communication).

Bloembergen, N., 1965, *Non-linear optics.* (New York: Benjamin).

Bloembergen, N., 1967, *Am. J. Phys.* **35,** 989.

Brillouin, L., 1922, *Ann. Phys. (Paris),* **77,** 88.

Chiao, R., Townes, C., and Stoicheff, B., 1964, *Phys. Rev. Lett.,* **12,** 592.

Cutter, M. A., Key, P. Y., and Little, V. I., 1974, *Appl. Optics.* to be published.

Debye, P., and Sears, F., 1932, *Proc. Nat. Acad. Sci.,* **18,** 409.

Denariez, M., and Bret, G., 1968, *Phys. Rev.,* **171,** 161.

Eckhardt, G., Hellwarth, R., McClung, F., Schwartz, S., Weiner, D., and Woodbury, E., 1962, *Phys. Rev. Lett.,* **9,** 455.

Fabelinskii, I., 1965, *Molecular scattering of light.* (New York: Plenum) (1968).

Fabelinskii, I., and Starunov, V., 1967, *Appl. Opt.* **6,** 1793.

Frenkel, J., 1946, *' Kinetic Theory of Liquids '.* New York: Dover Publications Inc.

Gross, E., 1930, *Nature,* **126,** 201, 400, 603.

Gross, E., 1940, *Compt. Rend. Acad. Bulgare,* **28,** 786.

Harrison, R. G., 1970, *Nonlinear optical effects in Liquids.* Ph.D. Thesis, London University.

Harrison, R. G., Key, P. Y. and Little, V. I. 1973, *Proc. Roy. Soc.* A, **334,** Paper I p. 193, Paper II p.215.

Harrison, R. G., Key, P. Y., Little, V. I., Magyar, G., and Katzenstein, J., 1968, *Appl. Phys. Lett.* **13,** 253.

Henderson, B. E., Getty, R. R., Leroi, G. E. and Rousseau, D. L., 1971, *Damage in Laser Materials,* ed. by Glass, A. J., and Guenther, A. H., National Bureau of Standards, Special Publication 356, 31.

Herman, R. M., and Gray, M. A., 1967, *Phys. Rev. Lett.* **19,** 824.

Key, P. Y. 1970, *The Scattering of light from light induced structures in liquids.* Ph.D. Thesis. London University.

Key, P. Y., and Harrison, R. G., 1972, *Phys. Rev.* A, **5,** 1899.

Key, P. Y., Harrison, R. G., Little, V., and Katzenstein, J., 1970, *I.E.E.E. J.Q. Elect.* **6,** 641.

Landau, L., and Lifshitz, E., 1960, *The electrodynamics of continuous media.* (London: Pergamon).

Landau, L., and Placzek, G., 1934, *Phys. Z. Sow.,* **5,** p. 172.

Little, V. I., Rowley, D. M., and Wiltsher, R., 1970, *Nature* **228,** 49.

Maier, M., Rother, W., and Kaizer, W., 1967, *Appl. Phys. Lett.* **10,** 80.

Mandelshtam, L., 1926, *J. Russ. Soc. Phys. Chem,* **58,** 381.

Mash, D., Morozov, V., Starunov, V., Tiganoff, E., and Fabelinskii, I., 1965, *J.E.T.P. Lett.,* **2,** p. 157.

Parks, J. H., and Alyassini, N., 1972, *Laser Induced Damage in Optical Materials,* ed. by Glass, A. J., and Guenther, A. H., National Bureau of Standards, Special Publication 372, 104.

Rank, D., Cho, C., Foltz, N., and Wiggins, T., 1967, *Phys. Rev., Lett.,* **19,** 828.

Raman, C., 1928, *Ind. J. Phys.,* **2,** 387.

Raman, C., and Krishnan, K., 1928, *Phil Mag.,* **4,** 498.

Shen, Y., and Shamam, Y., 1967, *Phys. Rev.* **163,** 224.

von der Linde, D., Laubereau, A., and Kaiser, W., 1971, *Phys. Rev. Lett.* **26,** 955.

Woodbury, E., and Ng, W., 1962, *Proc. I.R.E.,* **50,** 2367.

Ziatsev, G., Kyzylasov, Y., Starunov, V., and Fabelinskii, I., 1967, *J.E.T.P. Lett.,* **6,** 255.

The Authors:

In 1967 with Science Research Council support, Dr. V. I. Little established the non-linear optical research group at Royal Holloway College. Dr. R. G. Harrison and Dr. P. Y. Key were founder members of the group. Mr. M. A. Cutter graduated at Royal Holloway College, and is now in his third year of postgraduate study as an SRC research student. The work of the group is concerned principally with the optical probing of optically induced structures in liquids and thin films, and uses its specially developed techniques to investigate laser induced surface damage.